

# Durability of concrete with supplementary cementitious materials

**Ranger, Maxime**

*Publication date:*
2023

*Document Version*
Publisher's PDF, also known as Version of record

# Durability of concrete with supplementary cementitious materials

Maxime Ranger

PhD Thesis
August 2023

DTU Sustain
Department of Environmental and Resource Engineering
Technical University of Denmark

**Durability of concrete with supplementary cementitious materials**

**Maxime Ranger**

PhD Thesis, August 2023



Address: DTU Sustain
Department of Environmental and Resource Engineering
Technical University of Denmark
Bygningstorvet, Building 115
2800 Kgs. Lyngby
Denmark

Phone: +45 4525 1600

Homepage: https://www.sustain.dtu.dk
E-mail: info@sustain.dtu.dk

Cover: Concrete field exposure site at the Technical University of Denmark. Photo by Maxime Ranger.

# Acknowledgements

This PhD project was funded by the Danish Road Directorate and a joint grant from Innovation Fund Denmark and Realdania under the program “Circular Built Environment”. Their financial support is greatly acknowledged.

I am extremely grateful to my supervisor Marianne Tange Hasholt, who has been here since the beginning of my “concrete” journey. Thank you for your constant support and commitment during these three years, and for your sharp and always constructive feedback which strengthened my scientific reflexions.

I am also thankful to Ole Mejlhede Jensen for joining the supervision team for the last year. I truly appreciated your great advice when writing this thesis, and your availability to answer any questions and share your knowledge.

A warm thank to my supervisors Lene Højris Jensen and Ricardo Antonio Barbosa. Thank you for your availability, your good mood, and your support to help bringing my results from the lab to the “real world”.

Many thanks to Josée Duchesne and Benoit Fournier for a warm welcome in Quebec during my three-month external research stay at Laval University. Thank you for the access to the laboratory, for your availability to discuss my project and for sharing your experience. I would also like to thank Klaartje De Weerdt for a short but great research stay at NTNU, and for her support and contagious enthusiasm within RILEM Technical Committee 301.

Special thanks to Kurt Kielsgaard Hansen for his availability at DTU in all circumstances. I also thank the laboratory technicians at DTU who helped me along the project, especially Ebba Cederberg Schnell, Natasja Dueholm, Klaus Bræmer, Jørn Lykke Jensen and Jacob Friis-Grigoncza.

I am so glad to have met nice colleagues along the way and to have shared part of our PhD together: Jennifer A. Canul Polanco, Abdul Faheem, Gui Li, Pablo Alberdi Pagola, Miriam E. Krüger, Julie Bartholdy and Marvin Glißner. Special thanks to Jennifer for also sharing her knowledge on XRD.

I also had the pleasure to be part of the Circular Built Environment network supported by Bloxhub. Many thanks to Pernille Berg, Jule Rumpel and all my PhD fellows for broadening my mind and extending my knowledge on sustainability and circularity in the construction industry.

Finally, many thanks to my family and friends for nice times out of the office, refreshing holidays and talks about everything but concrete.

# Summary

The concrete industry currently is currently in a major transition phase to lower its $CO_2$ emissions. In this respect, using Supplementary Cementitious Materials (SCMs) is key to lower the amount of Portland cement in concrete. Traditional SCMs such as fly ash and blast furnace slag are industrial by-products which have been used for many years in concrete. However, the supply of these materials is expected to decline soon. This emphasises the need to find alternative SCMs and to adapt regulatory frameworks to allow their use in a safe and efficient way.

This PhD project intended to investigate the effect of SCMs on Alkali-Silica Reaction (ASR), one of the main issues that affect concrete durability. In particular, the main objective was to develop a generic procedure to qualify all types of SCMs with respect to ASR in the Danish concrete specifications. For this purpose, the experimental work was carried out on a selection of SCMs representing the diversity of sources.

The experiments focused on two main aspects. On the one hand, the influence of SCMs on the amount of alkalis in the pore solution was studied via cold water extraction (CWE). CWE is a simple method that can be performed with basic laboratory equipment, so it has the potential to be used at an industrial scale. On the other hand, several ASR expansion tests were carried out to evaluate the ability of SCMs to prevent the expansion induced by ASR. Field exposure cubes were cast to evaluate the validity of three accelerated laboratory tests: ASTM C1567, TI-B 51 and RILEM AAR-10.

The results showed a strong link between the SCM reactivity and their ability to reduce free alkalis in the pore solution. CWE allowed to determine the free alkali contribution from SCMs, which is a key value for calculating the alkali loading in concrete. The latter seemed to be linked with the ASR expansion via a threshold effect, i.e. no expansion occurred below a certain free alkali content around 2.4 kg/m$^3$ $Na_2O_{eq}$. This was only observed for AAR-10 and field cubes, which correlated well for all the mixes tested. Conversely, significant deviations occurred with ASTM C1567 and TI-B 51, which questions the suitability of these tests to assess the efficacy of SCMs.

A procedure was suggested to screen the suitability of SCMs with respect ASR. In addition, a proposal was formulated to update the Danish regulations regarding the qualification of SCMs.

# Sammenfatning

Betonindustrien undergår i disse år en betydelig ændring for at minimere $CO_2$-emissioner. I denne forbindelse er brugen af mineralske tilsætninger et vigtigt element for at reducere andelen af Portlandcement i beton. Traditionelle mineralske tilsætninger såsom flyveaske og højovnsslagge er industrielle biprodukter med en mangeårig anvendelse i beton, men det forventes at adgang til disse materialer bliver reduceret i de kommende år. Dette understreger behovet for at identificere alternative mineralske tilsætninger og modificere eksisterende normer og standarder, så sikker og effektiv anvendelse muliggøres.

Dette PhD-projekt havde til formål at undersøge effekten af mineralske tilsætninger på alkali-kiselreaktioner (AKR), der er en væsentlig nedbrydningsmekanisme som begrænser betons holdbarhed. Hovedformålet var at udvikle en generisk procedure der kan benyttes i danske betonstandarder til undersøgelse af alle typer af mineralske tilsætninger vedrørende AKR. Derfor blev der udført forsøg med et bredt udvalg af mineralske tilsætninger.

Forsøgene fokuserede på to hovedaspekter. Dels blev det med 'koldtvandsudtrækning' undersøgt hvordan mineralske tilsætninger påvirker mængen af alkalier i porevæsken. Koldtvandsudtrækning er en enkel metode der kan udføres med simpelt laboratorieudstyr, og den er derfor potentielt industrielt velegnet. Desuden blev en række AKR-ekspansionsforsøg udført for at undersøge, hvordan AKR påvirkes af mineralske tilsætninger. Felteksponeringskuber blev støbt for at undersøge anvendeligheden af tre accelererede laboratoriestandarder: ASTM C1567, TI-B 51 og RILEM AAR-10.

Resultaterne viste en stærk sammenhæng mellem reaktiviteten af mineralske tilsætninger og deres evne til at mindske frie alkalier i poreopløsningen. Koldtvandsudtrækning muliggjorde bestemmelse af mineralske tilsætningers bidrag til frie alkalier, der er en vigtig størrelse for at kunne beregne betons alkalibelastning. Sidstnævnte så ud til at være koblet til AKR-ekspansionen via en tærskeleffekt, dvs. ingen ekspansion finder sted under et vist frit alkaliindhold, ca. 2.4 kg/m$^3$ $Na_2O_{ækv}$. Dette blev kun observeret for AAR-10 og feltkuberne hvilket stemte godt overens for alle undersøgte blandinger. I modsætning hertil var der betydelige afvigelser i forhold til ASTM C1567 og TI-B 51, og anvendeligheden af disse standarder til de nævnte undersøgelser er derfor tvivlsom.

En procedure blev foreslået til screening af mineralske tilsætning mht. AKR. Ydermere blev der udarbejdet et forslag til opdatering af de danske standarder vedrørende acceptkritier for mineralske tilsætninger.

# Contents

# Preface

The thesis is organized into two parts: the first is a synopsis that contextualises the PhD findings; the second consists of the scientific publications listed below. These will be referred to by Roman numbers **I-VII.**

**I** Maxime Ranger, Marianne Tange Hasholt, Ricardo Antonio Barbosa, Pore solution alkalinity of cement paste as determined by Cold Water Extraction, *Published in CEMENT (2023), Volume 11, p. 100055*. *DOI: 10.1016/j.cement.2023.100055*

**II** Maxime Ranger, Marianne Tange Hasholt, Cold Water Extraction for determination of the free alkali metal content in blended cement pastes, *Published in CEMENT (2023), Volume 13, p. 100079. DOI: 10.1016/j.cement.2023.100079*

**III** Maxime Ranger, Marianne Tange Hasholt, Relationship between chloride migration, bulk electrical conductivity and formation factor of blended cements, *Submitted for publication.*

**IV** Maxime Ranger, Marianne Tange Hasholt, Ricardo Antonio Barbosa, Laboratory and field investigations of alkali-silica reaction prevention by supplementary cementitious materials: influence of the free alkali loading, *Manuscript in preparation.*

**V** Maxime Ranger, Marianne Tange Hasholt, Ricardo Antonio Barbosa, Lene Højris Jensen, Predicting the effect of SCMs on ASR in the accelerated mortar bar test with artificial neural networks, *Published in Proceedings of the 16$^{th}$ International Conference on Alkali-Aggregate Reaction in Concrete – Volume II, pp. 389–400, May 2022, Lisbon (Portugal).*

**VI** Maxime Ranger, Josée Duchesne, Reactivity of alternative supplementary cementitious materials assessed by the $R^3$ method, *Accepted for the 16$^{th}$ International Congress on the Chemistry of Cement, September 2023, Bangkok (Thailand).*

**VII** Maxime Ranger, Marianne Tange Hasholt, Ricardo Antonio Barbosa, Cold Water Extraction as a method to determine the free alkali content of cementitious binders, *Accepted for the 16$^{th}$ International Congress on the Chemistry of Cement, September 2023, Bangkok (Thailand).*

# Abbreviations

**General**

| | |
|---|---|
| ANN | Artificial Neural Network |
| AMBT | Accelerated Mortar Bar Test |
| ASR | Alkali-Silica Reaction |
| CPT | Concrete Prism Test |
| CWE | Cold Water Extraction |
| EDL | Electrical Double Layer |
| ICP-OES | Inductively Coupled Plasma – Optical Emission Spectroscopy |
| L/S | Liquid-to-Solid ratio by mass |
| PWE | Pore Water Extraction |
| PC | Portland Cement |
| RH | Relative Humidity |
| SCM | Supplementary Cementitious Material |
| TGA | Thermogravimetric Analysis |
| XRD | X-Ray Diffraction |
| XRF | X-Ray Fluorescence |

**Cement chemist notation**

| | |
|---|---|
| C | Calcium oxide – $CaO$ |
| S | Silicon dioxide – $SiO_2$ |
| A | Aluminium oxide – $Al_2O_3$ |
| F | Iron oxide – $Fe_2O_3$ |
| H | Water – $H_2O$ |
| $C_3S$ | Tricalcium silicate |
| $C_2S$ | Dicalcium silicate |
| $C_3A$ | Tricalcium aluminate |
| $C_4AF$ | Tetracalcium alumino ferrite |
| C-S-H | Calcium silicate hydrates |
| C-A-S-H | Calcium silicate aluminate hydrates |
| CH | Calcium hydroxide – Portlandite |
| AFm<br>AFt | Hydrated calcium aluminate, ferrite and sulfate phases |

# Variables

| Symbol | Unit | Description |
|---|---|---|
| $A_{t,y}(x)$ | [g/100 g binder] | Total content of compound *y* in material *x* |
| $A_{f,y}(x)$ | [g/100 g binder] | Free content of compound *y* in material *x* |
| $A_{ws,y}(x)$ | [g/100 g SCM] | Water-soluble content of compound *y* in powder *x* |
| $D_{nssm}$ | [$10^{-12}$ $m^2/s$] | Non-steady-state chloride migration coefficient |
| $w_{ps}$ | [wt.%] | Amount of pore solution |
| $w_{R3}$ | [g/100 g dry $R^3$ paste] | Bound water measured in the $R^3$ method |
| *w/b* | [-] | Water-to-binder ratio by mass |
| *w/c* | [-] | Water-to-cement ratio by mass |
| $\alpha_y(x)$ | [g/g SCM] | Apparent contribution of compound *y* from powder *x* |
| $\beta_y(x)$ | [g/100 g binder] | Net release of compound *y* from powder *x*, upon reaction of powder *x* |
| $\sigma_b$ | [mS/m] | Bulk electrical conductivity |

# 1 Introduction

For construction materials, durability may be defined as "the ability of a material to resist weathering action, chemical attack, abrasion, and other conditions of service" [1]. This PhD project focused on a specific mechanism affecting concrete durability: Alkali-Silica Reaction (ASR). The following gives a general introduction to concrete, cement chemistry and ASR, before presenting the research objectives.

## 1.1 General background

Concrete is a building material made of three main components: cement, water and aggregates. The most common type of cement is the so-called Portland cement, which is manufactured by sintering limestone and clay up to about 1450°C. In contact with water, Portland cement dissolves and forms new products that bind the aggregates together.

Concrete is the most used construction material on Earth [2]. The production of concrete worldwide was estimated to be around 14 billion $m^3$ in 2020 [3], and the demand is expected to rise in the coming years [2]. Two major challenges are therefore facing the concrete industry: carbon dioxide ($CO_2$) emissions and availability of raw materials. It is estimated that concrete accounts for around 8% of man-made $CO_2$ emissions [4,5], where the largest contribution comes from Portland cement. During its manufacturing, calcium carbonate ($CaCO_3$) in the limestone breaks down into calcium oxide (CaO) and $CO_2$ at around 800°C. This chemical breakdown accounts for about 60% of the $CO_2$ emissions, while the remaining 40% is related to energy consumption throughout the production [4].

Consequently, one of the most effective ways to reduce the carbon footprint of concrete is to replace Portland cement with substituents having less embodied carbon and/or bringing mechanical or durability benefits [6]. Such materials may be called Supplementary Cementitious Materials (SCMs). Traditional SCMs are primarily industrial by-products such as coal fly ash, silica fume or blast furnace slag. Using these materials in concrete also contribute to enhance circularity by creating new loops and avoiding waste handling. However, a decline in the production of traditional SCMs is expected in the coming years due to an overall decarbonisation of the industry [2]. This creates an urgent need to find alternative SCMs and make it possible to use them in practise [7]. As many concrete standards have separate regulations for each type of SCM, changes are needed to facilitate the introduction of new types [8].

Another important lever to reduce $CO_2$ emissions is to extend the service life of concrete constructions by improving durability [9]. For example, in 2020, the Danish Road Directorate set the design service life of new structures to 120 years. In the case of infrastructure, keeping them in use for longer has also financial benefits, since the projects usually require massive investments. Moreover, infrastructure is often challenging for concrete durability because they are located in harsh environments, with exposure to e.g. rainfalls, seawater or de-icing salts.

## 1.2 Cement hydration

Portland Cement (PC) is made of four main compounds, known as the clinker minerals: alite, belite, aluminate and ferrite. These are impure forms of $C_3S$, $C_2S$, $C_3A$ and $C_4AF$, respectively. When water is added, the clinker minerals dissolve and combine with water to form reaction products, called hydrates. Such process is referred to as hydration. The main types of hydrates include calcium silicate hydrates (C-S-H), portlandite (CH) and calcium aluminate phases (mainly AFm and AFt) [10]. When SCMs are used, additional reactions take place. If the SCM is hydraulic, it can directly react with water. If the SCM is pozzolanic, it reacts with portlandite formed during the hydration of PC. This pozzolanic reaction also produces C-S-H, but with a lower Ca/Si than the C-S-H produced during the hydration of PC [11].

The formation of these hydrates creates a solid porous matrix which binds the aggregates together. The pores may be partially or fully filled with a liquid called pore solution, which tries to be in thermodynamic equilibrium with the solid matrix. Due to the chemistry of cementitious materials, the pore solution is alkaline and mainly contains three types of ions: sodium ($Na^+$), potassium ($K^+$) and hydroxide ($OH^-$). As the concentrations are rather high (order of size: 0.5 mol/L), the pH of the pore solution is usually in the range 12-14 [12].

## 1.3 Alkali-silica reaction

Alkali-Silica Reaction (ASR) is a major concrete durability concern in many countries [13]. ASR is a complex physicochemical reaction which only occurs with certain types of aggregates containing a reactive form of silica (amorphous or poorly crystalline). The reaction can be summarised in three main steps [14]:

1) Hydroxide ions ($OH^-$) present in the pore solution attack the silanol groups at the surface of reactive silica grains, leading to the dissolution of silica.
2) Dissolved silica combines with calcium and alkali metals (Na and K) to form secondary products, called alkali-silica products.

3) The formation of these products causes internal pressures that may lead to the expansion of concrete and eventually cracking.

ASR is a slow process in real structures, where visible signs of damage typically appear after 5 to 10 years in temperate climates [15]. Besides concrete expansion, characteristic signs of surface damage include map cracking and pop-outs [16] as shown in Figure 1. Several strategies enable to delay or prevent ASR for new construction [17]:

- Select non-reactive aggregates.
- Limit the alkali content in the concrete, e.g. use low-alkali cement.
- Keep the concrete dry.
- Use adequate amounts of SCMs.
- Use adequate amounts of chemical admixtures, e.g. lithium-based products.

Using non-reactive aggregates and limiting the alkali content of concrete are usually prioritised, however these options may be challenging to implement. Indeed, cement and aggregates are often used locally, and their properties depend on the chemistry of raw materials. Similarly, for keeping the concrete dry, some structures like dams are not adapted for vapour barriers. In some cases, using SCMs or chemical admixtures is therefore the only efficient way to prevent deleterious ASR.

*Figure 1: Surface features of ASR damage. Left: map cracking on the deck of an ASR-affected railway bridge on Nivåvej (Nivå, Denmark), courtesy of Ricardo A. Barbosa. Right: pop-outs over porous opaline flint particles (picture size: 5 cm).*

It is acknowledged that the main mechanism by which SCMs prevent ASR is the reduction of the pore solution alkalinity [18]. Even though there are usually more alkalis per gram of powder in SCMs than in PC, less alkalis are present as ions in the pore solution (called “free alkalis”). However, contrary to PC, it is difficult to estimate the free alkalis contribution of SCMs. One possibility is to press a hardened sample to extract the pore solution and analyse its composition [19]. This method, called Pore Water Extraction (PWE), requires a specific and expensive setup which is only available in some research laboratories [20]. An alternative method called Cold Water Extraction (CWE) showed promising abilities [21] but needs to be explored further when SCMs are used.

Besides the pore solution alkalinity, other parameters can affect the ASR: the presence of aluminium in the pore solution, the type of aggregate, the moisture state, the temperature, and the exposure to external sources of alkalis, to cite a few [14]. Due to these numerous and complex relationships, the efficacy of SCMs must be assessed by performance testing. Like for many durability issues, accelerated laboratory tests are used to speed up the processes and to obtain results within a reasonable amount of time. However, accelerating measures may disturb the actual ASR process occurring in the field, and induce misleading conclusions [22]. Thus, it is difficult to design an “ideal test”, in particular one balancing validity and rapidity [23]. The validity of accelerated tests is generally evaluated via field studies, where concrete specimens are in outdoor conditions. Although such testing takes significantly longer time than accelerated tests, it is more representative of what occurs in real structures [24].

## 1.4 The Danish context

A comprehensive description of the ASR history in Denmark is presented in [25]. The paragraphs below summarise some of its key points relevant to the present work.

ASR studies in Denmark started in the 1950s with a large field investigation of concrete structures, where clear evidence of ASR was observed. Subsequent research led to the publication of the first ASR prevention guidelines in 1961, which were however not official requirements. In the meantime, the road infrastructure network developed considerably during the 1960s and the 1970s, and numerous concrete bridges were built with reactive aggregates. In 1987, the first official ASR requirements were enforced with the publication of the Basic Concrete Specification (in Danish: Basisbetonbeskrivelsen).

In 2013, the road and railway administrations estimated that 600 bridges were potentially affected by ASR, judging from the concrete composition and/or the year of construction. Special investigations have confirmed around 30 cases among the bridges still in service, while a handful have been removed from the list. No new case of ASR has been reported for bridges built after 1987.

The research conducted in the 1960s identified three main types of reactive minerals: porous opaline flint, porous calcareous opaline flint and opaline sandstone. The two first represent more than 90% of the ASR cases. Danish cements are typically below 0.6 wt.% $Na_2O_{eq}$, so that the alkali loading in the concrete is well below 3.0 kg/m$^3$ $Na_2O_{eq}$ and cannot explain the occurrence of ASR. Instead, ASR damage is attributed to the ingress of e.g. de-icing salts (NaCl). Thus, the main prevention measure has been the use of waterproofing membranes to prevent the ingress of water and NaCl.

For most exposure classes defined in EN 206 [26], the current Danish ASR regulations (EN 206 DK NA [27]) rely on two main pillars:

- **The use of aggregates classified as non-reactive.**
- **A maximum alkali loading of 3.0 kg/m$^3$ $Na_2O_{eq}$ in concrete**, where the contributions of coal fly ash, bio-coal fly ash and silica fume are not considered. If composite cements are used, their alkali content is defined according to the Danish standard INF 135 [28].

These requirements are particularly constraining for alternative SCMs because their total alkali content needs to be accounted for. This emphasises the urgent need for simple methods to determine their effective alkali contribution.

## 1.5 Research objectives

Considering the situation in Denmark, this project focuses on the role of SCMs with respect to ASR, intending to facilitate the introduction of alternative SCMs in ASR regulations. ASR regulations are essentially based on the strategies presented in Section 1.3. Two main types of requirements can be specified, namely prescriptive or performance-based:

- The prescriptive approach is based on a “recipe” to follow when designing a concrete mix.
- The performance-based approach sets a performance target but does not specify how this target should be reached.

Prescriptive rules have been traditionally used for concrete. However, they often hinder the use of new materials such as alternative SCMs, because their validity is limited to a certain range of materials [29].

The work reported in this thesis articulates around two research questions:

**Q1. How can one determine simply and accurately the free alkali contribution from SCMs?**

As stated in Section 1.3, there is no simple relationship between total and free alkalis for SCMs. This can be determined experimentally via Pore Water Extraction, but the method is not suited for large-scale uses due to the limited availability of the setup.

**Q2. What is the optimum way to test if an SCM can be used to mitigate ASR or poses an ASR risk?**

On the one hand, field testing is certainly the most effective way, but it may require several years or decades before any conclusion can be drawn. On the other hand, most of the accelerated tests were initially designed to test the reactivity of aggregates and may not be appropriate for testing the influence of SCMs.

# 2 Terminology

SCMs may be defined as “inorganic material such as fly ash, silica fume, metakaolin, or slag cement that reacts pozzolanically or hydraulically” [1]. For simplicity in this thesis, all materials used for PC replacement except limestone filler will be referred to as SCM, even if their pozzolanic or hydraulic behaviour has not been clearly demonstrated.

The terms “reactive” or “reactivity” are often used throughout the thesis, but the reader should be aware that their meaning is slightly different depending on the context. For SCMs, reactivity refers to the extent of hydraulic or pozzolanic reaction. For ASR, reactivity refers to the predisposition of an aggregate to suffer from ASR. In fact, the pozzolanic reaction and ASR are very similar, because they both start with the dissolution of amorphous silica. One may say that the only difference is the smaller particle size of pozzolanic-reactive materials compared to ASR ones, which implies that the pozzolanic reaction takes places significantly faster [30].

Many qualifying terms regarding alkalis can be found in the literature. In some cases, the same word is used for different concepts. One example of this is “available alkalis”, which can refer either to the standardised procedure in ASTM C311 [31] or to the alkalis above a certain threshold concentration in the pore solution, corresponding to the minimum level to sustain ASR [32]. Conversely, the same concept can be described by different words. For instance, the adjectives “active” [33], “effective” [34] or “free” [21] seem to have been used to designate alkali metals present as ions in the pore solution. For clarity and consistency, the terminology defined in Figure 2 will be systematically used throughout this thesis.

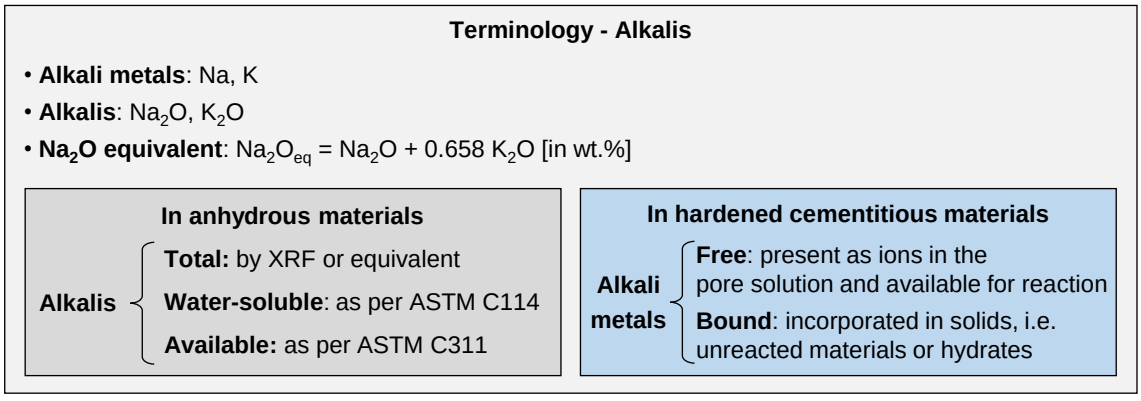


*Figure 2: Terminology related to alkalis used in this thesis. The intention is to provide the reader with a relatively short and visual list of terms to facilitate the reading and make a link with the literature. Adapted from Figure 1 in Paper II.*

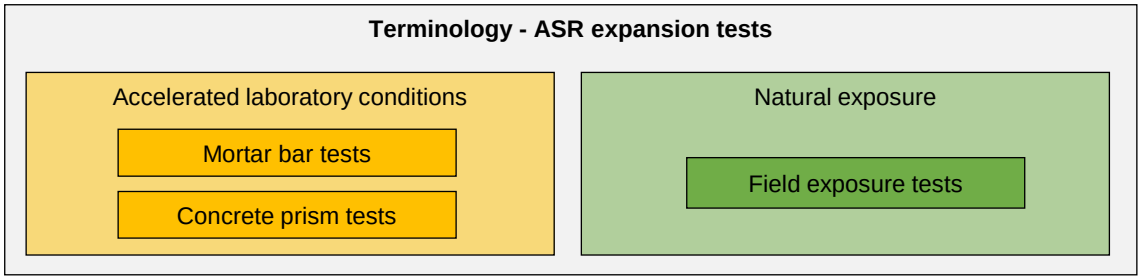


*Figure 3: Terminology related to ASR expansion tests used in this thesis. This division is likely not suited to classify all tests existing in the literature but should be sufficient in the present document.*

ASR expansion tests will be divided into two categories depending on the exposure conditions: accelerated in the laboratory or natural/outdoor. In addition, a distinction will be made for accelerated laboratory tests based on the material used, i.e. mortar or concrete. This division is presented in Figure 3. One should note that the name “accelerated mortar bar test” will be dedicated to ASTM C1260 [35] or C1567 [36], as it is often the case in the literature.

# 3 State-of-the-art

## 3.1 Alkali metals in concrete

Alkali metals (Na and K) originate from alkalis ($Na_2O$ and $K_2O$) that are naturally present in cementitious materials. In hardened cement paste, they can be found in three forms: bound to unreacted material, bound to hydrates – primarily C-S-H, or free in the pore solution [37]. In the pore solution, alkali metals are the major types of cations and ensure the electroneutrality of the solution against hydroxide ions. Thus, the ionic equilibrium in the pore solution can usually be described by $[Na^+] + [K^+] \approx [OH^-]$ [38,39]. In the case of PC, Helmuth et al. [40] proposed an empirical relationship where the hydroxide ion concentration can be calculated from the total alkali content of PC in wt.%, $A_{t,Na2Oeq}(PC)$, and the water-to-cement ratio, *w/c*, as per Equation (1).

$$[OH^-] = \frac{0.339 \cdot A_{t,Na2Oeq}(PC)}{w/c} + 0.022 \pm 0.06 \text{ mol/L} \quad (1)$$

Theoretically, the pore solution composition depends on the chemical equilibria with the solid matrix. The interface between the C-S-H and the bulk pore solution is called the Electrical Double Layer (EDL). In this layer, there must be a charge balance between the surface of the C-S-H (negatively charged) and the adsorbed cations in the EDL. In addition, the C-S-H, the EDL and the bulk pore solution must all be in thermodynamic equilibrium [41]. As a result, alkali metal binding by C-S-H increases if [42,43]:

- The amount of C-S-H increases.
- The Ca/Si of C-S-H decreases.
- The concentration of alkali metal ions increases.

When SCMs are used, the pozzolanic reaction produces C-S-H or C-A-S-H with a lower Ca/Si than C-S-H formed from PC [11]. Thus, more alkali metals can be bound, which reduces their concentrations in the pore solution. Taylor [37] proposed a method to predict the concentrations of $Na^+$, $K^+$ and $OH^-$ in the pore solution of samples with plain PC or PC with fly ash, based on a mass-balance approach in the paste. Subsequently, Duchesne and Bérubé [44] and Hemstad et al. [45] extended the experimental validation to systems containing other types of SCMs. Regarding the pore solution specifically, numerous data about the influence of traditional SCMs on the pore solution composition can be found in the review by Vollpracht et al. [12].

## 3.2 Techniques to measure free alkalis

A comprehensive review of the different techniques used to determine the free alkali metal content was made by Plusquellec et al. [21]. Among the different techniques, two will be presented in detail in the following: Pore Water Extraction (PWE) and Cold Water Extraction (CWE). For both methods, the amount of free alkali metals can either be expressed as a concentration (in mol/L) or as a weight fraction (in g/g cement or g/g paste) [21].

### 3.2.1 Pore Water Extraction

PWE is the most used technique to study the pore solution composition [46]. A pioneering setup was designed by Longuet et al. [47] and consists of extracting the pore solution mechanically by pressing a hardened sample with a piston, with a pressure usually in the range of 200-1000 MPa [21]. The method aims to collect the pore solution as is, so that all species can be accurately measured.

However, PWE is ineffective for specimens with a low free water content, caused by e.g. a low *w/c* or a high aggregate content [21,48]. Another limitation is the setup itself: due to its complexity and its cost, it is only available in a few laboratories [20]. Moreover, some safety concerns have been raised [45] due to the severe consequences of a potential failure of the metal body during the loading phase.

### 3.2.2 Cold Water Extraction

CWE is a leaching method, which relies on diluting the pore solution into a larger volume of solution that is easier to sample. Figure 4 illustrates the main steps of CWE: the hardened sample is first crushed, leached in deionised water, then the slurry is filtered and the filtrate is analysed [20]. The results must be converted to account for the dilution [21].

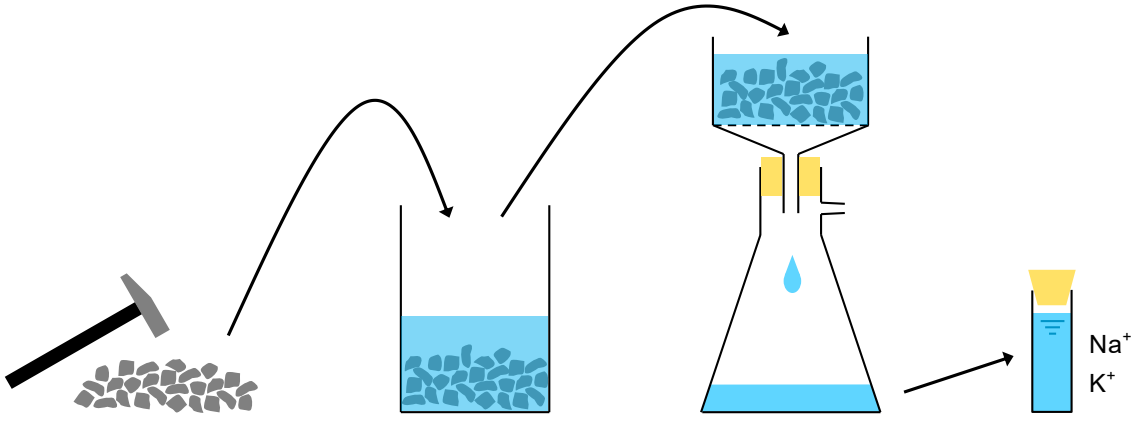


*Figure 4: CWE process: crushing, leaching, filtering and chemical analysis.*

The addition of water decreases the concentrations of alkali metals compared to the initial pore solution and increases the solubility of portlandite, via a reduction of the common ion effect [21]. Thus, the final CWE solution contains significantly more $Ca^{2+}$ and $OH^-$ than the initial pore solution. In theory, it is possible to correct the concentrations for portlandite dissolution [49], but it requires extra measurements to determine the portlandite content. Thus, the pH of the extracted solution is not representative of the pH of the initial pore solution. Unfortunately, most studies investigating the effect of test parameters like the size fraction, the liquid-to-solid ratio or the leaching time were based on pH measurements, which questions the validity of the conclusions [21].

The main advantage of CWE over PWE is the simplicity of the procedure and the equipment. However, CWE systematically gave higher concentrations than PWE [50]. One explanation may be the influence of the amount of pore solution, which needs to be determined to calculate the concentrations in the pore solution [51]. Another possible source of discrepancy is the potential release of alkali metals initially bound to hydrates during the leaching step [52]. Finally, secondary hydration of cement has also been mentioned as a reason for measuring a higher alkalinity by leaching methods [21].

## 3.3 Anticipating the free alkali contribution of SCMs

Equation (1) is not valid when SCMs are used. Thomas [18] observed a good correlation between a chemical index for the binder, $Na_2O_{eq} \times CaO / (SiO_2)^2$, and the $OH^-$ concentration in the pore solution of samples containing traditional SCMs. However, when alternative SCMs were used, the correlation became less evident [53]. The main reason behind this is the complexity of the chemical reactions occurring with SCMs. They contain multiple phases having different chemical and mineralogical properties, which influences their reactivity to a large extent. Even though the chemical composition gives an indication of the SCM performance, more characterisation is needed [7].

For example, efforts have been made to quantify the effect of SCMs on the compressive strength, through the development of reactivity tests such as the $R^3$ method [54]. The $R^3$ method relies on a simplified mixture containing an SCM, calcium hydroxide, calcium carbonate, water, alkalis and sulphates. By measuring different parameters such as heat release, bound water or portlandite consumption, it is possible to estimate the compressive strength contribution of an SCM with 7 days of testing [55,56].

Regarding alkalis, the only existing standard to quantify the contribution of an SCM to the alkalinity of the pore solution is the so-called "available alkalis" test in ASTM C311 [31]. In this test, an SCM is mixed with calcium hydroxide and water, and sealed cured for 28 days at 40°C. The hardened material is then crushed, leached in water and filtered. The amount of Na and K are measured and converted into alkalis. However, several studies showed that this test largely overestimates the contribution of SCMs when comparing the results with the pore solution of actual blended cement pastes [19,53].

## 3.4 Testing the effect of SCMs on ASR expansion

As deleterious ASR is characterised by concrete swelling, most requirements are based on expansion tests, where the test is passed if the expansion at a given point in time is below a certain threshold. According to Thomas et al. [23], an "ideal" method to test preventive measures should be "rapid, reliable and capable of determining the influence of aggregate reactivity, alkali availability and exposure conditions". The two most widely used methods are [57]:

- The Accelerated Mortar Bar Test (AMBT), standardised as e.g. ASTM C1567 [36]. Mortar bars are immersed in a 1M NaOH solution stored at 80°C. Provided that the exposure duration is limited to 14 days, the test was claimed to be realistic concerning the effect of SCMs on ASR [58], and corresponds fairly well with the field performance [57,59]. Nevertheless, some concerns were raised regarding changes in the pore solution chemistry such as ingress of $Na^+$, leaching of $K^+$ and dissolution of $SO_4^{2-}$ [60].
- The Concrete Prism Test (CPT), standardised as e.g. ASTM C1293 [61]. Concrete prisms are exposed to 100% RH and elevated temperature (38°C or 60°C). The test usually lasts for 2 years, after which the expansion flattens out due to alkali leaching [62]. Different possibilities exist to limit alkali leaching, such as increasing the size of the prisms [63], using an alkali wrapping [64] or placing the prisms in a synthetic pore solution [65]. Several authors observed that no expansion occurs in the CPT if the alkalinity of the pore solution is below a certain threshold value [66,67].

Fournier et al. [68] reported a reasonable correlation between CPT results and the expansion of field exposure cubes after 10 years. However, some blended mixtures passing the CPT failed in the field after 15 years of exposure. The same trend was observed by Tanesi et al. [69]. As significant changes in expansion features may occur even after 12 years of exposure in the field [70], longer durations (> 20 years) may be needed before concluding on the efficacy of prevention measures.

## 3.5 Danish regulations for cementitious materials

EN 206 DK NA [27] states that aggregates classified as non-reactive must be used for all exposure classes except X0 and XC1. In addition, the concrete alkali loading should be below 3.0 kg/m$^3$ $Na_2O_{eq}$. Fine reactive aggregates are allowed for exposure classes XC2, XC3, XC4, XF1 and XA1, but in this case the alkali loading should be lowered to 1.8 kg/m$^3$ $Na_2O_{eq}$.

The rules defining how the alkalis from cementitious materials should be accounted for when calculating the alkali loading are summarised in Figure 5. The alkali content of all constituents must be taken into account, except for coal fly ash, bio-coal fly ash and silica fume.

The declared alkali content for commercial cements is determined according to the Danish standard INF 135 [28], outlined in Figure 6. For CEM I, the declared value is the total content in the cement. For CEM II which can be used without further documentation, only alkalis from clinker, limestone and gypsum are accounted for. Based on the calculated alkali content, the cement is then classified into one of the four alkali classes: extra-low alkali (EA), low alkali (LA), medium alkali (MA) and high alkali (HA).

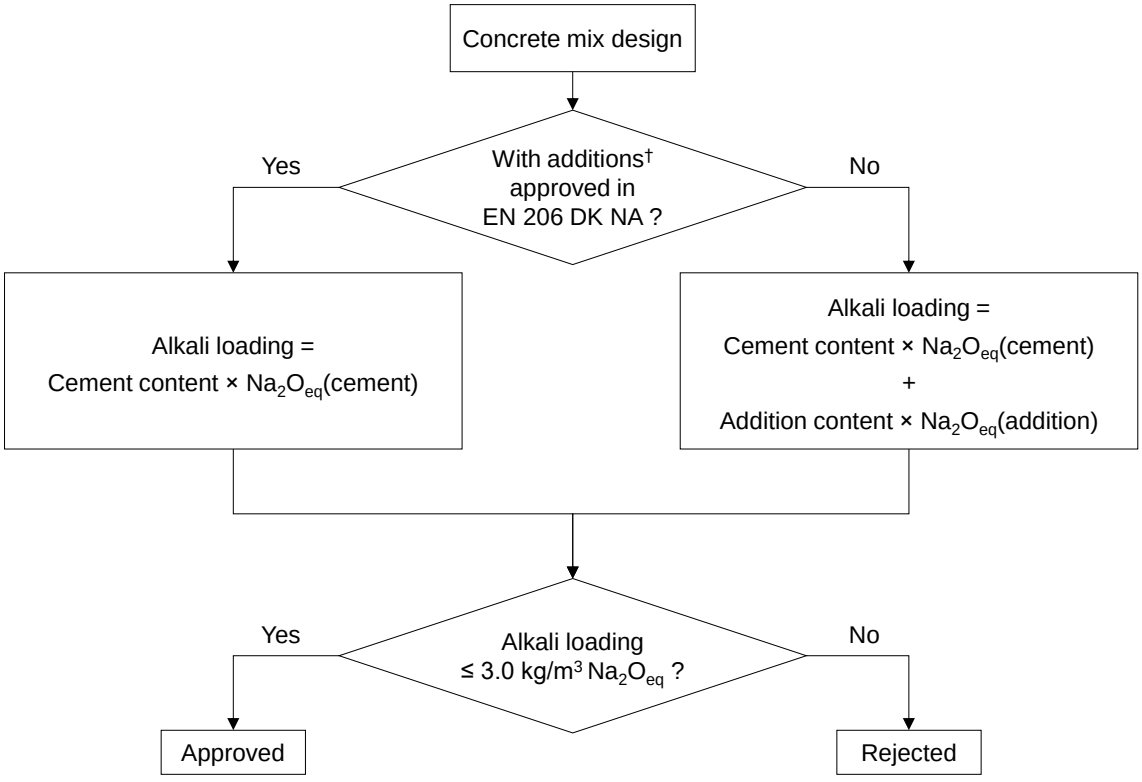


*Figure 5: Alkali loading calculation (binder part), graphical representation of EN 206 DK NA [27]. †) Coal fly ash, bio-coal fly ash and silica fume.*

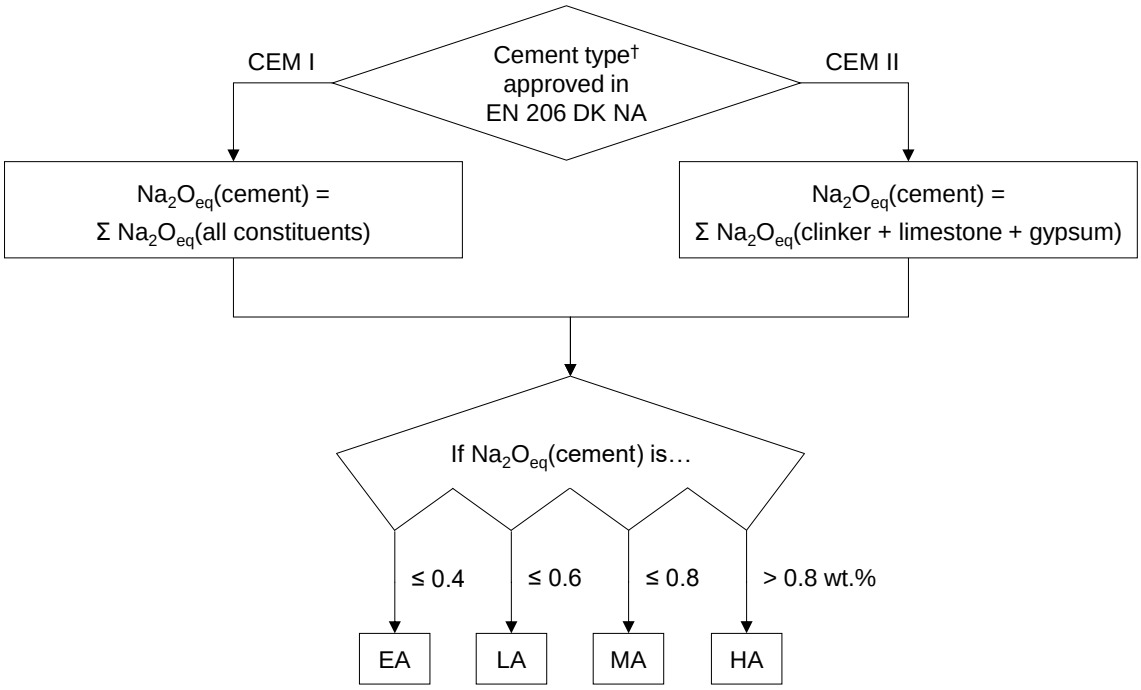


*Figure 6: Danish classification of cements depending on their alkali content, graphical representation of INF 135 [28]. †) CEM I, CEM II/A-L, CEM II/A-LL, CEM II/A-V, CEM II/B-V, CEM II/A-M and CEM II/B-M.*

As provided for in Annex N of EN 206 DK NA [27], a performance approach is possible if a binder does not comply with the rules presented above. This applies to new cement types, new SCMs, and also combinations that do not comply with EN 206 DK NA, e.g. a fly ash content higher than the maximum amount allowed (33 wt.%). In this case, Annex N states that the ASR performance of a binder should be documented with TI-B 51, the Danish mortar bar test [71]. The test should be performed in a comparative way, i.e. the candidate binder must be compared to a reference binder. The reference binder should consist of materials already fulfilling the requirements of the standards, for which there is a well-documented practical experience in Denmark.

The same approach is used to determine whether the alkalis from SCMs should be accounted for in composite cements (INF 135 [28]). Note that Annex N does not give a deemed-to-satisfy criterion regarding the expansion level obtained. The documentation is handed over to the standardisation committee, who is responsible for the final decision.

# 4 Methodology

## 4.1 Overall approach

This project intended to develop generic procedures that can be applied to any material. For this purpose, some SCMs representing the diversity of sources were selected and studied in parallel. The selection was made based on the type of material (natural resource, by-product or waste product), the chemical composition and the relevance in a Danish context.

The experimental plan was designed in a way to start from the effect of SCMs on paste properties and evolve towards their effect on ASR expansion. At the paste level, two main topics were investigated: the free alkali content and the transport properties. Additional method-related studies were added along the project to try to evaluate the accuracy and the representativity of the results.

## 4.2 Material and methods

Two types of PC were used throughout the project: a low alkali PC with 0.58 wt.% $Na_2O_{eq}$ (PC-LA) and a high alkali PC with 1.22 wt.% $Na_2O_{eq}$ (PC-HA). The alkali content of the cement was chosen as a variable because it affects SCM reactivity [72] and alkali metal binding [11]. The eight SCMs shown in Figure 7 were tested: coal fly ash (FA), sewage sludge ash (SSA), crushed brick (CB) glass beads (GB), two biomass ashes (BA1 and BA2) and two calcined clays (CC1 and CC2). A limestone filler (LL) was also used in paste studies as a reference for cement dilution.


*Figure 7: SCMs investigated in the project. A limestone filler was also included in paste experiments, as a reference inert material.*

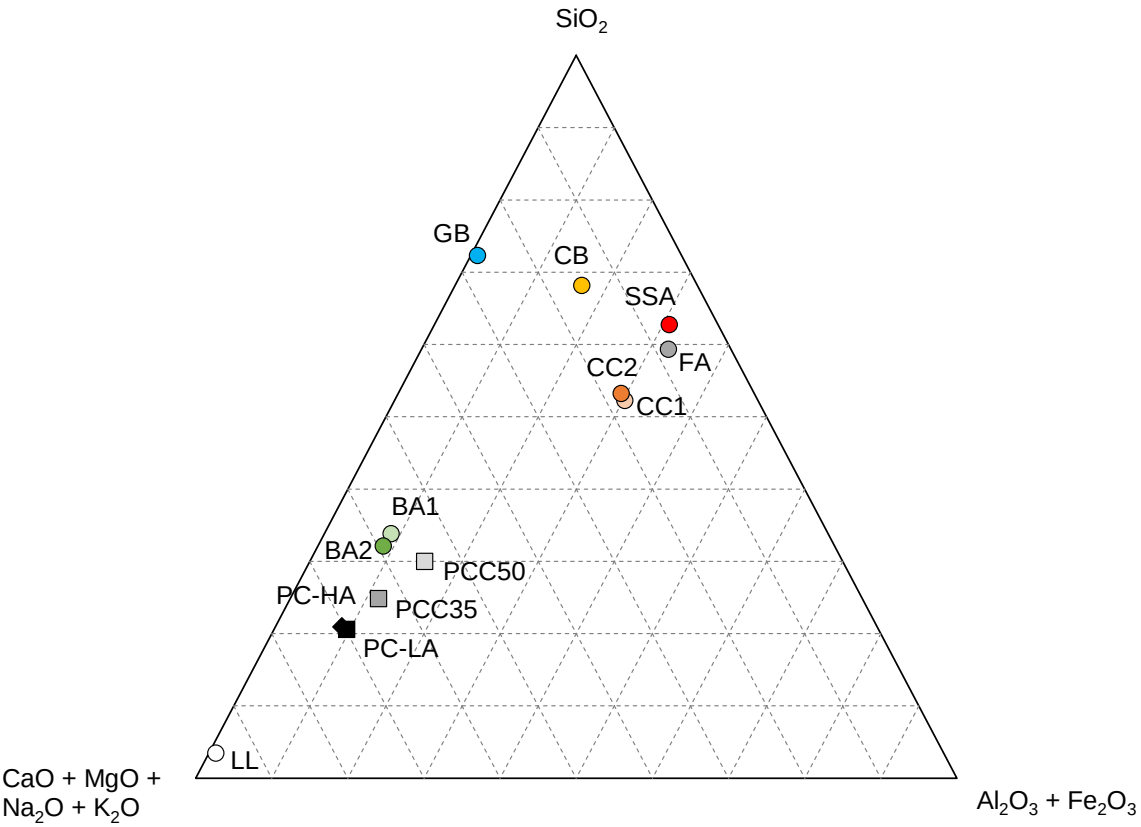


*Figure 8: Chemical composition of the cementitious materials (by mass). CaO, MgO, $Na_2O$ and $K_2O$ are grouped together because alkali and alkaline earth metals play similar roles in amorphous phases of SCMs [72,74].*

In addition, two composite cements containing limestone and calcined clay were tested: a CEM II/B-M (35 wt.% clinker replacement – PCC35) and a CEM II/C-M (50 wt.% clinker replacement – PCC50). The chemical compositions of the materials are presented in a ternary diagram in Figure 8.

For ASR testing, a typical Danish reactive sand from the Øde Hastrup quarry in Roskilde was used in all mixes. This sand contains around 3 wt.% of porous opaline flint and comes from the same geological layer as the one used by Chatterji [73]. The coarse fraction was made of a Danish non-reactive granite from Rønne, Bornholm.

Paste samples were produced by mixing 65 wt.% of PC and 35 wt.% of SCM, with $w/b$ = 0.50. This replacement level was chosen because it corresponds to the maximum clinker substitution level for CEM II in EN 197-1 [75], and it is close to the maximum fly ash content allowed in EN 206 DK NA [27] (33 wt.%). Moreover, it makes more visible the differences between blended cements and plain PC. Unless specifically mentioned, the specimens were sealed cured at 20°C. The phase assemblage was studied with traditional

analytical techniques: Thermogravimetric Analysis (TGA) and Quantitative X-Ray Diffraction (QXRD-Rietveld). Moreover, the samples were investigated with Cold Water Extraction (CWE), bulk electrical conductivity and "mini" chloride migration adapted from NT BUILD 492 [76]. These techniques were chosen because they can be performed with standard equipment available in most concrete laboratories, and thus have the potential to be used at a larger scale. For the same reasons, the reactivity of SCMs was evaluated via the bound water parameter of the $R^3$ method [56].

Regarding ASR testing, three accelerated expansion tests were carried out:

- **ASTM C1567** [36]: the most used method in the literature, and one of the accelerated tests with the shortest exposure duration.
- **TI-B 51** [71]: the only test method prescribed in EN 206 DK NA [27] to document the ASR performance of binders that are not yet included in the Danish standards.
- **RILEM AAR-10** [77]: a concrete performance test aiming to evaluate job mixes. It was also designed to limit leaching by using larger specimens than the traditional CPT. Note that the current procedure lacks documentation with respect to the laboratory/field correlation with porous opaline flint.

*Figure 9: ASR field exposure site at DTU, established in 2017 (GPS coordinates: 55.79103, 12.52619). In total, 90 cubes are currently exposed to test different aspects such as the aggregate type, the binder type or the effect of impregnation.*

| Test | Mix design | Specimen size [mm] | Curing | Exposure conditions | Exposure duration |
|---|---|---|---|---|---|
| ASTM C1567 | Mortar *w/b* = 0.47 | 25 x 25 x 285 | 1 day in water, 80°C | Immersion in 1M NaOH solution at 80°C | 14 days |
| TI-B 51 | Mortar *w/b* = 0.50 | 40 x 40 x 160 | 28 days in water, 20°C | Immersion in saturated NaCl solution at 50°C | 20 weeks |
| AAR-10 | Concrete *w/b* = 0.48 | 100 x 100 x 400 | None | Storage at 100% RH, 38°C | 2 years |
| Field | Concrete *w/b* = 0.50 | 300 x 300 x 300 | 4-5 weeks sealed, 20°C | Outdoor | > 2 years |

*Table 1: Main characteristics of the ASR tests used in the project. Since there is no well-defined procedure for field testing, the exposure duration is only indicative.*

To evaluate the accuracy of the accelerated tests presented above, air-entrained concrete cubes (edge length 300 mm) were cast for field testing. Due to the limited availability of some SCMs, only a subset was included in the field study (coal fly ash, two biomass ashes and one calcined clay). Two series were made, one with PC-LA and one with PC-HA. The cubes were sealed cured at 20°C for 4 to 5 weeks before being placed in an outdoor exposure test area located at DTU, shown in Figure 9. The exposure started in May 2021. A summary of the ASR tests carried out during the project is presented in Table 1.

An overview of the mixes produced during the project is shown in Table 2. Only PC-LA was used for mortar test, to avoid expansion during curing in TI-B 51 [71] and a too fast reaction in ASTM C1567 [36].

| | Paste | ASTM C1567 | TI-B 51 | AAR-10 | Field |
|---|---|---|---|---|---|
| Ref | 🔵🔴 | 🔵 | 🔵 | 🔵🔴 | 🔵🔴 |
| LL | 🔵🔴 | - | - | - | - |
| FA | 🔵🔴 | 🔵 | 🔵 | 🔴 | 🔵🔴 |
| CC1 | 🔵🔴 | - | 🔵 | 🔴 | 🔵🔴 |
| CC2 | 🔵🔴 | 🔵 | 🔵 | 🔴 | - |
| BA1 | 🔵🔴 | 🔵 | 🔵 | 🔵 | 🔵🔴 |
| BA2 | 🔵🔴 | 🔵 | 🔵 | 🔵 | 🔵🔴 |
| SSA | 🔵🔴 | 🔵 | 🔵 | 🔴 | - |
| CB | 🔵🔴 | 🔵 | 🔵 | 🔴 | - |
| GB | 🔵🔴 | 🔵 | 🔵 | 🔵 | - |
| GB_f | 🔵 | - | - | - | - |

*Table 2: Overview of the mixes produced during the project. 🔵: PC-LA. 🔴: PC-HA.*

Based on these results and to limit the experimental matrix, one cement type per SCM was selected for AAR-10 [77]. PC-LA was used with BA1, BA2 and GB to evaluate if these SCMs could trigger the expansion. PC-HA was used with the other to assess their efficacy in preventing expansion. In parallel, field cubes were produced with PC-LA and -HA to evaluate the effect of the PC alkali content in the long term.

## 4.3 Outline of the project

Figure 10 summarises the key steps of the PhD, the main investigation methods and the topics covered by the journal publications. More precisely, the following research questions were investigated in papers I-IV:

**I. How do CWE test parameters affect the accuracy of the calculated concentrations and free contents of alkali metals?**

The paper presents a parametric study about CWE, where the effect of four parameters was studied: the size fraction, the liquid-to-solid ratio, the leaching time and the method to determine the amount of pore solution. A comparison was made with PWE to assess the variability between the two methods.

**II. To what extent does CWE capture the influence of the binder composition on the free alkali metal content of blended cement pastes?**

CWE was used to determine the free alkali content of 18 different binders, containing PC-LA and PC-HA in binary combination with SCMs. The work was complemented by the quantification of clinker hydration, portlandite consumption and $R^3$ bound water to emphasise the link between the pore solution composition and the reactivity of cementitious materials.

**III. How does the binder composition affect the transport properties of paste?**

Transport properties influence the accelerated ASR test, both for the ingress/leaching of alkalis and moisture ingress in CPT tests [63]. The study was based on chloride migration and bulk electrical conductivity measured on paste specimens (testing the same binders as in Paper II).

**IV. Does the free alkali content correlate with ASR expansion?**

The influence of SCMs on ASR expansion was evaluated through different accelerated tests, as well as with field exposure cubes. Results from Papers II and III were used to discuss the outcomes of the expansion tests and link the ASR expansion with the binder properties.

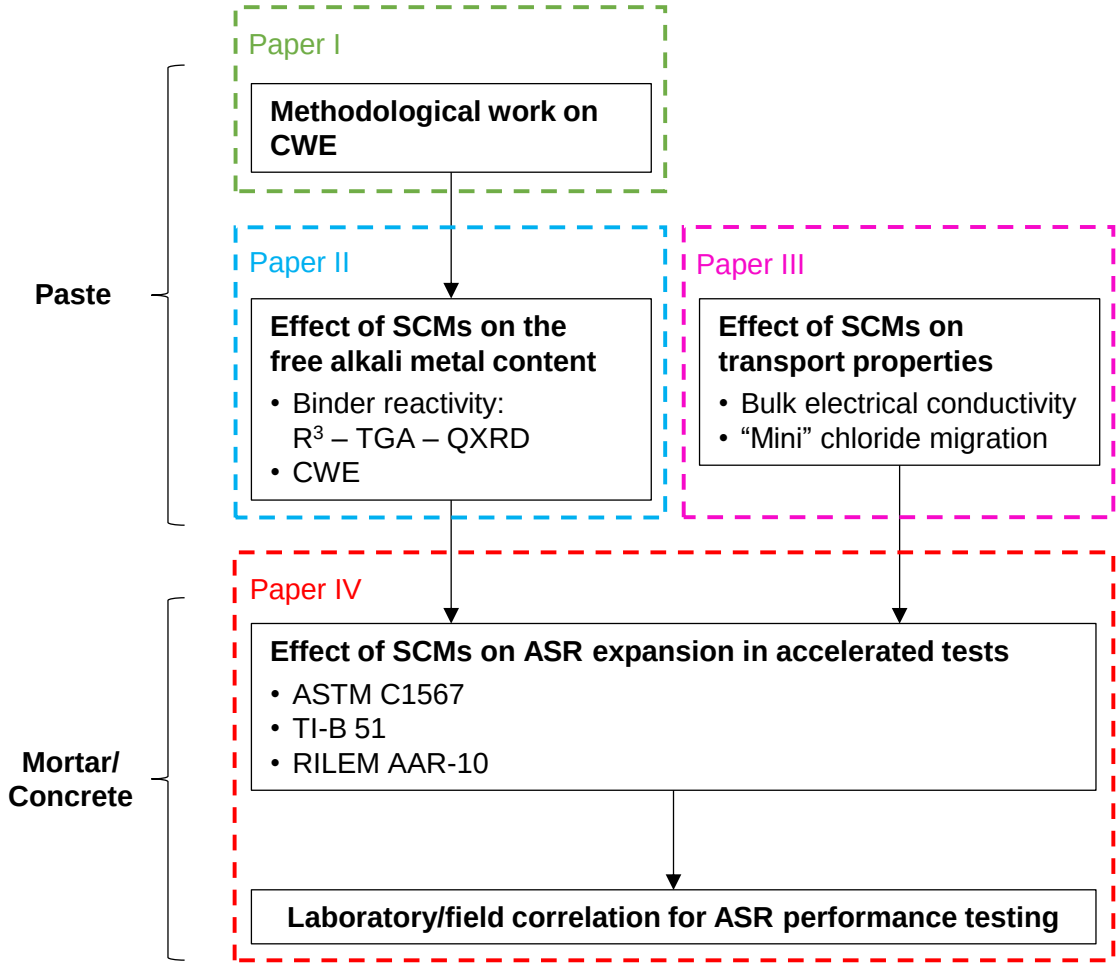


*Figure 10: Outline of the project, illustrating the connexions between the main steps and the investigation methods at different scales: paste, mortar and concrete.*

# 5 Results

This section presents the key results obtained in the project. They follow the same order as the journal papers in appendix, where more details can be found.

## 5.1 Sensitivity of CWE to test parameters

It was first decided to evaluate how CWE results are affected by four test parameters: the size fraction, the liquid-to-solid ratio by mass (L/S), the leaching time and the method to determine the amount of pore solution ($w_{ps}$). Figure 11 displays the calculated concentrations in the pore solution as a function of the size fraction of the crushed material and the leaching time for, 28-day-old paste samples cast with PC-LA. In both cases, the experiments were carried out with a L/S of 1:1, where the solid refers to the crushed paste and the liquid to the leaching water. The results show that a finer size fraction and a longer leaching time lead to higher concentrations, and that the effect is more pronounced for Na than for K. In Paper I, it is also shown that larger concentrations are obtained by increasing the L/S.

Figure 12 presents the results obtained by different drying methods to determine $w_{ps}$, and subsequently the effect on the calculated concentration and free content of Na as determined by CWE. Note that identical relative differences would be obtained for K. The concentration is greatly affected by $w_{ps}$ contrary to the free content, as expected. This is because for the latter, the dilution ratio between the pore solution and the leaching liquid is not as important as it is for the concentration. In this project, all calculations were made with $w_{ps}$ determined by drying with silica gel in a desiccator at 40°C.

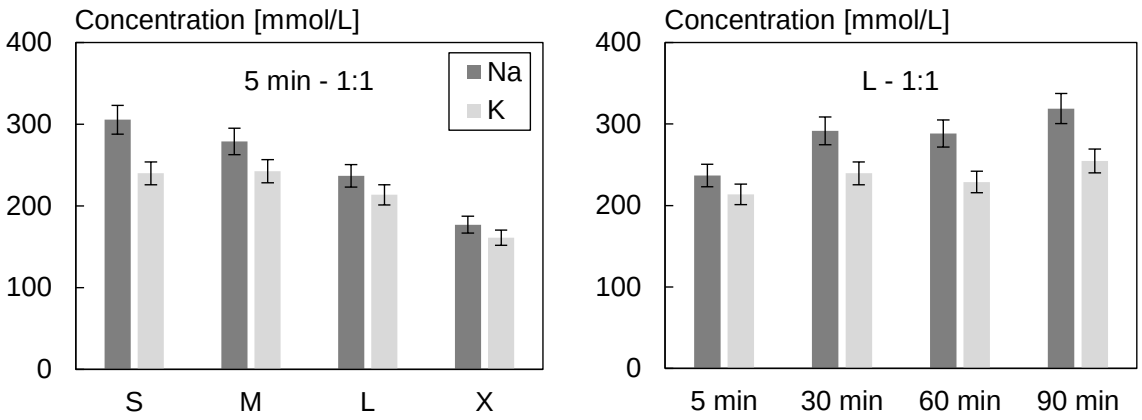


*Figure 11: Na and K concentrations in the pore solution, calculated from CWE results. Left: influence of the size fraction. Right: influence of the leaching time. Liquid-to-solid ratio of 1:1. S: < 0.15 mm, M: 0.15-0.50 mm, L: 0.50-1.00 mm, X: 1.00-2.00 mm. Adapted from Figures 5 and 7 in Paper I.*

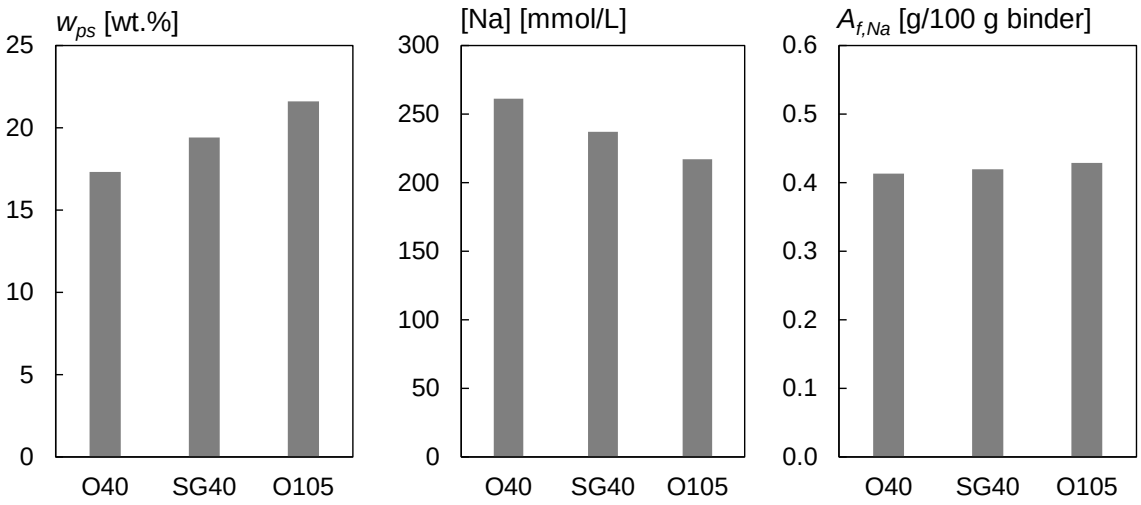


*Figure 12: Influence of the drying method. Left: on the amount of pore solution. Centre: on the Na concentration. Right: on the free Na content. O40: oven-drying at 40°C, SG40: drying with silica gel at 40°C, O105: oven-drying at 105°C. Paste samples cast with PC-LA and cured for 28 days. Adapted from Tables 7, 10 and 14 in Paper I.*

Using a desiccator prevented mass gain due to carbonation, silica gel enabled to dry relatively fast and to reproduce similar RH conditions between the tests, and 40°C prevented the destabilisation of some phases like ettringite.

## 5.2 Comparison between CWE and PWE

As PWE is the reference method to study the composition of the pore solution, it was of interest to compare PWE and CWE results, to detect any discrepancy between the two methods. The results on paste cast with PC-LA, PCC 35 and PCC50, and cured for 28 days at 20°C are shown in Figure 13.

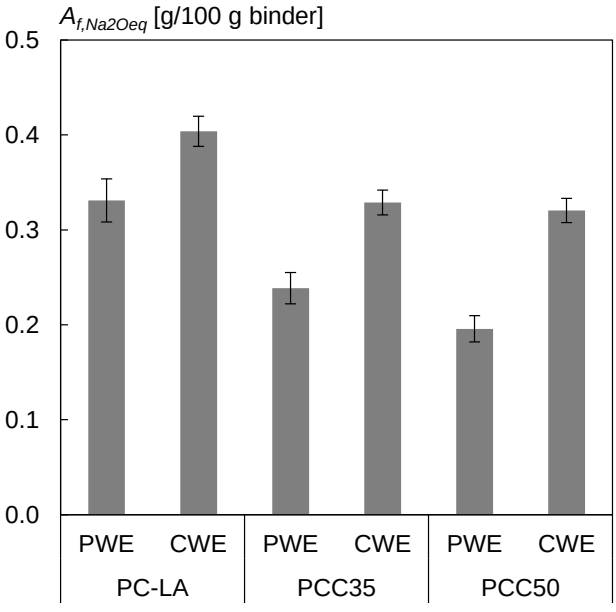


*Figure 13: Free alkali content determined on different cements at 28 days. Comparison between PWE and CWE (0.50-1.00 mm, 5 min leaching, liquid-to-solid ratio of 1:1). Adapted from Figure 1 in Paper VI.*

For these data, CWE was performed on the 0.50-1.00 mm size fraction, with 5 min of leaching and a L/S of 1:1. For all cement types, CWE systematically registers more free alkalis than PWE. The difference is even more pronounced for composite cements, where the clinker content is lower than in CEM I. A comparison in terms of concentrations is shown in Paper I, where similar observations can be made.

## 5.3 Influence of SCMs on free alkalis

SCMs are often characterised by their chemical composition. Its link with the free alkali metal concentration was investigated by using the chemical index proposed by Thomas [18] (already mentioned in Section 3.3). This is illustrated in Figure 14, which shows the total concentration of alkali metals calculated from CWE results on blended pastes. An overall trend is captured, but significant discrepancies are also visible. It is relatively clear that the chemical index has some flaws, as also observed in [53]. For example:

- For limestone (LL), the chemical index predicts an alkali metal concentration almost twice larger than the one measured, due to the large amount of CaO. However, CaO in limestone is present as calcite, which is thermodynamically stable in cement paste (except in the presence of reactive aluminate phases).
- For brick (CB), the opposite trend is predicted due to the $SiO_2$ contribution from brick. However, $SiO_2$ was mainly found as quartz, which does not influence the pore solution alkalinity other than via the dilution effect.

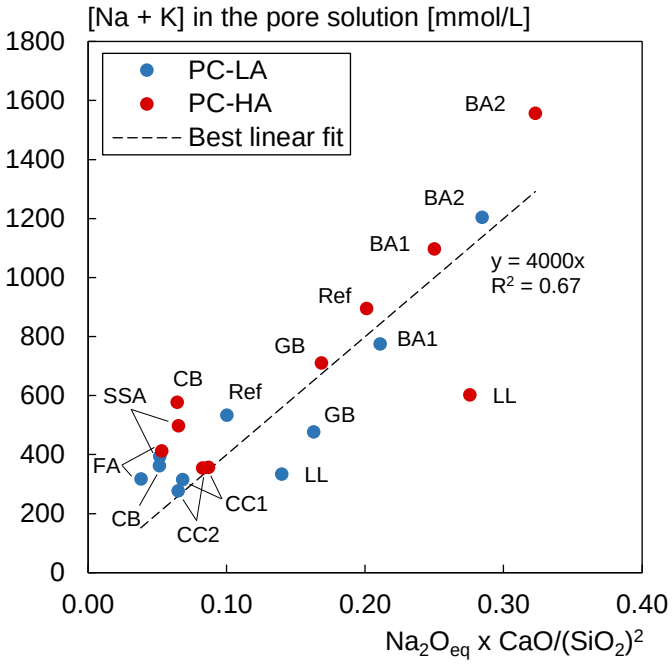


*Figure 14: Total alkali metal concentration in the pore solution at 140 days as a function of the chemical index proposed by Thomas [16]. Adapted from Figure 7 in Paper II.*

This is in line with reactivity measurements performed via the $R^3$ method. Bound water measurements up to 35 days are shown in Figure 15. All materials have more bound water than the inert limestone reference, but the range of values is wide. As expected, FA and CC are the SCMs reacting the most and the fastest. On the opposite, BA and GB reacted the least, even though crushing GB to a finer powder (GB_f) increased its reactivity. Measuring $w_{R3}$ over time also gives an indication of the kinetics. As such, CC2 and SSA experienced a negligible change between 7 and 35 days, while $w_{R3}$ increased significantly for the other materials, in particular FA and CC1.

From an engineering perspective, it may be convenient to isolate the alkali contribution of an SCM, $\alpha_{Na2Oeq}(SCM_i)$. This was calculated according to Equation 2, where the free alkali content determined on the sample with limestone is subtracted from the free content of the sample containing $SCM_i$. The value is then normalised by the total alkali content of $SCM_i$.

$$\alpha_{Na2Oeq}(SCM_i) = \frac{A_{f,Na2Oeq}(PC + SCM_i) - A_{f,Na2Oeq}(PC + LL)}{0.35 \cdot A_{t,Na2Oeq}(SCM_i)} \quad (2)$$

The results are displayed in Figure 16, together with the water-soluble and available alkalis. There are significantly less free alkalis than available alkalis, which is in agreement with [66]. The results also illustrate the possibility of net negative contributions from some SCMs, including fly ash and calcined clays. Moreover, the effect of the PC alkali content is clearly visible, as lower contributions are systematically obtained with PC-HA.

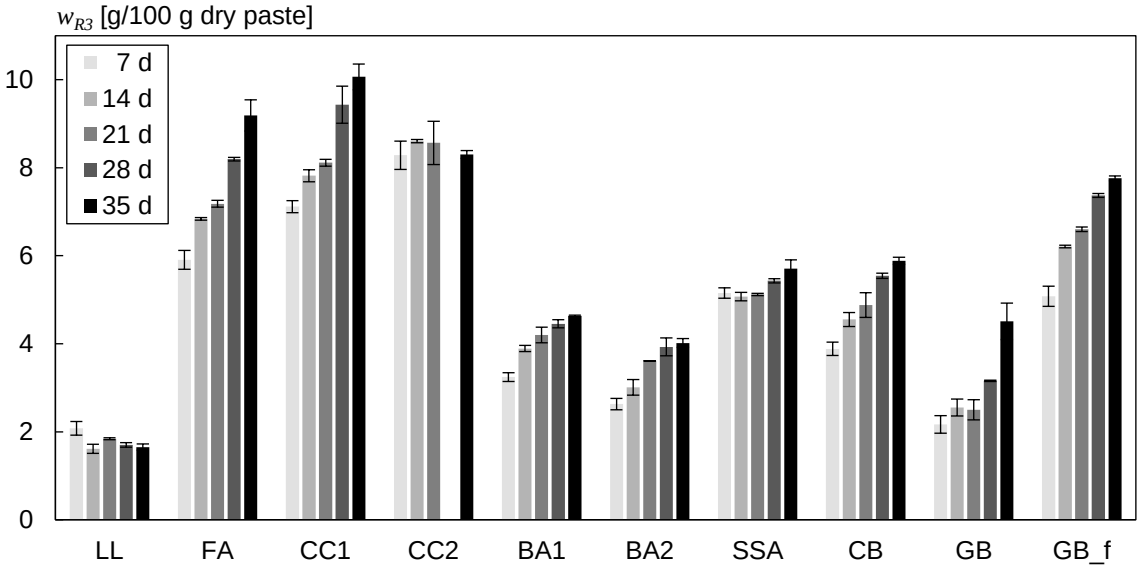


*Figure 15: Reactivity of SCMs from 7 and 35 days, expressed as $R^3$ bound water ($w_{R3}$). Adapted from Figure 4 in Paper II.*

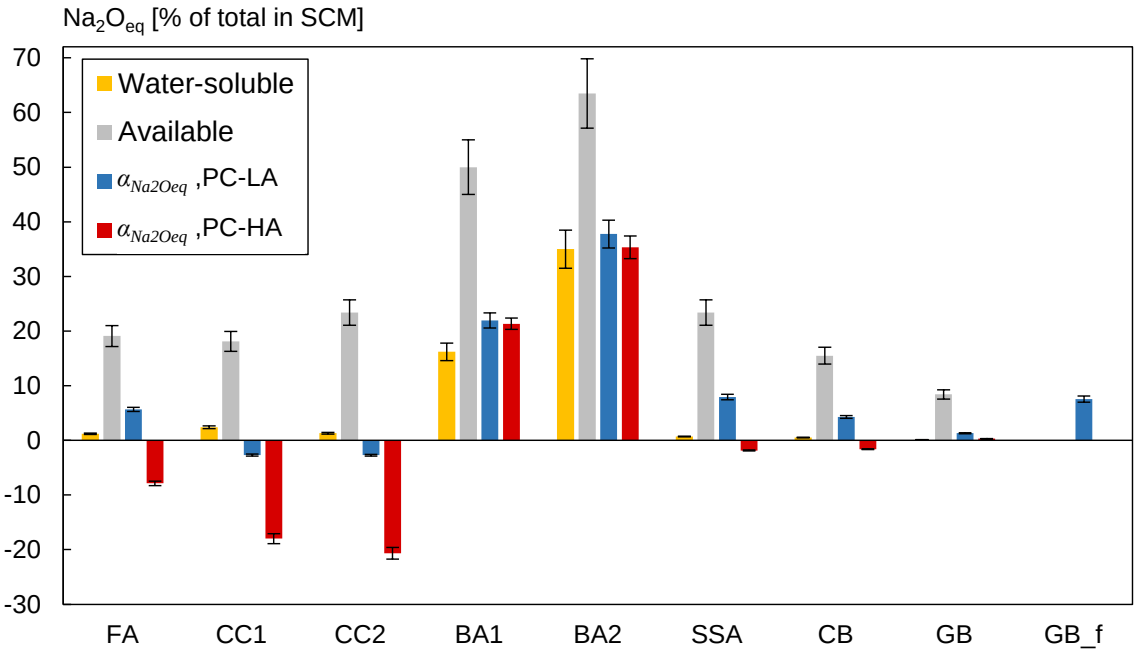


*Figure 16: Comparison between water-soluble alkalis as per ASTM C114 [78], available alkalis as per ASTM C311 [31], and free alkali contributions determined by CWE. Adapted from Figures 2 and 10 in Paper II.*

The SCMs with the highest levels of reactivity are expected to contribute the most to the release or the binding of alkali metals. To investigate this hypothesis, water soluble alkalis must be removed from the calculations, as they are released before the pozzolanic reaction starts. This can be done with Equation (3), which is similar to Equation (2) except that the alkali metals contribution from the SCM (member in brackets) is subtracted from the water-soluble alkali content of the SCM. It was chosen to calculate $\beta$ for both Na and K to show the effect of the type of alkali metal. Moreover, the values are expressed in g/100 g binder to emphasise that chemically speaking, it is alkali metals that are bound, not alkalis.

$$\beta_{Na}(SCM_i) = 0.35 \cdot A_{ws,Na}(SCM_i) - \left(A_{f,Na}(PC + SCM_i) - A_{f,Na}(PC + LL)\right) \quad (3)$$

The values obtained with Equation (3) for the 28 days data are plotted in Figure 17 against $w_{R3}$ at 7 days. A relatively clear trend stems from both graphs: the more reactive the SCM, the more binding, which corresponds to a negative $\beta$. One exception to the trend described above is GB_f, which shows the opposite behaviour. The probable explanation is that the extra binding capacity brought by the pozzolanic C-S-H cannot compensate for the large amount of Na in glass.

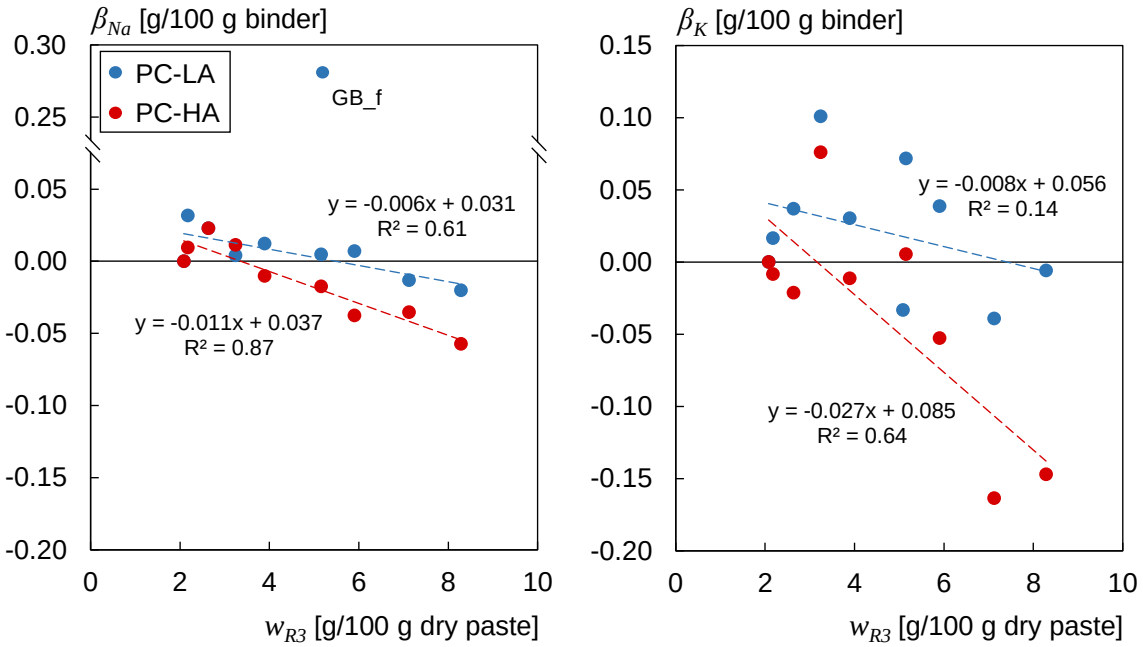


*Figure 17: Net alkali metal release (β) at 28 days as a function of the $R^3$ bound water ($w_{R3}$) at 7 days. Left: Na (GB_f is not included in the trend line). Right: K. Adapted from Figure 11 in Paper II. Details about $R^3$ results are given in Paper VI.*

## 5.4 Influence of SCMs on transport properties

In addition to the free alkali content, it was investigated how SCMs affect the transport properties of blended pastes. Figure 18 (left) displays the non-steady-state chloride migration coefficient $D_{nssm}$ determined on paste samples at 28 days. For all mixes, a lower value is obtained with PC-HA, but the magnitude of the difference depends on the SCM type. Figure 18 (right) demonstrates that the SCMs reacting the most also improve the resistance against chloride transport the most. Interestingly, a linear relationship seems to exist between $w_{R3}$ and the relative difference for $D_{nssm}$, calculated with respect to the plain PC sample. The PC alkali content appears to have a limited influence on the correlation.

The chloride migration test is a relatively simple and fast procedure (approx. 2 days), but it may be possible to obtain a similar outcome with an even simpler test. Figure 19 shows $D_{nssm}$ plotted against the bulk electrical conductivity $\sigma_b$ measured on sealed cured samples. A clear correlation can be observed between the two variables. In Paper II, the same figure was plotted with the bulk conductivity being normalised by the pore solution conductivity, namely the reciprocal of the formation factor. However, this resulted in a poorer correlation, in particular due to the mixes containing biomass ashes.

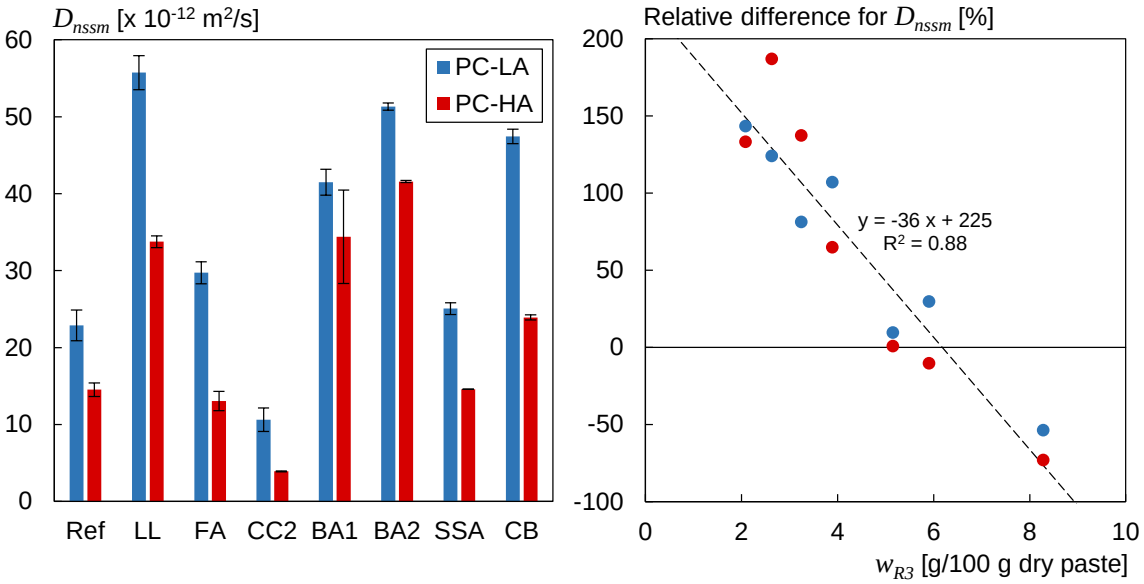


*Figure 18: Non-steady-state chloride migration coefficient ($D_{nssm}$) at 28 days. Left: Influence of the binder type. Right: Relative difference for $D_{nssm}$ (ref.: plain PC) versus $R^3$ bound water ($w_{R3}$) at 7 days. Adapted from Figure 8 in Paper III.*

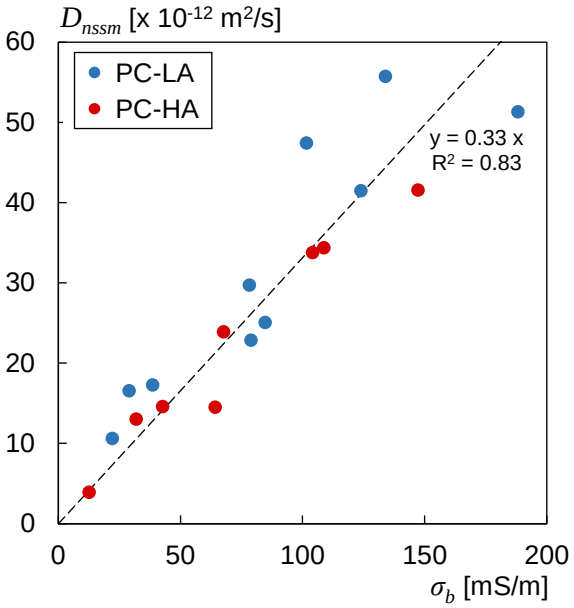


*Figure 19: Non-steady-state chloride migration coefficient ($D_{nssm}$) at 28 days as a function of the bulk electrical conductivity ($\sigma_b$). Adapted from Figure 9 in Paper III*

## 5.5 ASR expansion tests

### 5.5.1 Analysis of published results

Prior to the experimental work, ASR expansion data published in the literature were analysed with artificial neural networks (ANN) to investigate the link between the chemical composition of the binder (input) and the expansion (output). It was chosen to analyse ASTM C1567 [36] results to build a sufficiently large database, even though the validity of the test can be questioned. The results from the analysis are shown in Figure 20, and more detail is given in Paper V.

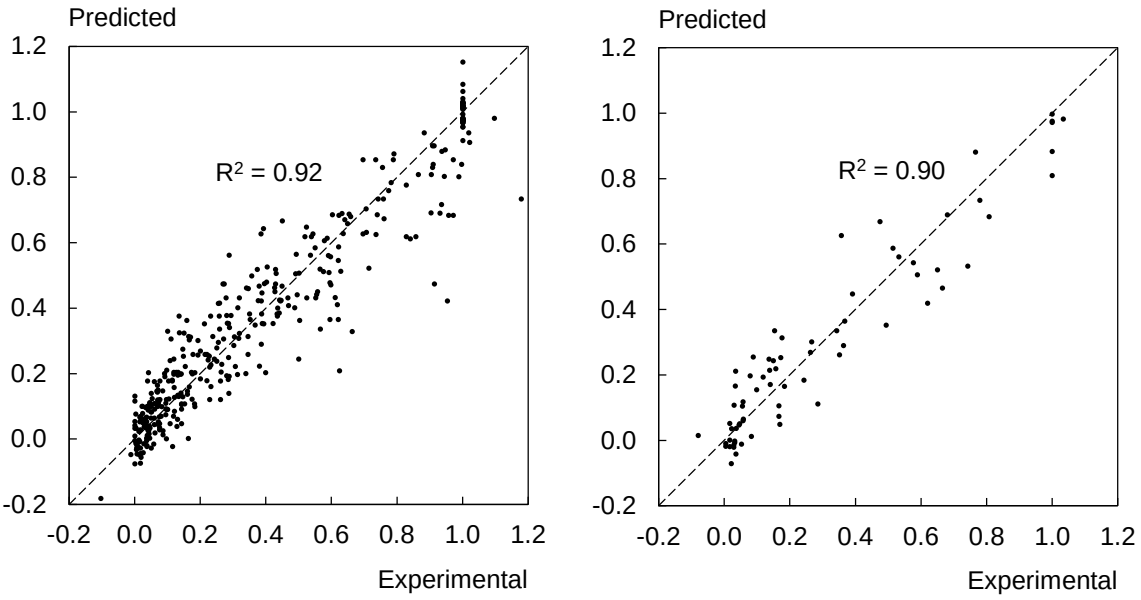


*Figure 20: Artificial neural network analysis. Left: training subset. Right: test subset. The graphs show the normalised expansion, i.e. the expansion of a mortar bar containing SCM divided by the expansion of the corresponding reference bar with plain PC and the same aggregate. Adapted from Figure 5 in Paper V.*

The results show a fairly good accuracy of the ANN prediction, with an $R^2$ equal to 0.92 for the training subset and 0.90 for the test subset. Considering the full dataset, approximately 70% of the data were within 10 percentage points compared to the experimental values. Some attempts were made to try to identify the influence of each input, but no effective method was found.

### 5.5.2 Experimental work

Different ASR expansion tests were performed during the project to evaluate the efficacy of the SCMs. All expansion curves can be found in Paper IV, and a summary of the result is presented in Table 3. The values are given after:

- 14 days for ASTM C1567 [36] (end of the test).
- 8 weeks for TI-B 51 [71] (the measurements were continued up to 20 weeks, but all curves flattened out after 8 weeks).
- 1.5 years for AAR-10 [77] (available data to date, but the measurements will be continued up to 2 years).
- 2 years for field (available data to date).

| Unit: mm/m | | ASTM C1567 (14 days) | TI-B 51 (8 weeks) | AAR-10 (1.5 years) | Field (2 years) |
|---|---|---|---|---|---|
| Acceptance limit | | 1.00 | 1.00 | 0.40 | 0.50 |
| Ref | PC-LA | 3.00 | 5.26 | 0.16 | -0.09 |
| | PC-HA | - | - | 3.05 | 5.61 |
| FA | PC-LA | -0.10 | -0.10 | - | -0.55 |
| | PC-HA | - | - | -0.20 | -0.03 |
| CC1 | PC-LA | - | -0.20 | - | -0.31 |
| | PC-HA | - | - | -0.34 | 1.90† |
| CC2 | PC-LA | 0.00 | -0.17 | - | - |
| | PC-HA | - | - | -0.08 | - |
| BA1 | PC-LA | 2.50 | 6.97 | 2.70 | 4.71 |
| | PC-HA | - | - | - | 3.85 |
| BA2 | PC-LA | 4.96 | 7.27 | 1.83 | 2.53 |
| | PC-HA | - | - | - | 1.78* |
| SSA | PC-LA | 0.04 | 2.27 | - | - |
| | PC-HA | - | - | -0.05 | - |
| CB | PC-LA | 0.85 | 4.21 | - | - |
| | PC-HA | - | - | 0.00 | - |
| GB | PC-LA | 1.65 | 6.20 | 2.03 | - |
| | PC-HA | - | - | - | - |

*Table 3: Summary of expansion test results. ■ : Expansion larger than the reference. ■ : Expansion lower than the reference but higher than the acceptance limit. ■ : Expansion below the acceptance limit. †) 20 wt.% of replacement only. *) With an additional 1.06% of expansion during curing. Adapted from Table 7 in Paper IV.*

From the available data, AAR-10 and field results are in total agreement. The field cube containing CC1 has only 20 wt.%, therefore it is not considered a mismatch. However, several discrepancies can be observed with mortar tests:

- There are two cases where the specimens expanded less than the reference in ASTM C1567 [36] but more in TI-B 51 [71] (BA1 and GB).
- Two cases where no expansion was measured in ASTM C1567 while the specimens did expand in TI-B 51, but less than the reference (SSA and CB).

The expansions measured in the different tests can be compared to the properties measured on paste, namely the free alkali content and the migration coefficient. This is done in Figure 21, where the results are grouped by expansion test.

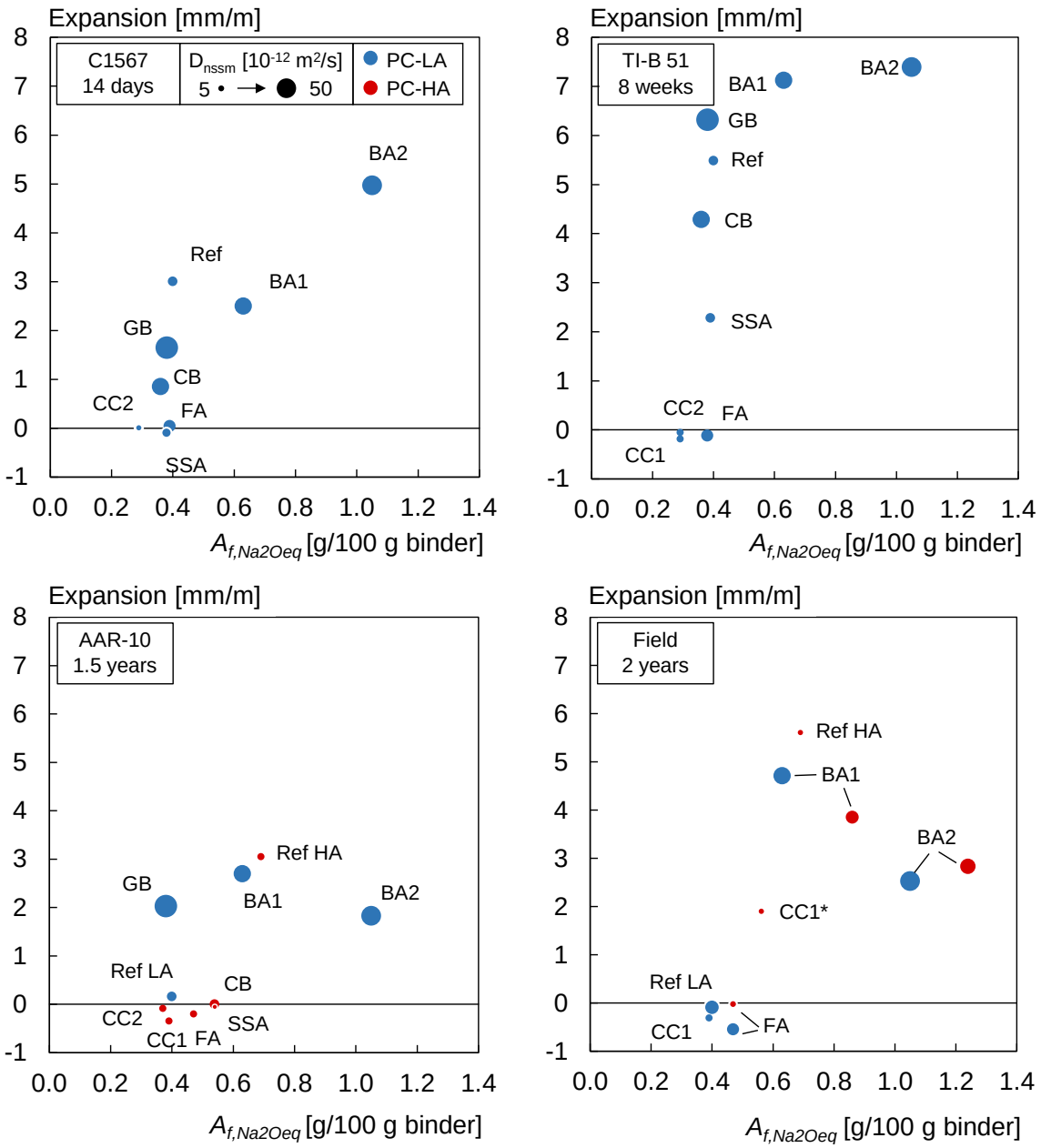


*Figure 21: Expansion in ASR expansion tests as a function of the free alkali content ($A_{f,Na2Oeq}$) determined on paste samples. The marker size represents the non-steady-state chloride migration coefficient ($D_{nssm}$). *) $A_{f,Na2Oeq}$ and $D_{nssm}$ were calculated proportionally to the replacement level (20 wt.% in field cube vs. 35 wt.% in paste specimens). Adapted from Figure 9 in Paper IV.*

For mortar tests, it is difficult to identify a trend. Several mixes have similar free alkali content, and yet very different expansions (Ref, GB, CB, SSA and FA). The differences in transport properties may be an explanation, because the mixes having a larger migration tend to expand more (GB and CB). However, it cannot explain why SSA differs from FA in TI-B 51 [71] or why both are below the reference.

For concrete tests, there seems to be a threshold around 0.5-0.6 wt.% free $Na_2O_{eq}$ below which the specimens do not expand Such threshold would correspond to a free alkali loading around 2.2-2.6 kg/m$^3$. In both AAR-10 [77] and in the field, the influence of transport properties is not clearly visible.

It should be mentioned that glass in AAR-10 is treated as an outlier here. The free alkali content measured at 28 days was relatively low, showing no sign of Na release despite the high content in glass. It is possible that the pozzolanic reaction started at a later age and led to high amounts of Na released, meaning that the free alkali content used in Figure 21 is not representative of the AAR-10 specimens. Another possibility is that since the glass beads are rather coarse ($d_{50}$ = 67 µm), they may act as ASR-reactive particles.

Some photographs of test specimens are presented in Figure 22.

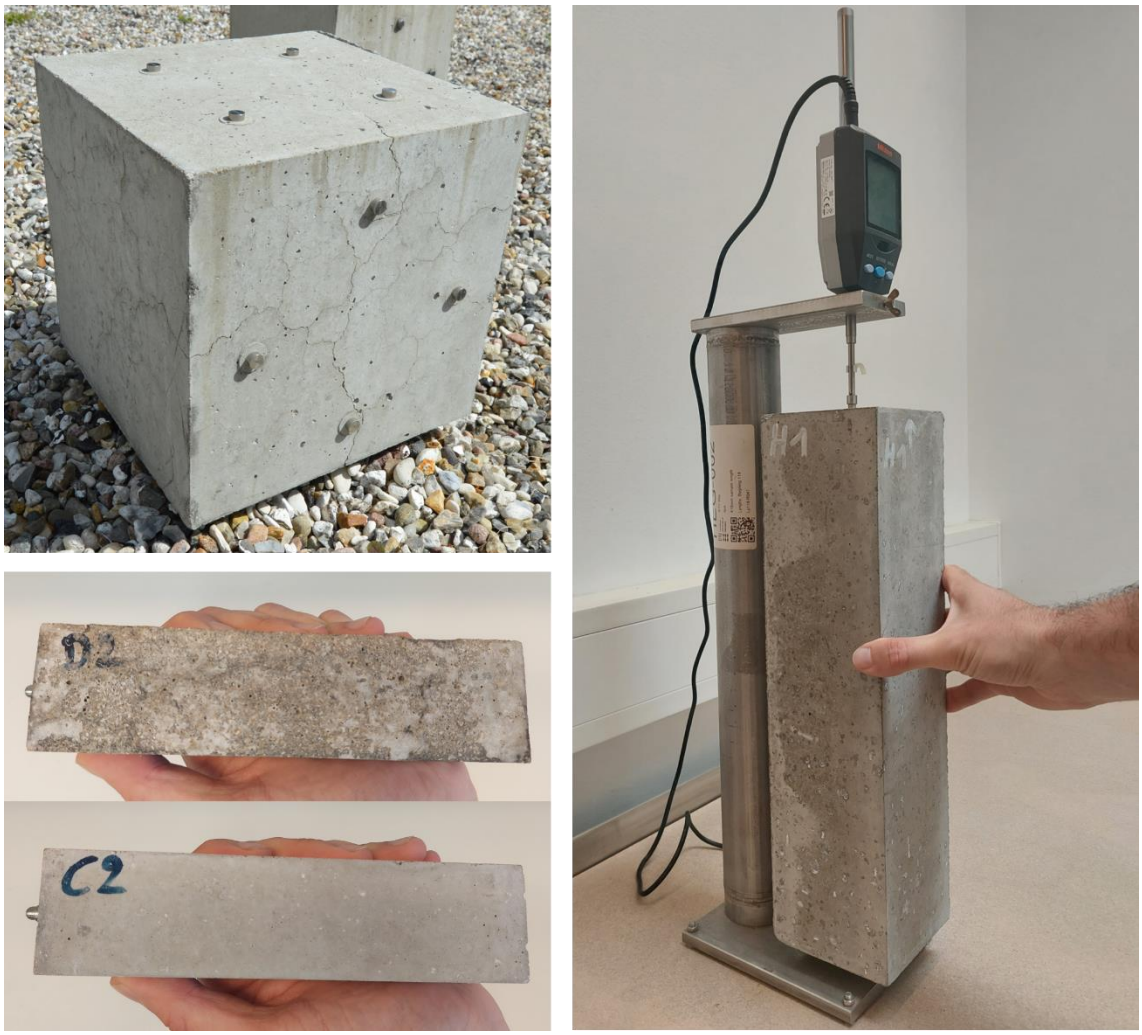


*Figure 22: Photographs of specimens from ASR expansion tests. Top-left: cracked 30 cm field cube with PC-HA. Bottom-left: TI-B 51 mortar bars after 20 weeks of exposure. Right: length measurement of an AAR-10 concrete prism.*

# 6 Discussion

## 6.1 Evaluation of Cold Water Extraction

Before the present PhD project, the literature on Cold Water Extraction mainly focused on mixes containing PC only. To advance knowledge on CWE, the work conducted here was primarily dedicated to blended cements.

The main advantage of CWE is the simplicity of the procedure, since the extraction can be performed with basic laboratory equipment. The only step that necessitates specific training is the chemical analysis of the leachate, but it is a common need for CWE and PWE.

When performing CWE, the thermodynamic equilibrium of the initial system is shifted. The addition of water dilutes the pore solution to a large extent, which in turn destabilises the solid matrix. In particular, portlandite is dissolved, meaning that the concentrations of $Ca^{2+}$ and $OH^-$ are not representative of the initial pore solution [21]. However, the new equilibrium is not reached with the settings used in this project, i.e. 0.50-1.00 mm, 5 min leaching and L/S of 1:1. This is shown in Figure 11, where the calculated concentrations increase for a longer leaching period or a smaller size fraction.

The results presented in Figure 13 seem to indicate that CWE systematically provides higher values than PWE. As discussed in Paper I, this raises the question of the *precision* of extraction methods. PWE is considered to be the reference method, even though some concerns have been raised regarding its *accuracy* [51]. The results obtained during this PhD project give insight on the accuracy of CWE, which is significantly affected by at least two factors:

- The pore solution volume, which influence was confirmed and quantified. It was shown that the calculated concentrations are roughly proportional to the measured pore solution volume.
- The release of alkali metals during leaching, due to the destabilisation of hydration products.

The latter is probably the most problematic aspect of CWE because it is intrinsic to the method, contrary to the determination of the pore solution amount which is performed in parallel. In hardened cement paste, CH acts as a calcium buffer ensuring the stability of C-S-H [79]. If all CH is depleted, C-S-H is destabilised, which may cause the release of some alkali metals initially bound to C-S-H. This is especially relevant for blended pastes

for two reasons: 1) the pozzolanic C-S-H contains more alkali metals due to its lower Ca/Si and 2) the CH buffer is smaller, because portlandite is consumed during the pozzolanic reaction. This may explain why the difference between PWE and CWE increases when the clinker content decreases in Figure 13.

This is a clear drawback of CWE for research applications because concentrations in the pore solution cannot be determined accurately. However, this may not be as problematic for engineering applications. Indeed, regulations are often based on maximum amounts of alkalis (e.g. 3.0 kg/m$^3$ $Na_2O_{eq}$). In this respect, CWE can be used to determine a conservative free alkali content. The next section will discuss how this can be done in practice.

## 6.2 Practical use of the concept of "free alkalis"

The free alkali content seems to be a better indicator of the ASR performance of a binder compared to the total alkali content. As discussed in the previous section, the free alkali content determined by CWE also contains a safety margin, due to the release of alkali metals initially bound. In addition to the CWE "settings" discussed in Paper I, several parameters should be chosen when determining free alkalis. This includes among others the *w/b*, the curing regime and the curing time. Based on the project work, the following comments can be made:

- *w/b* = 0.5 seems to be a convenient compromise between using a high enough value to produce workable paste with most SCMs, but not too high to remain realistic. The differences in the degree of hydration can be dealt with by adjusting the curing conditions. In paper I, it is also shown that secondary hydration during CWE on 28-day-old paste samples has a negligeable effect on the amount of alkali metals measured.
- Sealed curing is a well-defined curing regime and allows to avoid leaching. Paper II mentioned some limitations of curing blended cements pastes at 20°C. Indeed, a long curing period was necessary to register the impact of slowly reacting SCMs like fly ash. Increasing the curing temperature may solve this issue, provided that the phase assemblage is not thermo–dynamically modified. It was recently shown that 38°C leads to similar pore solution compositions as 20°C, contrary to 60°C which induces significant changes due to the destabilisation of sulphate-containing phases [45].
- The choice of the curing time largely depends on the curing temperature. The intention is to obtain a well-hydrated material, where the binder has significantly reacted within the shortest possible time. Regarding maturity, assuming an apparent activation energy of 33.5 kJ/mol, 28 days of curing

at 40°C correspond to 67 days at 20°C (factor of 2.4) [80]. A practical advantage of choosing 40°C is that the $R^3$ method is conducted at this temperature, so the same oven can be used to cure in parallel.

Once these parameters have been selected, the procedure to determine free alkalis slightly differs whether it is intended to evaluate a composite cement or an SCM alone. Both possibilities are detailed in the following.

### 6.2.1 Composite cement

For composite cements, the free alkali content can be directly determined on a paste sample. As shown in Paper II, the concentration and the free alkali content (to a lesser extent) increase when *w/c* decreases. For the concentrations, this is mainly due to the reduced pore solution volume for low *w/c*. The change in free content is probably caused by different degrees of hydration but remains relatively small.

The free content can be used as is, as a characteristic parameter of the cement. For example, using the classification in Figure 6, one could choose to classify a cement as LA if it has a total alkali content ≤ 0.6 wt.% $Na_2O_{eq}$ or a free alkali content determined by CWE ≤ 0.4 wt.% $Na_2O_{eq}$, based on results in Figure 13. However, more statistical data are needed to use an absolute value confidently. By then, a comparative approach seems to be the preferred option.

### 6.2.2 SCM

For SCMs tested as additions, the free alkali contribution requires a reference sample accounting for the dilution of the clinker. For instance, it can be a sample containing limestone with the same replacement level as the investigated SCM. Limestone does not bring additional alkalis but allows to account for the filler effect. A sample with plain PC can also be used, but the degree of hydration of the clinker may be slightly different compared to a blended paste, as shown in Paper II.

The free alkali contribution of an SCM can then be calculated, as shown by Equation (2). This value is convenient to use, because it appears as a scaling factor to be applied to the total alkali content. This is not a new concept, as it is already used in the British and French ASR regulations, e.g. 17% for fly ash, silica fume and metakaolin, and 50% for blast furnace slag [81,82].

The results from Paper II showed that the alkali content of the cement influences the SCM effect. Low-alkali PC seems to give conservative values but may not unveil the full alkali binding potential of some SCMs. Thus, in the perspective of establishing a standardised procedure, the system to be tested

should be specified. Using PC seems to be the most realistic choice, however it affects the reproducibility of the procedure because the composition of PC varies a lot from one production site to another, especially the alkali content. In this respect, an alternative may be to use $Ca(OH)_2$ and extra alkalis instead of PC, as it is done in the $R^3$ method. Such system is simpler than a [PC + SCM] mixture, and better defined chemically. These chemical compounds can be easily specified via chemical grades and are available in most laboratories, which is beneficial for the reproducibility of the method.

### 6.2.3 Limitations

In the present study, several parameters were fixed but may influence the results. For instance, a fixed replacement level of 35 wt.% was used in all blended pastes. It would be relevant to investigate the effect of this level on the free alkali contribution from an SCM ($\alpha_{Na2Oeq}$).

Another critical aspect is the long-term validity of the results. For some SCMs like FA, significant discrepancies were measured between 28 and 140 days. In this case, there seems to be more binding over time, so the value at 28 days is conservative. However, other authors observed the opposite trend with silica fume [66], which is problematic for determining a conservative value.

## 6.3 Effect of SCM on transport properties

The initial intention with the "mini" chloride migration test was to document the changes in transport properties induced by the binder composition, and include this in the analysis of ASR expansion data. Beforehand, bulk conductivity measurements were carried out on the paste specimens used for CWE, but without a specific goal at the time of the experiments. Thus, the idea of Paper III combining chloride migration, SCM reactivity and bulk electrical conductivity results came along during the project.

Theoretically, one expects the migration coefficient to be proportional to the formation factor, defined as the ratio between the bulk conductivity $\sigma_b$ and the pore solution conductivity $\sigma_{ps}$ [83]. However, the results show a proportionality with $\sigma_b$ only. Paper III discusses in more detail the reasons for such discrepancy, which is linked to the specimen conditioning when measuring $\sigma_b$.

Nevertheless, the linear relationships depicted in Figure 18 are particularly interesting, because they link the migration coefficient with an SCM reactivity parameter ($w_{R3}$) and a parameter measured with a non-destructive test ($\sigma_b$). Thus, an indication of transport properties can be obtained at a relatively low cost, which is convenient for screening processes.

## 6.4 Validity of accelerated ASR expansion tests

The results in Table 3 show an agreement between AAR-10 [77] and field cubes for the reference cubes with PC-LA and PC-HA. As illustrated in Paper IV, the kinetics of the expansion were similar in both tests, which is likely a coincidence. Even though a longer exposure time is needed for the cube with PC-LA, AAR-10 seems to be also valid for testing porous opaline flint.

In addition, to date, AAR-10 is the test with the best correlation with field results for cubes containing SCMs. The influence of SCMs is consistent, as well as the effect of the cement alkali content. Results from mortar tests showed some inconsistencies, in particular for alternative SCMs (BA, SSA and CB). Moreover, interpreting the results may be difficult when the specimen expands but less than the reference. In some cases, this seems to indicate that the SCM can indeed prevent or slow down ASR (SSA and CB in TI-B 51 [71]). However, in other cases, it conflicts with AAR-10 and field results (BA1 and GB in ASTM C1567 [36]), where the blended mixes expanded more and faster. Thus, it seems inappropriate to evaluate the suitability of a mix by only comparing it to a reference in mortar tests.

It must be underlined that all the conclusions regarding laboratory/field correlation are drawn after only two years of field exposure. Even though the reactive aggregate used in this project proved to react extremely fast, previous field studies demonstrated that prevention measures may be ineffective over time [68,70]. Therefore, it is important to prolong the field exposure to obtain long-term data and evaluate the validity of accelerated laboratory tests with more certainty.

## 6.5 ASR expansion and free alkali loading

One of the main objectives of the project was to compare the results obtained on paste with ASR expansion data. Regarding the correlation between ASR expansion and the free alkali content, there is a clear difference between mortar and concrete tests:

- No clear trend is visible with mortar tests, where the expansion can be significantly different despite a similar free alkali content. This is not so surprising, because mortar tests are based on an extra alkali supply to the system, which completely overshadows the role of the initial free alkali content. Moreover, the samples are cured in water before exposure, where some free alkalis are leached out. Some results may be explained by transport

properties differences, particularly for TI-B 51 [71]. This topic is currently under investigation, as a follow-up study of the present PhD project.

- On the contrary, there seems to be a threshold in concrete tests below which no expansion occurs, around 2.2-2.6 kg/m$^3$ free $Na_2O_{eq}$. This is consistent with the work done on alkali thresholds for reactive aggregate [84]. Assuming that about 70% of alkalis are free for plain PC mixes, this range matches fairly well with the common limit of 3.0 kg/m$^3$. It should however be mentioned that the term "threshold" solely refers to the expansion, and not on the ASR reaction itself. For example, some ASR products may already exist without building up sufficient internal stresses to damage the concrete.

This analysis was solely based on the free alkali content determined on paste samples at 28 days. However, this may not be representative of the concrete in AAR-10 [77]. For example, the pozzolanic reaction is likely more advanced in AAR-10 after several months of exposure at 40°C, which may affect alkali metal binding/release. Alkali release from aggregate may also cause some divergence, however this was not investigated during the project. Finally, other factors such as the presence of aluminium can influence the ASR process. More details are given in Paper IV.

## 6.6 Screening procedure to select SCMs

A framework to evaluate the suitability of alternative SCMs is given in ASTM C1709 [85]. Five main stages are identified: A) Characterisation of the material, B) Determination of the fineness, C) Testing to specifications for traditional SCMs, D) Concrete performance tests and E) Field trials and long-term performance and durability. Stages A, D and E of ASTM C1709 were largely addressed in the present PhD project, contrary to stages B and C. The reason for not selecting a particular fineness nor comparing it with existing standards for SCMs was the intention to develop a generic approach that applies to all materials. In this respect, dealing with different particle sizes emphasised the precautions to take when drawing conclusions, as shown with the example of glass beads. Moreover, fineness is not the only parameter influencing the performance of an SCM, and other adjustments may be necessary. This could for instance include the addition of limestone or the control of the sulfate balance.

Based on the framework of ASTM C1709, Figure 23 suggests a procedure to screen SCMs with respect to ASR. Each step is detailed in the following.

1. **Material composition (XRF and XRD)**

The chemical composition determined by XRF is probably the most basic test to perform as a starting point. However, SCMs often contain crystalline and amorphous phases, making it difficult to estimate their reactivity potential solely from their chemical composition. Adding a QXRD analysis is therefore valuable to estimate how much of the material may react and determine the chemical composition of the reactive phases. Nevertheless, QXRD is not the most practical analysis for a fast screening of materials, because it requires some data processing that may be complex and time-consuming.

2. **Water-soluble alkalis**

Water-soluble alkalis as determined by ASTM C114 [78] should not be used to estimate the alkali contribution from SCMs. However, they can be used to reject materials which cannot be used as is because they have too high contents of alkalis (e.g. biomass ashes).

3. **Reactivity ($R^3$ test)**

Results from $R^3$ tests can be correlated with changes in compressive strength, alkali metal binding and chloride migration coefficient, as shown in Papers II and III. The test was proven suitable for both traditional and alternative SCMs.

4. **Bulk electrical conductivity**

The bulk electrical conductivity measured on sealed cured samples was found to correlate with the chloride migration coefficient (Paper III), which can document the transport properties of the binder. The method is fully non-destructive, so the test specimens can be used for other measurements. Thus, it is suggested to measure the bulk conductivity on the same specimens as those used to determine the free alkali content.

5. **Free alkali content (CWE)**

This step corresponds to Section 6.2.

6. **For mitigation purposes: ASR performance test**

The results from Paper IV showed that even if there seems to be a threshold for the free alkali loading, there is likely a sensitive area where small variations in the compositions of the materials may tip the scale one way or the other. In absence of substantial experience with a particular aggregate, performance testing seems to be the preferred option. Based on the results presented earlier, it is recommended to use CPTs.

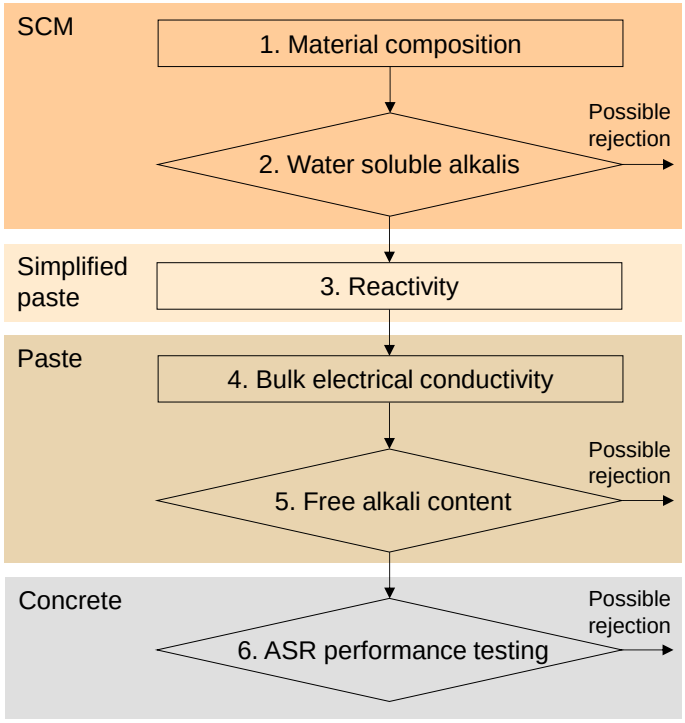


*Figure 23: Suggested procedure to screen and select SCMs with respect to ASR. The side arrows indicate where a rejection is possible. Even though steps 1, 3 and 5 are less directly connect–ed to ASR than steps 2, 5 and 6, they still provide valuable information about the SCM.*

## 6.7 Possible use in Danish regulations

The Danish regulations are essentially prescriptive, as different calculation rules specify how the alkalis should be accounted for (Section 3.5). The key aspect is to determine the contribution of SCMs, both in composite cements and for SCMs alone. The results from the present project have shown that this can be done by determining the free alkali of a mix containing the investigated binder, and comparing it to a reference, e.g. PC with limestone with the same replacement level. The contribution from the SCM can then be calculated as per Equation (2). The value can be used for both the cement alkali classes in INF 135 [28] and the concrete alkali loading in EN 206 DK NA [27].

In Denmark, non-reactive aggregates must be used for the exposure classes related to bridges, i.e. all except X0, XC1 to XC4, XF1 and XA1. This means that in practise, SCMs are not used as preventive measures against ASR. Therefore, the double requirement [non-reactive aggregate + maximum alkali loading] seems conservative enough without further testing. However, specifying a maximum alkali loading may be unsafe if reactive aggregates are used, especially if there is little experience with the selected aggregate and/or SCM. In this case, ASR performance testing will likely be the preferred option to qualify a mix. Once enough data have been collected, prescriptive rules may be established as it is the case in e.g. North America (ASTM C1778 [86] and CSA A23.2-27A [87]).

# 7 Conclusion

This conclusion is divided into two parts. First, some general conclusions dealing with the generic analysis of SCMs will be drawn. Then, the main outcomes of this project will be summarised with respect to the two research questions formulated in Section 1.5. Additional elements, more specific to each topic addressed in the project, can be found in the papers in appendix.

**Q1. How can one determine simply and accurately the free alkali contribution from SCMs?**

- Water soluble alkalis and available alkalis as per ASTM C114 and C311, respectively, are not representative of the alkalis in the pore solution. ASTM C114 can only document the amount of alkalis immediately leached out after mixing, which was negligible for most SCMs except biomass ashes. ASTM C311 overestimates the alkalis in the pore solution, probably due to too forced extraction conditions.
- Cold Water Extraction (CWE) was extensively investigated as an alternative to PWE. Both methods show the same trends for free alkali metals, even though CWE systematically gave higher amounts than PWE. The accuracy of CWE is probably affected by the release of alkali metals initially bound to hydrates, as well as the determination of the amount of pore solution. A procedure was suggested to limit the inaccuracy of CWE.
- Despite some drawbacks, CWE is a simple method to perform, which only requires basic laboratory equipment. CWE enables to determine the free alkali contribution of SCMs, which can then be used to calculate the alkali loading in concrete. For this purpose, CWE is more conservative than PWE.

**Q2. What is the optimum way to test if an SCM can be used to mitigate ASR or poses an ASR risk?**

- The analysis of published AMBT data with artificial intelligence showed a clear link between the chemical composition of an SCM and the AMBT expansion. However, the relationships are not straightforward, and the SCM level needed to prevent expansion could not be predicted with certainty.
- The results from the $R^3$ method were found to correlate with the release of alkali metals and the chloride migration coefficient, for both traditional and alternative materials. As these two aspects are relevant to ASR, performing the $R^3$ method is valuable to screen the effect of SCMs on ASR. Moreover, bound water measurements can be done with a simple oven.

- The different ASR expansion tests conducted in the project, namely ASTM C1567, TI-B 51, RILEM AAR-10 and field exposure showed some discrepancies. Results from mortar tests are difficult to interpret and may be unsafe. On the contrary, a satisfactory correlation was found between AAR-10 and field results, but the tests must be continued to evaluate the correlation in the long term.
- For concrete tests, there seems to be a threshold value below which no expansion occurs, around 2.2 – 2.6 kg/m$^3$ free $Na_2O_{eq}$. This value probably depends on the type of aggregate but is consistent with the common limit of 3.0 kg/m$^3$ for the total alkali content.
- It is recommended to use concrete prism tests or field exposure tests to evaluate the effect of SCMs, and not mortar bar tests. In the latter, the ingress of external compounds affects the pore solution composition. Such ingress depends on the transport properties of the material, which are significantly affected by the type of SCM.

# 8 Future research

The results and the conclusions presented earlier have underlined the need for further research to strengthen the knowledge that has been developed and ensure an effective and safe use of SCMs. The following lists some ideas which seem worthwhile exploring in future work.

## 8.1 Free alkali content

The accuracy and precision of pore solution extraction methods were briefly discussed in the thesis. As mentioned in the conclusion, this thesis addressed the accuracy of CWE. However, the accuracy of PWE has also been questioned in the literature, in particular the type of water released during mechanical extraction. **A more comprehensive comparison between CWE and PWE** would therefore be useful to better quantify their accuracy, and eventually conclude on the abilities of each technique. In addition, there is a need **to limit the release of alkali metals initially bound when performing CWE**, particularly with blended cements.

All the samples used to determine the free alkali content were cured at 20°C, and then tested at 28 and 140 days. For slowly reacting SCMs (e.g. fly ash), little effect was seen at 28 days probably because the pozzolanic reaction had not progressed significantly. One way to overcome this issue would be to **increase the curing temperature** to speed up hydration. Ideally, using a higher temperature should not affect the phase assemblage at equilibrium, but only allow it to reach the equilibrium stage faster.

Paper II showed how the free alkali content could be used to determine the alkali contribution from an SCM. This value is convenient for engineering uses, because it can be easily factored in when calculating the alkali loading of a concrete mix. As mentioned previously, this project did not aim to study specific SCMs; it was intended to develop a generic approach that could be used on any material. However, it could be interesting to **investigate the variability of the alkali contribution for a given type of SCM**, e.g. “fly ashes”, “calcined clays”, “biomass ashes”, etc. This could be helpful in prescriptive requirements, where the coefficients could be given per SCM type. A first step in this direction could be to use existing data published in the literature and make reasonable assumptions for the unknown parameters, in particular the amount of pore solution.

## 8.2 ASR expansion tests

TI-B 51 is a very common test in Denmark for testing local aggregates containing porous flint, and it is also prescribed in the standards to document the ASR performance of new cementitious materials. The relevance of TI-B 51 for the last point was highly questioned in this thesis, because the method strongly overshadows the role of free alkalis. However, there may be some potential in using TI-B 51 to test the specific issue of ASR induced by NaCl ingress. In this respect, as mentioned in Paper IV, **the mechanism by which NaCl triggers ASR needs to be better understood**. Little experimental evidence has been published, but it would be a valuable input before assessing definitively the suitability of the test.

The concrete tests showed that there may be a threshold for the free alkali content, below which no expansion occurs - which does not mean that ASR has not started. It would be relevant to **investigate the threshold behaviour further, particularly with local reactive aggregates that are susceptible to be used** in certain circumstances. One of the main objectives could be to determine with more confidence the threshold value, if any, and compare it with the current limit of 3.0 kg/m$^3$ $Na_2O_{eq}$ for the total alkali loading. This should be done with both plain PC mixes and blended mixes, to assess the validity of the approach for all cementitious binders. Regarding the experimental matrix, one could focus on the sensitive range around the threshold, i.e. a free alkali loading between 2.2 and 2.6 kg/m$^3$ $Na_2O_{eq}$.

Based on the available data, AAR-10 seems to be a promising method to evaluate the performance of blended mixes, even without boosting. However, this assessment only results from the comparison with the two-year expansion in the field. Thus, **field exposure must be continued and monitored for several years** to assess the long-term behaviour of the cubes and the efficiency of the preventive measures tested, mainly low-alkali PC and fly ash.

## 8.3 Data analysis

Many data have been published in the literature over the years. Since ASR is a complex and multi-factorial process, the studies only focus on fewer parameters to limit the experimental matrix. One option to exploit further the existing literature would be to **gather and analyse large datasets of already published data**, where a large amount of data can compensate for the lack of uniformity. For instance, the analysis of AMBT results with ANN done in this thesis could be extended to CPT or field exposure results.

# References


[1] American Concrete Institute, ACI CT-13 ACI Concrete Terminology, 2013.

[2] K.L. Scrivener, J.M. Vanderley, E.M. Gartner, Eco-efficient cements: Potential economically viable solutions for a low-$CO_2$ cement-based materials industry, Cem Concr Res. 114 (2018) 2–26. https://doi.org/10.1016/j.cemconres.2018.03.015.

[3] Global Cement and Concrete Association, Concrete Future - The GCCA 2050 Cement and Concrete Industry Roadmap for Net Zero Concrete, (2021). https://gccassociation.org/concretefuture/wp-content/uploads/2022/10/GCCA-Concrete-Future-Roadmap-Document-AW-2022.pdf (accessed May 19, 2023).

[4] L. Barcelo, J. Kline, G. Walenta, E. Gartner, Cement and carbon emissions, Mater Struct. 47 (2014) 1055–1065. https://doi.org/10.1617/s11527-013-0114-5.

[5] S.A. Miller, A. Horvath, P.J.M. Monteiro, Readily implementable techniques can cut annual $CO_2$ emissions from the production of concrete by over 20%, Environmental Research Letters. 11 (2016) 074029. https://doi.org/10.1088/1748-9326/11/7/074029.

[6] S.A. Miller, Supplementary cementitious materials to mitigate greenhouse gas emissions from concrete: can there be too much of a good thing?, J Clean Prod. 178 (2018) 587–598. https://doi.org/10.1016/j.jclepro.2018.01.008.

[7] M.C.G. Juenger, R. Snellings, S.A. Bernal, Supplementary cementitious materials: New sources, characterization, and performance insights, Cem Concr Res. 122 (2019) 257–273. https://doi.org/10.1016/j.cemconres.2019.05.008.

[8] J. Duchesne, Alternative supplementary cementitious materials for sustainable concrete structures: a review on characterization and properties, Waste Biomass Valorization. 12 (2021) 1219–1236. https://doi.org/10.1007/s12649-020-01068-4.

[9] R.D. Hooton, J.A. Bickley, Design for durability: The key to improving concrete sustainability, Constr Build Mater. 67 (2014) 422–430. https://doi.org/10.1016/j.conbuildmat.2013.12.016.

[10] H.F.W. Taylor, Cement Chemistry, Second Edition, Thomas Telford, 1997.

[11] B. Lothenbach, K. Scrivener, R.D. Hooton, Supplementary cementitious materials, Cem Concr Res. 41 (2011) 1244–1256. https://doi.org/10.1016/j.cemconres.2010.12.001.

[12] A. Vollpracht, B. Lothenbach, R. Snellings, J. Haufe, The pore solution of blended cements: a review, Mater Struct. 49 (2016) 3341–3367. https://doi.org/10.1617/s11527-015-0724-1.

[13] A.B. Poole, Chapter 1 – Introduction, Chemistry and Mechanisms, in: I. Sims, A. Poole (Eds.), Alkali-Aggregate Reaction in Concrete - A World Review, CRC Press, 2017: pp. 1–31.

[14] F. Rajabipour, E. Giannini, C. Dunant, J.H. Ideker, M.D.A. Thomas, Alkali-silica reaction: Current understanding of the reaction mechanisms and the knowledge gaps, Cem Concr Res. 76 (2015) 130–146. https://doi.org/10.1016/j.cemconres.2015.05.024.

[15] P. Nixon, B. Fournier, Chapter 2 – Assessment, Testing and Specification, in: I. Sims, A. Poole (Eds.), Alkali-Aggregate Reaction – A World Review, CRC Press, 2017: pp. 33–61.

[16] G.M. Idorn, Durability of concrete structures in Denmark, PhD Thesis, Technical University of Denmark, 1965.

[17] B. Fournier, M.-A. Bérubé, Alkali-aggregate reaction in concrete: A review of basic concepts and engineering implications, Canadian Journal of Civil Engineering. 27 (2000) 167–191. https://doi.org/https://doi.org/10.1139/l99-072.

[18] M. Thomas, The effect of supplementary cementing materials on alkali-silica reaction: A review, Cem Concr Res. 41 (2011) 1224–1231. https://doi.org/10.1016/j.cemconres.2010.11.003.

[19] J. Duchesne, M.-A. Bérubé, Available alkalies from Supplementary Cementing Materials, ACI Mater J. 91 (1994) 289–299. https://doi.org/10.14359/4335.

[20] M.C. Alonso et al., Development of an accurate pH measurement methodology for the pore fluids of low pH cementitious materials, Stockholm, 2012. https://www.skb.se/publication/2446525/R-12-02.pdf (accessed November 9, 2021).

[21] G. Plusquellec, M.R. Geiker, J. Lindgård, J. Duchesne, B. Fournier, K. De Weerdt, Determination of the pH and the free alkali metal content in the pore solution of concrete: Review and experimental comparison, Cem Concr Res. 96 (2017) 13–26. https://doi.org/10.1016/j.cemconres.2017.03.002.

[22] J. Lindgård, Ö. Andiç-Çakir, I. Fernandes, T.F. Rønning, M.D.A. Thomas, Alkali-silica reactions (ASR): Literature review on parameters influencing laboratory performance testing, Cem Concr Res. 42 (2012) 223–243. https://doi.org/10.1016/j.cemconres.2011.10.004.

[23] M. Thomas, B. Fournier, K. Folliard, J. Ideker, M. Shehata, Test methods for evaluating preventive measures for controlling expansion due to alkali-silica reaction in concrete, Cem Concr Res. 36 (2006) 1842–1856. https://doi.org/10.1016/j.cemconres.2006.01.014.

[24] B. Fournier, J. Lindgård, B.J. Wigum, I. Borchers, Outdoor exposure site testing for preventing Alkali-Aggregate Reactivity in concrete – a review, in: M.G. Alexander, H. Beushausen, F. Dehn, P. Moyo (Eds.), Proceedings of the 5th International Conference on Concrete Repair, Rehabilitation and Retrofitting, MATEC Web of Conferences, Cape Town (South Africa), 2018: p. 03002. https://doi.org/10.1051/matecconf/201819903002.

[25] J. Lindgård, B. Grelk, B.J. Wigum, J. Trägårdh, K. Appelqvist, E. Holt, M. Ferreira, M. Leivo, Chapter 7 – Nordic Europe, in: I. Sims, A. Poole (Eds.), Alkali-Aggregate Reaction in Concrete - A World Review, CRC Press, 2017: pp. 277–320.

[26] European Committee for Standardization, EN 206:2013+A1:2016+A2:2021 - Concrete - Specification, performance, production and conformity, 2021.

[27] Dansk Standard, EN 206 DK NA:2023 - Concrete - Specification, performance, production and conformity - Rules for application of EN 206 in Denmark (in Danish), 2023.

[28] Dansk Standard, INF 135 - Classification of cement - Classification concerning alkali content, sulphate resistance and rules for certification of additional requirements and conformity evaluation (in Danish), 2023.

[29] R.D. Hooton, J.A. Bickley, Prescriptive versus performance approaches for durability design - The end of innocence?, in: Materials and Corrosion, 2012: pp. 1097–1101. https://doi.org/10.1002/maco.201206780.

[30] M.D.A. Thomas, R.D. Hooton, K. Folliard, Chapter 4 – Prevention of Alkali-Silica Reaction, in: I. Sims, A. Poole (Eds.), Alkali-Aggregate Reaction in Concrete - A World Review, CRC Press, 2017: pp. 89–118.

[31] ASTM International, C311/C311M - Sampling and Testing Fly Ash or Natural Pozzolans for Use in Portland-Cement Concrete, 2018.

[32] M.H. Shehata, M.D.A. Thomas, Alkali release characteristics of blended cements, Cem Concr Res. 36 (2006) 1166–1175. https://doi.org/10.1016/j.cemconres.2006.02.015.

[33] R.B. Figueira, R. Sousa, L. Coelho, M. Azenha, J.M. de Almeida, P.A.S. Jorge, C.J.R. Silva, Alkali-silica reaction in concrete: Mechanisms, mitigation and test methods, Constr Build Mater. 222 (2019) 903–931. https://doi.org/10.1016/j.conbuildmat.2019.07.230.

[34] J. Lindgård, P.J. Nixon, I. Borchers, B. Schouenborg, B.J. Wigum, M. Haugen, U. Åkesson, The EU "PARTNER" Project — European standard tests to prevent alkali reactions in aggregates: Final results and recommendations, Cem Concr Res. 40 (2010) 611–635. https://doi.org/10.1016/j.cemconres.2009.09.004.

[35] ASTM International, C1260 - Potential Alkali Reactivity of Aggregates (Mortar-Bar Method), 2014.

[36] ASTM International, C1567 - Determining the Potential Alkali-Silica Reactivity of Combinations of Cementitious Materials and Aggregate (Accelerated Mortar-Bar Method), 2013.

[37] H.F.W. Taylor, A method for predicting alkali ion concentrations in cement pore solutions, Advances in Cement Research. 1 (1987) 5–17. https://doi.org/10.1680/adcr.1987.1.1.5.

[38] A.M. Boddy, R.D. Hooton, M.D.A. Thomas, Effect of product form of silica fume on its ability to control alkali-silica reaction, Cem Concr Res. 30 (2000) 1139–1150. https://doi.org/10.1016/S0008-8846(00)00297-0.

[39] P. Rivard, M.A. Bérubé, J.P. Ollivier, G. Ballivy, Decrease of pore solution alkalinity in concrete tested for alkali-silica reaction, Mater Struct. 40 (2007) 909–921. https://doi.org/10.1617/s11527-006-9191-z.

[40] R. Helmuth, D. Stark, S. Diamond, M. Moranville-Regourd, Alkali-Silica Reactivity: An Overview of Research, SHRP-C-342, Strategic Highway Research Program, National Research Council, Washington, D.C., 1993.

[41] B. Lothenbach, A. Nonat, Calcium silicate hydrates: Solid and liquid phase composition, Cem Concr Res. 78 (2015) 57–70. https://doi.org/10.1016/j.cemconres.2015.03.019.

[42] S.-Y. Hong, F.P. Glasser, Alkali binding in cement pastes: Part I. The C-S-H phase, Cem Concr Res. 29 (1999) 1893–1903. https://doi.org/10.1016/S0008-8846(99)00187-8.

[43] E. L'Hôpital, B. Lothenbach, K. Scrivener, D.A. Kulik, Alkali uptake in calcium alumina silicate hydrate (C-A-S-H), Cem Concr Res. 85 (2016) 122–136. https://doi.org/10.1016/j.cemconres.2016.03.009.

[44] J. Duchesne, M.A. Bérubé, Effect of supplementary cementing materials on the composition of cement hydration products, Advanced Cement Based Materials. 2 (1995) 43–52. https://doi.org/10.1016/1065-7355(95)90024-1.

[45] P. Hemstad, P. Zuschlag, P. Kjellemyr, J. Lindgård, K.O. Kjellsen, T.F. Rønning, H. Justnes, M. Zajac, M. Ben Haha, K. De Weerdt, Alkali metal distribution in composite cement pastes and its relation to accelerated ASR tests, Cem Concr Res. 173 (2023) 107283. https://doi.org/10.1016/j.cemconres.2023.107283.

[46] R.D. Hooton, M.D.A. Thomas, T. Ramlochan, Use of pore solution analysis in design for concrete durability, Advances in Cement Research. 22 (2010) 203–210. https://doi.org/10.1680/adcr.2010.22.4.203.

[47] P. Longuet, L. Burglen, A. Zelwer, The liquid phase of hydrated cement (in French: La phase liquide du ciment hydraté), Revue Des Matériaux de Construction et de Travaux Publics. 676 (1973) 35–41.

[48] R.S. Barneyback, S. Diamond, Expression and analysis of pore fluids from hardened cement pastes and mortars, Cem Concr Res. 11 (1981) 279–285. https://doi.org/https://doi.org/10.1016/0008-8846(81)90069-7.

[49] L. Li, J. Nam, W.H. Hartt, Ex situ leaching measurement of concrete alkalinity, Cem Concr Res. 35 (2005) 277–283. https://doi.org/10.1016/j.cemconres.2004.04.024.

[50] K. De Weerdt, P. Hemstad, H. Justnes, T. Østnor, T.F. Rønning, J. Lindgård, Fundamental study on ASR kinetics – effect of temperature on aggregate reactivity and pore water composition, in: A.L. Batista, A.S. Silva, I. Fernandes, L.O. Santos, J. Custódio, C. Serra (Eds.), Proceedings of the 16th International Conference on Alkali-Aggregate Reaction in Concrete, Volume I, Lisbon, 2021: pp. 837–849.

[51] A. Tuinukuafe, K.S.T. Chopperla, W.J. Weiss, J.H. Ideker, O.B. Isgor, Estimating $Na^+$ and $K^+$ concentrations of the pore solution based on exsitu leaching tests and thermodynamic modeling, RILEM Technical Letters. 7 (2022) 88–97. https://doi.org/10.21809/rilemtechlett.2022.164.

[52] K. De Weerdt, G. Plusquellec, A. Belda Revert, M.R. Geiker, B. Lothenbach, Effect of carbonation on the pore solution of mortar, Cem Concr Res. 118 (2019) 38–56. https://doi.org/10.1016/j.cemconres.2019.02.004.

[53] M. Kasaniya, M.D.A. Thomas, Role of the alkalis of supplementary cementing materials in controlling pore solution chemistry and alkali-silica reaction, Cem Concr Res. 162 (2022). https://doi.org/10.1016/j.cemconres.2022.107007.

[54] F. Avet, R. Snellings, A. Alujas Diaz, M. Ben Haha, K. Scrivener, Development of a new rapid, relevant and reliable ($R^3$) test method to evaluate the pozzolanic reactivity of calcined kaolinitic clays, Cem Concr Res. 85 (2016) 1–11. https://doi.org/10.1016/j.cemconres.2016.02.015.

[55] X. Li et al., Reactivity tests for supplementary cementitious materials: RILEM TC 267-TRM phase 1, Mater Struct. 51 (2018). https://doi.org/10.1617/s11527-018-1269-x.

[56] D. Londono-Zuluaga et al., Report of RILEM TC 267-TRM phase 3: validation of the $R^3$ reactivity test across a wide range of materials, Mater Struct. 55 (2022). https://doi.org/10.1617/s11527-022-01947-3.

[57] V. Sirivivatnanon, P. Thomas, M. Joshua Tapas, T. Nhu Nguyen, Reliability of AMBT and CPT in testing the effectiveness of SCM to mitigate alkali–silica reaction of field concrete, Constr Build Mater. 369 (2023) 130510. https://doi.org/10.1016/j.conbuildmat.2023.130510.

[58] M.-A. Bérubé, J. Duchesne, D. Chouinard, Why the accelerated mortar bar method ASTM C1260 is reliable for evaluating the effectiveness of supplementary cementing materials in suppressing expansion due to alkali-silica reactivity, Cement Concrete and Aggregates. 17 (1995) 26–34. https://doi.org/10.1520/CCA10333J.

[59] M. Thomas, F. Innis, Use of the Accelerated Mortar Bar Test for Evaluating the Efficacy of Mineral Admixtures for Controlling Expansion due to Alkali-Silica Reaction, Cement, Concrete, and Aggregates. 21 (1999) 157–164. https://doi.org/10.1520/CCA10429J.

[60] F. Golmakani, R.D. Hooton, Impact of pore solution concentration on the accelerated mortar bar alkali-silica reactivity test, Cem Concr Res. 121 (2019) 72–80. https://doi.org/10.1016/j.cemconres.2019.02.008.

[61] ASTM International, C1293 - Determination of Length Change of Concrete Due to Alkali- Silica Reaction, 2020.

[62] J. Duchesne, M.-A. Bérubé, Long-term effectiveness of supplementary cementing materials against alkali–silica reaction, Cem Concr Res. 31 (2001) 1057–1063. https://doi.org/10.1016/S0008-8846(01)00538-5.

[63] J. Lindgård, M.D.A. Thomas, E.J. Sellevold, B. Pedersen, Ö. Andiç-Çakir, H. Justnes, T.F. Rønning, Alkali-silica reaction (ASR) - Performance testing: Influence of specimen pre-treatment, exposure conditions and prism size on alkali leaching and prism expansion, Cem Concr Res. 53 (2013) 68–90. https://doi.org/10.1016/j.cemconres.2013.05.017.

[64] K. Yamada, S. Karasuda, S. Ogawa, Y. Sagawa, M. Osako, H. Hamada, M. Isneini, CPT as an evaluation method of concrete mixture for ASR expansion, Constr Build Mater. 64 (2014) 184–191. https://doi.org/10.1016/j.conbuildmat.2014.04.034.

[65] L. Sofia, T. Chappex, K. Scrivener, Impact of storage solution on expansion due to ASR, in: A.L. Batista, A.S. Silva, I. Fernandes, L.O. Santos, J. Custódio, C. Serra (Eds.), Proceedings of the 16th International Conference on Alkali-Aggregate Reaction in Concrete, Volume I, Lisbon, Portugal, 2022: pp. 731–742.

[66] J. Duchesne, M.A. Bérubé, The effectiveness of supplementary cementing materials in suppressing expansion due to ASR: Another look at the reaction mechanisms. Part 2: Pore solution chemistry, Cem Concr Res. 24 (1994) 221–230. https://doi.org/10.1016/0008-8846(94)90047-7.

[67] M. Bagheri, B. Lothenbach, K. Scrivener, The effect of paste composition, aggregate mineralogy and temperature on the pore solution composition and the extent of ASR expansion, Mater Struct. 55 (2022) 192. https://doi.org/10.1617/s11527-022-02015-6.

[68] B. Fournier, R. Chevrier, A. Bilodeau, P.-C. Nkinamubanzi, N. Bouzoubaa, Comparative field and laboratory investigations on the use of supplementary cementing materials (SCMs) to control alkali-silica reaction (ASR) in concrete, in: H. de M. Bernardes, N.P. Hasparyk (Eds.), Proceedings of the 15th International Conference on Alkali-Aggregate Reaction in Concrete, Sao Paulo (Brasil), 2016.

[69] J. Tanesi, T. Drimalas, K.S.T. Chopperla, M. Beyene, J.H. Ideker, H. Kim, L. Montanari, A. Ardani, Divergence between Performance in the Field and Laboratory Test Results for Alkali-Silica Reaction, Transp Res Rec. 2674 (2020) 120–134. https://doi.org/10.1177/0361198120913288.

[70] D. Hooton, B. Fournier, Long-term alkali-silica mitigation of high-alkali concrete with cement replacements, Proceedings of Institution of Civil Engineers: Construction Materials. 175 (2022) 125–136. https://doi.org/10.1680/jcoma.21.00049.

[71] Teknologisk Institut, TI-B 51 - Test method for alkali-silica reactivity of sand (in Danish: Prøvningsmetode Sands alkalikiselreaktivitet), 1985.

[72] J. Skibsted, R. Snellings, Reactivity of supplementary cementitious materials (SCMs) in cement blends, Cem Concr Res. 124 (2019) 105799. https://doi.org/10.1016/j.cemconres.2019.105799.

[73] S. Chatterjee, Z. Fördös, N. Thaulow, Alkali-silica reaction - Danish experience, in: R.N. Swamy (Ed.), The Alkali-Silica Reaction in Concrete, 1991.

[74] R. Snellings, P. Suraneni, J. Skibsted, Future and emerging supplementary cementitious materials, Cem Concr Res. 171 (2023) 107199. https://doi.org/10.1016/j.cemconres.2023.107199.

[75] European Committee for Standardization, EN 197-1 - Cement - Part 1: Composition, specifications and conformity criteria for common cements, 2011.

[76] NT BUILD 492: Concrete, mortar and cement-based repair materials: Chloride migration coefficient from non-steady-state migration experiments, 1999.

[77] T.F. Rønning, B.J. Wigum, J. Lindgård, Recommendation of RILEM TC 258-AAA: RILEM AAR-10: determination of binder combinations for non-reactive mix design using concrete prisms - 38 °C test method, Mater Struct. 54 (2021). https://doi.org/10.1617/s11527-021-01679-w.

[78] ASTM International, C114 - Chemical Analysis of Hydraulic Cement, 2018.

[79] B. Lothenbach, A. Nonat, Calcium silicate hydrates: Solid and liquid phase composition, Cem Concr Res. 78, Part A (2015) 57–70. https://doi.org/10.1016/j.cemconres.2015.03.019.

[80] P.F. Hansen, E.J. Pedersen, Maturity computer for controlled curing and hardening of concrete (in Danish), Nord Betong. 1 (1977) 21–25.

[81] BRE, Digest 330 - Alkali-silica reaction in concrete, 2004.

[82] AFNOR, FD P 18-464: Concrete - Provisions to prevent alkali-aggregate reaction (in French: Béton - Disposition pour prévenir les phénomènes d'alcali-réaction), 2021.

[83] Y. Bu, J. Weiss, The influence of alkali content on the electrical resistivity and transport properties of cementitious materials, Cem Concr Compos. 51 (2014) 49–58. https://doi.org/10.1016/j.cemconcomp.2014.02.008.

[84] R.G. Sibbick, C.L. Page, Threshold alkali contents for expansion of concretes containing British aggregates, Cem Concr Res. 22 (1992) 990–994. https://doi.org/10.1016/0008-8846(92)90123-D.

[85] ASTM International, C1709 - Standard Guide for Evaluation of Alternative Supplementary Cementitious Materials (ASCM) for Use in Concrete, 2018.

[86] ASTM International, C1778 - Reducing the Risk of Deleterious Alkali-Aggregate Reaction in Concrete, 2022.

[87] CSA Group, A23.2-27A - Standard practice to identify degree of alkali-reactivity of aggregates and to identify measures to avoid deleterious expansion in concrete, 2015.

# Appendix

Paper I

# Pore solution alkalinity of cement paste as determined by Cold Water Extraction

Maxime Ranger [a,b], Marianne Tange Hasholt [b], Ricardo Antonio Barbosa [c]

[a] Department of Environmental and Resource Engineering,
Technical University of Denmark (DTU), 2800 Kgs. Lyngby, Denmark

[b] Danish Road Directorate, 1577 Copenhagen V, Denmark

[c] Danish Technological Institute, 2630 Taastrup, Denmark

*Published in CEMENT (2023), Volume 11, p. 100055*
*DOI: 10.1016/j.cement.2023.100055 – Licence CC BY 4.0*

# Abstract

Cold Water Extraction (CWE) is a technique used to extract the pore solution of cementitious materials and to study its alkalinity. CWE can be used on paste, mortar or concrete, and requires only standard laboratory equipment. The method is not yet standardised, so several parameters must be arbitrarily selected when conducting the test.

This work investigated the influence of four parameters on the calculated alkali metal concentrations in the pore solution: the method for determining the amount of pore solution (oven-drying at 40 and 105°C, desiccator with silica gel and solvent exchange), the size fraction of the powdered material, the leaching duration and the liquid-to-solid ratio. A comparison with values obtained by Pore Water Extraction (PWE) on two cement types emphasises and quantifies the crucial impact of the amount of pore solution on CWE results. The results suggest that some bound alkali metals may be released during CWE. A mechanism is proposed, and recommendations are made to limit any effect of this on CWE results.

# Keywords

Alkalis, Pore Solution, Cement Paste, Blended Cement, Drying

# 1 Introduction

The nature of the pore solution of concrete determines a large number of durability issues. In particular, its alkalinity has a large effect on the alkali-silica reaction (ASR) and on steel corrosion in the case of reinforced concrete. Several studies have shown that the electroneutrality of the pore solution can be accurately described by considering only $OH^-$, $Na^+$ and $K^+$ ions [1–3], which implies that the pH value is mainly affected by the alkali metal concentrations. Different methods have been developed to measure the pH or the free alkali metal content of concrete, as summarised by Alonso et al. [4] and Plusquellec et al. [5].

Pore Water Extraction (PWE) as introduced by Longuet et al. [6] is often recommended as the preferred method and it is used as a reference to evaluate other procedures [7,8]. PWE requires special equipment to squeeze out the pore solution from a hardened specimen. This is done by compressing a sample (crushed or not) unilaterally, the other sides of the sample being restrained in a metal die. The magnitude of the maximum pressure applied has raised some concerns, some authors reporting an effect on the alkali metal concentration of the

extracted solution (200-1000 MPa in [9], 230-800 MPa in [10]). However, there is still no consensus on this question as other researchers concluded that there was no significant influence of the extraction pressure (200-560 MPa in [11], 500-1000 MPa in [12], 120-330 MPa in [13], 600-985 MPa in [14]). One possible explanation to the contradictory conclusions is the narrower pressure ranges used in [11–14] compared to [9,10]. Although PWE has been successfully used for many applications, it has proven to be relatively inefficient for materials with a low free water content, i.e. old samples or specimens with a low w/c (water-to-cement ratio by weight) [5,15]. Moreover, the main limitation of PWE remains the cost of the setup and therefore its availability [4].

The so-called Cold Water Extraction (CWE) is an alternative to PWE, and requires only basic equipment. CWE is an *ex situ* leaching method [4,5], where the sample is crushed, mixed with an extraction liquid, and filtered after a leaching period. As CWE includes more steps than PWE, the method is affected by more test parameters [4]. The influence of some of these parameters, such as the size fraction of the crushed particles, the liquid-to-solid ratio (L/S), the leaching time and the pH of the extracted solution were studied by e.g. Pavlík [16], Räsänen and Penttala [17], Li et al. [8], Loh et al. [18], and Wang et al. [19]. However, as pointed out by Plusquellec et al. [5], the pH value determined by direct measurement or hydroxide ion titration in the extracted solution is not representative of the pH of the pore solution. This is due to portlandite dissolution in water, which releases $OH^-$ ions. The pH of the extracted solution is therefore mainly influenced by the solubility of portlandite, and not by the original hydroxide ion concentration in the pore solution [9,20]. Only Li et al. [8] applied a correction based on the stoichiometric release of $OH^-$ and $Ca^{2+}$ from portlandite, to obtain realistic estimates of the concentration in the pore solution.

Other extraction techniques include *in-situ* leaching, variations of CWE (hot water extraction and “Espresso” method), or non-destructive methods (embedded potentiometric electrodes and fibre optic sensors) [4]. However, to date there is no standard method for determining the composition of the pore solution of hardened cementitious materials. All methods have advantages and limitations, and it is crucial to identify the critical parameters for each method, and to quantify their influence on the composition of the extracted solution [7]. In addition, the reliability of the methods with different binder types must be investigated. As an example, De Weerdt et al. [21] extracted the pore solution of mortar samples cast with a Portland cement, blended or not with fly ash. While all CWE results were overestimated compared to PWE, the differences (relative and absolute) varied

depending on the binder. In addition, the discrepancies increased even more when the curing temperature was increased.

The aim of the present work was to capture the sensitivity of the registered composition of the solution extracted by CWE to different parameters and discuss the accuracy of CWE results. In particular, the study focused on different drying methods to determine the amount of pore solution in hardened paste before extraction, and subsequently their influence on the results. In addition, the experimental matrix included test parameters such as size fraction, leaching duration, and liquid-to-solid ratio. Two cement types, a Portland cement and a Portland-composite cement (CEM I and CEM II/B-M according to EN 197-1, respectively) were used in a comparative study between CWE and PWE, in order to identify the possibilities and limitations of CWE when studying blended cements. It is important to mention that this study dealt with the accuracy of CWE, but did not address the precision of extraction methods, i.e. how to reconcile CWE and PWE results.

# 2 Background

To obtain an accurate estimation of the alkalinity of the pore solution by means of CWE, the method should fulfil three conditions:

(a) *Dilution of the pore solution.* The dissolved substances initially contained in the pore solution should be uniformly distributed in a larger liquid volume, which can easily be sampled. This is done either by intermixing the pore solution and the extraction liquid, or by transporting the dissolved substances.
(b) *No release of bound alkali metals* (from the hardened matrix or the unhydrated particles) *and no precipitation.*
(c) *Accurate estimation of the amount of pore solution*

As stated in the introduction, CWE does not give direct access to the original hydroxide ion concentration due to the dissolution of portlandite. Thus, it must be emphasised that studying the pore solution alkalinity with CWE is done indirectly through alkali metals (Na and K), which concentration is known to correlate well with that of $OH^-$ [1–3].

This section first describes the different mineral forms of alkali metals in Portland cement. Then, attention is drawn to the initial equilibrium that exists between the pore solution and the solid matrix before CWE has been performed. Finally, some relevant parameters of CWE are reviewed and referred to the three bullet points listed above.

## 2.1 Alkali metals in Portland cement

Alkali metals can essentially be found in two forms in Portland cement: either in sulphate phases, or in silicates and aluminates. The amount of alkali metals in sulphates is proportional to the ratio between $SO_3$ and $Na_2O + K_2O$, until a ratio around 1 above which 90% of $K_2O$ and 45% of $Na_2O$ are assumed to be in sulphates [22]. The remaining alkali metals are then distributed between the main clinker phases. The modified Bogue calculation proposed by Taylor allows to make this distribution [23]. Due to the high solubility of sulfate phases, alkali metals contained in these phases will be rapidly dissolved when water is added. On the contrary, the release of alkali metals from silicates and aluminates depends on the degree of hydration of the clinker.

## 2.2 Initial equilibrium: free and adsorbed alkali metals

In hardened paste, an equilibrium must always be maintained between the surface charge of C-S-H (negative) and the charge in the Electrical Double Layer (EDL) [24,25]. According to the Stern model, the EDL is made of a compact layer and a diffuse layer [26]. The thickness of the EDL, also referred to as Debye length, increases when the temperature increases or when the ionic strength of the pore solution decreases [27]. The charge compensation in the EDL is ensured by bound cations in competition with each other: $Ca^{2+}$, $Na^+$ and $K^+$. The proportion of each ion in the EDL is driven by the equilibrium between the C-S-H and the pore solution. Lothenbach and Nonat [25] summarised several studies dealing with alkali uptake in C-S-H, in particular the link with the Ca/Si of C-S-H. A high calcium concentration in the pore solution implies 1) a high Ca/Si due to thermodynamic equilibrium and 2) less alkali metal binding due to the preference for bivalent ions ($Ca^{2+}$) compared to monovalent ions ($Na^+$ or $K^+$) in the EDL. This is illustrated in Figure 1, which shows the alkali binding capacity of C-S-H as a function of the Ca/Si, calculated from the data published by Hong and Glasser [28] and L'Hôpital et al. [29]. The results also indicate that higher alkali concentrations in the pore solution enhance alkali metals uptake. The data were obtained by equilibrating synthetic C-S-H in alkaline solutions (KOH or NaOH) of different concentrations and sampling the solutions to determine the remaining alkali metal ions. It should be mentioned that the solution-to-solid ratio was significantly different between the two studies (15 in Hong and Glasser [28], 45 in L'Hôpital et al. [29]), and that C-A-S-H was used in [29]. However, the presence of aluminium was shown not to modify the alkali metal binding capacity of the gel [29].

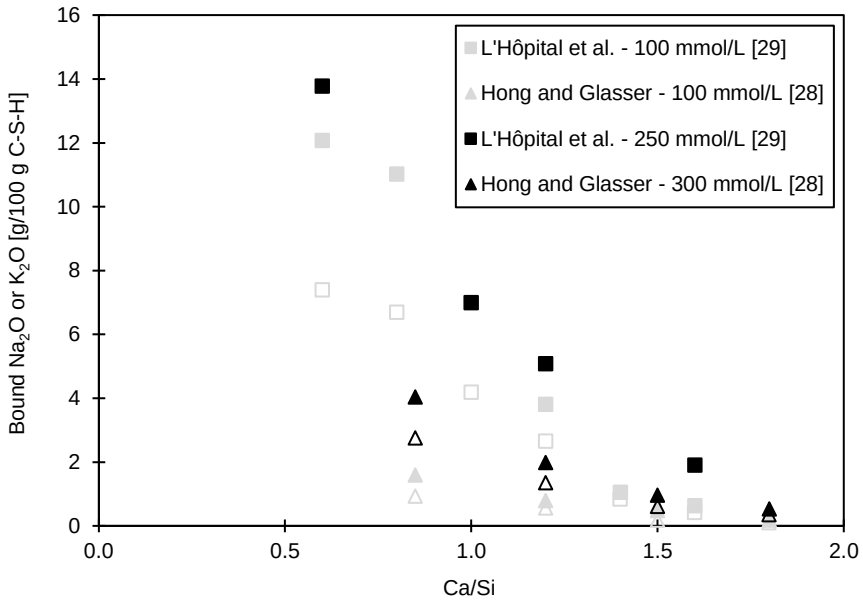


*Figure 1: Alkali binding capacity of C-S-H calculated from the data published by Hong and Glasser [28] and L'Hôpital et al. [29]. The concentration of the alkaline solution used for equilibrating the C-S-H is indicated in the legend. Plain markers = $K_2O$, empty markers = $Na_2O$.*

As mentioned in a discussion by Duchesne and Bérubé [30], a classical approach to this is to consider the equilibrium of each pair of competing ions in the EDL [31]: sodium–calcium and sodium–potassium, respectively, as shown in Equations (1a) and (1b).

$$2(Na^+)_b + (Ca)_{dl} = 2(Na)_{dl} + (Ca^{2+})_b \quad (1a)$$

$$(Na^+)_b + (K)_{dl} = (Na)_{dl} + (K^+)_b \quad (1b)$$

where the subscripts *b* and *dl* refer to the bulk solution (pore solution) and the double layer, respectively.

These two equilibria imply that the release of adsorbed alkali metals in the pore solution must be achieved by cation exchange, which is driven by the different concentrations and the surface charge. Finally, it must be recognised that a classification where alkali metals are either free or bound is a simplification, since there is a continuous transition from one to the other [32].

## 2.3 Relevant parameters when studying the pore solution composition with CWE

Bullet points (a) and (b) presented earlier in this section are related to chemical processes occurring during CWE and may be influenced by the test parameters. However, the determination of the amount of pore solution (c) is not part of CWE per se, but can affect the results. The following summarises the related theory and the existing literature on these aspects.

### 2.3.1 Particle size and leaching duration

CWE is based on leaching, which disturbs the equilibrium described in Section 2.2. The pore solution is diluted into the leaching liquid, which decreases the alkali metals concentrations. In parallel, depending on the leaching liquid, the calcium concentration may be increased by hydrate dissolution, in particular portlandite. During leaching, the system thus evolves towards a new stable state. However, this equilibrium may not be reached, so the kinetics of the reaction may influence the CWE results. In this respect, Levenspiel [33] describes two main rate-controlling processes for leaching: a chemical process that occurs at the surface of the particles, and a physical process based on diffusion from the unreacted part of the particles to the fluid.

For either of the mechanisms mentioned above, finer particles (larger specific surface) and longer leaching (higher degree of reaction) will favour the dilution of alkali metals (a) and increase their concentrations in the leachate. On the other hand, for the same reasons, they also favour secondary hydration [5] and thus potentially the release of extra alkali metals (b). Taking both aspects into consideration, the combination of a particle size below 80 µm and a leaching time of 5 min has been proposed in previous studies [4,5]. However, De Weerdt et al. [34] reported an overestimation of the alkali metals concentrations obtained with CWE compared to those predicted by thermodynamic modelling, which might be due to the release of loosely adsorbed alkali metals during CWE (particle size < 80 µm; L/S = 1; 5 min stirring).

### 2.3.2 Type of liquid

Plusquellec et al. [5] compared the effect of deionised water with three types of alcohol (methanol, ethanol and isopropanol) on the concentrations of alkali metals. Although alcohols seem to be promising candidates, as they both prevent further hydration during leaching and dissolution of hydrates (b), the alkalinity of the extracted solution is decreased compared to when water is used. The authors suggest that this is due to the molecular size of the alcohols. The alcohol molecules

are larger than water molecules, and therefore they cannot enter the small pores and extract alkali metals (a).

Castellote et al. [35] investigated three different leaching solutions: water (deionised and decarbonated), NaOH solution (0.3 mol/L), and saturated $Ca(OH)_2$ solution. Unlike water, the two alkaline solutions have pH values in the same range as the pore solution. However, if the pH of the extraction solution is higher than that of the pore solution, precipitation may occur. As a consequence, to ensure dissolution (a) and prevent precipitation (b), these authors recommend the use of water.

### 2.3.3 Liquid-to-solid ratio

The liquid-to-solid ratio (L/S) is a critical parameter for calculating the dilution factor between the pore solution and the extraction liquid (a). A correction must therefore be applied to the concentrations measured in the extracted solution, to be able to correctly estimate the pore solution concentration. The results obtained by Li et al. [8] show that the $OH^-$ concentration in the pore solution of a concrete with low-alkali cement ($Na_2O_{eq}$ = 0.36 wt.%) and w/c = 0.5 is not significantly affected by the L/S. However, when using concrete with a high-alkali cement ($Na_2O_{eq}$ = 0.97 wt.%) and w/c = 0.37, increasing the L/S does increase the calculated $OH^-$ concentration of the pore solution. The authors attribute the effect to hydration of unreacted cement particles, which releases alkali metals into the extracted solution. They suggest using L/S = 1 to obtain a sufficient amount of solution while limiting further hydration (b), a value that has also been used or recommended in other studies [4,5].

In addition to secondary hydration, a higher L/S further disturbs the equilibrium between the bulk solution and the solid matrix [5], by leading to a larger dilution of alkali metals and thus an increased dissolution of portlandite as the common ion effect decreases. This leads to larger concentration gradients, and therefore enhanced diffusion towards the extraction solution.

### 2.3.4 Amount of pore solution

The second parameter affecting the dilution factor in CWE is the volume of the pore solution in the sample (c), which must be determined in parallel of the leaching protocol. Plusquellec et al. [5] measured this value by oven-drying at 105°C and thermogravimetric analysis (TGA). They concluded that oven-drying was the preferred method of the two, mainly because of unquantifiable drying when crushing the sample for TGA.

Tuinukuafe et al. [36] proposed to normalise the amount of pore solution measured experimentally (oven-drying at 105°C) by a volume equal to the amount of evaporable water minus the amount of water bound to ettringite, monosulfate, hydrotalcite and hydrogarnet. This volume was determined by thermodynamic modelling coupled with an analytical partitioning of gel water, and resulted in a significantly larger amount (30 wt.%) compared to capillary water (19 wt.%) for the reference sample with Portland cement (w/c = 0.47). The rationale behind this suggestion was to account for interlayer water from C-S-H potentially released during PWE [37]. Normalising the calculations with the larger volume led to a clear improvement of the correspondence with PWE for the alkali metals concentrations in the pore solution.

Oven-drying aims to determine the amount of evaporable water, which is the sum of free water and physically bound (or adsorbed) water [38]. The evaporable water content is often determined as the mass loss obtained by oven drying at 105°C [38]. Strictly speaking, the amount of water that remains in the sample once equilibrium is reached depends on the temperature and the relative humidity (RH). It has been shown that adsorbed water is considerably affected in the RH interval 0–50% [39]. The RH is closely linked to the saturation vapour pressure, which strongly depends on the temperature: 2.34 kPa at 20°C, 7.38 kPa at 40°C and 120.97 kPa at 105°C [40]. The RH in an oven set to 40°C is therefore more sensitive to the ambient humidity than it would be at 105°C. As an example, saturated air at 20°C drops to ~2% RH at 105°C, but only to ~30% RH at 40°C.

However, the temperature and the RH also affect the stability of hydration products. Thus, at 105°C, ettringite decomposes and C-S-H is partly dehydrated [41]. This implies that chemically bound water is released, leading to an overestimation of the amount of evaporable water. Using a lower temperature (e.g. 40°C) can overcome this issue, although it would require longer drying time and may therefore induce further hydration [5,42] and carbonation. However, even at 40°C, low RH values can destabilise ettringite to form metaettringite, an amorphous product which only contains 10 to 13 moles of water per mole of $Al_2O_3$ (30 to 32 for ettringite) [43]. At 25°C, this has been reported to occur from 3% RH and below [44], leading to the release of water that was initially chemically bound.

Theoretically, CWE aims to collect free alkali metals which are, by definition, those present in free water. Logically, the volume of free water would therefore be the volume to consider in CWE calculations, as in Plusquellec et al [5]. However, as discussed in the previous paragraphs, the outcomes of drying methods are greatly influenced by the temperature and the RH, so that not only free water may

be removed. Consequently, there may be a difference between the actual quantity used in CWE calculations and the free water content. To make this distinction in the present paper, the term “amount of pore solution” will refer to the volume used in CWE calculations (independently of the method used and its outcome), while the term “free water” will only be used in opposition to “adsorbed water”

# 3 Materials and methods

The present work focused on the extraction of pore solution from cement paste samples. A parametric study of CWE was carried out to study the influence of different test parameters on the composition of the extracted solution. In parallel, different methods were investigated to determine the amount of pore solution. Finally, CWE was compared to PWE by applying both methods to samples cast with two different cement types, a Portland cement and a Portland-composite cement respectively.

## 3.1 Raw materials

Two cement types were used in this study: a type CEM I 52.5 N and a type CEM II/B-M 52.5 N (35% clinker replacement, with an equal amount of calcined clay and limestone). It should be mentioned that both cements were made from the same clinker. The chemical compositions were obtained by X-ray fluorescence (XRF) measurements, performed with a Malvern Panalytical Zetium spectrometer on powders sieved below 63 µm. The alkali metal content ($Na_2O$ and $K_2O$) was determined by wet chemistry methods according to EN 196-2. The results are summarised in Table 1. For CEM I, the mineral phases and their chemical composition determined by the modified Bogue calculation [23] are shown in Table 2. Alkali sulphates were determined first, and the remaining alkali metals were then divided between the clinker phases proportionally to the distribution in [23]. The amounts of free lime and calcite were set based on previous analysis of this particular cement.

*Table 1: Chemical composition of the cements (in wt.%) measured by XRF and physical characteristics.*

| Oxide | CEM I | CEM II/B-M |
|---|---|---|
| $SiO_2$ | 19.2 | 22.1 |
| $Al_2O_3$ | 5.2 | 6.4 |
| $Fe_2O_3$ | 3.67 | 3.95 |
| MgO | 1.0 | 1.1 |
| CaO | 63.4 | 54.2 |
| $Na_2O$ (EN 196-2) | 0.33 | 0.38 |
| $K_2O$ (EN 196-2) | 0.38 | 0.69 |
| $TiO_2$ | 0.19 | 0.27 |
| $P_2O_5$ | 0.26 | 0.24 |
| $SO_3$ | 3.14 | 2.73 |
| LOI (EN 196-2) | 3.21 | 7.86 |
| Cl | 0.04 | 0.07 |
| Sum | 100.2 | 99.9 |
| $Na_2O_{eq}$ | 0.58 | 0.83 |
| Fineness [$m^2/kg$] | 430 | 700 |
| Density [$kg/m^3$] | 3140 | 3020 |

*Table 2: Mineral composition of CEM I and chemical composition of the phases (in wt.% of total) derived from the modified Bogue calculation [23].*

| Phase | Phase fraction | Phase composition | | | | | | | |
|---|---|---|---|---|---|---|---|---|---|
| | | $SiO_2$ | $Al_2O_3$ | $Fe_2O_3$ | MgO | CaO | $Na_2O$ | $K_2O$ | $SO_3$ |
| $C_3S$ | 67.5 | 16.2 | 0.7 | 0.6 | 0.4 | 48.2 | 0.09 | 0.02 | 0.5 |
| $C_2S$ | 4.5 | 2.0 | 0.1 | 0.0 | 0.0 | 2.9 | 0.01 | 0.01 | 0.0 |
| $C_3A$ | 4.7 | 0.2 | 1.5 | 0.2 | 0.1 | 2.7 | 0.06 | 0.01 | 0.0 |
| $C_4AF$ | 13.0 | 0.5 | 2.8 | 2.8 | 0.4 | 6.2 | 0.02 | 0.01 | 0.0 |
| Periclase | 0.1 | 0.0 | 0.0 | 0.0 | 0.1 | 1.0 | 0.00 | 0.00 | 0.0 |
| Free lime | 0.5 | 0.0 | 0.0 | 0.0 | 0.0 | 0.5 | 0.00 | 0.00 | 0.0 |
| Calcite | 3.0 | 0.0 | 0.0 | 0.0 | 0.0 | 1.7 | 0.00 | 0.00 | 0.0 |
| $K_2SO_4$ | 0.6 | 0.0 | 0.0 | 0.0 | 0.0 | 0.0 | 0.00 | 0.34 | 0.3 |
| $Na_2SO_4$ | 0.3 | 0.0 | 0.0 | 0.0 | 0.0 | 0.0 | 0.15 | 0.00 | 0.2 |
| $CaSO_4$ | 2.9 | 0.0 | 0.0 | 0.0 | 0.0 | 1.2 | 0.00 | 0.00 | 1.7 |
| Others | 3.0 | 0.3 | 0.1 | 0.0 | 0.0 | 0.1 | 0.00 | 0.00 | 0.4 |

For the chemical experiments (PWE and CWE), deionised water was boiled, stored in a sealed glass bottle and cooled down to room temperature before the experiment, to remove air including $CO_2$ from the water and prevent subsequent carbonation. This water is denoted as *BDW* (Boiled, Deionised Water) in this paper.

## 3.2 Preparation of paste samples

The samples were prepared by first weighting 250 g of deionised water in the mixing bowl of a high shear laboratory blender (two speeds, capacity of 1.2 L, unloaded low speed and high speed stated by the manufacturer to be 15 800 rpm and 22 000 rpm respectively). 500 g of cement was then added before starting the blender. The mixing sequence was the following: 30 s at low speed, 90 s rest and 30 s at high speed. The inside of the bowl was scraped down at the beginning of the rest period to re-incorporate any dry material that was on the sides of the bowl.

The samples were cast in hollow POM cylinders. The casting procedure was slightly different for the parametric study and for the comparison between the two extraction methods. Table 3 shows the details for each procedure.

*Table 3: Comparison of the sample preparation for sample types A and B (geometry and casting procedure).*

| | Parametric study | Comparison between the extraction methods |
|---|---|---|
| Sample type | A | B |
| Mould size | Ø 25 mm x 100 mm | Ø 45 mm x 100 mm |
| Sealing | Rubber bungs | Rubber bung on one end, thick plastic foil and piece of plywood pressed against the cylinder on the other |
| Specimens per batch | 6 | 1 |
| Filling | Two layers<br>Vibrated for 15 s each time | Three layers<br>Vibrated for 15 s each time |

In both cases, the samples were rotated in a climate chamber at 20°C. After 24 h ± 1 h, the samples were demoulded, sealed with plastic foil and tape, and placed back in the same climate chamber until pore solution extraction.

## 3.3 Cold Water Extraction (CWE)

The CWE procedure was inspired by the method described in Plusquellec et al. [5], but it was adapted to the equipment that was available in the laboratory.

After 28 days of curing, the samples were unsealed and crushed manually. Depending on the size fraction, a hammer and/or a mortar and pestle were used. The crushed paste was regularly sieved until 20.00 g of material with an accuracy of 0.01 g was obtained. Between each sieving, the material passing through the sieve was put in a beaker and stored in a desiccator, which contained silica gel and soda lime to avoid carbonation. After completion, a magnet was added to stir the solution during the leaching stage. Subsequently, BDW was added directly to the beaker containing the crushed material with an accuracy of 0.01 g. The time after the addition of the last droplet of water was denoted $t_0$. At $t_0$ + 60 s, the beaker was placed in a glovebox where the $CO_2$ concentration of the air was below 80 ppm. At $t_0$ + 120 s, the beaker was sealed to entrap low $CO_2$ air. Finally, at $t_0$ + 180 s, the beaker was placed on the magnetic stirrer, and the stirring period was initiated.

At the end of the leaching time, the solution was immediately filtered by means of a Büchner filtration setup. A cellulose filter with 8 µm pore size was placed in the Büchner funnel. The pump was stopped when no liquid could be seen flowing out of the funnel. Filtrate dilution was made by pipetting 2 mL of filtrate and placing it in a plastic tube. Subsequently, 18 mL of BDW were added into the tube, and the solution was finally acidified by adding 280 µL of $HNO_3$ 32.5%. The tubes were stored between 2 and 7°C before performing inductively coupled plasma optical emission spectrometry (ICP-OES) with a Varian 720-ES instrument to determine the concentration of Na, K, Ca, Al and S. Before each extraction, the glassware was cleaned with a weak acid to eliminate any trace of precipitate or residues from previous experiments. To calculate the actual dilution factor and evaluate the uncertainty of each step, all masses were recorded to the nearest 0.001 g (mass of powder and BDW for leaching; mass of filtrate, BDW and acid for the dilution).

Table 4 gives an overview of the method and estimated durations.

*Table 4: Cold Water Extraction sequence and the estimated duration of each step.*

| Step | | Approximate duration |
|---|---|---|
| Crushing | | < 0.15 mm: 25 to 30 min<br>0.15 mm to 0.5 mm: 20 to 25 min<br>0.5 mm to 1 mm: 15 to 20 min<br>1 mm to 2 mm: 8 to 12 min |
| Addition of BDW | | 2 min |
| Leaching | Entrapment of low $CO_2$ air | 3 min |
| | Stirring | See Table 5 |
| Filtration | | 3 min |
| Dilution | | 2 min |
| Acidification | | 1 min |

## 3.4 Pore Water Extraction (PWE)

The device used in the present study was similar to the one depicted in Barneyback and Diamond [15]. The paste sample was placed in a die body where it fitted loosely into the bore hole. A disc of PTFE and the piston were subsequently placed on top of it. The entire setup was placed in a compressive strength testing machine that was used to load the piston. The pore solution was collected in a plastic vial connected to the surface of the base via a fluid drain, as shown in Figure 2.

The piston was loaded with a stress rate of 1.3 MPa/s until it reached 1000 MPa. The pressure was then maintained constant at 1000 MPa for 15 min. Immediately after the end of the extraction, the extracted solution was filtered through a cellulose filter (pore size 8 µm) by gravity. 2 mL of pore solution were sampled and transferred into a plastic tube, followed by 18 mL of BDW and 1 mL of $HNO_3$ 32.5%. More acid was added compared to CWE because the extracted solution in PWE is more concentrated. The tubes were stored in the fridge prior to ICP-OES analysis, which was performed with the same equipment as for CWE. The same elements were also investigated.

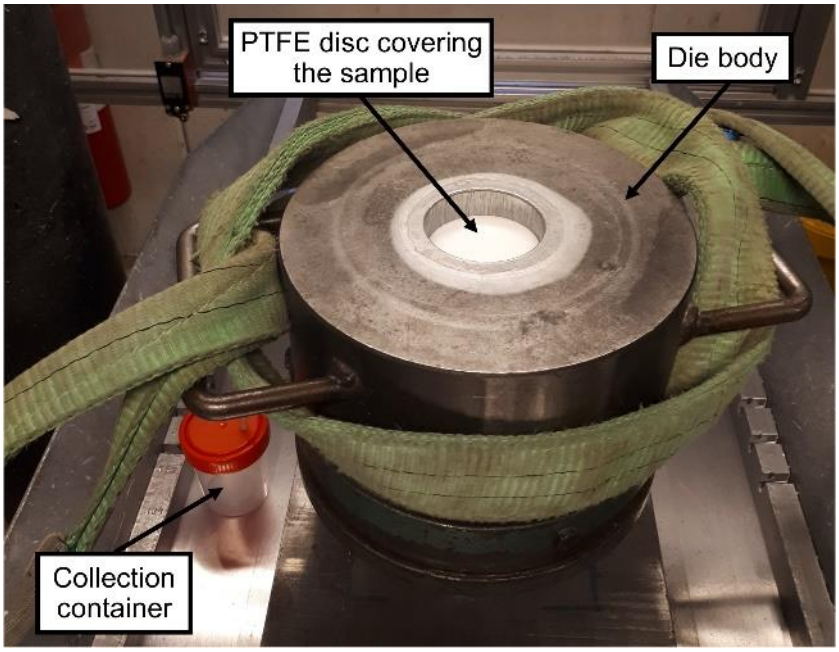


*Figure 2: Setup used for Pore Water Extraction.*

## 3.5 Amount of pore solution

A sample of paste was collected from each specimen used for CWE immediately after it was unsealed to determine the amount of pore solution. Different procedures based on mass loss were investigated, as detailed in the following sub-sections.

It is likely that some water was lost once the sample had been crushed. Therefore, additional Type A samples with CEM I were cast to measure the mass loss of the crushed sample (at 28 days) for all size fractions considered. This was achieved by following the same procedure as for CWE until 20.00 g of crushed paste had been collected.

A summary of the test program is presented in Table 5.

### 3.5.1 Oven-drying at 105°C

A broken slice of paste of approximately 25 g was sampled from each specimen immediately after they had been unsealed. The pieces were weighted with an accuracy of 0.001 g and placed in an oven at 105°C until they reached constant mass, i.e. a mass difference smaller than 0.1 wt.% between two consecutive measurements, with at least 24 h between. The samples were allowed to cool down to room temperature in a desiccator containing silica gel prior to weighting. In practice, it took approximately 5 days to reach constant mass. Once the mass

stabilised, some samples were divided to expose a fresh surface, which was sprayed with phenolphthalein to check the carbonation.

When measuring the mass loss of crushed samples, approximately 10 g out of the 20 g collected were dried. Constant mass was reached after 24 h. The mass loss during crushing $\Delta W_{105}$, defined as the difference between the mass loss of the bulk sample and that of the crushed sample, was calculated for all size fractions.

### 3.5.2 Oven-drying at 40°C

The same procedure was used, except that the oven temperature was set to 40°C. The time to reach constant mass was longer: around 14 days for bulk samples, and 48 h for crushed samples.

### 3.5.3 Silica gel at 40°C

To achieve better control of the relative humidity, 3 broken slices of approximately 25 g each were placed in a 5.5 L desiccator containing 400 g of silica gel (half at the bottom and half on the tray), which was itself stored in an oven set to 40°C. For each measurement, the desiccator was taken out of the oven and allowed to cool down to room temperature before opening. While weighing the samples, the silica gel was dried at 105°C for a few minutes.

An attempt was made to enhance water removal by creating some air circulation in the desiccator with small fans placed inside and activated for 5 min every hour.

### 3.5.4 Solvent exchange

This method was modelled on a procedure commonly used to stop hydration and preserve the microstructure [45]. A thin broken slice of paste of 2-3 mm was sampled, weighed and placed in ethanol, methanol or isopropanol for 7 days. A second solvent exchange was then performed with diethyl ether for an additional day. Finally, the slice was dried at 40°C to eliminate any trace of solvent. Due to the high volatility of diethyl ether, only 15 min of drying were required.

*Table 5: Test program to determine the amount of pore solution. The values correspond to the number of samples tested, and the letter in brackets refers to the sample type. [a]: all size fractions were tested. [b]: measured only on 0.5 – 1 mm. [c]: only on bulk samples.*

| | | Variable | CEM I | | CEM II/B-M | |
|---|---|---|---|---|---|---|
| | | | Type A | Type B | Type A | Type B |
| Oven-drying at 105 °C | Bulk | $W_{OD105}$ | 24 | 2 | 3 | 2 |
| | Powder | - | 1[a] | - | - | 1[b] |
| Oven-drying at 40 °C | Bulk | $W_{OD40}$ | 14 | 2 | 3 | 2 |
| | Powder | - | 1[a] | - | - | 1[b] |
| Desiccator with silica gel at 40°C | No fans | $W_{des40}$ | 3 | - | 3 | - |
| | Fans | $W_{des40f}$ | 3 | - | - | - |
| Solvent exchange[c] | Ethanol | $W_{eth}$ | 3 | - | - | - |
| | Methanol | $W_{meth}$ | 3 | - | - | - |
| | Isopropanol | $W_{isop}$ | 3 | - | - | - |

## 3.6 Data processing

For CWE, the concentration of a given element in the pore solution $[X]_{ps}$ can be calculated from the concentration in the extracted solution $[X]_{ex}$ via Equation (2a). The free alkali metal content in the sample $X_s$ can also be derived in a similar way, as shown in Equation (2b).

$$[X]_{ps} = \alpha \frac{m_{wp} + m_{CWE}}{m_{wb}} [X]_{ex} \quad (2a)$$

$$X_s = \alpha \frac{m_{wp} + m_{CWE}}{m_s} \gamma^{-1} [X]_{ex} \quad (2b)$$

where:

- $[X]_{ps}$: concentration in the pore solution [mol/L]
- $[X]_{ex}$: concentration in the extracted solution after dilution and acidification [mol/L]
- $X_s$: free alkali metal content in the sample [mol/g]
- $\alpha$: dilution factor [-], accounting for both water and acid addition. According to the procedure described in Section 3.3, the theoretical factor for CWE is $\alpha_{th}$ = (2+18+0.28)/2 = 10.14

- $m_{wp}$: mass of pore solution in the (crushed) sample [g]
- $m_{wb}$: mass of pore solution in the bulk specimen [g]
- $m_{CWE}$: mass of water used for leaching [g]
- $m_s$: mass of the sample [g]
- $\gamma$: density of water [g/L]. For all calculations, $\gamma$ = 998 g/L [40]

Equations (2a) and (2b) still hold in the case of PWE. However, a few changes apply:

- The theoretical dilution factor is $\alpha_{th}$ = (2+18+1)/2 = 10.50, due to the larger amount of acid
- $m_{wp}$ is equal to $m_{wb}$ since the sample is not crushed
- $m_{CWE}$ is equal to 0 because there is no leaching.

## 3.7 Parametric study of CWE

The present study quantified the influence of three parameters, namely the size fraction of crushed paste, the liquid-to-solid ratio (L/S) and the stirring time. Note that the stirring time differs from the leaching time: as shown in Table 4, the leaching time is the time needed for entrapping low $CO_2$ air plus the stirring time. All samples were Type A samples cast with CEM I. Table 6 describes the test program with the different parameters used for each test. Note that each test was performed in triplicate to assess the repeatability of the method. The test ID is based on the three parameters mentioned above. The first letter designates the size fraction: S for small (< 0.15 mm), M for medium (0.15 – 0.5 mm), L for large (0.5 – 1 mm) and X for extra large (1 – 2 mm). The following number refers to the stirring time in minutes, and the last number is the L/S. For example, M60-1 is the ID for the sample where the particle size is 0.15 – 0.5 mm (medium), the stirring time is 60 minutes, and L/S = 1.

*Table 6: Test program for the parametric study.*

| Test ID | Size fraction [mm] | Stirring time [min] | L/S [-] |
|---|---|---|---|
| S5-1 | < 0.15 | 5 | 1 |
| S5-2 | < 0.15 | 5 | 2 |
| S60-1 | < 0.15 | 60 | 1 |
| S60-2 | < 0.15 | 60 | 2 |
| M5-1 | 0.15 – 0.5 | 5 | 1 |
| M60-1 | 0.15 – 0.5 | 60 | 1 |
| L5-1 | 0.5 – 1 | 5 | 1 |
| L30-1 | 0.5 – 1 | 30 | 1 |
| L60-1 | 0.5 – 1 | 60 | 1 |
| L60-2 | 0.5 – 1 | 60 | 2 |
| L90-1 | 0.5 – 1 | 90 | 1 |
| X5-1 | 1 – 2 | 5 | 1 |
| X60-1 | 1 – 2 | 60 | 1 |

## 3.8 Comparison between PWE and CWE

The accuracy of CWE was assessed via a comparative study with PWE. Both methods were performed on Type B samples with CEM I and CEM II/B-M, at 28 days. CWE was carried out using the parameters corresponding to L5-1 and L90-1 (size fraction of 0.5 – 1 mm, 5 or 90 minutes of stirring and L/S = 1).

The mass losses used in the calculations were the ones obtained with Type A samples. However, oven-drying at 40 and 105°C were performed on Type B samples to verify that the specimen size did not significantly affect the measurements.

## 3.9 Thermodynamic modelling

Hydration kinetics and phase assemblage of the CEM I paste were studied via thermodynamic modelling using the Gibbs free energy minimisation software GEMS [46–48]. The degree of hydration of the clinker phases over time was calculated based on the Parrot and Killoh model [49,50]. The results were then used as inputs to determine the phase assemblage at 28 days, together with the mineral composition shown in Table 2. Thermodynamic data were taken from the PSI/Nagra database [51], extended with the Cemdata 18 database [52]. C-S-H was modelled according to the CSHQ model proposed by Kulik [53], which consists of 4 C-S-H end-members with Ca/Si varying from 0.67 to 2.25, and two alkali metals (K and Na) end-members.

# 4 Results

Raw data and the results of the detailed calculations described in this section are available online [54].

## 4.1 Determination of the amount of pore solution

The mass losses of bulk samples subjected to the different drying techniques specified in Section 3.5 are shown in Table 7.

*Table 7: Mass loss of bulk samples obtained with different drying techniques (in wt.%). The standard deviation is indicated in brackets, when available.*

| Method | | Variable | CEM I | | CEM II/B-M | |
|---|---|---|---|---|---|---|
| | | | Type A | Type B | Type A | Type B |
| Oven-drying at 105 °C | | $W_{OD105}$ | 21.6 (0.3) | 22.0 | 23.7 (0.2) | 23.7 |
| Oven-drying at 40 °C | | $W_{OD40}$ | 17.3 (0.2) | 17.0 | 18.4 (0.1) | 18.8 |
| Desiccator with silica gel at 40 °C | | $W_{des40}$ | 19.4 (0.1) | - | 20.8 (0.1) | - |
| Desiccator with silica gel and fans at 40 °C | | $W_{des40f}$ | 19.6 (0.1) | - | - | - |
| Solvent exchange | Methanol | $W_{meth}$ | 14.1 (1.1) | - | - | - |
| | Ethanol | $W_{eth}$ | 9.6 (1.4) | - | - | - |
| | Isopropanol | $W_{isop}$ | 7.7 (0.6) | - | - | - |

As expected, oven drying at 105°C gave the largest mass loss, 4 to 5 wt.% higher than at 40°C. Drying with silica gel gave an intermediate value, while solvent exchange methods led to significantly lower results. Note that the standard deviation is calculated as a sample standard deviation, to account for the bias introduced by the different numbers of samples tested using each method (see Table 5). The values for the crushed samples are shown in Table 8, together with the calculated mass loss during crushing ($\Delta W_{crushing,40}$ or $\Delta W_{crushing,105}$). The latter were derived by subtracting the mass loss of crushed samples (Table 8) from the mass loss of bulk samples (Table 7, Type B samples). The values indicate that the smaller the size fraction, the higher the mass loss during crushing. The carbonation depths flagged by a pH indicator (phenolphthalein) after drying at

40°C may be seen in Figure 3. The only sample not carbonated once stable mass was reached was the sample dried with silica gel.

*Table 8: Mass loss of crushed samples during oven-drying and calculated mass loss during crushing for different size fractions.*

| | | | Oven-drying 40°C | | Oven-drying 105°C | |
|---|---|---|---|---|---|---|
| Sample type | Cement type | Size fraction [mm] | Mass loss [wt.%] | $\Delta W_{crushing,40}$ [wt.%] | Mass loss [wt.%] | $\Delta W_{crushing,105}$ [wt.%] |
| A | CEM I | < 0.15 | 10.9 | 6.2 | 17.4 | 4.2 |
| | | 0.15 – 0.5 | 12.0 | 5.1 | 18.6 | 3.0 |
| | | 0.5 – 1 | 13.3 | 3.8 | 19.8 | 1.8 |
| | | 1 – 2 | 13.7 | 3.4 | 20.2 | 1.4 |
| B | CEM I | 0.5 – 1 | 13.4 | 3.7 | 20.1 | 1.9 |
| | CEM II/B-M | 0.5 – 1 | 15.2 | 3.6 | 21.9 | 2.8 |

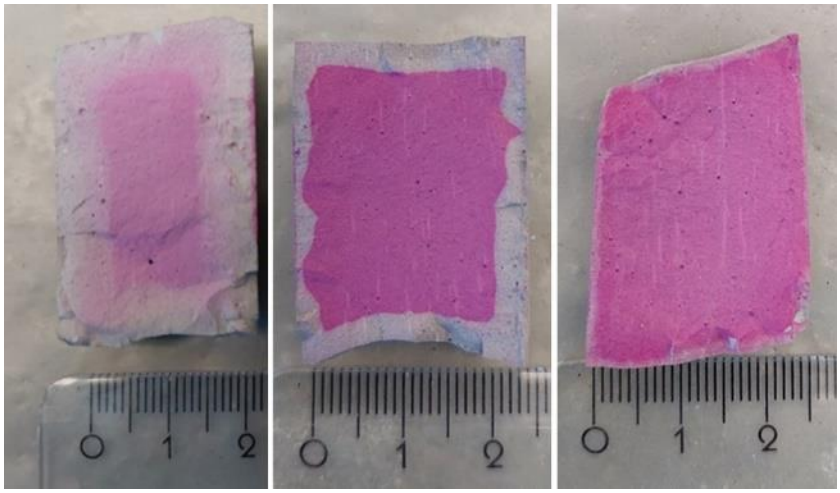

*Figure 3: Carbonation depth after 5 days of oven-drying at 105°C (left), 14 days of oven-drying at 40°C (centre) and 21 days in a desiccator with silica gel at 40°C (right).*

Figure 4 shows the mass loss over time of the samples dried at 40°C (oven-drying and desiccators with silica gel). All curves follow an exponential trend ($y = a + b \cdot exp(-x)$) with a high rate of mass loss over the first few days followed by a gradual slowdown before reaching constant mass. Oven-drying leads to the fastest initial removal, but the loss rate of the desiccator curves decreases more slowly so that there are no significant differences after 5 days.

Subsequently, the mass loss with desiccators is greater than with oven-drying and leads to a greater total mass loss. Figure 4 also shows the RH registered during drying in the oven and in the desiccator containing silica gel (without fans). Note that the peaks for the desiccator curve correspond to the measurements of the samples.

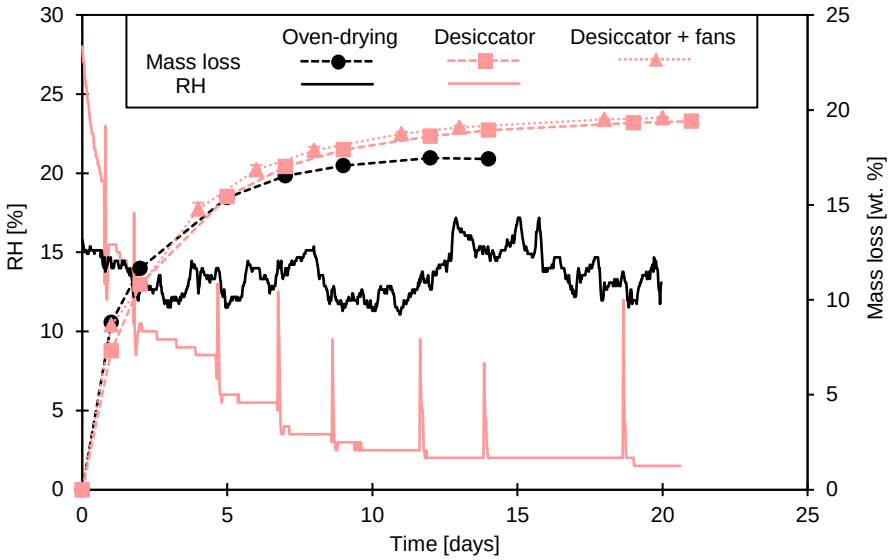


*Figure 4: Mass loss of the samples dried at 40°C (oven-drying and desiccator containing silica gel).*

## 4.2 Parametric study of CWE

The calculated concentrations for Na and K obtained from the parametric study detailed in Table 6 are reported in Table 9, after calculation according to Equation (2a). Based on all tests, the average experimental dilution factor is $\alpha_{exp}$ = 10.12. The mass of pore solution in the bulk specimen $m_{wb}$ is assumed to be $W_{des40}$ (in wt.%) multiplied by the mass of the sample ($m_{s,exp}$ = 20.00 g). The mass of pore solution in the crushed sample $m_{wp}$ is calculated in the same way, except that $\Delta W_{crushing,40}$ is subtracted from $W_{des40}$ to account for drying during crushing. Finally, the average mass of water used for leaching $m_{CWE,exp}$ is either 20.01 g or 40.01 g depending on the L/S. The table shows the average values as well as the standard deviations.

The results for Ca, Al and S are omitted here because of the uncertainty of the results. Regarding Ca, the reason lies in portlandite dissolution as explained in the introduction, which would lead to unrealistic concentrations. For Al and S, the ICP equipment used for the analyses was not calibrated to detect low-intensity signals

for these elements. Note that all ICP-OES results (Na, K, Ca, Al and S) are available online for information [54].

The standard deviations are calculated using propagation formulas [55] to account for the uncertainties of each parameter in Equation (2a). The uncertainty of a single ICP measurement is assumed to be 10%, based on observed deviations due to different dilution factors when performing the analysis. The detailed calculations are shown elsewhere [54].

*Table 9: Results of the parametric study on CWE: calculated Na and K concentrations in the pore solution. Each value is an average of three, as all tests were triplicated.*

| Test ID | Concentration [mmol/L] | | | |
|---|---|---|---|---|
| | Na | | K | |
| | Avg. | Std dev. | Avg. | Std dev. |
| S5-1 | 306 | 18 | 240 | 14 |
| S5-2 | 331 | 19 | 252 | 15 |
| S60-1 | 317 | 18 | 257 | 15 |
| S60-2 | 333 | 19 | 253 | 15 |
| M5-1 | 279 | 16 | 243 | 15 |
| M60-1 | 309 | 18 | 246 | 15 |
| L5-1 | 237 | 14 | 214 | 12 |
| L30-1 | 292 | 17 | 240 | 14 |
| L60-1 | 288 | 17 | 229 | 13 |
| L60-2 | 319 | 19 | 255 | 15 |
| L90-1 | 306 | 18 | 240 | 14 |
| X5-1 | 177 | 10 | 161 | 9 |
| X60-1 | 270 | 16 | 229 | 13 |

The effect of the size fraction on the alkali metal concentration in the pore solution is apparent in Figure 5, which shows the concentrations obtained with a stirring time of 5 min (left) and 60 min (right), the L/S being 1 in both cases. It may be seen that the concentrations decrease when the size fraction increases, which corresponds to the theoretical expectations. In addition, the difference is more pronounced with only 5 min stirring compared to 60 min.

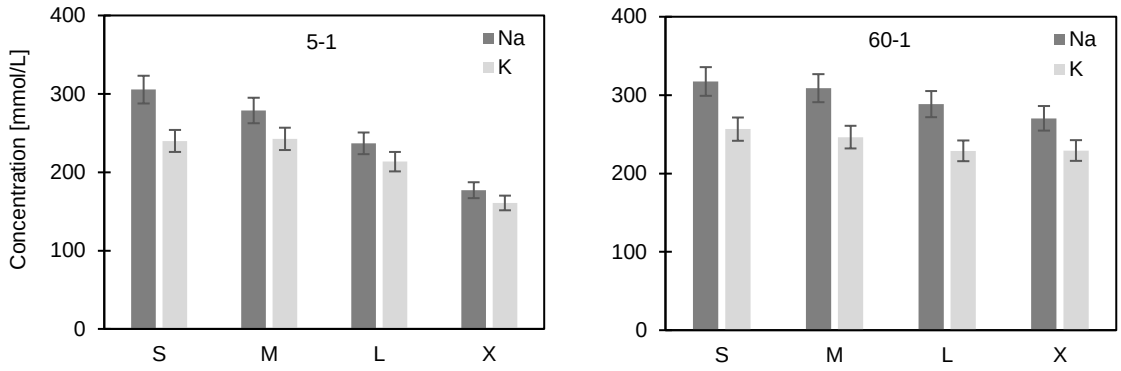


*Figure 5: Effect of the size fraction on the alkali metal concentration in the pore solution calculated from CWE results. The stirring time and the L/S are fixed (5 min (left) or 60 min (right), and 1:1 respectively).*

The effect of the L/S is shown in Figure 6, where the results of 6 tests are shown. The values should be compared two by two, for the same combination of size fraction and leaching time (S5, S60 and L60). The concentrations of Na and K increase when L/S increases in most cases. However, it must be emphasised that the differences may not be significant overall, as there is a considerable overlap between error bars.

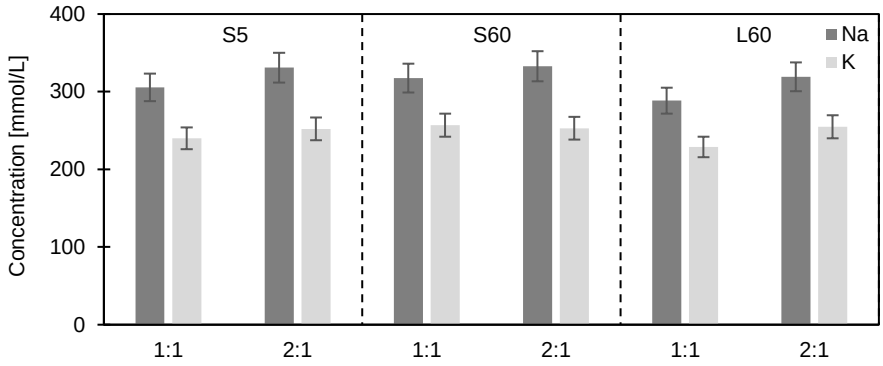


*Figure 6: Effect of the L/S on the alkali metal concentration in the pore solution calculated from CWE results.*

The influence of the stirring time is shown in Figure 7, which displays the results obtained with constant size fraction and L/S for 4 different stirring durations. Overall, the Na concentration tends to increase with time, which is in agreement with the expectations. Considering the two extreme durations, the trend for K may be the same but the significance of the results is again uncertain due to a strong overlap of error bars.

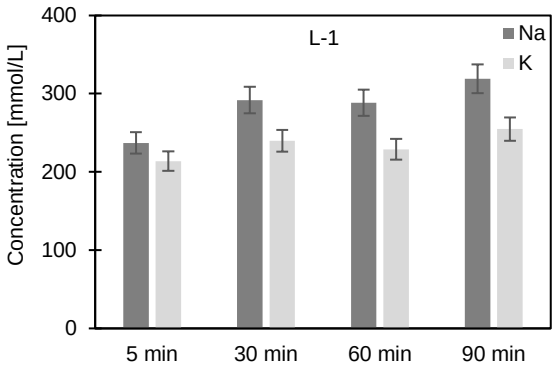


*Figure 7: Effect of the stirring time on the alkali metal concentration in the pore solution. The size fraction and the L/S are fixed (L and 1:1 respectively).*

Table 10 shows how the calculated concentrations are affected depending on the method chosen to determine the amount of pore solution. The baseline case corresponds to the results obtained by following the method described earlier with test L5-1. It must be mentioned that the results are presented for Na only, but the same relative differences apply for K since the amount of pore solution is a common parameter.

*Table 10: Influence of the method chosen for determining the amount of pore solution on the calculated Na concentration in the pore solution. The values in brackets represent the relative difference with the baseline (first row). The results correspond to L5-1.*

| | Concentration [mmol/L] |
|---|---|
| $m_{wp}$ and $m_{wb}$ determined by drying in a desiccator with silica gel at 40°C (baseline) | 237 (-) |
| $m_{wp}$ and $m_{wb}$ determined by oven-drying at 40°C | 261 (+10.1%) |
| $m_{wp}$ and $m_{wb}$ determined by oven-drying at 105°C | 217 (-8.5%) |
| Mass loss during crushing ignored ($m_{wp} = m_{wb}$) | 245 (+3.5%) |

## 4.3 Comparison between PWE and CWE

Table 11 shows the calculated concentrations of Na and K in the pore solution when comparing PWE and CWE, for the two cement types. The values are also plotted in Figure 8 and show that CWE overestimates the concentrations compared to PWE. The relative and absolute differences between CEM I and CEM II/B-M for PWE, CWE L5-1 and CWE L90-1 are listed in Table 12.

*Table 11: Comparison between PWE and CWE: calculated Na and K concentrations in the pore solution.*

| Cement type | Method | | Concentration [mmol/L] | |
|---|---|---|---|---|
| | | | Na | K |
| CEM I | PWE | | 200 | 172 |
| | CWE | L5-1 | 227 | 213 |
| | | L90-1 | 302 | 246 |
| CEM II/B-M | PWE | | 134 | 109 |
| | CWE | L5-1 | 196 | 169 |
| | | L90-1 | 252 | 204 |

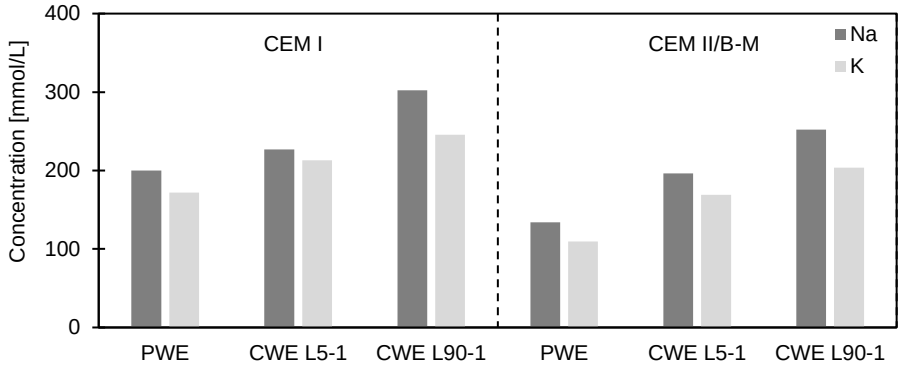


*Figure 8: Calculated concentrations of Na and K in the pore solution of CEM I and CEM II/B-M samples, for PWE and CWE.*

*Table 12: Relative and absolute differences between CEM I and CEM II/B-M for PWE, CWE L5-1 and CWE L90-1.*

| Method | Relative [%] | | Absolute [mmol/L] | |
|---|---|---|---|---|
| | Na | K | Na | K |
| PWE | 33 | 36 | 66 | 62 |
| CWE L5-1 | 14 | 21 | 31 | 44 |
| CWE L90-1 | 17 | 17 | 50 | 42 |

The alkali metal concentrations reported in Table 11 were used to calculate the free alkali metal content as calculated using Equation (2b). The results are shown in Table 13 and indicate the same trend as concentrations, i.e. higher values for CWE.

*Table 13: Free alkali metal content in the samples, with respect to the total alkali metal content reported in Table 1.*

| Cement type | Method | | Free alkali metal content [%] | |
|---|---|---|---|---|
| | | | Na | K |
| CEM I | PWE | | 63.6 | 52.7 |
| | CWE | L5-1 | 72.3 | 65.3 |
| | | L90-1 | 96.2 | 75.4 |
| CEM II/B-M | PWE | | 39.7 | 19.8 |
| | CWE | L5-1 | 58.1 | 30.7 |
| | | L90-1 | 74.7 | 36.9 |

Table 14 shows the influence of the method chosen for determining how the amount of pore solution affects the free alkali metal content, for PWE and CWE L5-1. As in Table 10, only the results for Na are displayed. One can note the relatively large influence of the amount of pore solution on the values calculated from PWE. On the contrary, CWE calculation are in this case barely affected by the drying method chosen.

*Table 14: Influence of the method chosen for determining the amount of pore solution on the free-Na content. The values in brackets represent the relative difference with the baseline (first row).*

| | Free Na content [%] | | | |
|---|---|---|---|---|
| | CEM I | | CEM II/B-M | |
| | PWE | CWE L5-1 | PWE | CWE L5-1 |
| $m_{wp}$ determined by drying in a desiccator with silica gel at 40°C (baseline) | 63.6 (-) | 72.3 (-) | 39.7 (-) | 58.1 (-) |
| $m_{wp}$ determined by oven-drying at 40°C | 56.7 (-10.8%) | 71.2 (-1.5%) | 35.1 (-11.5%) | 57.0 (-2.0%) |
| $m_{wp}$ determined by oven-drying at 105°C | 70.8 (+11.3%) | 73.9 (+2.2%) | 45.2 (+13.9%) | 59.6 (+2.5%) |
| Mass loss during crushing ignored ($m_{wp} = m_{wb}$) | 63.6 (0%) | 74.5 (+3.1%) | 39.7 (0%) | 59.7 (+2.7%) |
| $m_{wp}$ neglected | - | 62.4 (-13.6%) | - | 49.4 (-15.0%) |

## 4.4 Thermodynamic modelling

Hydration kinetics of the paste containing CEM I was determined according to the Parrot-Killoh model as described in Section 3.9. At 28 days, the degrees of hydration of $C_3S$, $C_2S$, $C_3A$ and $C_4AF$ were found to be respectively 0.85, 0.66, 0.85, 0.72 (weighted average = 0.81). The corresponding phase assemblage is reported in Table 15. The Ca/Si of the C-S-H at full hydration was found to be 1.7.

*Table 15: Phase assemblage of the CEM I paste (w/c = 0.5) at 28 days determined by thermodynamic modelling.*

| Phase | Weight fraction [g/100 g cement] |
|---|---|
| $C_3S$ | 10.5 |
| $C_2S$ | 1.6 |
| $C_3A$ | 0.7 |
| $C_4AF$ | 3.7 |
| C-S-H | 49.4 |
| Portlandite | 28.4 |
| Ettringite | 15.1 |
| AFm | 14.8 |
| Calcite | 2.5 |
| Hydrotalcite | 2.3 |
| Monocarbonate | 1.1 |
| Pore solution | 19.9 |

# 5 Discussion

The discussion is structured around five points. First, the modification of the alkali metal inventory due to CWE is analysed. Subsequently, the research questions mentioned in the introduction are examined: the influence of the test parameters (size fraction, leaching time and L/S) on the extracted solution in CWE, the influence of the method for determining the amount of pore solution on the calculated values in CWE and the choice of the method. Finally, the correspondence between CWE and PWE when comparing different cements is discussed.

## 5.1 Alkali metal inventory in CWE

In Table 13, it may be seen that the free alkali metal contents obtained with CWE L90-1 are unrealistic (in particular for Na, more than 90%). According to Equation (2b), only two factors are uncertain enough to potentially explain this high value:

the mass of pore solution in the crushed sample $m_{wp}$, or the concentration in the extracted solution $[X]_{ex}$.

The influence of $m_{wp}$ will be discussed in Section 5.3, but it is unlikely to be the explanation here. It is already known to have little influence on the free alkali metal content [5], which is also confirmed by the results shown in Table 14. The only remaining cause of the discrepancy is thus $[X]_{ex}$, and obtaining a value larger than expected suggests that not only the alkali metals present in the pore solution were leached out, but also some alkali metals that had initially been bound.

### 5.1.1 Alkali metals in unreacted clinker

The first possibility is to release alkali metals from unreacted clinker phases, due to further hydration during leaching in CWE. However, due to the high $SO_3$ to $Na_2O$ + $K_2O$ ratio (above 4), most alkali metals are readily soluble in sulphates. To confirm this, one can quantify the maximum amount of alkali metals that can be released from unreacted clinker during CWE, by combining the degrees of hydration from Section 4.4 and the alkali metal content of the clinker phases from Table 2. The calculations lead to 9 and 2% of the total $Na_2O$ and $K_2O$ contents respectively. Even considering the worst-case scenario. i.e. full hydration achieved within 90 minutes of leaching, alkali metal release from unreacted clinker would not significantly lower the amount of free alkali metals. Moreover, it is the authors' opinion that a leaching time of 5 minutes (as in CWE L-5) would strongly limit the risk of further hydration.

### 5.1.2 Alkali metals bound to C-S-H

The other possibility is to release alkali metals bound to hydrates (mainly C-S-H). As a starting point, one should estimate the amount bound before extraction. This can be done by evaluating three parameters of the C-S-H: 1) the Ca/Si, 2) the alkali metal binding capacity and 3) the amount of C-S-H formed. As reported in Section 4.4, the Ca/Si at full hydration was found to be approximately 1.7. For the binding capacity, the data from Hong and Glasser presented in Figure 1 can be interpolated to obtain values for Ca/Si = 1.7 and alkali metals concentrations of 200 mmol/L (which are approximately the values determined by PWE). This approach results in a binding capacity of 0.28 g $Na_2O$ and 0.42 g $K_2O$ per 100 g of C-S-H. Considering 49 g of C-S-H formed per 100 g of cement (Table 15) and normalising the results with respect to the total contents leads to 42% of $Na_2O$ and 54% $K_2O$ being bound at 28 days. Thus, despite the relatively high Ca/Si, these numbers suggest that a significant amount of alkali metals are bound to the C-S-H before CWE.

Assuming no leaching, all alkali metals are either in unreacted clinker, bound to C-S-H or free in the pore solution. Thus, the alkali inventory can be derived from

the calculations in Sections 5.1.1 and 5.1.2, and is shown in Table 16. The free alkali metal contents, obtained by mass balance, are relatively consistent with experimental values reported by other authors (39–57% in Rivard et al. [3], 46–59% in Drolet et al. [56], 50–62% in Plusquellec et al. [5]).

*Table 16: Alkali metal inventory before CWE. The values are given in % of total.*

| | In unreacted clinker | Bound to C-S-H | Free in the pore solution |
|---|---|---|---|
| $Na_2O$ | 9% | 42% | 49% |
| $K_2O$ | 2% | 54% | 44% |

Since there are only two possible sources of alkalis in the system, and that hydration of unreacted clinker cannot explain why CWE overestimates free alkali metal contents (Section 5.1.1), the behaviour of alkali metals bound to C-S-H during CWE must be investigated further. As discussed in Section 2.2, bound alkali metals cannot be removed from the EDL unless other cations replace them, typically $Ca^{2+}$ in cementitious systems. Duchesne and Bérubé [30] argue that such an exchange takes place between the bulk solution and the EDL until an equilibrium is reached. Before CWE, the bulk solution in question is the pore solution. However, when adding water in CWE, the bulk solution of the system is changed: ionic diffusion occurs from the pore solution to the added water, so that the concentrations of $Na^+$ and $K^+$ decrease. In the meantime, portlandite dissolves which increases the concentration of $Ca^{2+}$. The thermodynamic equilibrium of the system is therefore shifted, and the consequence on alkali metal binding can be described in two ways:

- Increasing the calcium concentration in the liquid phase changes the equilibrium with the C-S-H, so that the Ca/Si increases [29]. According to Figure 1, this goes in the direction of a lower binding capacity, i.e. release of alkali metals into the bulk solution
- From Equation (1a), the equilibrium is broken so that the amount of $(Na^+)_b$ decreases and that of $(Ca^{2+})_b$ increases. Bringing back the system to equilibrium implies that the calcium concentration in the EDL $(Ca)_{dl}$ increases, and so that of sodium $(Na)_{dl}$ decreases. Consequently, $Na^+$ ions that were initially in the EDL are released into the leaching solution, and the same occurs with $K^+$.

Furthermore, it should be mentioned that the concentration shift in the bulk solution induces a change of the ionic strength. As a result, the thickness of the

EDL is probably modified during the leaching phase of CWE, which also has an influence on the equilibrium.

The mechanism described above suggests that two processes must take place during CWE: the extraction of free alkali metals, and the release of bound alkali metals. There may thus be a trade-off between the two, which depends on the kinetics of each process.

## 5.2 Influence of the test parameters on the extracted solution

As CWE is performed in a non-equilibrium state, most results are in agreement with Section 2.3 and can be explained by considering the evolution of the systems towards a stable state.

As shown in both graphs of Figure 5, smaller size fractions accelerate the evolution of the system and therefore lead to higher concentrations. A larger specific surface will favour diffusion of free alkali metals through the pores, cation exchange between the bulk solution and the EDL, and the hydration of unreacted particles. In other words, larger size fractions are likely to limit the release of bound alkali metals and further hydration, but they may also slow down the extraction of free alkali metals [5], especially those located in the small pores. In addition, the authors' impression was that from a certain size (2 – 4 mm), the crushed paste was not well immersed in water with L/S = 1, which can significantly affect the results. It is likely that the crushing technique also influences the effect of the size fraction. Finer size fractions are typically more difficult to obtain manually, which increases the water loss and the risk of carbonation.

The kinetics of the evolution is well illustrated by Figure 7. The concentrations increase with longer leaching times, but the rate decreases as the system gets closer to equilibrium. This can also be seen by comparing the two graphs of Figure 5: for a short leaching time (left), the difference between the size fractions is much more pronounced than for a longer one (right), which is a sign of convergence as all systems are brought closer to equilibrium.

The effect of the L/S depicted in Figure 6 is also in line with the theory described in Section 2.3.3 There is a larger difference for systems further from equilibrium (S5 – fine size fraction but short leaching time and L60 – long leaching time but coarse size fraction) compared to those closer (S60 – fine size fraction and long leaching time) when changing the L/S.

As mentioned in the introduction, other authors investigated the same parameters in previous publications [8,16–19], leading to the same conclusions. However, these results were subjected to caution since most studies focused on the pH of the extracted solution, which is known to be dramatically affected by portlandite dissolution [5,20]. Although studying alkali metals with CWE also presents some challenges as discussed in this paper, it allows to eliminate a major source of error in the interpretation of the data (non-representativity of $OH^-$ ions).

## 5.3 Influence of different methods used to determine the amount of pore solution on the final results

The results displayed in Table 7 show some important differences between the drying methods used in this study, and a significant influence on the calculated concentrations is reported in Table 10. Oven-drying at 105°C gives the largest mass loss, which was expected due to the decomposition of hydrates, especially ettringite, as explained in Section 2.3.4. When comparing the drying tests conducted at 40°C, it may be seen that higher values were reached in the desiccators than in the oven. The values in Table 10 are in agreement with the results reported by Natkunarajah et al. [20], who indicated that a 10% change in the free water content induced a 10% change in the back-calculated CWE results for concrete samples.

The difference between drying tests at 40°C can partly be attributed to different RH values, as illustrated in Figure 4. The lower the RH, the more adsorbed water was removed. In the oven, the RH was not stable and varied between 11 and 17%. In the desiccator, the RH decreased and stabilised around 1.5% due to the presence of silica gel. It should also be mentioned that according to Section 2.3.4, 1.5% RH may destabilise ettringite and therefore extract some chemically bound water. In addition, carbonation is also disturbing oven-drying measurements, and probably caused some mass gain for some samples. Indeed, the oven-dried samples were carbonated to a depth of 3 mm after 14 days at 40°C and to a depth of 6 mm after 5 days at 105°C, while the samples dried in the desiccators were not affected at all, as shown in Figure 3.

Since the time for reaching stable mass is longer for samples dried at 40°C, secondary hydration has to be considered. Figure 4 shows that mass loss during the first 24 hours of oven-drying is more than 8.5 wt.%, which corresponds to the removal of most free water so that further hydration is largely limited after 1 day. The mass loss with the desiccator method is almost as fast (around 7.5 wt.%), provided that enough silica gel is used (preliminary tests with only 200 g at the bottom gave only 3% loss during the first day). The air circulation created by the fans results in an additional

1 wt.% mass loss during the first 24 hours. However, the final value is very close to the one obtained without the fans, so it was decided not to use the fans in the other measurements. Note that drying can also be accelerated by using smaller samples, if they are large enough to be representative of the specimen.

Even though hydration is about 2.5 times faster at 40°C compared to 20°C (with an Arrhenius reaction rate [57]), further hydration at 40°C for 1 day would correspond to a sample tested at approximately 30 days instead of 28 days. In the authors' opinion, this cannot cause significant changes in the amount of evaporable water that is measured. However, it would if CWE must be performed at early age (e.g. at 7 days), as the change would no longer be negligible.

Solvent exchange methods lead to lower values, suggesting that not all evaporable water is removed. In contrast with drying methods, the measurements are not made at equilibrium since the final weight was taken after an arbitrary duration. However, for a given exchange time, the alcohol type influences the amount of water removed. This confirms the explanation of Plusquellec et al. [5] as to why CWE with alcohols yields lower concentrations, since the mass loss is correlated with the molecular size (methanol = 4.1 Å, ethanol = 5.2 Å, isopropanol = 5.8 Å [58]) and therefore with the degree of penetration in the smaller pores.

Table 17 gives an overview of the abilities and limitations of the drying methods investigated in the present work.

*Table 17: Overview of the abilities and limitations of the different methods investigated to determine the amount of pore solution.*

| Method | Expected degree of removal | | | Secondary hydration | Carbonation |
|---|---|---|---|---|---|
| | Free water | Adsorbed water | Chemically bound water | | |
| Oven-drying 105°C | Very high | Very high | Very high | ? | Yes |
| Oven-drying 40°C | Very high | Medium | Low | Limited | Yes |
| Desiccator + silica gel 40°C | Very high | High | Medium | Limited | No |
| Solvent exchange | High | Low | Very low | No | No |

In light of this, one must consider the most appropriate value to use in the CWE calculations. On the one hand, as stated in Section 2.3.4, evaporable water corresponds to a larger volume compared to free water, which would lead to an

underestimation of the concentrations. There are methods that can be used to distinguish between the two (e.g. sorption isotherms, DVS [39]), but they are time consuming and complex to carry out. On the other hand, if bound alkali metals are released as suggested in Section 5.1, considering free water only would lead to an overestimation of the concentrations.

Another point investigated in this study was the water loss during crushing. This is illustrated by $\Delta W_{crushing}$ in Table 8 which increased when reducing the size fraction, as a fine powder has a larger specific surface which facilitates water evaporation. Although the mass loss does affect the concentrations, the influence is rather limited as shown in Table 10, especially for large size fractions. Note that only oven-drying was performed on the crushed samples. However, the water loss during crushing is likely to be mainly capillary water, so a similar loss would apply to oven-drying values or desiccator values (at 40°C).

Finally, it must be mentioned that unlike for mortar or concrete [5], it is not possible to disregard completely $m_{ws}$ in Equation (2b) for paste (see Table 14), as the amount of pore solution in the sample is not negligible compared to the amount of leaching water.

## 5.4 Choice of the amount of pore solution

In the present study, the decision to assume that $m_{wp}$ was equal to the mass loss determined by drying in a desiccator with silica gel at 40°C was taken for three reasons: it allows more reproducible test conditions (due to a better control on the RH), it limits secondary hydration and it prevents carbonation. Even though this volume is larger than the free water content and may be overestimated compared to the amount that is relevant for free alkali metals, it can, to some extent, compensate for the fact that bound alkali metals are probably released.

The correction of the amount of pore solution proposed by Tuinukuafe et al. [36] brought CWE and PWE concentrations significantly closer to a 1:1 match. However, the method relies on accurate thermodynamic modelling and gel water partitioning for the system, which can be challenging for blended cements. Moreover, it is important to mention that the focus was different than the present work: Tuinukuafe et al. suggested a correction to improve the *precision* of extraction methods (how close the measurements are from each other), while the present paper discusses the *accuracy* of CWE (how close the measurements are from the true value).

As shown in Tables 10 and 14, the amount of pore solution is a critical parameter when determining the concentrations in the pore solution with CWE and the free alkali metal content with PWE, which confirm the results of previous studies

[5,20,36]. It is difficult to directly compare results across studies because different methods were used, e.g. oven-drying at 105°C [5,20] or thermodynamic modelling [36]. However, each method raised a different aspect to take into consideration, which highlights the importance of identifying the scope of the study.

## 5.5 Correspondence between CWE and PWE when comparing cement types

### 5.5.1 Pore solution concentration

The results plotted in Figure 8 show that both CWE tests (L5-1 and L90-1) capture the same trend as PWE, namely the lower alkalinity for CEM II/B-M compared to CEM I. It is well known that blended cements usually reduce the pH of the pore solution [59], and similar results have been reported with limestone and calcined clay blends [60].

Table 12 shows that the relative difference between the two cements is smaller with CWE than with PWE, whereas the leaching duration in CWE and the ion type seem to barely affect the difference. This seems to be due to an offset of the CWE results (the absolute differences are fairly constant), which lowers the relative difference. The results reported by De Weerdt et al. [21] for a Portland cement, pure and blended with 20% fly ash, respectively, show the same discrepancies (approx. 22% lower with PWE, but only 11% with CWE). However, Plusquellec et al. [5] found an almost constant relative drop between a CEM I and a CEM II/B-V (45% with PWE, 40% with CWE).

The representativity of the extracted solution has been extensively discussed in Section 5.1 for CWE. Since PWE is based on a direct extraction of the pore solution, measuring all ion concentrations (both cations and anions) would be a good quality check to verify the consistency of the results, although this was not done in the present study. As an example, a potential source of inconsistency is the presence of fine C-S-H of silicate anions in the extracted solution, which would require more cations to be in the solution to keep the charge balance. Moreover, the type of water expelled in PWE also influences the accuracy of the method [36,37], which should be considered when comparing it with CWE.

The discussions in the previous sections have emphasised the difficulty of obtaining a systematic match between CWE and PWE with the methods investigated in the present paper. Whether or not this is problematic depends on the intended use of the results. For the purpose of comparing binder types across each other, focusing on differences rather than on absolute concentrations may be

a way to overcome this issue. In this respect, it is a disadvantage if PWE and CWE lead to different relative differences. However, a somewhat constant absolute difference would enable some data processing of CWE results and the same quantitative conclusions as in PWE. It would therefore be useful to extend the comparison between the two methods to more blended cements.

### 5.5.2 Free alkali metal content

The free alkali metal contents calculated from PWE results on CEM I (Table 13) are in the range of values reported in the literature, as mentioned in Section 5.1.2 [3,5,56]. The values calculated from CWE L5-1 are higher, but still in a realistic range for both CEM I and CEM II/B-M. Finally, as mentioned above, the values obtained from CWE L90-1 are unrealistic. Overall, these results follow the trend of the pore solution concentrations, i.e. lower free alkali metal content for CEM II/B-M.

The conclusions regarding the evaluation of the free alkali metal content are essentially the same as for the pore solution concentrations. Both PWE and CWE indicate a smaller amount of free alkali metals in CEM II/B-M, but the relative differences between CEM I and CEM II/B-M differ depending on the extraction method.

# 6 Conclusion

The present paper focused on different parameters influencing the concentrations and the free contents of alkali metals in cement paste obtained by CWE. The work particularly focused on the accuracy of CWE results and discussed alternative drying methods to determine the amount of pore solution, compared to the conventional oven-drying at 105°C. CWE was performed on two cement types and the results were compared to those obtained by PWE, to explore the suitability of CWE with blended cements. The work has highlighted the following points:

- CWE is performed in a non-stable state, where the bulk solution is dramatically changed compared to the pore solution, due to the dilution of alkali metals and portlandite dissolution in water during leaching. The evolution of the system over time is likely to include the release of alkali metals that were initially bound to the hydrates, so that the final state is very different from what it would be in a simple dilution of the pore solution. This hypothesis still needs to be verified experimentally.
- The effects of the different test parameters, namely the size fraction, the leaching duration and the L/S depend on their effects on the equilibrium:
  - A smaller size fraction accelerates the evolution towards equilibrium, leading to higher concentrations of alkali metals

  - A longer leaching duration brings the system closer to equilibrium, with a similar effect on the alkali metals
  - A higher L/S shifts the equilibrium even more, so that the total amount of alkali metals extracted (free and bound) will eventually be still larger.
- There is some water loss during crushing. However, the influence on both the concentrations and the free contents of alkali metals is limited
- The method used to determine the amount of pore solution is a critical parameter in the calculations, which strongly influences the correspondence between CWE and PWE, both for the concentrations in the pore solution and the free alkali metal contents.
- The drying methods used to determine the amount of pore solution led to a value larger than the free water content, due to the release of adsorbed water. However, to some extent this overestimated volume can compensate for the probable release of bound alkali metals when calculating the concentrations in the pore solution
- CWE performed in a consistent way seems able to capture the same trends as PWE for different cement types, although further work is needed to quantify the difference between both methods for blended cements.
- Several sources of inaccuracy seem to exist for both PWE and CWE, which eventually affect the precision of extraction methods. It is therefore crucial to identify the purpose of the study, to make consistent use of the results.

Based on these conclusions, the authors propose the following recommendations to improve CWE accuracy:

- Choose a short leaching time, ideally 5 min
- Select a size fraction below 1 mm, which is convenient to obtain with the available equipment in the laboratory
- Use L/S = 1
- Use the mass loss determined by drying in a desiccator containing silica gel and stored at 40°C as the amount of pore solution in CWE calculations
- Perform both PWE and CWE on reference samples cast with the same mix and cured in the same way to document the difference between the two methods.

As discussed in this paper, other choices may be more appropriate if the purpose is different, e.g. a direct quantitative comparison of PWE and CWE results.

# Acknowledgements

The work presented is part of an industrial PhD project financed by the Danish Road Directorate and a joint grant from Innovation Fund Denmark (Innovationsfonden) and Realdania under the program Circular Built Environment. This financial support is gratefully acknowledged. The Research and Quality Centre of Aalborg Portland, in particular Lasse Frølich, are warmly thanked for supplying the cements, hosting Pore Water Extraction tests, and performing the XRF analysis. The authors would also like to thank Professor Georgios M. Kontogeorgis (Department of Chemical and Biochemical Engineering, DTU) for the fruitful discussions on electrical double layers. Finally, we would like to thank the contribution of three anonymous reviewers, which significantly helped to improve the quality of the present paper.

# CRediT authorship contribution statement

Maxime Ranger: Conceptualisation, Methodology, Formal analysis, Investigation, Writing – original draft, Visualisation.

Marianne Tange Hasholt: Conceptualisation, Methodology, Writing – review and editing, Supervision, Funding acquisition.

Ricardo Antonio Barbosa: Conceptualisation, Writing – review and editing, Supervision, Funding acquisition.

# References

[1] A.M. Boddy, R.D. Hooton, M.D.A. Thomas, Effect of product form of silica fume on its ability to control alkali-silica reaction, Cement and Concrete Research. 30 (2000) 1139–1150. https://doi.org/10.1016/S0008-8846(00)00297-0.

[2] H. Kagimoto, M. Sato, M. Kawamura, Evaluation of the degree of deterioration in AAR damaged concretes and analysis of their pore solutions, in: M.-A. Bérubé, B. Durand, B. Fournier (Eds.), Proceedings of the 11th International Conference on Alkali-Aggregate Reaction in Concrete, Québec, 2000: pp. 859–868.

[3] P. Rivard, M.-A. Bérubé, J.P. Ollivier, G. Ballivy, Decrease of pore solution alkalinity in concrete tested for alkali-silica reaction, Materials and Structures. 40 (2007) 909–921. https://doi.org/10.1617/s11527-006-9191-z.

[4] M.C. Alonso, J.L. García Calvo, Walker C, Naito M, S. Pettersson, I. Puigdomenech, M.A. Cuñado, M. Vuorio, H. Weber, H. Ueda, K. Fujisaki, Development of an accurate pH measurement methodology for the pore fluids of low pH cementitious materials, Svensk Kärnbränslehantering (Swedish Nuclear Fuel and Waste Management Company), Stockholm, 2012. Report R-12-02, ISSN 1402-3091.

[5] G. Plusquellec, M.R. Geiker, J. Lindgård, J. Duchesne, B. Fournier, K. De Weerdt, Determination of the pH and the free alkali metal content in the pore solution of concrete: Review and experimental comparison, Cement and Concrete Research. 96 (2017) 13–26. https://doi.org/10.1016/j.cemconres.2017.03.002.

[6] P. Longuet, L. Burglen, A. Zelwer, La phase liquide du ciment hydraté (in French), Revue Des Matériaux de Construction et de Travaux Publics. 676 (1973) 35–41.

[7] A. Behnood, K. van Tittelboom, N. de Belie, Methods for measuring pH in concrete: A review, Construction and Building Materials. 105 (2016) 176–188. https://doi.org/10.1016/j.conbuildmat.2015.12.032.

[8] L. Li, J. Nam, W.H. Hartt, Ex situ leaching measurement of concrete alkalinity, Cement and Concrete Research. 35 (2005) 277–283. https://doi.org/10.1016/j.cemconres.2004.04.024.

[9] M.-A. Bérubé, C. Tremblay, Chemistry of pore solution expressed under high pressure - Influence of various parameters and comparison with the hot-water extraction method, in: M. Tang, N. Deng (Eds.), Proceedings of the 12th International Conference on Alkali-Aggregate Reaction in Concrete, Beijing, 2004: pp. 833–842.

[10] T. Chappex, K. Scrivener, Alkali fixation of C-S-H in blended cement pastes and its relation to alkali silica reaction, Cement and Concrete Research. 42 (2012) 1049–1054. https://doi.org/10.1016/j.cemconres.2012.03.010.

[11] J. Duchesne, M.-A. Bérubé, Evaluation of the validity of the pore solution expression method from hardened cement pastes and mortars, Cement and Concrete Research. 24 (1994) 456–462. https://doi.org/10.1016/0008-8846(94)90132-5.

[12] M. Cyr, P. Rivard, F. Labrecque, A. Daidié, High-pressure device for fluid extraction from porous materials: Application to cement-based materials,

Journal of the American Ceramic Society. 91 (2008) 2653–2658. https://doi.org/10.1111/j.1551-2916.2008.02525.x.

[13] B. Lothenbach, Thermodynamic equilibrium calculations in cementitious systems, Materials and Structures. 43 (2010) 1413–1433. https://doi.org/10.1617/s11527-010-9592-x.

[14] L. Montanari, J. Tanesi, H. Kim, A. Ardani, Influence of loading pressure and sample preparation on ionic concentration and resistivity of pore solution expressed from concrete samples, Journal of Testing and Evaluation. 49 (2020). https://doi.org/10.1520/JTE20190765.

[15] R.S. Barneyback, S. Diamond, Expression and analysis of pore fluids from hardened cement pastes and mortars, Cement and Concrete Research. 11 (1981) 279–285. https://doi.org/10.1016/0008-8846(81)90069-7.

[16] V. Pavlík, Water extraction of chloride, hydroxide and other ions from hardened cement pastes, Cement and Concrete Research. 30 (2000) 895–906. https://doi.org/10.1016/S0008-8846(00)00261-1.

[17] V. Räsänen, V. Penttala, The pH measurement of concrete and smoothing mortar using a concrete powder suspension, Cement and Concrete Research. 34 (2004) 813–820. https://doi.org/10.1016/j.cemconres.2003.09.017.

[18] P.Y. Loh, P. Shafigh, H.Y.B. Katman, Z. Ibrahim, S. Yousuf, pH measurement of cement-based materials: the effect of particle size, Applied Sciences (Switzerland). 11 (2021) 8000. https://doi.org/10.3390/app11178000.

[19] W.C. Wang, W.H. Huang, M.Y. Lee, H.T.H. Duong, Y.H. Chang, Standardised procedure of measuring the pH value of cement matrix material by ex-situ leaching method (ESL), Crystals (Basel). 11 (2021) 436. https://doi.org/10.3390/cryst11040436.

[20] K. Natkunarajah, K. Masilamani, S. Maheswaran, B. Lothenbach, D.A.S. Amarasinghe, D. Attygalle, Analysis of the trend of pH changes in concrete pore solution during the hydration by various analytical methods, Cement and Concrete Research. 156 (2022) 106780. https://doi.org/10.1016/j.cemconres.2022.106780.

[21] K. De Weerdt, P. Hemstad, H. Justnes, T. Østnor, T.F. Rønning, J. Lindgård, Fundamental study on ASR kinetics – effect of temperature on aggregate reactivity and pore water composition, in: A.L. Batista, A.S.

Silva, I. Fernandes, L.O. Santos, J. Custódio, C. Serra (Eds.), Proceedings of the 16th International Conference on Alkali-Aggregate Reaction in Concrete, Volume I, Lisbon, 2021: pp. 837–849.

[22] H.F.W. Taylor, Distribution of sulfate between phases in Portland cement clinkers, Cement and Concrete Research. 29 (1999) 1173-1179. https://doi.org/10.1016/S0008-8846(98)00241-5.

[23] H.F.W. Taylor, Modification of the Bogue calculation, Advances in Cement Research. 2 (1989) 73-77. https://doi.org/10.1680/adcr.1989.2.6.73.

[24] S. Chatterji, M. Kawamura, Electrical double layer, ion transport and reactions in hardened cement paste, Cement and Concrete Research. 22 (1992) 774–782. https://doi.org/10.1016/0008-8846(92)90101-Z.

[25] B. Lothenbach, A. Nonat, Calcium silicate hydrates: Solid and liquid phase composition, Cement and Concrete Research. 78 (2015) 57–70. https://doi.org/10.1016/j.cemconres.2015.03.019.

[26] P.T. Nguyen, O. Amiri, Study of electrical double layer effect on chloride transport in unsaturated concrete, Construction and Building Materials. 50 (2014) 492–498. https://doi.org/10.1016/j.conbuildmat.2013.09.013.

[27] G.M. Kontogeorgis, S. Kiil, Introduction to applied colloid and surface chemistry, John Wiley and Sons, Inc, 2016.

[28] S.Y. Hong, F.P. Glasser, Alkali binding in cement pastes: Part I. The C-S-H phase, Cement and Concrete Research. 29 (1999) 1893–1903. https://doi.org/10.1016/S0008-8846(99)00187-8.

[29] E. L'Hôpital, B. Lothenbach, K. Scrivener, D.A. Kulik, Alkali uptake in calcium alumina silicate hydrate (C-A-S-H), Cement and Concrete Research. 85 (2016) 122–136. https://doi.org/10.1016/j.cemconres.2016.03.009.

[30] J. Duchesne, M.-A. Bérubé, A reply to a discussion by S. Chatterji of the paper: "The effectiveness of supplementary cementing materials in suppression expansion due to the ASR. Part 2. Pore solution chemistry," Cement and Concrete Research. 24 (1994) 1579–1581. https://doi.org/10.1016/0008-8846(94)90176-7.

[31] W. Stumm, Chemistry of the solid-water interface: Processes at the mineral-water and particle-water interface in natural systems, John Wiley & Sons, Inc, 1992.

[32] H. Friedmann, O. Amiri, A. Aït-Mokhtar, Physical modeling of the electrical double layer effects on multispecies ions transport in cement-based materials, Cement and Concrete Research. 38 (2008) 1394–1400. https://doi.org/10.1016/j.cemconres.2008.06.003.

[33] O. Levenspiel, Chemical Reaction Engineering, Third Edition, John Wiley & Sons, Inc, 1998.

[34] K. De Weerdt, G. Plusquellec, A. Belda Revert, M.R. Geiker, B. Lothenbach, Effect of carbonation on the pore solution of mortar, Cement and Concrete Research. 118 (2019) 38–56. https://doi.org/10.1016/j.cemconres.2019.02.004.

[35] M.C. Castellote, M.C. Alonso, C. Andrade, Determination of the $OH^-$ content in the aqueous phase of hardened cementitious materials by an empirical leaching method, Materiales De Construccion. 52 (2002) 39–56. https://doi.org/10.3989/mc.2002.v52.i265.343.

[36] A. Tuinukuafe, K.S.T. Chopperla, W.J. Weiss, J.H. Ideker, O.B. Isgor, Estimating $Na^+$ and $K^+$ concentrations of the pore solution based on ex-situ leaching tests and thermodynamic modeling, RILEM Technical Letters. 7 (2022) 88–97. https://doi.org/10.21809/rilemtechlett.2022.164.

[37] J. Xu, K. Zhang, L. Chen, X. Zhou, Q. Yuan, Effect of pore solution expression on solid composition of cement paste, Advances in Cement Research. 34 (2022) 301–310. https://doi.org/10.1680/jadcr.21.00122.

[38] T.C. Hansen, Physical structure of hardened cement paste. A classical approach, Materials and Structures. 19 (1986) 423–436. https://doi.org/10.1007/BF02472146.

[39] O. Linderoth, Binding of moisture in fly ash blended Portland cement paste and mortar: Impact of replacement level and curing temperature, PhD Thesis, Lund University, 2018.

[40] J.R. Rumble, CRC Handbook of Chemistry and Physics, 102nd Edition (Internet Version 2021), 102nd Edition, CRC Press/Taylor & Francis, Boca Raton, FL, 2021. https://hbcp.chemnetbase.com/ (accessed February 25, 2022).

[41] C. Gallé, Effect of drying on cement-based materials pore structure as identified by mercury intrusion porosimetry A comparative study between oven-, vacuum-, and freeze-drying, Cement and Concrete Research. 31 (2001) 1467–1477. https://doi.org/10.1016/S0008-8846(01)00594-4.

[42] A. Korpa, R. Trettin, The influence of different drying methods on cement paste microstructures as reflected by gas adsorption: Comparison between freeze-drying (F-drying), D-drying, P-drying and oven-drying methods, Cement and Concrete Research. 36 (2006) 634–649. https://doi.org/10.1016/j.cemconres.2005.11.021.

[43] Q. Zhou, F.P. Glasser, Thermal stability and decomposition mechanisms of ettringite at <120°C, Cement and Concrete Research. 31 (2001) 1333–1339. https://doi.org/10.1016/S0008-8846(01)00558-0.

[44] L.G. Baquerizo, T. Matschei, K. Scrivener, Impact of water activity on the stability of ettringite, Cement and Concrete Research. 79 (2016) 31–44. https://doi.org/10.1016/j.cemconres.2015.07.008.

[45] K. Scrivener, R. Snellings, B. Lothenbach, A practical guide to microstructural analysis of cementitious materials, CRC Press, 2016.

[46] Paul Scherer Institut, GEM-Selektor v.3, https://gems.web.psi.ch/, 2021 (accessed October 21, 2022).

[47] D.A. Kulik, T. Wagner, S.V. Dmytrieva, G. Kosakowski, F.F. Hingerl, K.V. Chudnenko, U.R. Berner, GEM-Selektor geochemical modeling package: revised algorithm and GEMS3K numerical kernel for coupled simulation codes, Computational Geosciences. 17 (2013) 1–24. https://doi.org/10.1007/s10596-012-9310-6.

[48] T. Wagner, D.A. Kulik, F.F. Hingerl, S.V. Dmytrieva, GEM-Selektor geochemical modeling package: TSolMod library and data interface for multicomponent phase models, Canadian Mineralogist. 50 (2012) 1173–1195. https://doi.org/10.3749/canmin.50.5.1173.

[49] L.J. Parrot, D.C. Killoh, Prediction of cement hydration, British Ceramic Proceedings. 35 (1984) 41–53.

[50] B. Lothenbach, T. Matschei, G. Möschner, F.P. Glasser, Thermodynamic modelling of the effect of temperature on the hydration and porosity of Portland cement, Cement and Concrete Research. 38 (2008) 1–18. https://doi.org/10.1016/j.cemconres.2007.08.017.

[51] T. Thoenen, W. Hummel, U. Berner, E. Curti, The PSI/Nagra Chemical Thermodynamic Database 12/07, PSI Report 14-04, Villigen PSI, Switzerland, 2014.

[52] B. Lothenbach, D.A. Kulik, T. Matschei, M. Balonis, L. Baquerizo, B. Dilnesa, G.D. Miron, R.J. Myers, Cemdata18: A chemical thermodynamic database for hydrated Portland cements and alkali-activated materials, Cement and Concrete Research. 115 (2019) 472–506. https://doi.org/10.1016/j.cemconres.2018.04.018.

[53] D.A. Kulik, Improving the structural consistency of C-S-H solid solution thermodynamic models, Cement and Concrete Research. 41 (2011) 477–495. https://doi.org/10.1016/j.cemconres.2011.01.012.

[54] M. Ranger, M.T. Hasholt, Datasets for journal article "Pore solution alkalinity of cement paste as determined by Cold Water Extraction," DTU Data. (2022). https://doi.org/10.11583/DTU.19137326.

[55] Chemistry LibreTexts, Propagation of Error, https://chem.libretexts.org/@go/page/353, 2020 (accessed February 26, 2022).

[56] C. Drolet, J. Duchesne, B. Fournier, Validation of the alkali contribution by aggregates to the concrete pore solution, Cement and Concrete Research. 98 (2017) 10–23. https://doi.org/10.1016/j.cemconres.2017.04.001.

[57] P. Kumar Mehta, P. Monteiro, Concrete: microstructure, properties, and materials, McGraw-Hill Education, 2014.

[58] B. Van der Bruggen, J. Schaep, D. Wilms, C. Vandecasteele, Influence of molecular size, polarity and charge on the retention of organic molecules by nanofiltration, Journal of Membrane Science. 156 (1999) 29–41. https://doi.org/10.1016/S0376-7388(98)00326-3.

[59] A. Vollpracht, B. Lothenbach, R. Snellings, J. Haufe, The pore solution of blended cements: a review, Materials and Structures. 49 (2016) 3341–3367. https://doi.org/10.1617/s11527-015-0724-1.

[60] Q.D. Nguyen, M.S.H. Khan, A. Castel, Engineering properties of limestone calcined clay concrete, Journal of Advanced Concrete Technology. 16 (2018) 343–357. https://doi.org/10.3151/jact.16.343.

Paper II

# Cold Water Extraction for determination of the free alkali metal content in blended cement pastes

Maxime Ranger [a,b], Marianne Tange Hasholt [b]

[a] Department of Environmental and Resource Engineering,
Technical University of Denmark (DTU), 2800 Kgs. Lyngby, Denmark

[b] Danish Road Directorate, 1577 Copenhagen V, Denmark

*Published in CEMENT (2023), Volume 13, p. 100079*
*DOI: 10.1016/j.cement.2023.100079 – Licence CC BY 4.0*

*Note: In the original published version of this article, there is a scaling error in Figure 10 regarding the free alkali contribution of SCMs. This thesis shows a corrected version of Figure 10.*

# Abstract

In this work, Cold Water Extraction (CWE) was performed on blended cement pastes to extract the pore solution and determine the free alkali metal content. To better understand CWE results, the reactivity of cementitious materials was also investigated, complemented by TGA and quantitative XRD analysis. The study aimed at being generic to assess the suitability of the methods, and included 9 SCMs with various compositions: limestone, coal fly ash, two calcined clays, two biomass ashes, sewage sludge ash, crushed brick and glass beads.

The study highlighted the importance of assessing the reactivity of SCMs in parallel to performing CWE, as this contributes to a more certain interpretation of the results. In general, results obtained with CWE were consistent with the existing literature about the effect of binder composition on the free alkali metal content. From a practical view, CWE and SCM reactivity tests could be performed with basic laboratory equipment and appeared to be applicable to both traditional and alternative SCMs.

# Keywords

Pore Solution, Cold Water Extraction, Alkalis, Blended Cement, Cement Paste

# 1 Introduction

The use of supplementary cementitious materials (SCMs) is one of the most effective measures to lower $CO_2$ emissions associated with the production of concrete. However, an expected production decline of traditional SCMs such as coal fly ash or blast furnace slag has highlighted the necessity to introduce alternative SCMs [1]. These alternatives represent a broader range of materials with varying compositions, and they are often produced locally in limited amounts [2]. There is therefore a need for generic test methods applicable to a wide range of SCMs [3], to enable the use of marginal materials that do not fit in the current standards [4]. Historically, SCMs have been used to improve concrete properties and especially durability [5], which can also contribute to limit $CO_2$ emissions and material use on a life-cycle perspective [1,6]. As an example, traditional SCMs are often incorporated in concrete to mitigate deleterious alkali-silica reaction (ASR) [7].

ASR is a chemical reaction starting with the dissolution of amorphous silica from aggregates, caused by a high pH in the pore solution. The efficacy of SCMs to mitigate ASR is generally associated with a lower alkalinity of the pore solution

[8]. Because of complex dissolution and precipitation reactions, the amount of free alkalis in the pore solution cannot be easily forecast for blended systems. ASTM C311 is the only standardised procedure to determine available alkalis from SCMs, however the results do not correlate with the direct analysis of the pore solution of hardened cement paste [9,10]. The pore solution is often studied with Pore Water Extraction (PWE), a method which consists in drawing out the liquid phase by pressing a sample [11]. However, PWE requires special equipment which is not available in all laboratories. Cold Water Extraction (CWE) is an alternative to PWE based on leaching of a crushed sample, which can be carried out with standard laboratory equipment. To date in the literature, CWE has mainly been used to determine the free alkali metal content of concrete where PWE could not be used due to an insufficient amount of free water [12,13].

The present work explores the possibility of using CWE to study blended cement pastes. More specifically, it is intended to address the following research question: to what extend does CWE capture the influence of the binder composition on the free alkali metal content of blended cement pastes? The study aims at being generic, with the intention to develop an approach that can be generalised to as many SCMs as possible. For this reason, various traditional and alternative SCMs are included in the experimental matrix. In addition, the reactivity of cementitious materials is assessed with different methods (TGA, QXRD and $R^3$ reactivity tests) and used to interpret free alkali metal results.

# 2 Background

## 2.1 Terminology

The terminology related to alkalis used in the present paper is presented in Figure 1.

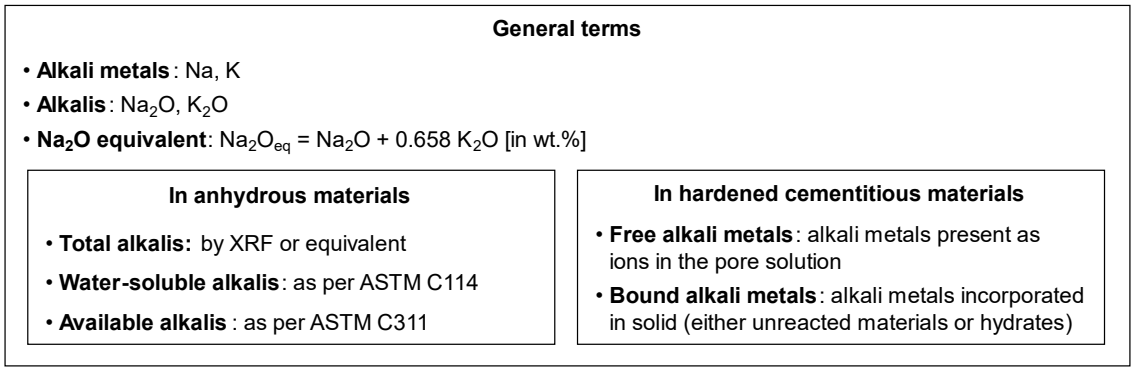


*Figure 1: Terminology related to alkalis used in the present paper.*

More terms than the ones mentioned in Figure 1 can be found in the literature. For example, “rapidly-soluble” [14] or “readily-soluble” [15] alkalis were used to designate alkali sulphates. Some terms were also used with a different meaning, such as available alkalis. Shehata and Thomas [16] defined as “available” the alkalis released in a solution maintained at a certain alkali concentration, for example the minimum concentration necessary to sustain ASR (around 250 mmol/L).

## 2.2 Screening of SCM reactivity

The work carried out by RILEM TC 267-TRM concluded that among existing reactivity tests, results obtained with the $R^3$ method showed the best correlation with the 28-day compressive strength [17]. The correlation was confirmed across a wide range of traditional SCMs [18]. The $R^3$ method is based on a paste where water is mixed with portlandite, SCM, calcite, alkalis and sulphates. The paste composition aims at simulating the environment of a Portland cement paste, where the contribution of the clinker is simplified [19]. Different parameters can then be measured to quantify the reactivity of an SCM: cumulative heat release (isothermal calorimetry), bound water (oven-drying) and chemical shrinkage. Portlandite consumption can also be measured by thermogravimetry to help distinguish between pozzolanic and latent hydraulic SCMs, however it does not correlate well with the compressive strength [20,21].

## 2.3 The impact of SCMs on free alkalis

The ionic composition of the pore solution is usually dominated by hydroxide ions ($OH^-$), which are counterbalanced by alkali metal ions ($Na^+$ and $K^+$) [10,22,23]. Once alkali metals are dissolved, they can either remain as ions in the pore solution or become bound to hydrates. Indeed, C-S-H adsorbs cations ($Ca^{2+}$ or $Na^+/K^+$) to neutralise its negative surface charge [24]. The alkali metal binding capacity of C-S-H depends on the thermodynamic equilibrium with the pore solution and is enhanced by a lower Ca/Si and a higher alkalinity of the pore solution [25,26]. When silica-rich SCMs are used, the pozzolanic C-S-H formed has typically a lower Ca/Si compared to when Portland cement is used alone, therefore more alkali metals can be bound [27]. Vollpracht et al. [28] summarised pore solution data and highlighted the efficacy of traditional pozzolanic SCMs (fly ash, silica fume and metakaolin) to lower the alkalinity of the pore solution. Conversely, some SCMs may lead to a higher alkalinity, as it is the case for some high calcium (class C) and/or high-alkali fly ashes [29].

Some analytical relationships have been proposed in the literature to calculate the hydroxide ion concentration in the pore solution. Helmuth et al. [30] derived an empirical relationship which is a function of the total $Na_2O_{eq}$ (in wt.%) and the water-to-cement ratio (w/c), as shown in Equation (1).

$$[OH^-] = \frac{0.339 \cdot Na_2O_{eq}}{w/c} + 0.022 \pm 0.06\, mol/L \quad (1)$$

Later, Thomas [8] observed a linear correlation between the $OH^-$ concentration and a chemical index of the binder, $Na_2O_{eq} \times CaO / (SiO_2)^2$. However, this relationship does not account for the complexity and the diversity of chemical reactions taking place in cement pastes containing SCMs, which strongly affects the correlation [8,10]. Kawabata and Yamada [31] proposed a model to determine the $OH^-$ concentration based on the degree of reaction of each phase and 3 factors: the amount of C-(A)-S-H, the Ca/Si of C-(A)-S-H, and the amount of free water. However, these parameters require the use of additional analytical techniques (e.g. QXRD, selective dissolution or SEM-EDS), which seems to limit its application at a large scale.

## 2.4 Cold Water Extraction

As stated in the introduction, CWE is an alternative to PWE to extract the pore solution of hardened specimens. CWE includes four main steps: crushing of the material, leaching, filtration and sampling. When water is used as leaching liquid, which is often the case in the literature [12,13,32–34], portlandite is dissolved in the solution. As a result, the original hydroxide ion concentration in the pore solution is significantly affected, and cannot be measured accurately directly. For this reason, CWE mainly aims at studying alkali metals. An essential parameter is the amount of pore solution, necessary to calculate the concentrations. As pointed out in previous publications [33,34], a change of 10% in the amount of pore solution results in approximately 10% change for the concentrations.

Several studies reported a significant mismatch between CWE and PWE results [32,34,35]. Ranger et al. [34] investigated different techniques to determine the amount of pore solution in paste samples, but CWE results were systematically higher compared to PWE. However, the authors emphasised the possibility of alkali metals being released from hydrates, increasing the concentrations in the extracted solution. Tuinukuafe et al. [35] proposed a method to reconcile CWE and PWE results, by correcting the volume extracted in PWE based on thermodynamic modelling. These studies enlightened the challenges of precision and accuracy that extraction methods pose.

It is important to mention that CWE shifts the thermodynamic equilibrium of the system due to the addition of water. With only 5 min of leaching, it is unlikely that a new equilibrium is reached, so that the measured value represents a state somewhere between two equilibria. To soften this issue, one could use an alkaline leaching liquid to limit the thermodynamic mismatch. Shehata and Thomas [16] implemented such method and let the systems equilibrate before analysing the leaching solution. 3 months were necessary to reach equilibrium, which significantly extended the test duration compared to regular CWE.

# 3 Materials and methods

## 3.1 Raw materials

In this study, two types of Portland cement (PC) were used: a low-alkali CEM I 52.5 N (0.58 wt.% $Na_2O_{eq}$) and a high-alkali CEM I 52.5 R (1.23 wt.% $Na_2O_{eq}$). In the following, they are denoted as PC-LA and PC-HA, respectively. In addition, 9 different SCMs were tested in combination with the two PC: limestone filler (LL), coal fly ash (FA), two calcined clays (CC1 and CC2), two biomass ashes (BA1 and BA2), sewage sludge ash (SSA) pre-treated to recover the phosphorous content [36], crushed brick (CB) obtained by milling old bricks from demolished buildings and soda-lime glass beads (GB). Some glass beads were also crushed in a ball-mill to achieve a finer particle size ($d_{50}$ = 9.3 µm, denoted as GB_f). The chemical compositions were measured by X-ray fluorescence (XRF) on powders sieved below 63 µm (Malvern Panalytical Zetium spectrometer). The particle size distribution was measured with a laser diffractometer (Malvern Mastersize 2000). The values are presented in Table 1. The mineral compositions determined by quantitative X-ray diffraction (QXRD, Rietveld) are given in Table 2 for PC and Table 3 for SCMs.

*Table 1: Chemical composition of the materials (in wt.%) and physical characteristics.*

| Oxide | Portland cement | | Limestone | Fly ash | Calcined clay | | Biomass ash | | Sewage sludge ash | Crushed brick | Glass beads |
|---|---|---|---|---|---|---|---|---|---|---|---|
| | PC-LA | PC-HA | LL | FA | CC1 | CC2 | BA1 | BA2 | SSA | CB | GB / GB_f |
| $SiO_2$ | 19.2 | 19.2 | 2.0 | 56.2 | 46.6 | 49.0 | 25.5 | 23.2 | 56.8 | 63.4 | 72.0 |
| $Al_2O_3$ | 5.2 | 5.1 | 0.4 | 23.8 | 17.4 | 17.3 | 4.8 | 4.3 | 8.4 | 11.2 | 0.7 |
| $Fe_2O_3$ | 3.67 | 2.99 | 0.12 | 6.9 | 9.58 | 9.74 | 1.8 | 1.93 | 19.57 | 4.32 | 0.17 |
| MgO | 1.0 | 2.4 | 0.3 | 1.8 | 2.5 | 2.5 | 3.5 | 4.0 | 0.9 | 1.2 | 3.8 |
| CaO | 63.4 | 60.6 | 54.2 | 3.9 | 9.7 | 10.1 | 34.1 | 30.9 | 1.4 | 9.0 | 9.1 |
| $Na_2O$ | 0.33 | 0.45 | 0.03 | 0.49 | 0.92 | 0.81 | 0.87 | 0.71 | 1.03 | 2.81 | 13.63 |
| $K_2O$ | 0.38 | 1.18 | 0.06 | 1.64 | 2.47 | 2.66 | 4.93 | 7.35 | 2.43 | 0.43 | 0.21 |
| $TiO_2$ | 0.19 | 0.35 | 0.03 | 0.93 | 0.97 | 0.97 | 0.28 | 0.29 | 1.54 | 0.63 | 0.07 |
| $P_2O_5$ | 0.26 | 0.08 | 0.11 | 1.02 | 0.21 | 0.24 | 2.91 | 3.03 | 2.97 | 0.15 | 0.01 |
| $SO_3$ | 3.14 | 3.81 | 0.08 | 0.79 | 0.97 | 0.98 | 4.58 | 12.66 | 0.38 | 0.63 | 0.24 |
| $Na_2O_{eq}$ | 0.58 | 1.23 | 0.07 | 1.57 | 2.54 | 2.55 | 4.12 | 5.55 | 2.63 | 2.91 | 13.77 |
| LOI (EN 196-2) | 3.21 | 3.56 | 42.52 | 1.57 | 7.97 | 4.94 | 15.83 | 10.26 | 3.77 | 5.37 | 0.09 |
| Sum | 100.1 | 99.9 | 100.0 | 99.6 | 99.8 | 99.7 | 99.8 | 99.6 | 99.4 | 99.8 | 100.0 |
| Density [kg/m³] | 3150 | 3130 | 500 | 2300 | 2700 | 2700 | 2620 | 2650 | 2650 | 2640 | 2500 |
| $d_{50}$ [µm] | 14 | 10.7 | 3.8 | 18 | 9.6 | 39.4 | 15.5 | 70.2 | 11.1 | 42.8 | 67.0 / 9.3 |

*Table 2: Mineralogical composition of Portland cements (in wt.%, normalised to 100% crystalline) determined by QXRD analysis. The numbers are given with one decimal, but the uncertainty is estimated to be around 1 wt.%.*

| Phase | ICSD nb | PC-LA | PC-HA |
|---|---|---|---|
| $C_3S$ (M1) | From [37] | 48.0 | 41.9 |
| $C_3S$ (M3) | 94742 | 17.2 | 21.7 |
| $C_2S$ | 81096 | 10.2 | 8.3 |
| $C_3A$ | 1841 | 3.6 | 6.6 |
| $C_4AF$ | 98836 | 10.8 | 10.2 |
| Bassanite | 79529 | 2.7 | 3.0 |
| Calcite | 73446 | 4.5 | 3.4 |
| Anhydrite | 15876 | 2.8 | - |
| Spurrite | 4332 | - | 3.0 |
| Quartz | 174 | 0.3 | 0.6 |
| Periclase | 9863 | - | 1.1 |
| Aphthitalite | 26018 | - | 0.1 |
| $R_{wp}$ | | 7.85 | 8.11 |

*Table 3: Mineralogical composition of SCMs (in wt.%) determined by QXRD analysis. The numbers are given with one decimal, but the uncertainty is estimated to be around 1 wt.%.*

| Phase | ICSD nb | LL | FA | CC1 | CC2 | BA1 | BA2 | SSA | CB | GB/ GB_f |
|---|---|---|---|---|---|---|---|---|---|---|
| Quartz | 174 | 0.6 | 11.7 | 5.2 | 7.0 | 4.1 | 5.3 | 21.1 | 32.7 | - |
| Calcite | 73446 | 95.3 | - | 9.1 | 5.6 | 16.3 | 10.0 | - | 9.0 | - |
| Mullite | 158098 | - | 16.2 | - | - | - | - | - | - | - |
| Hematite | 201096 | - | 0.5 | 0.4 | 0.6 | - | - | 15.4 | 1.3 | - |
| Magnetite | 195702 | - | 0.5 | - | - | - | - | - | - | - |
| Anhydrite | 15876 | - | - | 0.4 | 0.5 | 4.2 | 8.9 | - | - | - |
| Syngenite | 157072 | - | - | - | - | - | 14.3 | - | - | - |
| Illite | 90144 | - | - | 5.0 | 6.1 | - | - | - | - | - |
| Paragonite | 158607 | - | - | 7.7 | 2.0 | - | - | - | - | - |
| Rutile | 93097 | - | - | 0.1 | 0.4 | - | 0.2 | - | - | - |
| Microcline | 100495 | - | - | - | - | 3.2 | - | 18.8 | - | - |
| | 202423 | - | - | - | - | - | - | - | 17.1 | - |
| Anorthite | 86327 | - | - | - | - | 1.5 | - | 8.2 | - | - |
| Albite | 87660 | - | - | - | - | - | - | 4.7 | - | - |
| | 87658 | - | - | - | - | - | - | - | 16.8 | - |
| Aluminium phosphate | 262932 | - | - | - | - | - | - | 1.4 | - | - |
| Diopside | 16905 | - | - | - | - | - | - | - | 3.1 | - |
| Sanidine | 69965 | - | - | - | - | 1.1 | - | - | - | - |
| Portlandite | 202220 | - | - | - | - | 1.7 | 10.7 | - | - | - |
| Sylvite | 154214 | - | - | - | - | 0.7 | 0.8 | - | - | - |
| $KAlCl_4$ | 1704 | - | - | - | - | 4.4 | - | - | - | - |
| Halite | 41411 | - | - | - | - | 0.4 | - | - | - | - |
| Calcium chloride | 56769 | - | - | - | - | - | 0.4 | - | - | - |
| Amorphous/Unknown | | 4.1 | 71.0 | 72.1 | 77.9 | 62.4 | 47.9 | 30.4 | 20.0 | 100.0 |
| $R_{wp}$ | | 8.79 | 2.89 | 3.20 | 3.83 | 6.49 | 6.23 | 3.95 | 8.37 | - |

## 3.2 Water-soluble alkalis

The quantification of water-soluble alkalis was done according to ASTM C114. 25.0 g of SCM was mixed with 250 mL of deionised water and stirred mechanically for 10 min with a magnet. The solution was then vacuum filtered with a Büchner setup, using a cellulose filter with 8 µm pore size. 10 mL of the filtrate was then diluted by a factor of 2 and acidified with 0.5 mL of nitric acid

32.5%. The final solution was analysed with ICP-OES (Varian 720-ES) to determine the concentrations of Na and K.

## 3.3 Available alkalis

Available alkalis were measured as per ASTM C311. 5.0 g of SCM was pre-mixed with 2.0 g of calcium hydroxide (laboratory grade). 10 mL of deionised water was added, and the mix was stirred manually for 60 s. Paste samples of approximately 10 g were cast in sealed plastic vials and stored at 38°C. After 28 days of curing, the paste samples were crushed and mixed with deionised water to reach a total of 200 mL. The solution was stirred mechanically for 1 h, then vacuum filtered and rinsed 10 times with hot water (around 65°C). The filtrate was then acidified with hydrochloric acid 25% (5 mL in excess after the phenolphthalein indicator turned colourless) and the volume was adjusted to 500 mL. The solution was also analysed with ICP-OES to quantify Na and K.

## 3.4 Preparation of cement paste samples

All pastes were produced with a water-to-binder ratio (w/b) of 0.50. Each batch was prepared by mixing 500 g of binder and 250 g of deionised water. The latter was added first into the mixing bowl, followed by the cement and the SCM (weighted separately). The blend was mixed with a high shear laboratory blender (capacity of 1.2 L, unloaded speed announced at 22 000 rpm) according to this sequence: 30 s mixing followed by 90 s rest and 30 s mixing. During the rest period, the inside of the bowl was scraped down to incorporate any material left on the sides. For each batch, 6 samples were cast in hollow POM cylinders. The moulds were filled in two layers, each vibrated for 15 s. The moulds were then sealed with rubber bungs and rotated along their longitudinal axis in a room maintained at 21°C. The samples were demoulded after 24 h ± 2 h and placed in aluminium pouches, which were sealed and stored in a climate chamber at 20°C until testing. A fixed replacement level of 35 wt.% was used for all mixes containing SCMs. Each SCM presented in Table 1 was tested with both PC-LA and PC-HA (all tests were triplicated). Finally, other w/c values were tested for the reference mix with PC-LA (w/c = 0.4 and 0.6).

In the following, the mix ID is composed of the alkali level of the cement (LA or HA) followed by the SCM. As an example, HA-CC1 refers to the mix with 65 wt.% PC-HA and 35 wt.% CC1. The two reference mixes are referred to as LA-Ref and HA-Ref.

## 3.5 Pore solution extraction

The pore solutions of the paste samples were studied by performing Cold Water Extraction (CWE) at 28 and 140 days. In the literature, results on pore solution composition are often reported after 28, 90 or 180 days of curing. However, in the present study, the important aspect is that the second curing period is considerably longer than the first one. For practical reasons, the experiments were run in parallel with testing the same SCMs with the Danish accelerated mortar bar test for ASR (TI-B 51), and here the exposure time is 140 days. The CWE procedure is described in the following.

### 3.5.1 Cold Water Extraction (CWE)

The CWE procedure was similar to the one presented in Ranger et al. [34] (L5-1 settings). The hardened paste was crushed manually and sieved until collecting 20.0 g of the 0.5 – 1 mm size fraction. The crushed material was then mixed with 20.0 g of deionised water (at room temperature). 2 min after the addition of water, the slurry was stirred for 5 min before being vacuum filtered (same setup as for water-soluble alkalis). The filtrate was then diluted 20 times (1 mL of filtrate for 19 mL of deionised water) and acidified with 280 µL of nitric acid 32.5%. All masses were registered to the nearest 0.001 g to calculate the actual dilution factors. The samples were analysed by ICP-OES to determine the concentrations of Na and K.

### 3.5.2 Amount of pore solution

Samples of approximately 10 g were dried in desiccators (5.5 L) stored in ovens set to 40°C. The desiccators contained 400 g of silica gel, placed in a large Petri dish on the tray to cover the largest area possible. During the first 48 h of drying, no more than 6 samples were placed in the same desiccator to speed up the mass loss and prevent further hydration. The samples were dried until reaching constant mass (defined as mass change smaller than 0.1% per 24h of drying).

### 3.5.3 Data processing

The concentrations in the pore solution in mol/L and the amounts of free alkali metals in g/g binder were calculated from Equations (2a) and (2b), respectively.

$$[X]_{ps} = \alpha \cdot \frac{m_{wp} + m_{CWE}}{m_{wb}} \cdot [X]_{ex} \quad (2a)$$

$$X_b = \alpha \cdot \frac{m_{wp} + m_{CWE}}{m_s} \cdot \gamma^{-1} \cdot M_X \cdot (1 + w/b) \cdot [X]_{ex} \quad (2b)$$

where $[X]_{ps}$ is concentration in the pore solution [mol/L], $[X]_{ex}$ the concentration in the extracted solution after dilution and acidification [mol/L], α the dilution factor [-] accounting for both water and acid addition, $m_{wp}$ the mass of pore solution in the crushed powder [g], $m_{wb}$ the mass of pore solution in the bulk specimen [g], $m_s$ the mass of the powdered sample [20.0 g], γ the density of water at 23°C [998 g/L], $M_X$ the molar mass of element X [g/mol] and $m_{CWE}$ the mass of water used for leaching [20.0 g]. Based on previous results [34], it was chosen to assume $m_{wp} = 0.8\ m_{wb}$.

## 3.6 Phase analysis

For all mixes with PC-LA, one extra paste sample was cast and investigated by thermogravimetric analysis (TGA) and QXRD at 28 and 140 days. TGA was also conducted on $R^3$ samples at 7 days to determine portlandite consumption (see Section 3.7). Prior to all analyses, hydration was stopped according to the procedure described in [38]. The crushed samples (< 1 mm) were then stored in a desiccator containing silica gel and soda lime under light vacuum until characterisation, which occurred within 24h. The samples were powdered to pass a 150 μm sieve just before conducting TGA and XRD.

### 3.6.1 Thermogravimetric analysis (TGA)

TGA was performed with a STA 449 F3 Jupiter® thermal analyser from NETZSCH. Approximately 50 mg of powdered paste were placed in an 85 μL alumina crucible, and the mass was recorded while heating from 30°C to 1050°C at a rate of 10°C/min. The sample chamber was purged with $N_2$ at a rate of 50 mL/min [39].

The amount of chemically bound water was determined by considering the mass loss between 105°C and 1000°C [40], correcting for the $CO_2$ loss between approximately 550°C and 800°C. The amount of portlandite was calculated from the mass loss occurring between approximately 450°C and 550°C determined by the tangential method [13,39]. The exact temperature boundaries were defined manually for each curve, based on the derivative.

For mixes containing SCMs, the portlandite consumption was calculated as the difference to the reference mix, correcting for the cement replacement level and the degree of hydration of the clinker. The formula is shown in Equation (3), where $m_{CH}$ is the mass of portlandite in g/g PC, α is the degree of hydration of the clinker, and the subscripts PC and PC+SCM refer to the reference mix (plain PC) and a mix with SCM (65 wt.% PC + 35 wt.% SCM), respectively.

$$m_{CH,consumed} = m_{CH,PC} \cdot (1 - RL) \cdot \frac{\alpha_{PC+SCM}}{\alpha_{PC}} - m_{CH,PC+SCM} \quad (3)$$

### 3.6.2 X-ray diffraction (XRD)

The XRD measurements were performed with a PANalytical X-Pert$^3$ diffractometer, using a Bragg-Brentano geometry in a θ-2θ configuration. The X-ray radiation was a CuKα (λ = 1.5408 Å) operated at 45 kV and 40 mA. The optical configuration included 0.5° divergence slit, 1° antiscatter slits (incident and receiving), 0.04 rad soller slits (incident and receiving) and a 10 mm beam mask. The X-Celerator detector was used in a step scanning mode. The samples were backloaded and scanned between 5 and 70°, with a step size of 0.02° and a total measurement time of 15 minutes (to limit carbonation of hydrated samples). Two samples of each powder were scanned, and the averaged diffractogram was used for phase identification and quantification.

Qualitative and quantitative analyses were conducted with the HighScore Plus software. The Rietveld refinement method was applied to quantify the amount of each phase. The background was fitted with a 5$^{th}$ degree polynomial whenever possible (i.e. for materials mainly crystalline), and with the algorithm proposed by Sonneveld and Visser [41] for hydrated pastes and amorphous anhydrous materials [42]. The refinement was carried out in the following order: scale factors, unit cell parameters (limited to 1% shift), the w Cagliotti parameter for the full-width at half maximum (constrained between 0.0001 and 0.2), and the preferred orientations for some phases according to the March-Dollase model (constrained between 0.7 and 1). The quantification was carried out with the external standard method [39], using a NIST-certified α-quartz sample (SRM 1878b) with a declared crystallinity of 96.73%. The quality of the fit was assessed with the $R_{wp}$ agreement index. For hydrated samples, the results were back calculated to be expressed in g/100 g PC. The degree of hydration was calculated from the amount of clinker phases left in hydrated pastes.

## 3.7 SCM reactivity tests

The reactivity of the SCMs was evaluated through two parameters of the R$^3$ method, namely bound water and portlandite consumption. The mix design for each batch is shown in Table 4 [17]. The R$^3$ solution (deionised water, KOH and $K_2SO_4$) was prepared before the tests and stored in a closed plastic bottle; the dry materials (SCM, portlandite and calcite) were pre-mixed manually with a spatula for 2 min. Both the R$^3$ solution and the dry mix were stored at 40°C before mixing.

Approximately 75 g of paste was produced by mixing the dry mix and the $R^3$ solution manually for 30 s and then mechanically for 90 s (laboratory mixer). Samples of approximately 8 g were cast in sealed plastic vials and cured at 40°C for up to 35 days.

*Table 4: $R^3$ mix design based on [17].*

| | SCM | $Ca(OH)_2$ | DI water | KOH | $K_2SO_4$ | $CaCO_3$ | Total |
|---|---|---|---|---|---|---|---|
| Mass [g] | 9.97 | 29.91 | 53.84 | 0.22 | 1.08 | 4.99 | 100.00 |

After 7, 14, 28 and 35 days of curing, approximately 5 g of paste were oven-dried in two steps, first at 40°C for 24h and then at 350°C for 2h. The tests were triplicated at 7 days and duplicated at later ages. $R^3$ bound water ($w_{R3}$) was calculated as the mass loss between 40°C and 350°C and expressed in g/100 g SCM. The amount of portlandite in the hardened $R^3$ paste at 7 days was determined by TGA, as described in Section 3.6.1. The portlandite consumption was then calculated in g/100 g SCM.

In parallel, the compressive strength potential at 28 days of the different binders was determined on mortar bars according to EN 196-1: 450 g of cementitious materials, 225 g of deionised water and 1350 g of CEN standard sand per batch (3 bars). The mortars were produced by blending 65 wt.% of PC-LA with 35 wt.% of SCM at a fixed w/b = 0.5. Superplasticizer (Dynamon XTend-200) was used if the initial flow value determined according to EN 1015-3 was below 150 mm. After demolding, each bar was weighted in air and water to estimate the air content, and the compressive strength was corrected on the basis of 5% strength loss for 1% of air [43]. $R^3$ test results were then compared with the relative compressive strength, where the mix with plain PC-LA was taken as the reference.

# 4 Results

The results presented in Section 4 and raw data are available online, see reference [44].

## 4.1 Water-soluble and available alkalis

The water-soluble and available alkalis determined as per ASTM C114 and C311, respectively, are shown in Figure 2. Both PC have similar relative amounts of water-soluble alkalis, around 60-70% of all $Na_2O$ and 40-50% of all $K_2O$. For most SCMs except biomass ashes, the water-soluble alkali content is negligible. There are significantly more available alkalis, but the extent varies depending on the type of SCM. No clear trend can be seen between Na and K.

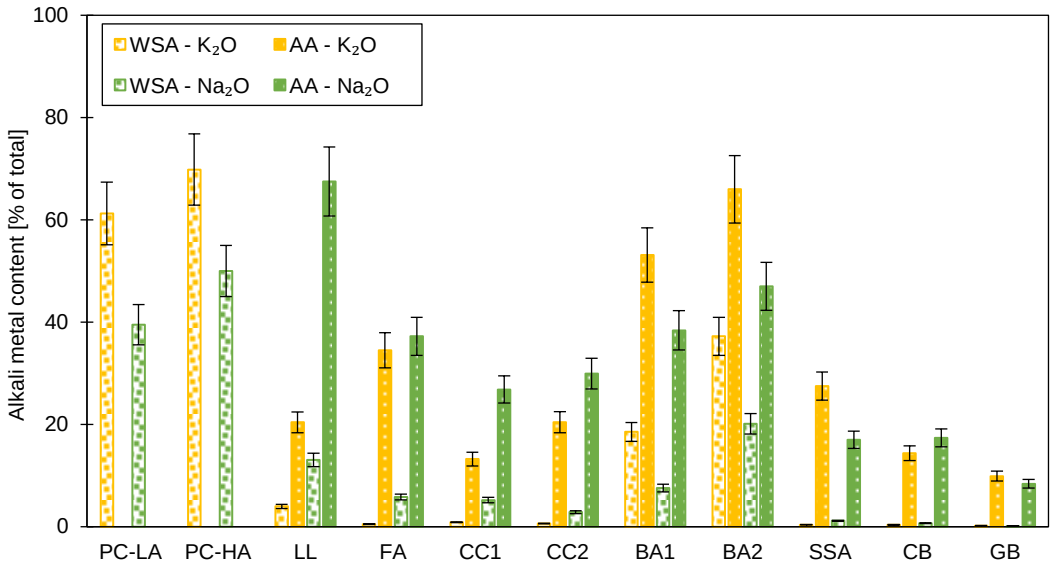


*Figure 2: Water-soluble (WSA) and available alkalis (AA), determined according to ASTM C114 and C311, respectively. Note that the tests were not performed for GB_f, and only water-soluble alkalis were measured for PC-LA and -HA.*

## 4.2 Reactivity of SCMs

The results from the $R^3$ tests are presented in Figure 3. The bound water at 7 days (Figure 3A) correlates well with the relative compressive strength at 28 days ($R^2 = 0.80$). From Figure 3B, it can be seen that there is a fairly constant molar ratio of 1.5 between bound water and portlandite (H/CH) for all materials except the two biomass ashes and limestone. Note that the bound water is expressed in g/100 g SCM to allow the comparison with portlandite consumption.

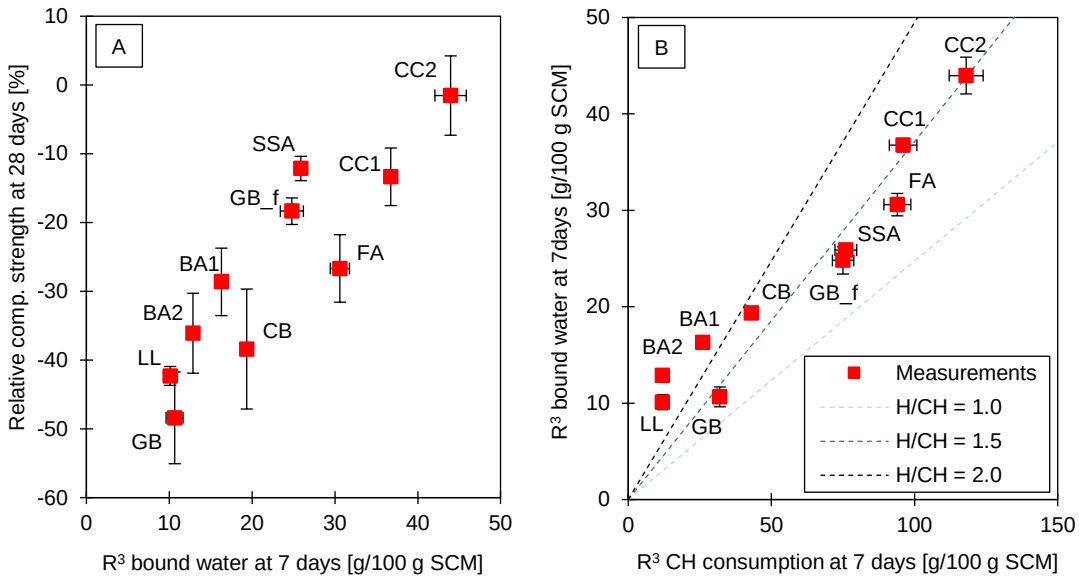


*Figure 3: Results from $R^3$ tests. A: 28-day relative compressive strength (reference = plain PC-LA) as a function of R3 bound water at 7 days. B: $R^3$ bound water as a function of portlandite consumption at 7 days. Dashed lines are guides for the eyes for different molar ratios between water (H) and portlandite (CH).*

The evolution of the $R^3$ bound water over time is illustrated in Figure 4, where weekly results are reported up to 35 days. Here, the values are given in g/100 g dry paste, as in previous studies (e.g. [17]). Three types of evolutions can be observed: no significant change (LL, CC2 and SSA), a linear trend (FA, CC1, BA1, BA2, CB and GB_f) and an exponential trend (GB). One can also notice the good repeatability of the results, which is illustrated by the error bars representing the standard deviation (3 samples at 7 days, 2 samples otherwise).

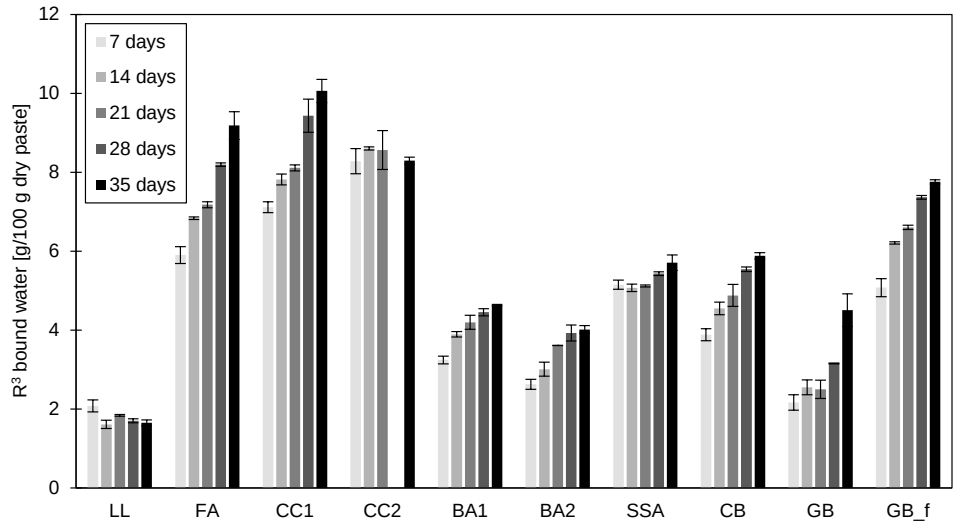


*Figure 4: Bound water in $R^3$ paste as a function of time. Note: the CC2 samples at 28 days were accidentally dropped and could not be measured.*

## 4.3 Free alkali metals in plain cement pastes

Figure 5A shows the effect of the w/c on the total concentration of alkali metals in the pore solution of plain cement pastes at 28 days, calculated from CWE results. The figure also shows the calculated hydroxide ion concentration from Equation (1). Figure 5B presents the distribution between free and bound alkalis. Even though the concentration decreases when the w/c increases, the free alkali content slightly increases (0.37, 0.40 and 0.43 wt.% for w/c = 0.4, 0.5 and 0.6, respectively).

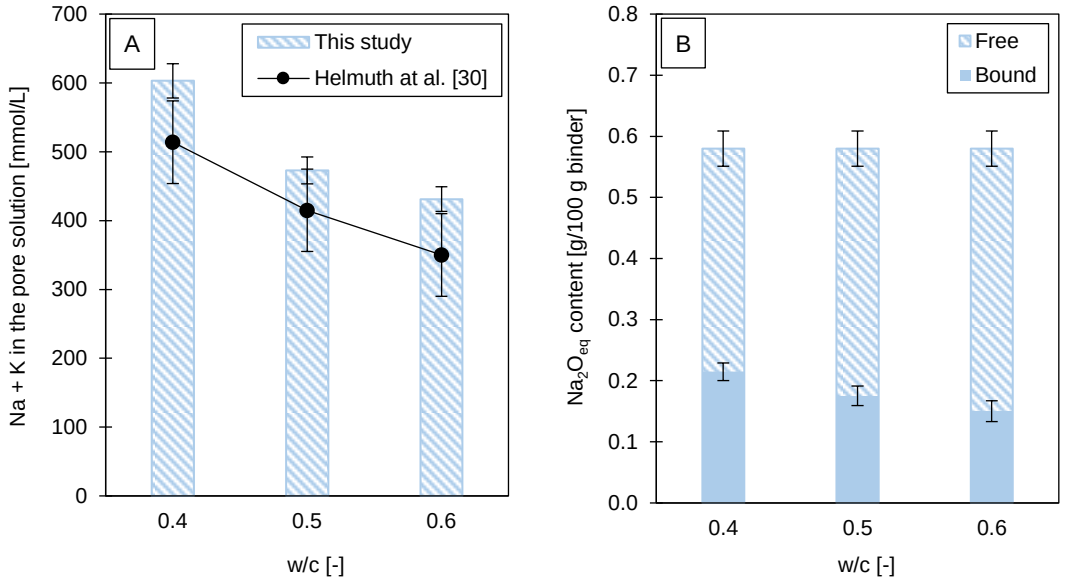


*Figure 5: Calculated total alkali metal concentration in the pore solution (A) and calculated free and bound alkali content (B) for plain cement pastes at 28 days as a function of the w/c. Figure 5A also includes the calculated [$OH^-$] from Equation (1).*

## 4.4 Free alkali metals in blended cement pastes

### 4.4.1 Concentrations in the pore solution

The calculated total concentration of alkali metals (Na + K) in the pore solution determined from CWE measurements is presented in Figure 6. The amount of pore solution used in the calculations is given in [44]. The replacement of cement by SCMs led to a decrease of the alkali metal concentration except for the two biomass ashes. The magnitude of the decrease is fairly close to that obtained by dilution with a limestone filler (LL) for LA-PC, however trends appear more clearly for HA-PC. In particular, FA, CC1 and CC2 appear to be more effective than the dilution effect only, and bring the alkali metal concentration almost to the same level as when LA-PC is used. When comparing the results between 28 and

140 days, 3 trends can be observed: an increase (Ref, BA1, BA2 and GB), a steady concentration (LL and CB) and a decrease (FA, CC1, CC2 and SSA).

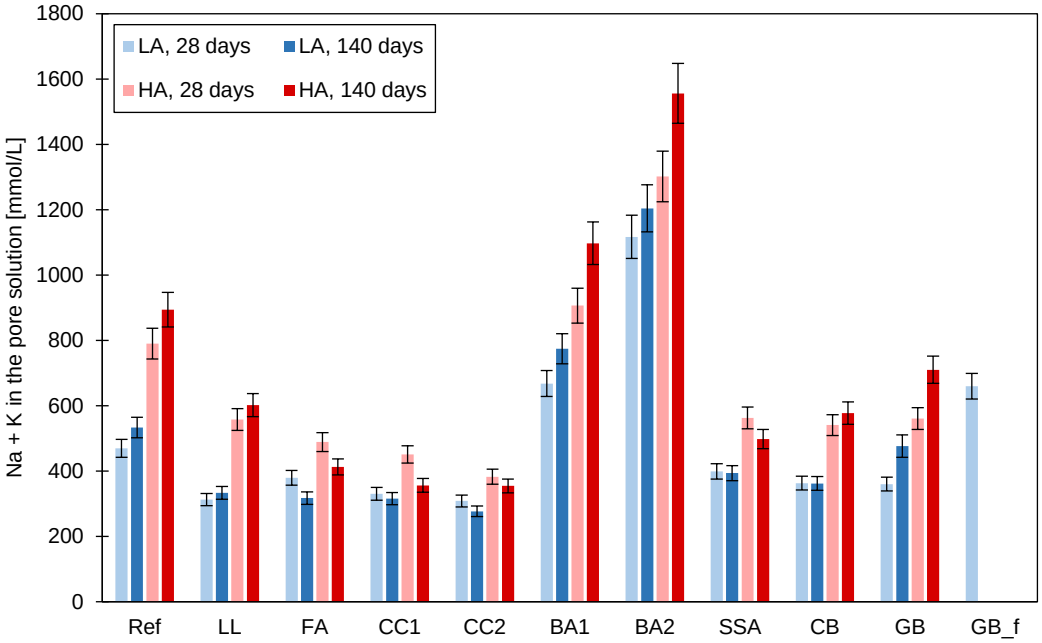


*Figure 6: Calculated concentration of alkali metals in the pore solution of cement paste.*

Figure 7 depicts the correlation between the chemical index proposed by Thomas [8] and the total alkali metal concentration in the pore solution after 140 days of curing. The chemical index was derived from the binder composition determined by XRF (weighted average between PC and SCMs). Thomas [8] compared it with the hydroxide ion concentration at 2 years and found a best linear fit following $y = 6000x$ and with $R^2 = 0.92$. Although a similar dependency is relatively evident from Figure 7, the data are quite scattered which results in a lower $R^2$.

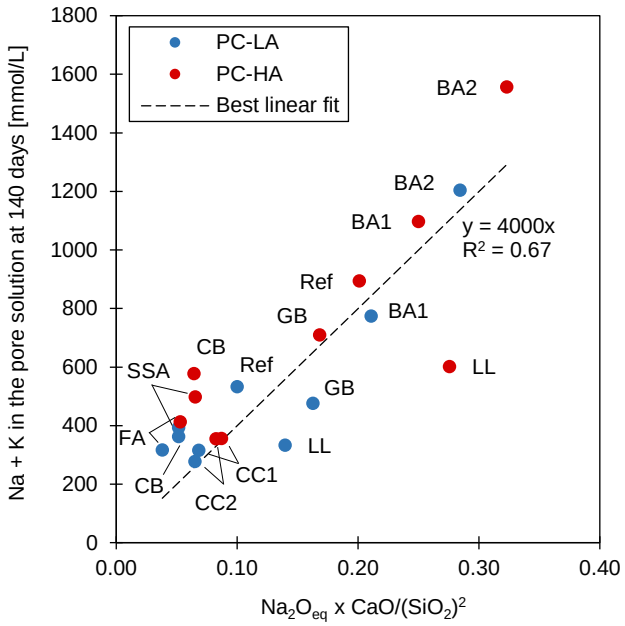


*Figure 7: Total alkali metal concentration in the pore solution of cement paste at 140 days as a function of the chemical index proposed by Thomas [8].*

### 4.4.2 Free alkali metal content

The influence of the type of alkali metal (Na or K) is illustrated in Figure 8, where the results are expressed both in mmol/L and in % of total. In Figures 8A and 8B, there is little difference in terms of concentrations between Na and K for PC-LA (except for biomass ashes and glass), but higher concentrations of K with PC-HA. Conversely, when examining Figures 8C and 8D, the relative amount of K in the pore solution is always lower than that of Na, irrespective of the alkali content of the cement (except for glass). The free alkali metal content remains relatively constant over time for some mixes (Ref, LL, BA1, BA2 and CB) and tend to decrease for others (FA, CC1, CC2 and SSA). The only exception is for GB, which shows an increase for Na (small relative change, but large total content).

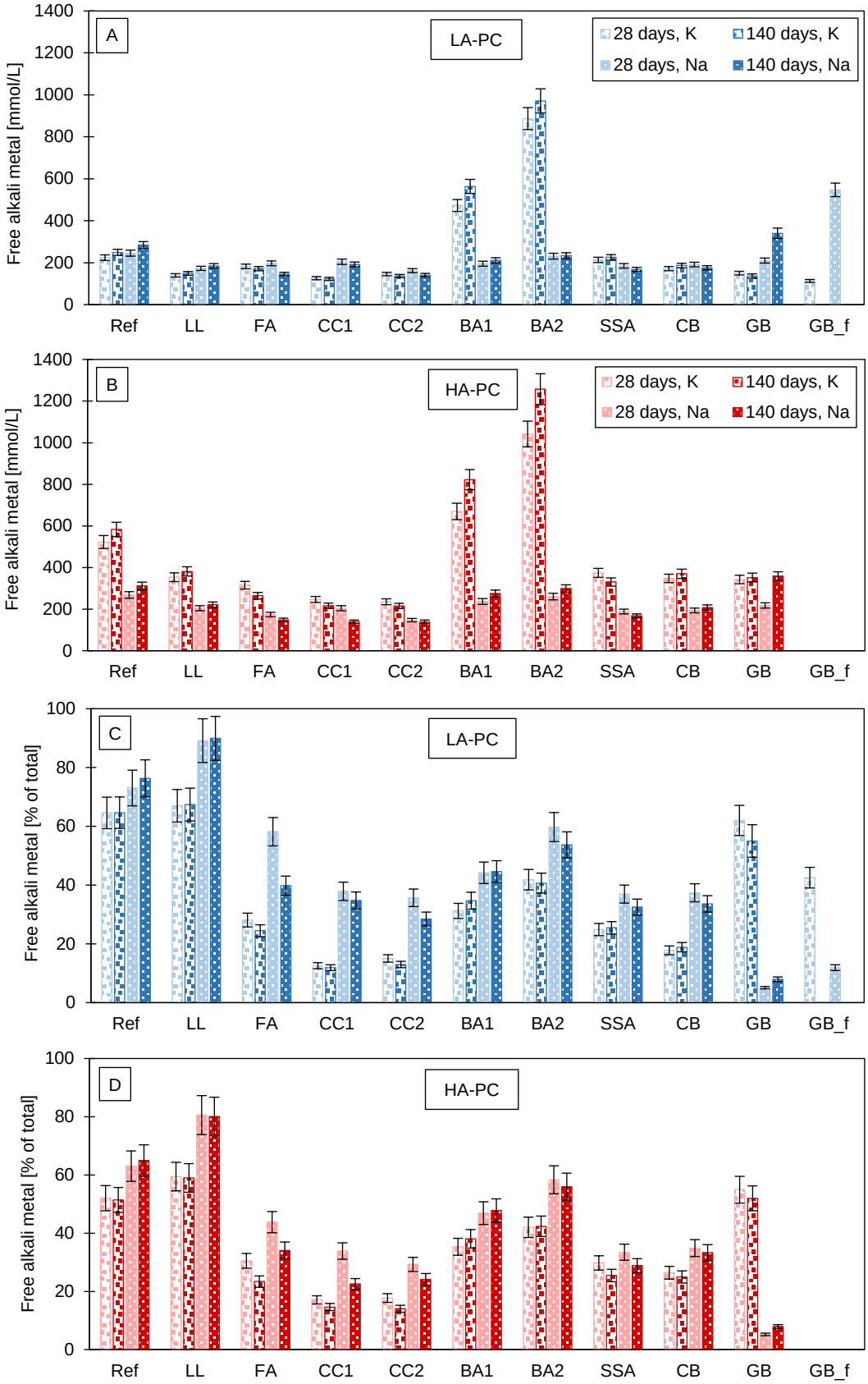


*Figure 8: Free metal alkali content in cement paste (A and B: in mmol/L, C and D: in % of total) at 28 and 140 days with low-alkali PC (A and C) and high-alkali PC (B and D).*

Figure 9 presents the distribution between free and bound alkalis in cement paste expressed in $Na_2O_{eq}$ (in g/100 g binder) at 28 days. It must be observed that the values were calculated by converting all free "alkali metals" into "alkalis". This assumption will be discussed in Section 5. One can see that when SCMs are used, the ratio between free and total alkalis decreases. This is also true for biomass ashes (BA1 and BA2), even though their free content exceeds that of the references.

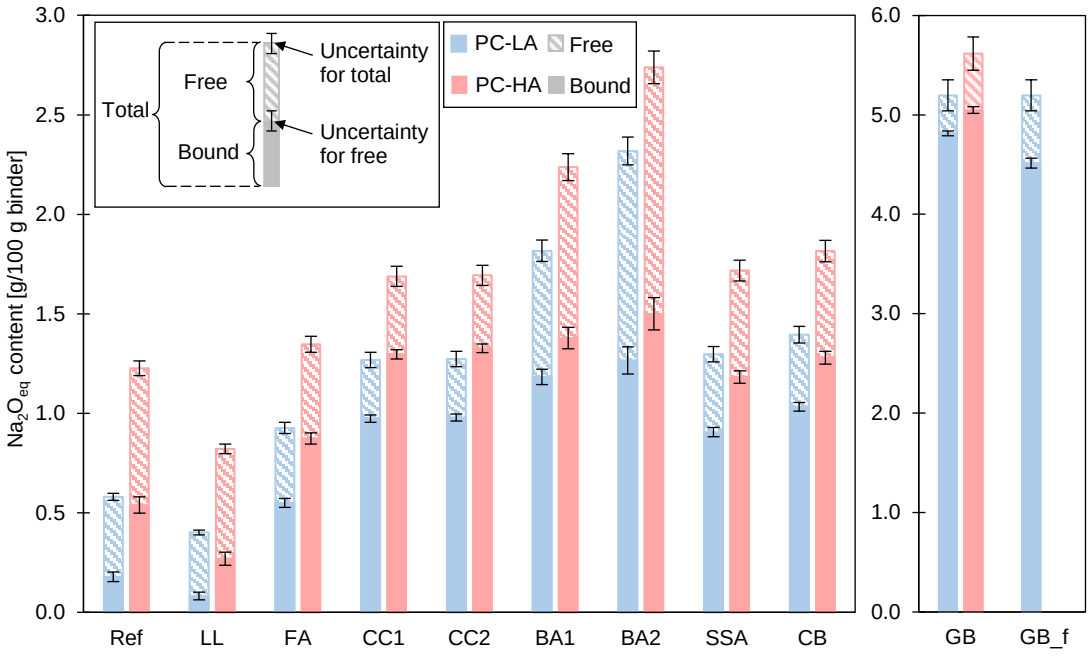


*Figure 9: Distribution between free and bound alkalis in cement paste (in g/100 g binder) at 28 days. Note that the scale on the y-axis is different for GB and GB_f.*

To compare free and available alkalis, the results from Figure 9 were processed to determine the contribution of each SCM (in g/100 g SCM). This was done by calculating the difference in free alkalis between a given paste and the one containing LL (with the same PC) to account for the dilution effect. The values were then expressed with respect to the total $Na_2O_{eq}$ content of the SCM. The results are displayed in Figure 10 and show that there are always significantly less free alkalis than available alkalis. A negative contribution was found for several SCMs (FA, CC1 and CC2), which was even more pronounced with HA-PC.

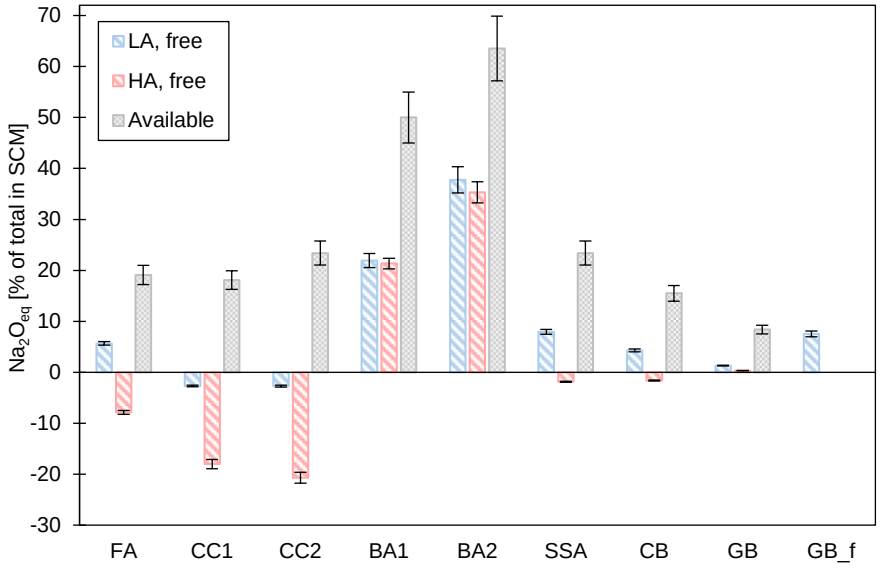


*Figure 10: Comparison between free and available alkalis (in % of total in SCM).*

### 4.4.3 Alkali metal binding

An attempt was made to study the changes in alkali metal binding induced by SCMs, in particular with respect to their reactivity. The results are presented in Figure 11, where the values on the y-axis were calculated according to Equation (4) (all variables refer to $Na_2O_{eq}$, WS = water-soluble).

$$Net\ release\ (SCM_i) = Free\ (LL) + WS\ (SCM_i) - Free\ (SCM_i) \qquad (4)$$

A negative value on the y-axis therefore means that the SCM reaction leads to alkali metal binding. The reason for subtracting water-soluble alkalis is that they are dissolved during mixing, i.e. before SCMs start to react.

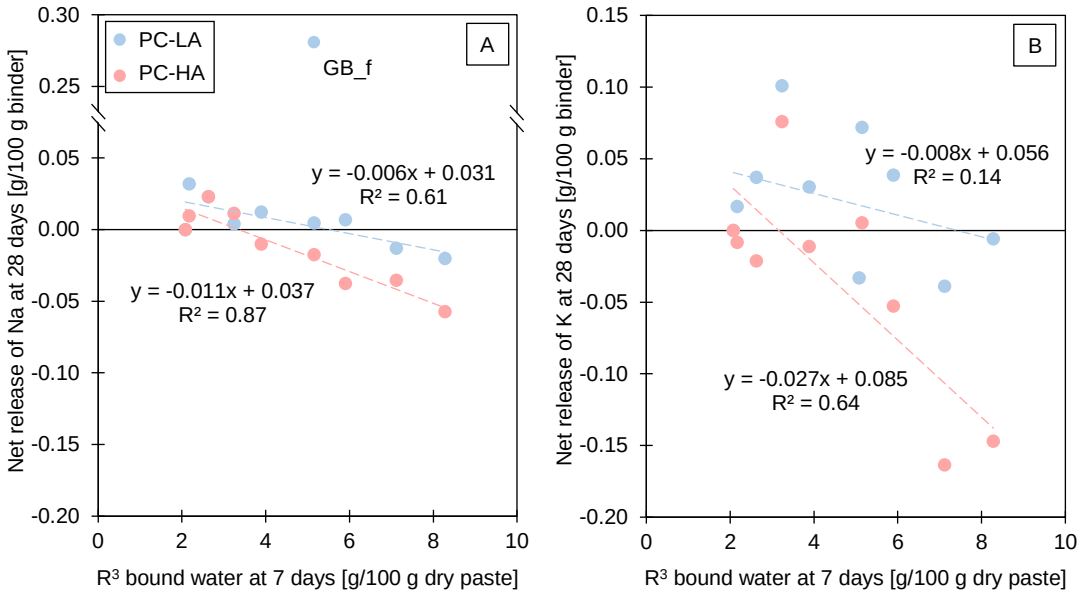


*Figure 11: Net alkali metal release (in g/100 g binder) at 28 days as a function of the $R^3$ bound water at 7 days. A: Sodium, Na (the trend line for PC-LA was calculated without GB_f). B: Potassium, K.*

Figure 11A shows that there is a clear relationship between the level of reactivity of an SCM and its effect on Na binding. The only notable exception is GB_f, which shows the opposite behaviour. Similar trends can be seen in Figure 11B for the relationship between the level of reactivity and the effect on K binding, although the data are significantly more scattered. In both figures, there is a tendency for PC-HA to enhance binding, as the trend line is below and steeper than with PC-LA.

## 4.5 Phases in blended cement pastes

The degree of hydration of the clinker calculated from QXRD results and the portlandite content determined by TGA are given in Table 5. The detailed QXRD and TGA results can be found online [44]. As expected, a higher degree of hydration and more portlandite were obtained by increasing the w/b of the reference mix (LA-Ref). A higher degree of hydration was also obtained on all blended mixes compared to the reference one. The portlandite content varied significantly between the binders, which indicates different extends of pozzolanic reaction. The results from Table 5 were then used to calculate the portlandite consumption according to Equation (3). The results are shown in Figure 12. The negative values for BA1 are probably caused by the portlandite already present in the ash (Table 3). Little to no portlandite consumption was measured for LL, BA2 and GB, which is in agreement with the reactivity measurements displayed in Figure 3. The largest values were registered for CC1, CC2, SSA and FA, the latter having the largest increase from 28 to 140 days.

*Table 5: Degree of hydration of the clinker (DoH) calculated from QRXD results and portlandite (CH) content calculated from TGA results.*

| Mix | w/b | 28 days | | 140 days | |
|---|---|---|---|---|---|
| | | DoH [-] | CH [g/100 g PC] | DoH [-] | CH [g/100 g PC] |
| | 0.4 | 0.85 | 14.5 | - | - |
| LA-Ref | 0.5 | 0.90 | 18.1 | 0.95 | 18.7 |
| | 0.6 | 0.93 | 19.6 | - | - |
| HA-Ref | 0.5 | 0.91 | 17.2 | - | - |
| LA-LL | 0.5 | 0.96 | 20.3 | 0.99 | 19.6 |
| LA-FA | 0.5 | 0.95 | 18.2 | 0.97 | 12.2 |
| LA-CC1 | 0.5 | 0.93 | 8.3 | 0.95 | 7.2 |
| LA-CC2 | 0.5 | 0.93 | 10.5 | 0.95 | 8.2 |
| LA-BA1 | 0.5 | 0.94 | 21.1 | 0.97 | 22.5 |
| LA-BA2 | 0.5 | 0.94 | 18.4 | 0.96 | 18.2 |
| LA-SSA | 0.5 | 0.94 | 10.3 | 0.97 | 9.1 |
| LA-CB | 0.5 | 0.96 | 17.9 | 0.98 | 16.8 |
| LA-GB | 0.5 | 0.96 | 20.6 | 0.99 | 19.9 |
| LA-GB_f | 0.5 | 0.94 | 16.4 | - | - |

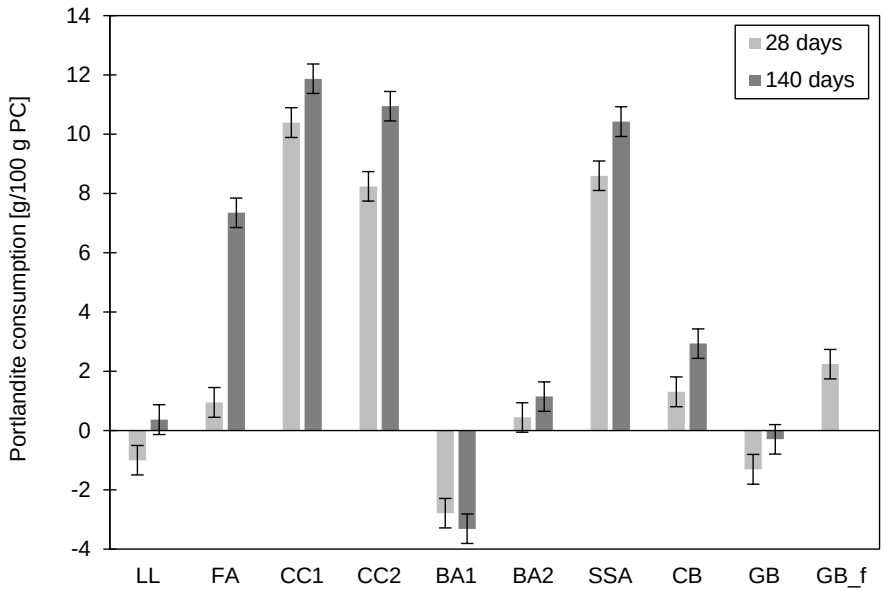


*Figure 12: Portlandite consumption calculated from TGA results (blended cement pastes with LA-PC). The error bars represent the observed uncertainty (0.5 g/100 g PC).*

# 5 Discussion

The results from the previous section will be discussed starting from the simplest system (raw materials) towards more complex ones (hardened blended cement pastes). The section will be concluded with a critical discussion on the practical use of CWE.

As a preliminary remark, it should be mentioned that most analytical techniques used to measure “alkalis” (XRF, ICP, flame photometry) are in reality quantifying “alkali metals”. Thus, converting the results directly into alkalis ($Na_2O$, $K_2O$, $Na_2O_{eq}$) may be fundamentally wrong. However, “alkalis” is the most common engineering parameter, widely used in product declarations and requirements. For this reason, it was chosen to display “alkalis” results in Figures 5, 9 and 10, calculated by a direct conversion from alkali metals to alkalis. The validity of such assumption will be discussed throughout the section.

## 5.1 Direct determination of the alkali metal contribution from SCMs

As it can be seen in Figure 2, there are significantly more available alkalis than water-soluble ones, which is consistent with previous studies [9,10,45]. Apart from the mix design and curing, the available alkali procedure is quite similar to CWE. The hardened paste is crushed, leached in water and filtered. Duchesne and Bérubé [9] mentioned that the leaching and rinsing steps in ASTM C311 probably lead to the release of alkali metals bound to hydrates. In fact, Ranger et al. [34] suspected the same effect for CWE on cement paste samples. With such a long leaching time in ASTM C311 (1 h), it is likely that the effect is even amplified compared to CWE. In both cases, this may result in overestimating the actual alkali metal content of the pore solution. Kasaniya and Thomas [10] also raised some concerns regarding the mix design in ASTM C311, in particular the effect of the SCM-to-lime ratio and the absence of additional alkalis in the mix. These two points have a direct influence on the pozzolanic reaction and were investigated when developing the $R^3$ method [19]. This emphasises the importance of hydration reactions when quantifying free alkali metals, which will be developed in Section 5.2.

The results of ASTM C311 should also be interpreted with caution, in particular for BA1 and BA2. These materials contain salts (halite, sylvite and $KAlCl_4$), which release alkali metals without a proportional amount of hydroxide ions. The name of the test may therefore be misleading because it is “alkali metals” that are

quantified, not “alkalis”. In this case, identifying the type of alkali metal bearing phases can be useful to interpret the results (e.g. by QXRD, or by analysing the chloride and sulphate contents of the solution).

In summary, although ASTM C311 aims to consider all relevant mechanisms involving alkalis from SCMs, it seems to give inaccurate results compared to what is seen in the pore solution of blended cement pastes. In addition, other authors concluded on no clear link between ASTM C311 results and ASR expansion in the concrete prism test [16]. One alternative may be to replace lime with Portland cement, and therefore cast a proper blended cement paste. This has already been suggested by other authors [9,10] to better capture the behaviour of SCMs in cementitious binders and will be discussed extensively in Section 5.3.

## 5.2 Hydration reactions

Alkali metal release from reactive phases mainly depends on the degree of reaction of each material. The following section first deals with the SCM reactions separated from clinker hydration, and subsequently combines both.

### 5.2.1 Isolated SCM reactions

The reactivity results presented in Figure 3 are in agreement with previous work on bound water [18], and demonstrate that the $R^3$ method performs well with alternative SCMs. When plotting bound water against portlandite consumption, it may be seen that the water-to-portlandite molar ratio varies significantly between the materials. However, the 4 most reactive SCMs at 7 days (CC2, CC1, FA and SSA) as well as GB and GB_f seem to have a similar ratio close to 1.5. In the case of a pure pozzolanic reaction, one would expect a molar ratio close to 1 [46]. The results therefore suggest that hydrates holding more water than C-S-H are also formed, such as ettringite and AFm phases. For the other materials (LL, BA1, BA2 and CB), the ratio is higher and indicates that the materials are probably more latent hydraulic (or inert) than pozzolanic [47].

For any chemical reaction, two approaches are needed to describe accurately the state of the system: thermodynamics and kinetics. This also applies to SCM reactions, and therefore it is important to consider reaction kinetics when evaluating the reactivity of an SCM [48]. As shown in Figure 4, the evolution of bound water over time differed from one SCM to another. As an example, while CC2 had roughly 30% more bound water than FA after 7 days, FA exceeded CC2 after 35 days. Another example of interest is GB: at 7 days, the bound water content was similar to the inert reference LL. However, the measurements took off from 28 days to start following an exponential trend. In this case, the kinetics is probably

closely linked to the size and the shape of the glass beads, as GB_f reacted significantly faster. Extending the test duration can therefore give some indication about the reaction speed of the materials.

### 5.2.2. Combined cement hydration and SCM reaction

When mixing Portland cement and SCMs, two reactions take place simultaneously: clinker hydration and SCM reaction, the latter made possible by the former through the formation of portlandite. From Table 5 it can be seen that the introduction of SCMs in the mix speeds up clinker hydration, the degree of hydration of the clinker being systematically higher than the reference mix at 28 days.

The portlandite consumption results presented in Figure 12 are overall in agreement with the $R^3$ results from Figures 3 and 4. In both cases, there is no evidence of pozzolanic reaction with LL, BA1, BA2 and GB. LL was most likely inert, GB had a slow reaction rate (as explained in Section 5.2.1), while BA1 and BA2 acted as latent hydraulic materials to form in particular ettringite (due to the high sulphur content), which explains the higher bound water content compared to inert materials. An interesting difference to notice is the behaviour of FA, which had a similar portlandite consumption as CC1 in $R^3$ tests, but significantly smaller in cement pastes. However, the portlandite consumption of FA in cement paste greatly increased from 28 to 140 days, which could indicate different reaction kinetics in the two experiments.

## 5.3 Influence of the binder composition on free alkalis

CWE was used to evaluate the free alkali metal content in blended cement pastes. This part explores the influence of the binder composition (alkali content of PC and type of SCM) on free alkali metals.

### 5.3.1 Alkali content of Portland cement

It is well known that the more alkalis in PC, the higher the alkalinity of the pore solution [30]. This is illustrated by the results presented in Figures 6 and 9, which show that both the calculated concentrations of alkali metals and the free alkali content are higher with PC-HA compared to PC-LA. Figure 8 also highlights that there are proportionally more free alkalis with PC-LA (69%) compared to PC-HA (58%). This is consistent with previous studies showing that alkali metal binding by C-S-H is enhanced by a higher alkalinity of the surrounding liquid [25,26].

In a paste containing PC only, it is possible to make an alkali inventory by combining water-soluble alkalis, degrees of hydration and CWE results. The alkali inventory for the two cement pastes cast with PC (LA and HA) is presented in

Table 6. The values show that with a degree of reaction around 0.90, alkalis left in unreacted clinker make up around 5% of the total. This suggests that even in the event of further hydration during CWE, the amount of alkalis released is within the uncertainty range of the method. Consequently, such potential phenomena could not significantly impact the results presented in the present paper.

*Table 6: Alkali inventory ($Na_2O_{eq}$ in % of total) at 28 days of cement pastes containing PC only.*

| Mix | Bound | | Free |
|---|---|---|---|
| | Clinker | Hydrates | |
| LA-Ref | 5% | 26% | 69% |
| HA-Ref | 6% | 38% | 56% |

### 5.3.2 SCM composition

In agreement with Section 2.3, Figure 7 illustrates the limitations of the chemical index to correlate with the alkali metal concentration in the pore solution. As underlined by Thomas [8] and Kasaniya and Thomas [10], the chemical index does not accurately reflect the availability of compounds, in particular for SCMs containing crystalline non-reactive phases. This explanation probably applies to Figure 7, since the data deviating the most from the best linear fit include limestone (LL) and crushed brick (CB), two materials which are mainly crystalline (95% and 80% respectively).

Figures 6 and 9 show that only biomass ashes lead to higher levels of free alkali metals compared to the reference mixes. The explanation is probably twofold: on the one hand, Figure 2 shows that the biomass ashes have the largest content of water-soluble alkalis. On the other hand, the reactivity parameters presented in Figures 3 and 4 are among the lowest, implying that little pozzolanic C-(A)-S-H is formed (if any). This is not surprising given the chemical and mineralogical composition of the ashes (40-50% crystalline, high amorphous calcium and alkali contents). As a consequence, the alkali metal binding capacity of the hydrates is quite limited.

It must be mentioned that the two biomass ashes contain large amounts of sulphur, in the form of anhydrite and syngenite. When dissolving, these phases also release sulphates in the pore solution, which partly counterbalance alkali metal ions. This has already been observed when elevating the temperature, which destabilises sulphate-bearing phases like ettringite [49]. A similar effect is possible with chlorides released from halite and sylvite. Consequently, the relationship

$[Na^+] + [K^+] \approx [OH^-]$ may not hold completely true, so that the hydroxide ion concentration cannot be accurately described by alkali metal ions only. However, both chloride and sulphates are anions ($Cl^-$ and $SO_4^{2-}$), meaning that only looking at alkali metals would overestimate the $OH^-$ concentration, which seems to be on the safe side regarding ASR. The inaccuracy becomes more problematic if cations are dissolved (e.g. fine silicates), because they could lead to the opposite trend.

Figures 6 and 9 demonstrate that all other SCMs were able to decrease the concentration of alkali metals and the free alkali content. With LA-PC, it is difficult to say whether it is solely due to the dilution effect, as the values are quite close to the ones obtained with limestone. However, with HA-PC, it becomes clear that the dilution effect is not the only explanation, as FA, CC1, CC2, SSA and CB led to lower values compared to LL.

The $R^3$ results in Figures 3 and 4, as well as the portlandite consumption in Figure 12 indicate that all these SCMs present signs of pozzolanic activity. Figure 11 illustrates that for most SCMs, their alkali metal binding capacity seems linked to their reactivity, which can be explained by the production of pozzolanic C-(A)-S-H. There is a fairly good linear correlation for Na; the trend is also visible for K, even though the data are more scattered (the reason for this is not known). However, both graphs point towards an increased binding for more reactive SCMs, and also confirm that binding is enhanced by PC-HA. It should also be mentioned that after subtracting water-soluble alkalis, only one biomass ash (BA1, with a $R^3$ bound water value of 3.24 g/100 g dry paste) releases some K. The fact that BA2 has the largest amount of free alkali metals can therefore be attributed to water-soluble alkalis only. For future work, it may be of interest to expand the range of reactivity for the SCMs and investigate the potential of the $R^3$ method to estimate the gain in binding capacity brought by SCMs.

In the case of glass, one can see that the alkali metal concentration in the pore solution increases significantly when using finer particles, which is also striking in Figure 11 where GB_f appears as an outlier. An enhanced glass dissolution increases both silica and alkali metal contents, which have opposite effects on the pore solution alkalinity. More silica favours a low Ca/Si of the C-S-H, thereby increasing its alkali binding capacity. However, in the present case, this is probably not enough to compensate for the increase in alkali metals. This was highlighted by Kasaniya and Thomas, who also noted that silica may have the dominant effect if higher replacement levels are used [10].

As a result, some SCMs have a negative effective contribution to the free alkali content as illustrated by Figure 10. Such conclusion cannot be made from ASTM

C311 results (only positive contributions can be found), which was highlighted by other authors [9,10]. It should be mentioned that the pastes probably have different maturities because of different curing temperatures (20°C for CWE, 38°C for ASTM C311). However, Figure 8 indicates a steady or slight decrease of the free alkali metal content over time, while ASTM C311 results are expected to increase with a longer curing time [9,10]. Thus, these opposite trends suggest an even larger difference at later ages.

The results presented in Figure 10 also emphasise the influence of the alkali content of the cement, as all SCMs have a lower contribution when tested with HA-PC. This is probably because a higher alkalinity enhances the pozzolanic reaction [19]. For further research, it would be valuable to assess the effect of the SCM replacement ratio on the free alkali contribution from the SCM, as in the present study only one ratio was studied (35 wt.%).

## 5.4 Influence of other parameters on the free alkali content

In addition to the binder composition, the results also gave insights into the influence of other parameters, such as the w/c, the type of alkali metal (Na or K) and the curing time. The role of these factors is discussed in the following.

### 5.4.1 Water-to-cement ratio

The drop in alkali metal concentration when the w/c increases (Figure 5A) was also observed previously [28,50]. It is also in agreement with Equation (1), which links the hydroxide ion concentration and the w/c (similar trends but higher values with CWE results, as explained in Section 2.4). However, Figure 5B shows that there are proportionally more free alkalis with a higher w/c, which implies that another mechanism is also playing a role. It could be hydration, because the degree of hydration increases when the w/c increases. If the clinker releases more alkalis than what the corresponding C-S-H can bind, it results in a net increase. Another possible explanation could be that due to the more concentrated pore solution at low w/c, the alkali metal binding capacity of the C-S-H is enhanced [25,26]. Even though the explanation remains unclear, the change induced by the w/c is quite limited (0.37 to 0.43). Thus, choosing a relatively high w/c to quantify free alkalis for engineering applications seems to be the most conservative option.

### 5.4.2 Type of alkali metal

The influence of the type of alkali metal is illustrated in Figure 8. In Figures 8A and 8B, Na and K are fairly evenly distributed for PC-LA. This does not apply to

biomass ashes and glass, due to the chemistry of these materials. With PC-HA, the molar concentration of K is twice that of Na for most mixes, which reflects the distribution in the reference mix. Free contents in Figures 8C and 8D give a somewhat different perspective to the results because there is a systematic tendency for K to be relatively more bound than Na (except for GB), which is in agreement with the work of Plusquellec et al. [32].

In the literature, it seems that there is no consensus about the binding capacity of C-S-H as a function of the type of alkali metal [24]. Among the studies reporting higher binding of K, Bach et al. [51] concluded that potassium can penetrate the interlayer of C-S-H and can therefore be bound both on the outside and also on the inside, contrary to sodium. However, the results from the present study cannot be used to conclude on a preferential binding, because no distinction can be made between alkali metals bound to hydrates and those bound to unreacted phases.

Nevertheless, the fact that alkali metals may behave differently implies that some information may be lost when only looking at $Na_2O_{eq}$. Everything else being equal, a 1:1 molar substitution of Na with K (or vice versa) in the raw materials could therefore lead to a different free alkali content. The relevance of the $Na_2O$ equivalent concept has already been discussed [52], because the ratio between Na and K seems to influence the extent of ASR expansion.

### 5.4.3 Curing time

When extending the curing time, the amount of free water decreases, which naturally raises the concentrations. It is therefore difficult to interpret the results from Figure 6 for the mixes where the concentrations increase. On the opposite, a reduction in concentration over time certainly implies that alkali binding is taking place, as any other behaviour would lead to the opposite trend. This is the case for FA, CC1, CC2 and possibly SSA.

To better understand what happens in the other mixes, it may be of interest to examine Figure 8. The free alkali metal content seems to remain constant for the two references (LA-Ref and HA-Ref) as well as for the mixes containing limestone (LL), suggesting that the increase in concentration in the pore solution is mainly due to the decrease in volume. Moreover, irrespective of the cement alkali content, all SCMs except BA1 and GB lead to a decrease in the free alkali metal content, which indicates a net binding.

The behaviour of GB can be linked with the observations on its reactivity presented in Section 5.2.1. Indeed, glass is entirely amorphous and contains a high quantity of alkali metals. As it reacts slowly (Figure 4), no traces of alkali metals are seen

at early age. However, at a later stage, glass particles start dissolving and release alkali metals. When evaluating the free alkali metal content of a mix containing SCM, it is therefore essential to have a critical interpretation of the results and preferably have some insights about the state of reactivity of SCMs.

## 5.5 Practical use of CWE

### 5.5.1 Possibilities

ASR mitigation with alternative SCMs usually relies on performance testing, mainly because of the lack of long-term data as specified in ASTM C1778 (guideline for preventing deleterious ASR). In this respect, CWE appears to be a simple and affordable option to screen the efficacy of SCMs. For instance, CWE could be used to evaluate the effective free alkali contribution of an SCM, as it is done in Figure 10. Such reasoning (already proposed by Hobbs [53]) is convenient for engineering applications because it allows the determination of a coefficient for each material, which can then be used in prescriptive requirements for the alkali loading in concrete.

It must be emphasised that screening with CWE does not exempt from further performance testing of the concrete mixes when SCMs are used to mitigate ASR, because other factors affect their efficacy (e.g. presence of aluminium or resistance to moisture ingress). However, in the authors' opinion, CWE is a relatively fast method to select the most promising binders, and therefore better target the mixtures that are worthwhile testing further.

### 5.5.2 Limitations

Several methodological limitations of CWE were already mentioned in a previous publication [34]. As highlighted in Section 2.4, alkali metals initially bound to hydrates are probably released during leaching. This phenomenon may be influenced by the binder composition, since the latter drives the initial thermodynamic equilibrium in the paste. More data are needed to better understand and quantify this aspect. Regarding further hydration during leaching in CWE, the results from Table 6 prove that the amount of alkalis left in unreacted clinker is quite limited at 28 days and onwards. However, if CWE is performed at an earlier age, there is a possibility that this amount becomes significant and disturbs the interpretation. As a consequence, CWE seems more appropriate for systems containing a well hydrated clinker.

One of the main limitations of CWE is that the method does not give access to a complete ion inventory. With portlandite dissolution during leaching, the hydroxide concentration is significantly higher than what it was initially in the pore

solution. It is therefore not possible to verify that $[Na^+] + [K^+] \approx [OH^-]$. Other anions may be involved in the inventory, such as chlorides, sulphates or silicates. Moreover, even though the present study was conducted on paste samples only, CWE can also be used with concrete. In the case of concrete prone to ASR, there may be a risk that CWE destabilises alkali-silica reaction products, which contain some alkali metals. Thus, the method may give misleading results with respect to the actual amounts of free alkali metals.

The example of glass (GB) also showed that the result is only valid for the SCM tested as it is. If any material processing is done, like grinding, the test should be performed again. In addition, the behaviour of glass stressed the importance of the SCM reactivity when interpreting the results. For slowly reactive materials, it is critical to use a sufficiently long curing time to capture the chemical influence of the SCM.

### 5.5.3 Possible improvements

As shown in Figure 12, curing at 20°C for 28 days may not induce a sufficient maturity to unveil the long-term effect of SCMs reacting slowly. One possibility to overcome this issue is to raise the curing temperature, e.g. to 40°C as in ASTM C311. However, it should be verified that raising the temperature only accelerates the reactions, without significantly changing the thermodynamic equilibrium (especially with respect to alkali metal binding).

Considering the possible use of CWE described in Section 5.5.1, the present study emphasised the effect of the alkali content of PC and the curing time on the results, but there may be more (e.g. the SCM replacement ratio). A complementary parametric study would therefore be useful to determine which parameters should be used when qualifying an SCM with respect to its free alkali contribution. In this respect, one might have to reconsider the size fraction and the leaching time used in CWE. The effect of SCMs on the chemical composition of hydrates was largely developed in this paper, but SCMs also affect the microstructure. The penetration of the leaching liquid into the pores is likely modified in blended mixes compared to OPC, which may also influence the results.

In future studies, it may be interesting to use CWE on samples containing silica fume. This SCM has a peculiar behaviour, where alkali metals are bound at early age but released in the pore solution over time [54]. The size and the type of particle (agglomerated or sintered) also have an influence on the behaviour of silica fume, which can either act as an ASR inhibitor or as a nucleation site for expansion alkali silica gels [55]. Such systems may be enlightening challenges with regards to the reliability of CWE.

# 6 Conclusion

This study explored the use of CWE to determine the free alkali metal content in blended cement pastes. The free alkali metal content obtained by CWE on blended cement pastes is consistent with the expected effect of the binder composition as reported for similar binders in the literature. The results were complemented by an assessment of the reactivity of cementitious materials.

The following points were highlighted:

- Contrary to ASTM C311 which evaluates available alkalis from a system containing SCM only (no cement), CWE on blended cement paste takes into account the interactions between the cement and the SCM. As a result, net negative contributions can be detected, which is not the case with ASTM C311.
- The w/b and the curing time affect the free alkali content as determined by CWE on paste specimens. More parameters, not investigated in the present study, may also influence the results (e.g. the SCM replacement ratio). Strictly speaking, the free alkali content is therefore a paste property, not a binder property. Based on the present study, w/b = 0.5 and 28 days of curing at 20°C seem to be appropriate and relatively conservative parameters, unless the SCM is slowly reacting (see below).
- $R^3$ tests and water-soluble alkalis appear to be useful and widely accessible methods to better interpret CWE results. $R^3$ tests give some thermodynamic and kinetic indications of the SCM reactivity, which is particularly useful for slowly reacting materials. The free alkali content should only be evaluated after a significant amount of the SCM has reacted, otherwise there is a risk to overlook the SCM contribution.
- CWE enables to determine the free alkali metal content (Na or K). In practise, the free alkali content ($Na_2O$, $K_2O$ or $Na_2O_{eq}$) seems more convenient because total contents are commonly reported as oxides. However, the two quantities may not be equivalent if alkali metals are present in other forms. The conversion should thus be done having this in mind, and additional measurements may be useful if the presence of other compounds (chloride, sulphate) is suspected.

# Acknowledgements

The work presented is part of an industrial PhD project financed by the Danish Road Directorate and a joint grant from Innovation Fund Denmark (Innovationsfonden) and Realdania under the program Circular Built

Environment. The financial support is gratefully acknowledged. We thank the Research and Quality Centre of Aalborg Portland for the XRF analyses, as well as the following companies for supplying the materials: EasyMining (sewage sludge ash), Emineral (biomass ashes), Norcem (PC-HA) and Norrecco (crushed brick). In addition, a warm thank you to Jennifer Anette Canul Polanco (DTI) for the help with QXRD analyses. We would also like to thank Prof. Josée Duchesne (Laval University) for the guidance and the discussions about SCMs reactivity during a research stay of the first author at Laval University. Finally, we also thank Prof. Ole Mejlhede Jensen (DTU) for reviewing the present manuscript and providing valuable comments, as well as two anonymous reviewers who provided valuable comments with respect to the possible uses and limitations of CWE.

# CRediT authorship contribution statement

Maxime Ranger: Conceptualisation, Methodology, Formal analysis, Investigation, Writing – original draft, Visualisation.

Marianne Tange Hasholt: Conceptualisation, Methodology, Writing – review and editing, Supervision, Funding acquisition.

# References

[1] K.L. Scrivener, J.M. Vanderley, E.M. Gartner, Eco-efficient cements: Potential economically viable solutions for a low-$CO_2$ cement-based materials industry, Cem Concr Res. 114 (2018) 2–26. https://doi.org/10.1016/j.cemconres.2018.03.015.

[2] J. Duchesne, Alternative supplementary cementitious materials for sustainable concrete structures: a review on characterisation and properties, Waste Biomass Valorization. 12 (2021) 1219–1236. https://doi.org/10.1007/s12649-020-01068-4.

[3] R. Snellings, K.L. Scrivener, Rapid screening tests for supplementary cementitious materials: past and future, Mater Struct. 49 (2016) 3265–3279. https://doi.org/10.1617/s11527-015-0718-z.

[4] S. Al-Shmaisani, R.D. Kalina, R.D. Ferron, M.C.G. Juenger, Critical assessment of rapid methods to qualify supplementary cementitious materials for use in concrete, Cem Concr Res. 153 (2022). https://doi.org/10.1016/j.cemconres.2021.106709.

[5] N. de Belie, M. Soutsos, E. Gruyaert, Properties of Fresh and Hardened Concrete Containing Supplementary Cementitious Materials - State-of-the-Art Report of the RILEM Technical Committee 238-SCM, Working Group 4, Springer, 2018. http://www.springer.com/series/8780.

[6] M.C.G. Juenger, R. Snellings, S.A. Bernal, Supplementary cementitious materials: New sources, characterisation, and performance insights, Cem Concr Res. 122 (2019) 257–273. https://doi.org/10.1016/j.cemconres.2019.05.008.

[7] M.D.A. Thomas, K.J. Folliard, Concrete aggregates and the durability of concrete, in: C.L. Page, M.M. Page (Eds.), Durability of Concrete and Cement Composites, Woodhead, Cambridge, 2007: pp. 247–281. https://doi.org/10.1533/9781845693398.247.

[8] M. Thomas, The effect of supplementary cementing materials on alkali-silica reaction: A review, Cem Concr Res. 41 (2011) 1224–1231. https://doi.org/10.1016/j.cemconres.2010.11.003.

[9] J. Duchesne, M.-A. Bérubé, Available alkalies from Supplementary Cementing Materials, ACI Mater J. 91 (1994) 289–299. https://doi.org/10.14359/4335.

[10] M. Kasaniya, M.D.A. Thomas, Role of the alkalis of supplementary cementing materials in controlling pore solution chemistry and alkali-silica reaction, Cem Concr Res. 162 (2022). https://doi.org/10.1016/j.cemconres.2022.107007.

[11] R.D. Hooton, M.D.A. Thomas, T. Ramlochan, Use of pore solution analysis in design for concrete durability, Advances in Cement Research. 22 (2010) 203–210. https://doi.org/10.1680/adcr.2010.22.4.203.

[12] J. Lindgård, T. Østnor, B. Fournier, Ø. Lindgård, T. Danner, G. Plusquellec, K. De Weerdt, Determining alkali leaching during accelerated ASR performance testing and in field exposed cubes using cold water extraction (CWE) and μXRF, in: MATEC Web of Conferences, EDP Sciences, 2018. https://doi.org/10.1051/matecconf/201819903004.

[13] K. De Weerdt, G. Plusquellec, A. Belda Revert, M.R. Geiker, B. Lothenbach, Effect of carbonation on the pore solution of mortar, Cem Concr Res. 118 (2019) 38–56. https://doi.org/10.1016/j.cemconres.2019.02.004.

[14] H.F.W. Taylor, Cement Chemistry, Second Edition, Thomas Telford, 1997.

[15] B. Lothenbach, F. Winnefeld, C. Alder, E. Wieland, P. Lunk, Effect of temperature on the pore solution, microstructure and hydration products of Portland cement pastes, Cem Concr Res. 37 (2007) 483–491. https://doi.org/10.1016/j.cemconres.2006.11.016.

[16] M.H. Shehata, M.D.A. Thomas, Alkali release characteristics of blended cements, Cem Concr Res. 36 (2006) 1166–1175. https://doi.org/10.1016/j.cemconres.2006.02.015.

[17] X. Li et al., Reactivity tests for supplementary cementitious materials: RILEM TC 267-TRM phase 1, Mater Struct. 51 (2018). https://doi.org/10.1617/s11527-018-1269-x.

[18] D. Londono-Zuluaga et al., Report of RILEM TC 267-TRM phase 3: validation of the $R^3$ reactivity test across a wide range of materials, Mater Struct. 55 (2022). https://doi.org/10.1617/s11527-022-01947-3.

[19] F. Avet, R. Snellings, A. Alujas Diaz, M. Ben Haha, K. Scrivener, Development of a new rapid, relevant and reliable ($R^3$) test method to evaluate the pozzolanic reactivity of calcined kaolinitic clays, Cem Concr Res. 85 (2016) 1–11. https://doi.org/10.1016/j.cemconres.2016.02.015.

[20] P. Suraneni, J. Weiss, Examining the pozzolanicity of supplementary cementitious materials using isothermal calorimetry and thermogravimetric analysis, Cem Concr Compos. 83 (2017) 273–278. https://doi.org/10.1016/j.cemconcomp.2017.07.009.

[21] P. Suraneni, A. Hajibabaee, S. Ramanathan, Y. Wang, J. Weiss, New insights from reactivity testing of supplementary cementitious materials, Cem Concr Compos. 103 (2019) 331–338. https://doi.org/10.1016/j.cemconcomp.2019.05.017.

[22] A.M. Boddy, R.D. Hooton, M.D.A. Thomas, Effect of product form of silica fume on its ability to control alkali-silica reaction, Cem Concr Res. 30 (2000) 1139–1150. https://doi.org/10.1016/S0008-8846(00)00297-0.

[23] M.H. Shehata, M.D.A. Thomas, Effect of fly ash composition on the expansion of concrete due to alkali-silica reaction, Cem Concr Res. 30 (2000) 1063–1072. https://doi.org/10.1016/S0008-8846(00)00283-0.

[24] B. Lothenbach, A. Nonat, Calcium silicate hydrates: Solid and liquid phase composition, Cem Concr Res. 78 (2015) 57–70. https://doi.org/10.1016/j.cemconres.2015.03.019.

[25] S.-Y. Hong, F.P. Glasser, Alkali binding in cement pastes: Part I. The C-S-H phase, Cem Concr Res. 29 (1999) 1893–1903. https://doi.org/10.1016/S0008-8846(99)00187-8.

[26] E. L'Hôpital, B. Lothenbach, K. Scrivener, D.A. Kulik, Alkali uptake in calcium alumina silicate hydrate (C-A-S-H), Cem Concr Res. 85 (2016) 122–136. https://doi.org/10.1016/j.cemconres.2016.03.009.

[27] B. Lothenbach, K. Scrivener, R.D. Hooton, Supplementary cementitious materials, Cem Concr Res. 41 (2011) 1244–1256. https://doi.org/10.1016/j.cemconres.2010.12.001.

[28] A. Vollpracht, B. Lothenbach, R. Snellings, J. Haufe, The pore solution of blended cements: a review, Mater Struct. 49 (2016) 3341–3367. https://doi.org/10.1617/s11527-015-0724-1.

[29] M.H. Shehata, M.D.A. Thomas, R.F. Bleszynski, The effects of fly ash composition on the chemistry of pore solution in hydrated cement pastes, Cem Concr Res. 29 (1999) 1915–1920. https://doi.org/10.1016/S0008-8846(99)00190-8.

[30] R. Helmuth, D. Stark, S. Diamond, M. Moranville-Regourd, Alkali-Silica Reactivity: An Overview of Research, SHRP-C-342, Strategic Highway Research Program, National Research Council, Washington, D.C., 1993.

[31] Y. Kawabata, K. Yamada, Evaluation of alkalinity of pore solution based on the phase composition of cement hydrates with supplementary cementitious materials and its relation to suppressing ASR expansion, Journal of Advanced Concrete Technology. 13 (2015) 538–553. https://doi.org/10.3151/jact.13.538.

[32] G. Plusquellec, M.R. Geiker, J. Lindgård, J. Duchesne, B. Fournier, K. De Weerdt, Determination of the pH and the free alkali metal content in the pore solution of concrete: Review and experimental comparison, Cem Concr Res. 96 (2017) 13–26. https://doi.org/10.1016/j.cemconres.2017.03.002.

[33] K. Natkunarajah, K. Masilamani, S. Maheswaran, B. Lothenbach, D.A.S. Amarasinghe, D. Attygalle, Analysis of the trend of pH changes of concrete pore solution during the hydration by various analytical methods, Cem Concr Res. 156 (2022). https://doi.org/10.1016/j.cemconres.2022.106780.

[34] M. Ranger, M.T. Hasholt, R.A. Barbosa, Pore solution alkalinity of cement paste as determined by Cold Water Extraction, CEMENT. 11 (2023) 100055. https://doi.org/10.1016/j.cement.2023.100055.

[35] A. Tuinukuafe, K.S.T. Chopperla, W.J. Weiss, J.H. Ideker, O.B. Isgor, Estimating $Na^+$ and $K^+$ concentrations of the pore solution based on exsitu leaching tests and thermodynamic modeling, RILEM Technical Letters. 7 (2022) 88–97. https://doi.org/10.21809/rilemtechlett.2022.164.

[36] L.M. Ottosen, D. Thornberg, Y. Cohen, S. Stiernström, Utilization of acid-washed sewage sludge ash as sand or cement replacement in concrete, Resour Conserv Recycl. 176 (2022). https://doi.org/10.1016/j.resconrec.2021.105943.

[37] M.-N. de Noirfontaine, M. Courtial, F. Dunstetter, G. Gasecki, M. Signes-Frehel, Tricalcium silicate $Ca_3SiO_5$ superstructure analysis: a route towards the structure of the M1 polymorph, Zeitschrift Für Kristallographie. 227 (2012) 102–112. https://doi.org/10.1524/zkri.2011.1425.

[38] R. Snellings et al., RILEM TC-238 SCM recommendation on hydration stoppage by solvent exchange for the study of hydrate assemblages, Mater Struct. 51 (2018). https://doi.org/10.1617/s11527-018-1298-5.

[39] K. Scrivener, R. Snellings, B. Lothenbach, A practical guide to microstructural analysis of cementitious materials, CRC Press, 2016.

[40] T.C. Hansen, Physical structure of hardened cement paste. A classical approach, Mater Struct. 19 (1986) 423–436. https://doi.org/10.1007/BF02472146.

[41] E.J. Sonneveld, J.W. Visser, Automatic Collection of Powder Data from Photographs, J Appl Crystallogr. 8 (1975) 1–7. https://doi.org/10.1107/S0021889875009417.

[42] G. Le Saoût, T. Füllmann, V. Kocaba, K.L. Scrivener, Quantitative study of cementitious materials by X-ray diffraction/Rietveld analysis using an external standard, in: J.J. Beaudoin, J.K. Makar, L. Raki (Eds.), Proceedings of the 12$^{th}$ International Congress on the Chemistry of Cement, Montreal, Canada, 2007.

[43] ACI Committee 212, ACI PRC-212.3-16 Report on Chemical Admixtures for Concrete, 2016.

[44] M. Ranger, Dataset for journal article “Cold Water Extraction for determination of the free alkali metal content in blended cement pastes,” DTU Data. (2023). https://doi.org/10.11583/DTU.22155284.

[45] J. Duchesne, M.A. Bérubé, The effectiveness of supplementary cementing materials in suppressing expansion due to ASR: Another look at the reaction mechanisms. Part 2: Pore solution chemistry, Cem Concr Res. 24 (1994) 221–230. https://doi.org/10.1016/0008-8846(94)90047-7.

[46] R. Snellings, G. Mertens, J. Elsen, Supplementary cementitious materials, Rev Mineral Geochem. 74 (2012) 211–278. https://doi.org/10.2138/rmg.2012.74.6.

[47] P. Suraneni, A. Hajibabaee, S. Ramanathan, Y. Wang, J. Weiss, New insights from reactivity testing of supplementary cementitious materials, Cem Concr Compos. 103 (2019) 331–338. https://doi.org/10.1016/j.cemconcomp.2019.05.017.

[48] S. Ramanathan, L.R. Pestana, P. Suraneni, Reaction kinetics of supplementary cementitious materials in reactivity tests, Cement. 8 (2022) 100022. https://doi.org/10.1016/j.cement.2022.100022.

[49] F. Golmakani, R.D. Hooton, Impact of pore solution concentration on the accelerated mortar bar alkali-silica reactivity test, Cem Concr Res. 121 (2019) 72–80. https://doi.org/10.1016/j.cemconres.2019.02.008.

[50] R. Qian, Y. Zhang, C. Liu, Z. Liu, Y. Zhang, G. Liu, Effects of supplementary cementitious materials on pore-solution chemistry of blended cements, J Sustain Cem Based Mater. 11 (2022) 389–407. https://doi.org/10.1080/21650373.2021.1988754.

[51] T.T.H. Bach, E. Chabas, I. Pochard, C. Cau Dit Coumes, J. Haas, F. Frizon, A. Nonat, Retention of alkali ions by hydrated low-pH cements: Mechanism and $Na^+/K^+$ selectivity, Cem Concr Res. 51 (2013) 14–21. https://doi.org/10.1016/j.cemconres.2013.04.010.

[52] A. Leemann, B. Lothenbach, The $Na_2O$-equivalent of cement: A universal parameter to assess the potential alkali-aggregate reactivity of concrete?, in: M.A.T.M. Broekmans, B.J. Wigum (Eds.), Proceedings of the 13$^{th}$ International Conference on Alkali-Aggregate Reaction in Concrete, Trondheim, Norway, 2008: pp. 909–919.

[53] D.W. Hobbs, Alkali-silica reaction in concrete, Thomas Telford, London, 1988.

[54] M.H. Shehata, M.D.A. Thomas, Use of ternary blends containing silica fume and fly ash to suppress expansion due to alkali-silica reaction in concrete, Cem Concr Res. 32 (2002) 341–349. https://doi.org/10.1016/S0008-8846(01)00680-9.

[55] M.C.G. Juenger, C.P. Ostertag, Alkali-silica reactivity of large silica fume-derived particles, Cem Concr Res. 34 (2004) 1389–1402. https://doi.org/10.1016/j.cemconres.2004.01.001.

Paper III

# Relationship Between Chloride Migration, Bulk Electrical Conductivity and Formation Factor of Blended Cements

Maxime Ranger [a,b], Marianne Tange Hasholt [b]

[a] Department of Environmental and Resource Engineering, Technical University of Denmark (DTU), 2800 Kgs. Lyngby, Denmark

[b] Danish Road Directorate, 1577 Copenhagen V, Denmark

*Submitted for publication*

# Abstract

This study investigates the links between the non-steady-state chloride migration coefficient, the bulk electrical conductivity and the formation factor of blended cement paste specimens. 18 different binders were tested: two Portland cements (low- and high-alkali) in combination with limestone filler, fly ash, calcined clay, two biomass ashes, sewage sludge ash and crushed brick, as well as two Portland composite cements. In addition, three binders were tested in concrete as well for comparison.

Mixes with high-alkali cement showed better resistance to chloride transport, and the effect of supplementary cementitious materials was found to be strongly linked with their reactivity. Moreover, the results showed a clear correlation of the migration coefficient with the bulk electrical conductivity and, to a lesser extent, with the formation factor. However, these relationships are strongly influenced by the methods used to determine conductivities. Finally, the results suggested a fairly good correspondence between the results obtained on paste and concrete.

# Keywords

Chloride migration, Electrical conductivity, Formation factor, Supplementary cementitious materials (SCMs), Transport.

# 1 Introduction

Supplementary cementitious materials (SCMs) have significant effects on the phase assemblage [1], the pore structure [2] and the pore solution composition [3] of blended cement pastes. Consequently, moisture and ion transport properties are affected [4], which has implications for most durability issues.

The formation factor $FF$ was proposed as a measure of transport properties in concrete [5]. It is defined as the ratio between the electrical conductivity of the pore solution $\sigma_{ps}$ and the bulk electrical conductivity $\sigma_b$, as shown in Equation (1) [6]. The formation factor is also linked with the porosity $\Phi$ and a pore connectivity parameter $\beta$ [7].

$$FF = \frac{\sigma_{ps}}{\sigma_b} = \frac{1}{\Phi\beta} \quad (1)$$

Huang et al. [8] showed a proportionality between the non-steady-state chloride migration coefficient $D_{nssm}$ and the reciprocal of *FF* for paste samples, as per Equation (2). The coefficient of proportionality $D_{ps}$ matched with the chloride migration coefficient in the bulk pore solution ($D_{ps} = 2.03 \cdot 10^{-9}$ m$^2$/s). However, different trends were reported by other authors. Baroghel-Bouny et al. [9] found a correlation between the steady-state migration coefficient $D_{ssm}$ and *1/FF* (on concrete), while Wilson et al. [10] reported a relationship between $D_{ssm}$ and $\sigma_b$ (on paste).

$$D_{nssm} = \frac{D_{ps}}{FF} \quad (2)$$

The present work was carried out as part of a study related to the effects of SCMs on the alkali-silica reaction (ASR). Transport properties play a large role in accelerated ASR testing, whether it is in immersion tests like accelerated mortar bar tests (transport of water and ions) or in high relative humidity (*RH)* tests like concrete prism tests (transport of vapour and leaching of alkali metals). Chopperla and Ideker [11] found a relationship between the expansion in the miniature concrete prism test and the ratio between the hydroxide ion concentration and *FF*. Additionally, the measurements performed by Lindgård et al. [12] on ASR concrete prisms (38°C, 100% *RH*) showed that the internal *RH* was usually above 80% after 4 weeks of exposure, even for low water-to-cement ratios (*w/c* = 0.30) or for binders containing fly ash. For this range of *RH*, Huang et al. [4] noticed that the vapour diffusion coefficient was also linearly linked to *1/FF*, with a relationship similar to Equation (2).

Based on Equation (2) and the dependencies mentioned in the previous paragraph, the influence of a binder on ions and moisture transport properties may be documented via chloride migration. However, the diverging conclusions from the literature create some uncertainty as to which parameter correlates best with chloride migration results. Thus, the present paper aims to explore these relationships further when the binder composition varies, i.e. the type of SCM and the alkali content of Portland cement (PC). In addition, it is intended to evaluate the sensitivity of the pore solution and bulk electrical conductivity results when different approaches are used. The study is primarily based on paste samples, however some results on concrete specimens are also presented for comparison. Experimental work includes non-steady-state chloride migration according to NT BUILD 492 adapted for paste and bulk conductivity measurements. The conductivity of the pore solution was calculated based on pore solution compositions published previously [13,14].

# 2 Materials and methods

## 2.1 Raw materials

Two types of Portland cement (PC) and two types of Portland composite cement (PCC) were used in the study. Each row starts with their designation in the present paper:

- PC-LA – CEM I low alkali (0.58 $Na_2O_{eq}$ wt.%).
- PC-HA – CEM I high alkali (1.23 $Na_2O_{eq}$ wt.%).
- PCC35 – CEM II/B-M (35 wt.% clinker replacement, calcined clay and limestone).
- PCC50 – CEM II/C-M (50 wt.% clinker replacement, calcined clay and limestone).

PC-LA, PCC35 and PCC50 were all manufactured with the same clinker. In addition, seven different SCMs were tested in combination with the two PC: limestone filler (LL), fly ash (FA), calcined clay (CC), two biomass ashes (BA1 and BA2), sewage sludge ash (SSA) and crushed brick (CB). The chemical compositions were measured by X-ray fluorescence (XRF) on powders sieved below 63 µm (Malvern Panalytical Zetium spectrometer). The particle size distribution was measured with a laser diffractometer (Malvern Mastersize 2000). Moreover, it was assumed that PCC50 had the same density as PCC35. The values are presented in Table 1 for cements, and in Table 2 for SCMs. Reference [13] contains more information about the mineralogical composition of the cementitious materials, as well as the reactivity of the SCMs. The reactivity was investigated with the $R^3$ method, explained in [15]. The $R^3$ bound water values measured at 7 days are also reported in Table 2.

*Table 1: Chemical composition of the cements measured by XRF.*

| Oxide | Portland cement | | Composite cement | |
|---|---|---|---|---|
| | PC-LA | PC-HA | PCC35 | PCC50 |
| $SiO_2$ | 19.2 | 19.2 | 22.1 | 26.6 |
| $Al_2O_3$ | 5.2 | 5.1 | 6.4 | 8.5 |
| $Fe_2O_3$ | 3.67 | 2.99 | 3.95 | 4.94 |
| MgO | 1.0 | 2.4 | 1.1 | 1.4 |
| CaO | 63.4 | 60.6 | 54.2 | 45.7 |
| $Na_2O$ | 0.33 | 0.45 | 0.38 | 0.45 |
| $K_2O$ | 0.38 | 1.18 | 0.69 | 1.09 |
| $SO_3$ | 3.14 | 3.81 | 2.73 | 2.47 |
| $Na_2O_{eq}$ | 0.58 | 1.23 | 0.83 | 1.17 |
| LOI | 3.21 | 3.56 | 7.86 | 7.88 |
| Density [kg/m$^3$] | 3150 | 3130 | 3020 | 3020 |
| $d_{50}$ [µm] | 14.0 | 10.7 | 17.4 | 14.0 |

*Table 2: Chemical composition of the SCMs measured by XRF and reactivity measured by the $R^3$ bound water test at 7 days [13].*

| Oxide | Limestone | Fly ash | Calcined clay | Biomass ash | | Sewage sludge ash | Crushed brick |
|---|---|---|---|---|---|---|---|
| | LL | FA | CC | BA1 | BA2 | SSA | CB |
| $SiO_2$ | 2.0 | 56.2 | 49.0 | 25.5 | 23.2 | 56.8 | 63.4 |
| $Al_2O_3$ | 0.4 | 23.8 | 17.3 | 4.8 | 4.3 | 8.4 | 11.2 |
| $Fe_2O_3$ | 0.12 | 6.90 | 9.74 | 1.80 | 1.93 | 19.57 | 4.32 |
| MgO | 0.3 | 1.8 | 2.5 | 3.5 | 4.0 | 0.9 | 1.2 |
| CaO | 54.2 | 3.9 | 10.1 | 34.1 | 30.9 | 1.4 | 9.0 |
| $Na_2O$ | 0.03 | 0.49 | 0.81 | 0.87 | 0.71 | 1.03 | 2.81 |
| $K_2O$ | 0.06 | 1.64 | 2.66 | 4.93 | 7.35 | 2.43 | 0.43 |
| $SO_3$ | 0.08 | 0.79 | 0.98 | 4.58 | 12.66 | 0.38 | 0.63 |
| $Na_2O_{eq}$ | 0.07 | 1.57 | 2.55 | 4.12 | 5.55 | 2.63 | 2.91 |
| LOI | 42.52 | 1.57 | 4.94 | 15.83 | 10.26 | 3.77 | 5.37 |
| $d_{50}$ [µm] | 3.8 | 18.0 | 39.4 | 15.5 | 70.2 | 11.1 | 42.8 |
| $R^3$ bound water [g/100 g dry paste] | 2.08 | 5.90 | 8.28 | 3.24 | 2.63 | 5.15 | 3.89 |

The aggregrates in concrete consisted of a Danish 0-2 mm sand (Storebælt) and two fractions of granite (Blå Rønne), 4-8 and 11-16 mm. When necessary, a superplasticiser (SP) was added to the mixes (MasterGlenium SKY 851, active substance: polycarboxylates).

## 2.2 Preparation of samples

### 2.2.1 Paste

Paste samples were produced by mixing 300 g of dry cementitious materials and 150 g of deionised water ($w/b$ = 0.5) with a high-shear laboratory mixer (capacity of 1.2 L, unloaded speed announced at 22 000 rpm). The constituents were added into the mixing bowl in the following order: water, cement and SCM. The blend was mixed two times 30 s, with a resting time of 90 s in between. The specimens were cast in hollow POM cylinders sealed with rubber bungs. The cylinders were approx. 120 mm long, diameter 22 mm for migration tests and diameter 25 mm for conductivity and pore solution analysis. The specimens were rotated along their longitudinal axis for 24 ± 2 h until demoulding, and then cured at 20°C in sealed pouches of aluminium-plastic composite foil ("coffee-bag foil").

### 2.2.2 Concrete

Concrete batches of 20 L were prepared in a 50 L pan mixer. The dry constituents were mixed for 1 min, then water was added ($w/b$ = 0.50), and the concrete was mixed for 2 min. If the slump measured according to EN 12350-2 was below 80 mm, the concrete was mixed again for 1 min with the addition of superplasticiser. The air content was measured as per EN 12350-7. The concrete compositions and the fresh properties are given in Table 3.

*Table 3: Concrete compositions (in kg/m$^3$) and fresh properties.*

| | Cement | Water | Aggregates | | | SP | Slump [mm] | Air content [vol.%] |
|---|---|---|---|---|---|---|---|---|
| | | | 0-2 mm | 4-8 mm | 11-16 mm | | | |
| Density [kg/m$^3$] | See Table 1 | 1000 | 2620 | 2720 | 2640 | 1050 | - | - |
| PC-LA | 440 | 220 | 586 | 489 | 598 | 0.0 | 80 | 1.4 |
| PCC35 | 440 | 220 | 580 | 485 | 593 | 1.3 | 120 | 1.1 |
| PCC50 | 440 | 220 | 580 | 485 | 593 | 2.6 | 100 | 1.2 |

For each batch, three cylinders (diameter 100 mm x 200 mm) were cast on a vibrating table (filled in two layers) and demoulded after 24 h ± 2 h. The specimens were sealed cured in aluminium-plastic bags stored at 20°C.

## 2.3 Chloride migration

Chloride migration was performed according to NT BUILD 492 on both concrete and paste specimens. After 28 days of curing, 50 mm long pieces were cut and vacuum saturated with a saturated $Ca(OH)_2$ solution for 18 h ± 1 h. The specimens were then placed in the migration setup (anolyte: 0.3 mol/L NaOH, catholyte: 10 wt.% NaCl) with 30 V applied to determine the initial current.

For concrete samples, the test settings (voltage, current and duration) were determined according to Appendix 2 in NT BUILD 492. At the end of the test, the specimens were split into two parts, and the broken surfaces were sprayed with $AgNO_3$. The penetration depth of chlorides was measured with a calliper in seven different locations, evenly distributed along the penetration front. The outer 10 mm on each side was avoided. All tests were duplicated in a setup where the two specimens shared the same catholyte solution (12 L in total).

A similar procedure was used for paste specimens, but several adjustments were made to deal with the smaller sample size and the difference in transport properties. Some illustrations of the setup are shown in Figure 1. First, the volume of anolyte and catholyte were reduced to 20 mL and 3.5 L per sample, respectively. Second, Appendix 2 in NT BUILD 492 could not be used to choose the voltage and the test duration. For practical reasons, the test duration was chosen to be 24 h. A series of trial-and-error tests were then performed to determine appropriate voltages as a function of the initial current, where the objective was to obtain a penetration depth of around 25 mm. Finally, only two measurements of the chloride front were taken (omitting the outer 5 mm on each side).

For both paste and concrete, the non-steady-state chloride migration coefficient was calculated according to Equation (3).

$$D_{nssm} = \frac{0.0239 \cdot (273 + T) \cdot L}{(U - 2) \cdot t} \left( x_d - 0.0238 \sqrt{\frac{(273 + T) \cdot L \cdot x_d}{U - 2}} \right) \quad (3)$$

Where:

- $D_{nssm}$: non-steady-state chloride migration coefficient [$10^{-12}$ $m^2/s$].
- $U$: absolute value of the applied voltage [V].
- $T$: average value of the initial and final temperatures in the anolyte solution [°C].
- $L$: Thickness of the test specimen [mm].
- $x_d$: average value of the penetration depths [mm].
- $t$: test duration [h].

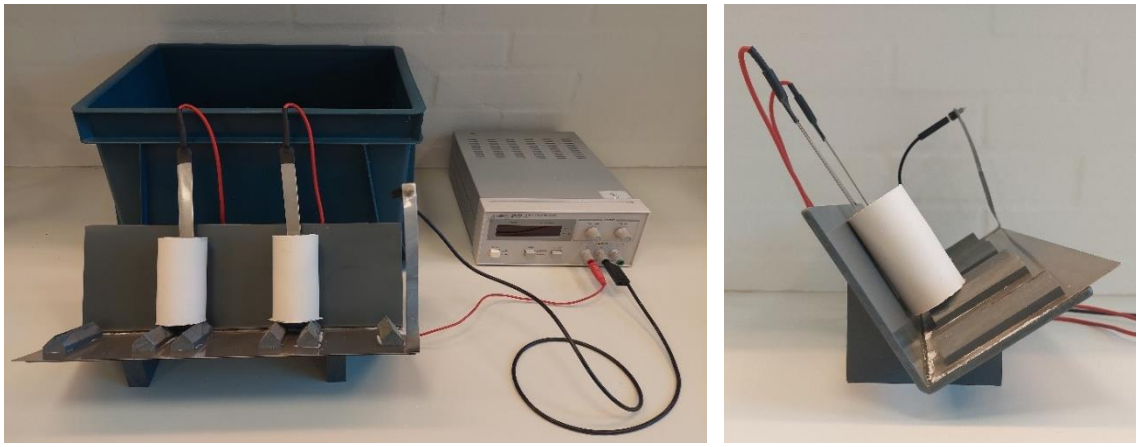

*Figure 1 – Chloride migration setup for paste samples. The plastic support where the sleeves are resting is normally placed in the box, which is filled with 10 wt.% NaCl solution.*

## 2.4 Porosity and degree of saturation

The porosity was measured according to the PF method [16] on paste specimens cast with PC-LA, PCC35 and PCC50. After 23 days of sealed curing (mass $m_1$), the specimens were immersed in the simulated pore solutions for 5 days ($m_2$), and then dried at 105°C until reaching constant mass ($m_3$). The porosity ($\Phi$) and the degree of saturation ($S$) were determined according to Equations (4a) and (4b) respectively, where $v$ is the volume of the specimen calculated from its dimensions and $\rho_w$ the density of water (1000 kg/$m^3$).

$$\Phi = \frac{m_2 - m_3}{\rho_w \cdot v} \quad (4a)$$

$$S = \frac{m_1 - m_3}{m_2 - m_3} \quad (4b)$$

## 2.5 Formation factor

As shown in Equation (1), the formation factor can be calculated from the bulk conductivity and the conductivity of the pore solution. The procedure to determine these two values is detailed below.

### 2.5.1 Bulk conductivity

The bulk conductivity for paste specimens was measured with a procedure similar to the volumetric method in EN 12390-19. On each end of a cylindrical specimen were placed: a sponge soaked in deionised water, an electrode, and a non-conductive POM plate (1 cm thick). The specimen stood vertically, and a steel mass of 500 g was placed on the top POM plate. Two conductive rings with 40 mm spacing were clamped onto the specimen, with a sponge between the specimen surface and the ring. A picture of the setup is shown in Figure 2.

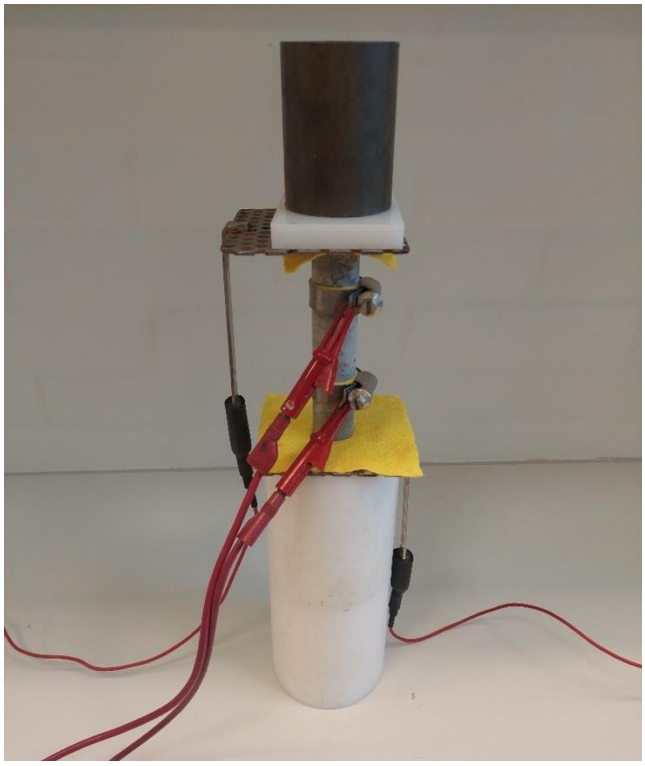

*Figure 2: Bulk electrical conductivity setup for paste samples. The measurements are made between the inner rings (voltage) and through the outer electrodes (current).*

An alternative voltage (amplitude 5 V, frequency 50 Hz) was applied to the outer electrodes. Two parameters were measured: the current passing through the outer electrodes, and the voltage between the inner electrodes. The bulk conductivity $\sigma_b$ (in S/m) was then calculated according to Equation (5).

$$\sigma_b = \frac{I}{U_e} \cdot \frac{L_e}{A} \quad (5)$$

Where:

- $I$: amplitude of the current applied on the outer electrodes [A].
- $U_e$: amplitude of the voltage between the inner electrodes [V].
- $L_e$: distance between the inner electrodes [m].
- $A$: cross-sectional area of the specimen [$m^2$].

Most measurements were conducted on sealed cured samples which were not saturated before the test. This is because the same paste samples were also used for Cold Water Extraction, where it was desired not to disturb the pore solution. To evaluate the influence of such conditioning, companion specimens made of plain PC-LA, PCC35 and PCC50 (both paste and concrete) were cured in simplified pore solutions at 20°C. The simplified pore solutions were prepared by dissolving NaOH and KOH pellets in deionised water. The concentrations were based on previous studies on the same materials [14,17] and are summarised in Table 4. $Ca(OH)_2$ was then added to the solutions until saturation. The intention was to avoid 1) leaching of alkalis (not to alter the conductivity of the pore solution) and 2) leaching of calcium hydroxide (not to increase the porosity [5]).

*Table 4: Concentrations of alkali hydroxides in the simplified pore solutions used for curing some of the specimens.*

| Mix | NaOH [mol/L] | KOH [mol/L] |
|---|---|---|
| PC-LA | 0.25 | 0.23 |
| PCC35 | 0.18 | 0.17 |
| PCC50 | 0.17 | 0.15 |

For comparison, the bulk resistivity was also determined on concrete specimens for PC-LA, PCC35 and PCC50. Both curing regimes were implemented. The bulk conductivity was calculated as the reciprocal of the resistivity, which was measured according to the Wenner probe method with a Proceq Resipod instrument. Measurements were taken at four locations around the cylinders (90° between each) and averaged.

### 2.5.2 Pore solution conductivity

The pore solution composition was determined by Cold Water Extraction (CWE) on paste specimens sealed cured for 28 days. CWE was performed by crushing paste to obtain 20 g of the 0.5-1 mm fraction, which was then mixed with 20 g of deionised water and stirred for 5 min. The slurry was vacuum filtered, and the filtrate was analysed with ICP-OES (Varian 720-ES) to determine the concentrations of Na and K. The volume of pore solution was estimated by drying pieces of paste of approximately 30 g in a desiccator containing silica gel, stored at 40°C. The results were published in previous publications [14,17]. For PC-LA, PCC35 and PCC50, the pore solution was also studied by Pore Water Extraction (PWE, high-pressure extraction).

The conductivity of the pore solution was then derived from the concentrations of $Na^+$, $K^+$ and $OH^-$, as proposed in [18]. Since $[OH^-]$ was not measured, it was assumed that $[OH^-] \approx [Na^+] + [K^+]$. The calculated conductivity is given by Equations (6a)-(6c).

$$\sigma_{ps} = \sum_i z_i \cdot c_i \cdot \lambda_i \quad (6a)$$

$$\lambda_i = \frac{\lambda_i^0}{1 + G_i \cdot \sqrt{I_M}} \quad (6b)$$

$$I_M = \frac{1}{2} \sum_i z_i^2 \cdot c_i \quad (6c)$$

Where:

- $\sigma_{ps}$: calculated conductivity [S/m].
- $z$: valence of [-].
- $c$: concentration [mol/L].
- $\lambda$: equivalent conductivity [$cm^2 \cdot S/mol$].
- $\lambda^0$: equivalent conductivity at infinite dilution [$cm^2 \cdot S/mol$].
- $G$: empirical conductivity coefficient $[mol/L]^{-1/2}$.
- $I_M$: ionic strength of the solution [mol/L].

The values of $\lambda^0$ and $G$ used in the calculations were taken from [18] and are shown in Table 5.

*Table 5: Equivalent conductivity at infinite dilution and conductivity coefficient at 25°C [18].*

| Species | $\lambda^0$ [cm$^2$·S/mol] | $G$ [mol/L]$^{-1/2}$ |
|---|---|---|
| $OH^-$ | 198.0 | 0.353 |
| $K^+$ | 73.5 | 0.548 |
| $Na^+$ | 50.1 | 0.733 |

# 3 Results and discussion

The results and the associated raw data presented in this section are available online, see reference [19]. All tests were carried out 28 days after casting. As a preliminary remark, the authors would like to highlight that some graphs contain a limited number of data points. Even though some elaboration will be made on the visible trends, one must remain cautious with respect to the validity of these observations.

## 3.1 Comparison of properties measured on paste and concrete

### 3.1.1 Non-steady-state migration coefficient

Figure 3 displays the non-steady-state migration coefficient ($D_{nssm}$) determined on paste and concrete samples cast with the same binders. The value for concrete cast with PC-LA is in agreement with Hasholt and Jensen [20], who used the same cement and *w/c*, and a similar paste content. Moreover, PCC35 and PCC50 perform better than PC against chloride ingress, which was already observed by other authors for limestone calcined clay cements [2]. Based on the three data points, the relationship between concrete and paste can be reasonably well described by a linear fit.

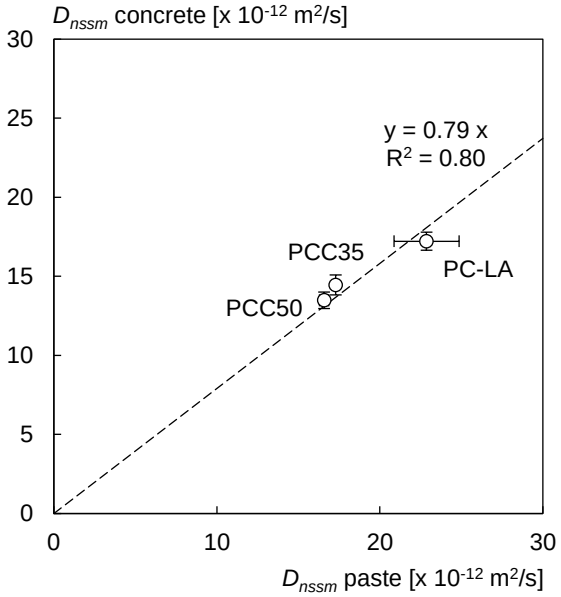


*Figure 3: Non-steady-state migration coefficient (in $10^{-12}$ $m^2/s$) at 28 days for paste and concrete samples cast with the same binders and w/b. The trend line was forced to pass through (0,0) for physical reasons.*

Previous work by Delagrave et al. [21] and Yang and Su [22] investigated the changes in steady-state chloride migration coefficient ($D_{ssm}$) induced by the presence of aggregates. Both studies were conducted on mortar samples, where the sand volume fraction was increased from 0% to 40% [22] or 57% [21]. It was concluded that increasing the aggregate content leads to:

- On the one hand, a decrease of $D_{ssm}$ due to paste dilution and increased tortuosity.
- On the other hand, an increase of $D_{ssm}$ due to enhanced transport properties in the interfacial transition zone (ITZ).

The studies also showed that increased tortuosity and modified transport properties in the paste (increased in the ITZ, hampered otherwise) roughly compensate each other, so that accounting for paste dilution only gives a reasonably accurate estimate. Jensen et al. [23] conducted diffusion tests and highlighted this fact as well. Moreover, it was shown that similar chloride profiles were obtained on paste and corresponding mortar exposed to the same conditions [24].

Non-steady-state migration experiments are based on measuring the chloride penetration depth, not the chloride flux through the entire cross-section. Thus, the pure paste dilution effect caused by aggregates is expected to have a smaller influence on non-steady-state results compared to steady-state ones. This was

experimentally observed by Luping and Nilsson [25], who found that $D_{nssm}$ for mortar was about 70% of that in a corresponding paste, with $w/c$ = 0.4 and a sand volume fraction of 51% in the mortar. This is in line with the trend stemming from the data shown in Figure 3.

### 3.1.2 Bulk conductivity

The bulk conductivity correspondence between paste and concrete is shown in Figure 4 for PC-LA, PCC35 and PCC50. For each curing regime, a linear relationship exists independently of the binder type. The data published by Princigallo et al. [26] show that a concrete containing 60 vol.% of aggregates has approximately 35% of the bulk conductivity of a corresponding paste after 2 days of sealed curing. This ratio for sealed cured specimens in Figure 4 varies between 20 and 40%, which is a similar order of size. Higher values are obtained with specimens cured in solution, which will be discussed in detail in Section 3.2.

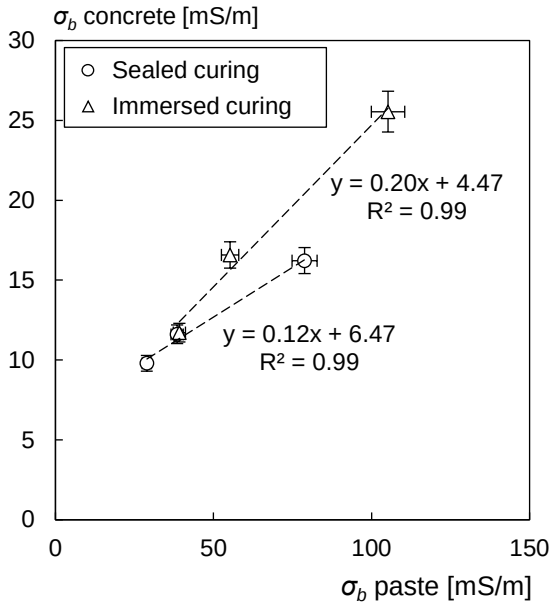


*Figure 4: Bulk conductivity at 28 days measured on paste and concrete, for specimens sealed cured or cured in simplified pore solution (PC-LA, PCC35 and PCC50).*

## 3.2 Influence of specimen conditioning and measuring methods on conductivities

### 3.2.1 Bulk conductivity

The influence of the curing regime on $\sigma_b$ is presented in Figure 5, which shows the same data as in Figure 4 but plotted in a different way. As observed by Weiss et al. [27], samples cured in solutions have a higher $\sigma_b$ than sealed cured

specimens. However, a linear relationship with a very good fit ($R^2$ = 0.99) seems valid for both paste and concrete.

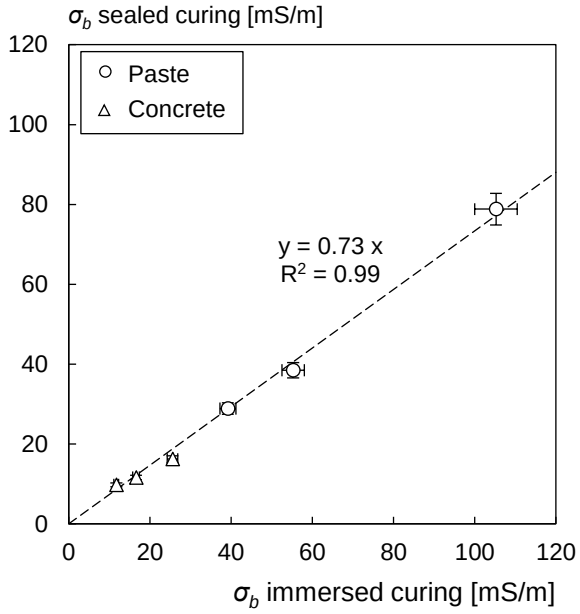


*Figure 5: Bulk conductivity at 28 days measured on specimens cured under two different regimes: sealed curing and immersed curing (in simplified pore solution).*

According to Bentz and Stutzman [28], sealed curing creates a more disconnected pore network. Hydration products in sealed cured specimens tend to concentrate in the smallest pores between unhydrated cement particles, contrary to saturated curing where hydration products are more evenly distributed. Another significant difference is the degree of saturation of the specimens. The work of Weiss et al. [27] suggests that the ratio between the bulk conductivity of a non-saturated sample and that of a saturated sample is equal to $S^{n-1+\delta}$, where $S$ is the degree of saturation, $n$ is an empirical coefficient typically between 4 and 5 for cementitious materials and $\delta$ is a correction term accounting for the increased ionic strength of the pore solution in non-saturated samples, which varies between 0.1 and 0.3.

The porosity and the degree of saturation of the sealed cured samples are shown in Table 6, together with the factor $S^{n-1+\delta}$ calculated with $n$ = 5 and $\delta$ = 0.15. These values were taken from reference [27], for an ionic strength around 0.3-0.4 mol/L.

*Table 6: Porosity and degree of saturation measured on sealed cured specimens. The term $S^{n-1+\delta}$ was calculated with n = 5 and $\delta$ = 0.15.*

| Mix | $\Phi$ [vol.%] | $S$ [-] | $S^{n-1+\delta}$ [-] |
|---|---|---|---|
| PC-LA | 45.5 | 0.925 | 0.723 |
| PCC35 | 48.3 | 0.930 | 0.740 |
| PCC50 | 49.4 | 0.926 | 0.728 |

The values for $S^{n-1+\delta}$ presented in Table 6 fit well with the slope in Figure 5, which suggests that the degree of saturation is the main reason for the deviation from the 1:1 line. The degree of hydration may also play a role [27], however it was found to be relatively high for a sealed cured paste specimen with PC-LA at 28 days (0.89) [13]. Thus, no significant increase is expected with immersed curing.

### 3.2.2 Pore solution conductivity

Figure 6 shows the pore solution conductivity calculated from Equations (6a)-(6c), using two different datasets obtained on paste samples with PWE and (CWE) [13,14].

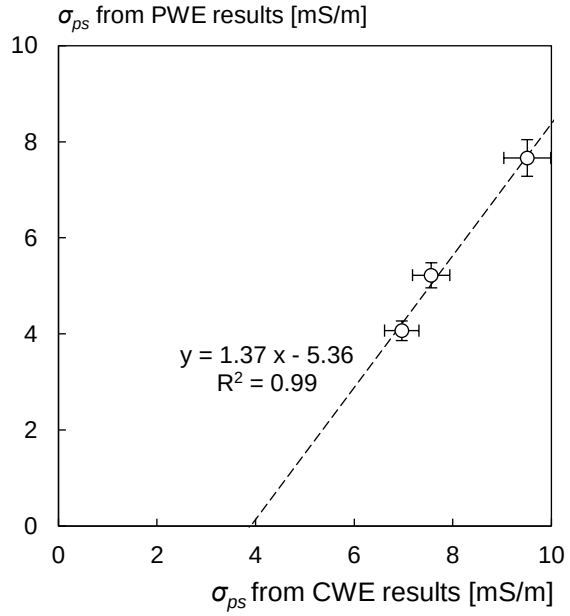


*Figure 6: Pore solution conductivity for PC-LA, PCC35 and PCC50 calculated from CWE and PWE results at 28 days.*

The calculations with CWE lead to higher conductivities, which is a direct consequence of CWE giving systematically larger alkali metal concentrations in the pore solution compared to PWE [13,14].

Huang et al. [4] already underlined the influence of the method to determine the conductivity of the pore solution. The authors argued that squeezing out the pore solution may not extract ions present in the diffusion layer of the electrical double layer, which would underestimate the conductivity of the pore solution. This explanation was put forward to explain the difference between their results and those of Wilson et al. [10]. As mentioned in a previous study [17], it is suspected that alkali metals initially present in the electrical double layer may be released during CWE. This might partly compensate for the pitfall mentioned above, but a quantitative analysis is necessary to evaluate the magnitude of the change.

### 3.2.3 Formation factor

The results from the previous sections can be combined to evaluate the sensitivity of the formation factor to the different methods used to determine conductivities. Figure 7 shows *1/FF* for PC-LA, PCC35 and PCC50 for the four combinations: bulk conductivity measured on sealed cured specimens or specimens cured in their pore solution, and pore solution conductivity determined from CWE results or PWE results.

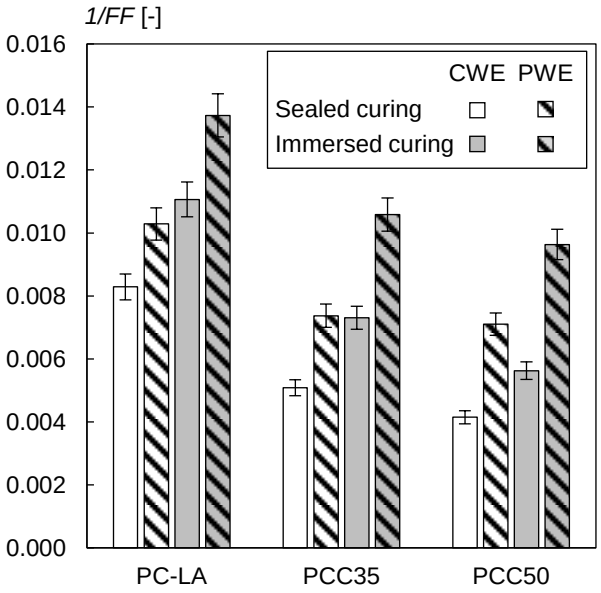


*Figure 7: Sensitivity of the formation factor reciprocal (1/FF) for paste specimens. The bulk conductivity was measured on specimens either sealed cured or cured in solution, and the pore solution conductivity was calculated from CWE or PWE results.*

One can see that *1/FF* may vary by a factor >2 between the two extreme combinations. Even though it is not intended to discuss here which approaches are the most appropriate, it must be highlighted that the choice significantly influences the results. A more in-depth discussion on the topic can be found in

Weiss et al. [27], where it is emphasised that *FF* depends on both the saturation state and hydration.

## 3.3 Influence of the binder composition on the migration coefficient

Table 7 presents the parameters used in the migration test with paste samples: initial current at 30 V, adjusted voltage and subsequent intensity. In addition, the chloride penetration depth at the end of the test (average of two samples) is also given.

*Table 7: Settings used in the chloride migration test on paste (given for one paste specimen). The test duration was set to 24 h for practical reasons.*

| Mix | | Initial current at 30 V [mA] | Adjusted voltage [V] | New current [mA] | Cl penetration depth [mm] |
|---|---|---|---|---|---|
| PC-LA | Ref | 25 | 12 | 9 | 19.7 |
| | LL | 39 | 9 | 10 | 32.8 |
| | FA | 20 | 10 | 12 | 40.9 |
| | BA1 | 35 | 10 | 10 | 28.1 |
| | BA2 | 47 | 8 | 10 | 27.2 |
| | CC | 6 | 30 | 6 | 22.9 |
| | SSA | 11 | 20 | 10 | 34.8 |
| | CB | 35 | 10 | 10 | 31.7 |
| PC-HA | Ref | 20 | 20 | 13 | 21.0 |
| | LL | 31 | 11 | 10 | 25.6 |
| | FA | 11 | 25 | 9 | 23.4 |
| | BA1 | 35 | 10 | 10 | 23.7 |
| | BA2 | 48 | 8 | 9 | 22.6 |
| | CC | 3 | 45 | 5 | 13.1 |
| | SSA | 11 | 12 | 9 | 26.0 |
| | CB | 23 | 15 | 11 | 25.3 |

The calculated $D_{nssm}$ is shown in Figure 8A as a function of the binder composition (i.e. PC alkali content and SCM type). For all mixes, using PC-HA systematically leads to a lower migration coefficient compared to PC-LA. Bu et Weiss [29] observed the same effect of the cement alkali content on diffusion properties and related it to a densification of the microstructure. Figure 8B illustrates the relationship between 1) the reactivity of SCMs

measured by the $R^3$ bound water test [13] and 2) the relative difference for $D_{nssm}$, where PC samples were taken as the references.

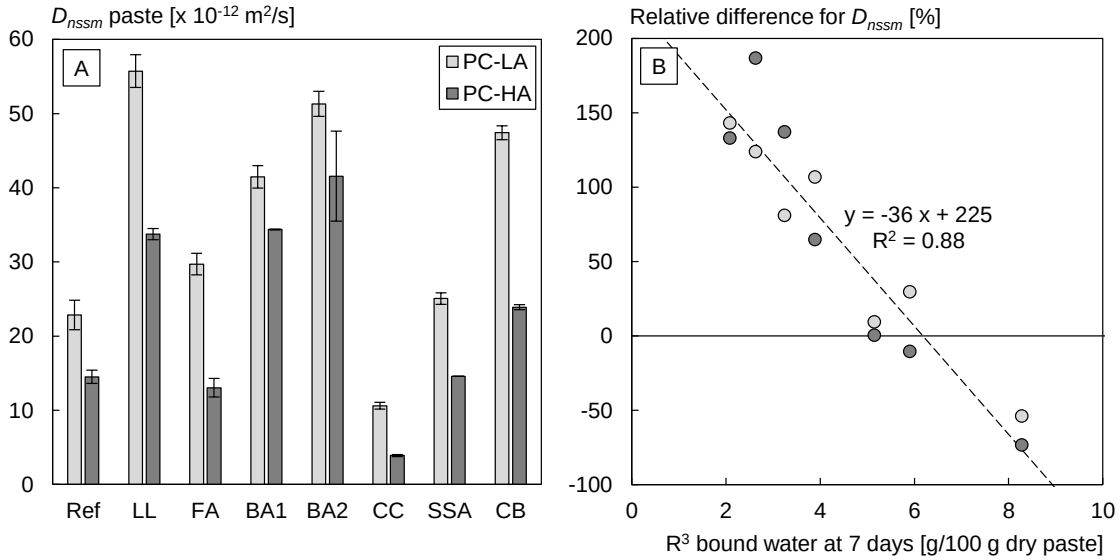


*Figure 8: A: Non-steady-state migration coefficient (in $10^{-12}$ $m^2$/s) at 28 days determined on paste samples. B: Relative non-steady-state migration coefficient plotted (with respect to the plain PC samples) as a function of the $R^3$ bound water at 7 days (in g/100 g dry paste) [13].*

Figure 8B shows a strong correlation, which emphasises the dominant effect of the SCM reactivity on $D_{nssm}$. Such influence of the reactivity is clearly visible in long-term studies, for instance with fly ash which is known to barely affect transport properties at early age but dramatically reduce chloride ingress in the long run [30]. It is however promising to see that the SCM effect can be anticipated with a simple $R^3$ bound water test. For future studies, it would be interesting to test the influence of the SCM replacement level in the mixes and expand the reactivity range to validate the linearity observed in Figure 8B, for instance by including metakaolin and silica fume.

## 3.4 Relationship between the migration coefficient and conductivities

Figure 9 displays $D_{nssm}$ as a function of $\sigma_b$ (9A) and *1/FF* (9B). $\sigma_b$ is the one measured on sealed cured samples, and $\sigma_{ps}$ is the one calculated from CWE results. As shown in Figure 9A, a reasonable proportionality exists between $D_{nssm}$ and $\sigma_b$. A subsequent link with *1/FF* is also observed in Figure 9B, even though the data are more scattered and all above the straight-line representing Equation (2).

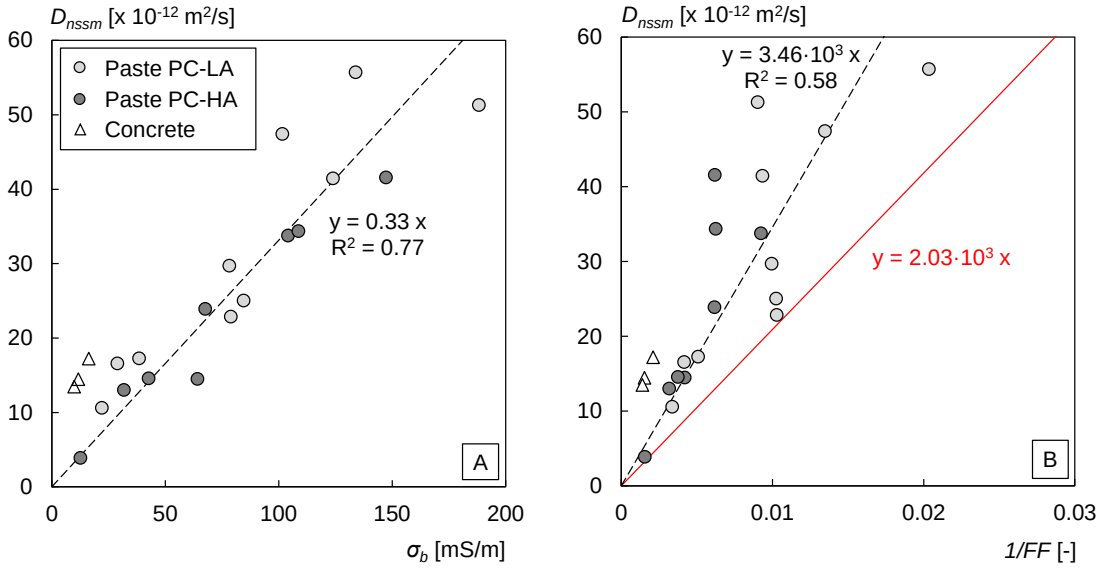


*Figure 9: Non-steady-state migration coefficient (in $10^{-12}$ $m^2/s$) at 28 days. A: as a function of the bulk conductivity. B: as a function of the reciprocal of the formation factor. Best linear fits are represented by dashed lines, and Equation (2) by a red solid line.*

None of the studies mentioned in the introduction [4,9,10] concluded on a correlation between $D_{nssm}$ and $\sigma_b$. Huang et al. [4] did see a correlation between $D_{nssm}$ and *1/FF*, however the data in Figure 9B do not match the theoretical coefficient of proportionality. Given the large variations for conductivities and for *1/FF* illustrated in Figure 7, it seems not so surprising to find different conclusions across the studies.

Assuming that the relationship found in Figure 5 holds true for all mixes, the correlation between $D_{nssm}$ and $\sigma_b$ exits whether the specimens are sealed cured or cured in their pore solution. Indeed, Figure 5 is a pure proportionality relationship, so using one value or the other in Figure 9A would only change the slope and not the $R^2$ value. By using the proportionality coefficient from Figure 5 (0.73), one can also "correct" *1/FF* and estimate what the value would be for saturated and non-leached specimens. This is done in Figure 10, and results in a significantly better fit with Equation (2), except for concrete specimens (triangles) and mixes containing BA1 and BA2 (circled in green).

The reason for the mixes containing biomass ashes to deviate from Equation (2) in Figure 10 may be due to the inaccuracy of the pore solution conductivity. As explained in Section 2.5.2, it was calculated by only considering [$Na^+$] and [$K^+$], and deducing [$OH^-$] to maintain the charge balance. However, BA1 and BA2 contain some chloride [13], so a significant amount of $Cl^-$ is probably present in the pore solution. Because the conductivity of $Cl^-$ is about 2.6 times

lower than that of $OH^-$ [18], the actual conductivity of the pore solution is likely lower than the one calculated previously. As a result, the actual *1/FF* may be larger than the one shown in Figure 10, bringing the data points closer to the expected relationship.

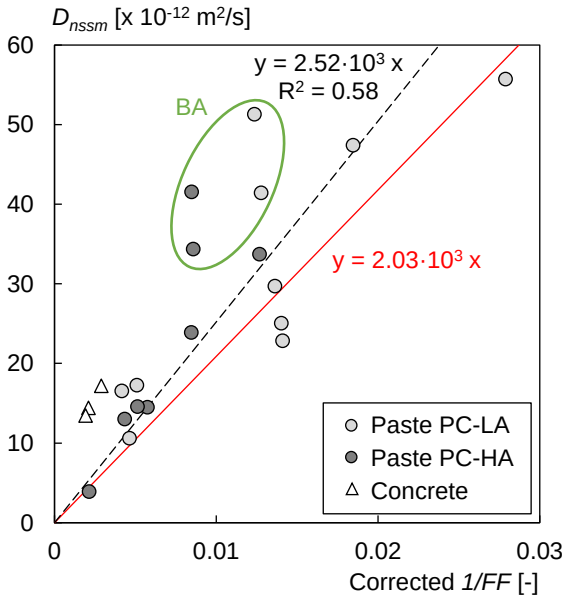


*Figure 10: Non-steady-state migration coefficient (in $10^{-12}$ $m^2/s$) at 28 days as a function of the reciprocal of the formation factor, corrected according to the relationship found in Figure 5 (division by 0.73 of the bulk conductivity measured on sealed cured specimens).*

Regarding concrete mixes, the deviation is probably due to the presence of aggregates that do not affect bulk conductivity and non-steady-state migration in the same way. Different conclusions may be drawn from steady-state experiments [9], where the presence of aggregates strongly affects the migration coefficient. In this case, the ratio between concrete and paste is expected to be significantly more related to the volume fraction of aggregates than in Figure 3.

## 3.5 Perspectives with respect to ASR testing

The beneficial effect of SCMs against ASR is generally associated with a reduction of the pore solution alkalinity [31]. However, the results presented in the previous sections combined with the conclusions of other studies [4,12] suggest that SCMs can also greatly affect the kinetics of the ASR, particularly in accelerated tests. As an example, the permeability of blended mixes was listed as a key factor to consider when using ASTM C1260/C1567 to test SCMs (immersion in 1 M NaOH at 80°C) [32].

The role of the alkali content on transport properties (Figure 8) is particularly relevant to consider. Even though high alkali contents are associated with a larger ASR risk, it was shown that they also contribute to lower the permeability of the paste. Thus, there might be a sensitive area where both phenomena have a comparable influence (but an opposite effect on the results), which should be factored in when interpreting the outcomes of the test.

# 4 Conclusion

The present study investigated the relationship between the non-steady-state migration coefficient ($D_{nssm}$), the bulk electrical conductivity ($\sigma_b$) and the formation factor ($FF$) for 18 different binders. Most of the experiments were carried out on paste specimens, however a comparison with concrete was made for a selected set of binders. The following conclusions can be drawn:

- For paste, a proportionality relationship was observed between $D_{nssm}$ and $\sigma_b$ measured on sealed cured specimens. A clear link was also observed with $1/FF$, even though the data were more scattered. From a practical perspective, measuring the bulk conductivity on sealed cured specimens has the advantage of being completely non-destructive, so that the same specimen can be measured over time or used for another test.
- Increasing the PC alkali content reduces $D_{nssm}$ and $\sigma_b$, for both plain PC and blended mixes. Moreover, the effect of SCMs varies significantly from one type to another and is correlated with their reactivity. The simple $R^3$ bound water test seems able to predict the change in $D_{nssm}$ compared to a reference PC sample.
- The methods used to determine electrical conductivities significantly influence the results, both for the bulk specimen and the pore solution. In particular, curing the samples in their own pore solution increased $\sigma_b$ by nearly 40%. Using this value to calculate $FF$ seems to better fit with the expected theoretical relationship between $D_{nssm}$ and $1/FF$. This also calls for a more specific definition of the formation factor.
- There is a clear link between the properties measured on paste and concrete, which appeared to be independent of the binder type. However, $D_{nssm}$ and $\sigma_b$ seem to be affected in different ways by the presence of aggregates. As a result, the proportionality between $D_{nssm}$ and $\sigma_b$ seems to hold, but with a different coefficient.

The points mentioned above suggest that comparing transport properties of concrete can be done on corresponding pastes, provided that the type, the volume fraction and the grading curve of aggregates are the same across all concrete mixes.

# Acknowledgments

The work presented is part of an industrial PhD project financed by the Danish Road Directorate and a joint grant from Innovation Fund Denmark (Innovationsfonden) and Realdania under the program Circular Built Environment. The financial support is gratefully acknowledged. Finally, we would like to acknowledge the support of the CALLISTE project for developing and supplying the prototype CEM II/C-M. We would also like to thank Ole Mejlhede Jensen for reviewing the manuscript and providing valuable insights.

# References

[1] Lothenbach B, Scrivener K & Hooton R D: "Supplementary cementitious materials". *Cement and Concrete Research*, Vol. 41, No. 12, 2011, pp. 1244-1256.

[2] Sui S, Georget F, Maraghechi H, Sun W & Scrivener K: "Towards a generic approach to durability: Factors affecting chloride transport in binary and ternary cementitious materials". *Cement and Concrete Research*, Vol. 124, 2019, p. 105783.

[3] Vollpracht A, Lothenbach B, Snellings R & Haufe J: "The pore solution of blended cements: a review". *Materials and Structures*, Vol. 49, No. 8, 2016, pp. 3341-3367.

[4] Huang L, Tang L, Löfgren I, Olsson N, Yang Z & Li Y: "Moisture and ion transport properties in blended pastes and their relation to the refined pore structure". *Cement and Concrete Research*, Vol. 161, 2022, p. 106949.

[5] Weiss W J, Barrett T J, Qiao C & Todak H: "Toward a specification for transport properties of concrete based on the formation factor of a sealed specimen". *Advances in Civil Engineering Materials*, Vol. 5, No. 1, 2016, pp. 179-194.

[6] Whittington H W, McCarter J & Forde M C: “The conduction of electricity through concrete”. *Magazine of Concrete Research*, Vol. 33, No. 114, 1981, pp. 48-60.

[7] Garboczi E J: “Permeability, diffusivity, and microstructural parameters: A critical review”. *Cement and Concrete Research*, Vol. 20, No. 4, 1990, pp. 591-601.

[8] Huang L, Tang L, Löfgren I, Olsson N & Yang Z: “Real-time monitoring the electrical properties of pastes to map the hydration induced microstructure change in cement-based materials”. *Cement and Concrete Composites*, Vol. 132, 2022, p. 104639.

[9] Baroghel-Bouny V, Kinomura K, Thiery M & Moscardelli S: “Easy assessment of durability indicators for service life prediction or quality control of concretes with high volumes of supplementary cementitious materials”. *Cement and Concrete Composites*, Vol. 33, No. 8, 2011, pp. 832-847.

[10] Wilson W, Georget F & Scrivener K: “Unravelling chloride transport/microstructure relationships for blended-cement pastes with the mini-migration method”. *Cement and Concrete Research*, Vol. 140, 2021, p. 106264.

[11] Chopperla K S T & Ideker J H: “Using electrical resistivity to determine the efficiency of supplementary cementitious materials to prevent alkali-silica reaction in concrete”. *Cement and Concrete Composites*, Vol. 125, 2022, p. 104282.

[12] Lindgård J, Sellevold E J, Thomas M D A, Pedersen B, Justnes H & Rønning T F: “Alkali-silica reaction (ASR) - Performance testing: Influence of specimen pre-treatment, exposure conditions and prism size on concrete porosity, moisture state and transport properties”. *Cement and Concrete Research*, Vol. 53, 2013, pp. 145-167.

[13] Ranger M & Hasholt M T: “Cold Water Extraction for determination of the free alkali metal content in blended cement pastes”. *CEMENT*, Vol. 11, 2023, p. 100079.

[14] Ranger M, Hasholt M T & Barbosa R A: “Cold Water Extraction as a method to determine the free alkali content of cementitious binders”. *Proceedings*, 16th International Congress on the Chemistry of Cement, Bangkok, Thailand, September 2023.

[15] Londono-Zuluaga D et al.: “Report of RILEM TC 267-TRM phase 3: validation of the $R^3$ reactivity test across a wide range of materials”. *Materials and Structures*, Vol. 55, No. 5, 2022, p. 142.

[16] Sellevold E J & Farstad T: “The PF-method - A simple way to estimate the w/c-ratio and air content of hardened concrete”. *Proceedings*, ConMat’05 and Mindess Symposium, Vancouver, Canada, August 2005.

[17] Ranger M, Hasholt M T & Barbosa R A: “Pore solution alkalinity of cement paste as determined by Cold Water Extraction”. *Cement*, Vol. 11, 2023, p. 100055.

[18] Snyder K A, Feng X, Keen B D & Mason T O: “Estimating the electrical conductivity of cement paste pore solutions from $OH^-$, $K^+$ and $Na^+$ concentrations”. *Cement and Concrete Research*, Vol. 33, No. 6, 2003, pp. 793-798.

[19] Ranger M: “Dataset for journal article “Relationship Between Chloride Migration, Bulk Electrical Conductivity and Formation Factor of Blended Cements””. *DTU Data*, https://doi.org/10.11583/DTU.23388200, 2023.

[20] Hasholt M T & Jensen O M: “Chloride migration in concrete with superabsorbent polymers”. *Cement and Concrete Composites*, Vol. 55, 2015, pp. 290-297.

[21] Delagrave A, Bigas J P, Ollivier J P, Marchand J & Pigeon M: “Influence of the interfacial zone on the chloride diffusivity of mortars”. *Advanced Cement Based Materials*, Vol. 5, No. 3-4, 1997, pp. 86-92.

[22] Yang C C & Su J K: “Approximate migration coefficient of interfacial transition zone and the effect of aggregate content on the migration coefficient of mortar”. *Cement and Concrete Research*, Vol. 32, No. 10, 2002, pp. 1559-1565.

[23] Jensen O M, Hansen P F, Coats A M & Glasser F P: “Chloride ingress in cement paste and mortar”. *Cement and Concrete Research*, Vol. 29, No. 9, 1999, pp. 1497-1504.

[24] Jensen O M: “Chloride ingress in cement paste and mortar measured by Electron Probe Micro Analysis”, *Report* No. R-51, Technical University of Denmark, Department of Structural Engineering and Materials, Kgs. Lyngby, Denmark, 1998, 64 pp.

[25] Tang L & Nilsson L O: “Rapid determination of the chloride diffusivity in concrete by applying an electrical field”. *ACI Materials Journal*, Vol. 89, No. 1, 1993, pp. 49-53.

[26] Principigallo A, Van Breugel K & Levita G: “Influence of the aggregate on the electrical conductivity of Portland cement concretes”. *Cement and Concrete Research,* Vol. 33, No. 11, 2003, pp. 1755-1763.

[27] Weiss J, Snyder K, Bullard J & Bentz D: “Using a Saturation Function to Interpret the Electrical Properties of Partially Saturated Concrete”. *Journal of Materials in Civil Engineering,* Vol. 25, No. 8, 2013, pp. 1097-1106.

[28] Bentz D P & Stutzman P E: “Curing, hydration, and microstructure of cement paste”. *ACI Materials Journal*, Vol. 105, No. 5, 2006, pp. 348-356.

[29] Bu Y & Weiss J: “The influence of alkali content on the electrical resistivity and transport properties of cementitious materials”. *Cement and Concrete Composites,* Vol. 51, 2014, pp. 49-58.

[30] Thomas M D A & Bamforth P B: “Modelling chloride diffusion in concrete: Effect of fly ash and slag”. *Cement and Concrete Research*, Vol. 29, No. 4, 1999, pp. 487-495.

[31] Thomas M: “The effect of supplementary cementing materials on alkali-silica reaction: A review”. *Cement and Concrete Research,* Vol. 41, No. 12, 2011, pp. 1224-1231.

[32] Bérubé M A, Duchesne J & Chouinard D: “Why the accelerated mortar bar method ASTM C1260 is reliable for evaluating the effectiveness of supplementary cementing materials in suppressing expansion due to alkali-silica reactivity”. *Cement Concrete and Aggregates,* Vol. 17, No. 1, 1995, pp. 26-34.

Paper IV

# Laboratory and field investigations of alkali-silica reaction prevention by supplementary cementitious materials: influence of the free alkali loading

Maxime Ranger [a,b], Marianne Tange Hasholt [b], Ricardo Antonio Barbosa [c]

[a] Department of Environmental and Resource Engineering,
Technical University of Denmark (DTU), 2800 Kgs. Lyngby, Denmark

[b] Danish Road Directorate, 1577 Copenhagen V, Denmark

[c] Danish Technological Institute, 2630 Taastrup, Denmark

*Manuscript in preparation*

*It is expected to submit this manuscript for publication when the AAR-10 specimens reach 2 years of exposure, as it is the recommended duration when testing SCMs. The current version was written with the data available, up to 1.5 years.*

# Abstract

The effect of various supplementary cementitious materials (SCMs) on the expansion induced by alkali-silica reaction (ASR) was investigated with outdoor exposure and different accelerated laboratory tests: ASTM C1567, TI-B 51 and RILEM AAR-10. A highly reactive sand containing porous flint was tested in combination with fly ash, two biomass ashes, two calcined clays, sewage sludge ash, crushed brick and glass beads.

The results show a correlation between the expansion at 1.5 years in AAR-10 and 2 years in the field, while some divergences were observed with ASTM C1567 and TI-B 51. It was noticed that below a certain threshold for the free alkali loading around 2.4 kg/m$^3$ free $Na_2O_{eq}$, no expansion occurred neither in AAR-10 nor in the field. The effect is less clear in ASTM C1567 and TI-B 51, which is probably partly explained by the effect of SCMs on transport properties and chemical interactions with the surrounding media.

# Keywords

Alkali-silica reaction, Blended cement, Alkalis, Accelerated tests, Field exposure

# 1 Introduction

Accelerated laboratory tests are commonly used to assess the ability of supplementary cementitious materials (SCMs) to mitigate the alkali-silica reaction (ASR). Most of these methods are directly inspired by those used to determine aggregate reactivity, e.g. the accelerated mortar bar test (AMBT) and the concrete prism test (CPT):

- The AMBT (ASTM C1260/C1567, RILEM AAR-2) is probably the most used procedure in the industry due to its relatively short duration (16 days in total), even though the mechanism by which SCMs act in the AMBT is fundamentally different than in the field [1]. Nevertheless, several studies have concluded that limiting the exposure period to 14 days and using an expansion limit of 0.10% provide a reasonable assessment of the expected field performance of the same [SCM + aggregate] combination [2–4].
- Contrary to the AMBT, the CPT (ASTM C1293, RILEM AAR-3) is by design closer to what occurs in real structures and shows a good correlation with field data [5]. However, the duration of the CPT is significantly longer than for the AMBT, as 2 years of testing are usually required for SCMs, after which the expansion is likely to flatten out due to alkali leaching [6,7].

The validity of accelerated tests is generally assessed by conducting field exposure studies, where equivalent specimens are exposed to outdoor conditions [8]. However, the long exposure period often needed is a major obstacle to a more systematic use of field testing. It was reported that specimens from field studies can expand continuously for more than 25 years, which affect the correlation with accelerated test results when evaluating preventive measures [9].

In addition to performance-based requirements, many national guidelines include prescriptive rules via maximum limits for the alkali loading in concrete. This is supported by previous works showing a clear correlation between the pore solution alkalinity and the concrete expansion [10–12]. One of the key challenges is therefore to anticipate the free alkali content, i.e. the amount of alkalis present in the pore solution available for further reaction. The main difficulty is to account for the SCM contribution, which is significantly more complex than for Portland cement.

In previous publications by the same authors, various blended mixes were investigated to determine their influence on the free alkali content [13] and on transport properties [14]. The present work compares these results with the ASR expansion obtained in field exposure cubes and in various accelerated tests: ASTM C1567, TI-B 51 and RILEM AAR-10. In particular, it is intended to investigate if the free alkali content is a reliable parameter to evaluate the ASR performance of a binder. With the emergence of alternative SCMs, there is a need to screen their ability to prevent or worsen ASR. Such assessment can be made with ASR performance tests, but they may be impractical when many materials should be tested within a limited time.

# 2 Materials and methods

This part first presents the raw materials in Section 2.1. The different ASR expansion tests are then introduced in Sections 2.2-2.4, followed by a summary of the mixes produces and the rationale for selecting them in Section 2.5. Finally, a short description of the results obtained on paste samples in previous publications [13,14] is given in Section 2.6.

## 2.1 Raw materials

### 2.1.1 Cementitious materials

Two types of Portland cement (PC) were used: a type CEM I 52.5 N low alkali (0.58 wt.% $Na_2O_{eq}$) and a type CEM I 52.5 R high alkali (1.23 wt.% $Na_2O_{eq}$). In the following, they are denoted as PC-LA and PC-HA respectively. In addition, eight different SCMs were tested in combination with the two PC: coal fly ash (FA), two calcined clays (CC1 and CC2), two biomass ashes (BA1 and BA2),

sewage sludge ash (SSA), crushed brick (CB) and glass beads (GB) Unless otherwise stated, 35 wt.% of cement replacement was used. The chemical compositions were measured by X-ray fluorescence (XRF) on powders sieved below 63 µm (Malvern Panalytical Zetium spectrometer). The particle size distribution was measured with a laser diffractometer (Malvern Mastersize 2000). The values are presented in Table 1. More information about the mineralogical composition of the cementitious materials is given in [13].

*Table 1: Chemical composition of the cementitious materials (in wt.%) measured by XRF.*

| Oxide | Portland cement | | Fly ash | Calcined clay | | Biomass ash | | Sewage sludge ash | Crushed brick | Glass beads |
|---|---|---|---|---|---|---|---|---|---|---|
| | PC-LA | PC-HA | FA | CC1 | CC2 | BA1 | BA2 | SSA | CB | GB |
| $SiO_2$ | 19.2 | 19.2 | 56.2 | 46.6 | 49.0 | 25.5 | 23.2 | 56.8 | 63.4 | 72.0 |
| $Al_2O_3$ | 5.2 | 5.1 | 23.8 | 17.4 | 17.3 | 4.8 | 4.3 | 8.4 | 11.2 | 0.7 |
| $Fe_2O_3$ | 3.67 | 2.99 | 6.9 | 9.58 | 9.74 | 1.8 | 1.93 | 19.57 | 4.32 | 0.17 |
| MgO | 1.0 | 2.4 | 1.8 | 2.5 | 2.5 | 3.5 | 4.0 | 0.9 | 1.2 | 3.8 |
| CaO | 63.4 | 60.6 | 3.9 | 9.7 | 10.1 | 34.1 | 30.9 | 1.4 | 9.0 | 9.1 |
| $Na_2O$ | 0.33 | 0.45 | 0.49 | 0.92 | 0.81 | 0.87 | 0.71 | 1.03 | 2.81 | 13.63 |
| $K_2O$ | 0.38 | 1.18 | 1.64 | 2.47 | 2.66 | 4.93 | 7.35 | 2.43 | 0.43 | 0.21 |
| $TiO_2$ | 0.19 | 0.35 | 0.93 | 0.97 | 0.97 | 0.28 | 0.29 | 1.54 | 0.63 | 0.07 |
| $P_2O_5$ | 0.26 | 0.08 | 1.02 | 0.21 | 0.24 | 2.91 | 3.03 | 2.97 | 0.15 | 0.01 |
| $SO_3$ | 3.14 | 3.81 | 0.79 | 0.97 | 0.98 | 4.58 | 12.66 | 0.38 | 0.63 | 0.24 |
| $Na_2O_{eq}$ | 0.58 | 1.23 | 1.57 | 2.54 | 2.55 | 4.12 | 5.55 | 2.63 | 2.91 | 13.77 |
| LOI | 3.21 | 3.56 | 1.57 | 7.97 | 4.94 | 15.83 | 10.26 | 3.77 | 5.37 | 0.09 |
| Sum | 100.1 | 99.9 | 99.6 | 99.8 | 99.7 | 99.8 | 99.6 | 99.4 | 99.8 | 100.0 |
| Density [kg/m³] | 3150 | 3130 | 2300 | 2700 | 2700 | 2620 | 2650 | 2650 | 2640 | 2500 |
| $d_{50}$ [µm] | 14 | 10.7 | 18 | 9.6 | 39.4 | 15.5 | 70.2 | 11.1 | 42.8 | 67.0 |

### 2.1.2 Aggregates

A typical 0-4 mm Danish reactive sand from a quarry located in Øde Hastrup (Roskilde, Denmark) was used in all mixtures, with about 3 wt.% of porous opaline flint. This sand is coming from the same geological layer as the one used by Chatterji [15]. For concrete tests, the coarse aggregate consisted of 2 fractions of a non-reactive crushed granite from Rønne (Bornholm, Denmark), 4-8 mm and 11-16 mm. The mineralogical composition of the aggregates determined by X-ray diffraction and Rietveld refinement on powdered samples is shown in Table 2, together with the declared density and absorption values.

*Table 2: Mineralogical composition determined by XRD-Rietveld (in wt.%) and physical characteristics of the aggregates.*

| Phase | Øde Hastrup sand | Rønne granite |
|---|---|---|
| Quartz | 55 | 23 |
| Plagioclase | 10 | 49 |
| Alkali feldspar | 12 | 15 |
| Calcite | 19 | - |
| Mica | 3 | 5 |
| Amphibole | - | 5 |
| Chlorite | 1 | 1 |
| Pyroxene | - | 1 |
| Clay minerals | - | 1 |
| Amorphous/ Unidentified | 3 | <1 |
| Density [-] | 2.62 | 2.72 (4-8 mm)<br>2.64 (11-16 mm) |
| Absorption [%] | 0.9 | 0.7 (4-8 mm)<br>1.2 (11-16 mm) |

### 2.1.3 Admixtures

When necessary, a superplasticizer (SP) was used to ensure acceptable workability of the mixes (Dynamon XTend 200, active substance: acrylic polymer). For the field exposure cubes, an air-entraining agent (AEA) was added to obtain frost-resistant concrete (Mapeair® 25, active substance: synthetic tensides).

## 2.2 Mortar bar tests: ASTM C1567 and TI-B 51

Two mortar bar tests were performed on all SCMs: ASTM C1567 and TI-B 51 [16,17]. Table 3 summarizes the main steps of the methods. In both cases, mixing was carried out according to EN 196-1, except the amounts of constituents were

increased to obtain 1.5 L of mortar. The flow was measured according to EN 1015-3. For each batch, three bars were cast with stainless steel pins on both ends. The length of the bars was measured after demoulding and before exposure, to check for any expansion during curing.

*Table 3: Summary of the main steps in ASTM C1567 and TI-B 51.*

| | ASTM C1567 | TI-B 51 |
|---|---|---|
| Aggregate preparation | Sieving and recombination according to the grading curve in AAR-2 (European sieve sizes) | Particles above 4 mm discarded |
| Binder composition | 65 wt.% PC-LA + 35 wt.% SCM (+ reference with 100 wt.% PC-LA) | |
| Mix design (by mass) | 1 part of binder to 2.25 parts of aggregates<br>w/b = 0.47 | 1 part of binder to 3 parts of aggregates<br>w/b = 0.50 |
| Flow | Target between 150 and 200 mm<br>Superplasticizer added if flow value < 150 mm | |
| Specimen size | 25 x 25 x 185 mm | 40 x 40 x 160 mm |
| Curing | 24 h in deionised water at 80°C | 28 days in deionised water at 20°C |
| Exposure | 14 days in 1 M NaOH at 80°C (preheated, 2.3 L of solution for 3 bars) | 20 weeks in saturated NaCl at 50°C (not preheated, 5 L of solution for 3 bars) |
| Measurements | Immediately after taking the boxes out of the oven<br>Measurements after 3, 7, 11 and 14 days of exposure | After 20 h ± 2 h of cooling at room temperature<br>Measurements after 1, 2, 3, 4, 5, 6, 8, 10, 15 and 20 weeks of exposure |

## 2.3 Concrete prism test: RILEM AAR-10

Concrete prims were cast and tested according to the AAR-10 test procedure proposed by RILEM TC 258 [18]. It should be noted that the AAR-10 procedure had not been validated so far for aggregates containing porous flint, due to a lack of data [19].

### 2.3.1 Mixing, casting and exposure

Each batch contained 440 kg/m$^3$ of cementitious materials and 210 kg/m$^3$ of water (w/b = 0.48). The fine aggregate fraction was adjusted to 37% of the total mass of aggregates to obtain an acceptable slump for the reference mixes. The aggregate

volume slightly varied in different mixes, to account for the different densities of the cementitious materials. 25 L of concrete were produced for each batch.

The mixing sequence was the following: 2 min of dry mixing, 2 min of break, 2 min of wet mixing, 1 min of break and 1 min of mixing. The slump and the fresh air content were measured according to EN 12350-2 and EN 12350-7, respectively. Superplasticizer was added when necessary to obtain a slump of at least 80 mm. No extra alkali (NaOH) was used. The concrete compositions are shown in Table 4.

*Table 4: Concrete compositions for RILEM AAR-10 (in kg/m$^3$) and fresh properties.*

| Mix ID | PC-LA | PC-HA | SCM | Water | Aggregates | | | SP | Slump [mm] | Air content [%] |
|---|---|---|---|---|---|---|---|---|---|---|
| | | | | | 0-4 mm | 4-8 mm | 11-16 mm | | | |
| LA-REF | 440 | - | - | 211 | 627 | 427 | 640 | - | 80 | 1.5 |
| HA-REF | - | 440 | - | 211 | 626 | 427 | 640 | - | 150 | 0.7 |
| HA-FA | - | 286 | 154 | 211 | 609 | 415 | 622 | - | 140 | 1.0 |
| HA-CC1 | - | 286 | 154 | 211 | 619 | 421 | 632 | 3.52 | 70 | 1.0 |
| HA-CC2 | - | 286 | 154 | 211 | 619 | 421 | 632 | 2.20 | 170 | 1.1 |
| LA-BA1 | 286 | - | 154 | 211 | 618 | 421 | 631 | 0.44 | 120 | 0.9 |
| LA-BA2 | 286 | - | 154 | 211 | 618 | 420 | 361 | 0.64 | 120 | 0.7 |
| HA-SSA | - | 286 | 154 | 211 | 618 | 421 | 631 | 1.76 | 160 | 1.2 |
| HA-CB | - | 286 | 154 | 211 | 617 | 420 | 631 | - | 130 | 1.1 |

Three prisms (100 x 100 x 400 mm) were cast in parallel wooden forms, with stainless steel pins embedded on both ends. The forms were covered with a plastic foil and cured in a climate chamber at 20°C for 21 h ± 2 h. The prisms were then demoulded and weighted, and their length was measured with a length gauge while the specimen stood vertically. They were then placed in 50 L sealed plastic containers. The containers were filled with 25 mm of deionised water (approx. 2L), and their walls were covered with felt cloth. The specimens rested on 50 mm high plastic racks to keep them over water. The containers were stored in a walk-in climate chamber at 38°C.

### 2.3.2 Expansion measurements

Before each measurement, the containers were transported two by two from the climate chamber to the laboratory in an insulated box to limit temperature drop. The transport time was less than 3 minutes. The measurement procedure was the following: $t_0$ = remove prism A from the container, $t_0$ + 30 s = measure length of prism A, $t_0$ + 60 s = weight prism A and put it back, $t_0$ + 90 s = remove prism B

from the container, etc. The total measurement time per container did not exceed 6 min, and the containers were placed back in the climate chamber within 20 min.

### 2.3.3 Alkali leaching

Prior to the tests, a curve “volume of water” versus “height of water” was established for the container type used for the tests, as suggested in [18]. Subsequently, only the height of water was measured, and the volume could be deduced from the calibration curve. This was done with a wooden stick after measuring the three prisms. 20 mL of liquid were, and deionised water was added to keep the water level at 25 mm ± 5 mm. The sampled liquid was then analysed with ICP-OES (Varian 720-ES) to determine the concentrations in Na and K.

## 2.4 Field exposure cubes

Due to material availability, only fly ash, biomass ashes 1 and 2 and calcined clay 1 were used to produce field exposure cubes. For HA-CC1, the replacement level was only 20 wt.% for the same reasons. One batch with 35 wt.% replacement was lost due to a failure of the casting equipment.

### 2.4.1 Mixing, casting and curing

The concrete compositions are given in Table 5. The concretes were air-entrained to prevent frost damage during the exposure. Batches of 75 L were produced with a 150 L mixer (Eirich R09T), with 2 min of dry mixing followed by 2 min of wet mixing. The cubes (300 x 300 x 300 mm) were cast in wooden forms, filled in three layers with vibration after each layer. 4 embedded stainless-steel pins were placed on two adjacent sides. The forms were covered with a plastic foil and demoulded after 22 h ± 2 h at 20°C. The lengths between the pins were measured with a 200 mm DEMEC length gauge. After taking the initial readings, the cubes were wrapped in plastic and cured for 4 to 5 weeks at 20°C, so that all cubes started the outdoor exposure on the same day. The lengths were measured again just before exposure, to detect any expansion during curing.

*Table 5: Concrete compositions for field exposure cubes (in kg/m$^3$) and fresh properties.*

| Mix ID | PC-LA | PC-HA | SCM | Water | Aggregates | | | SP | AEA | Slump [mm] | Air content [%] |
|---|---|---|---|---|---|---|---|---|---|---|---|
| | | | | | 0-4 mm | 4-8 mm | 11-16 mm | | | | |
| REF-LA | 440 | - | - | 220 | 656 | 344 | 562 | - | 2.20 | 100 | 5.0 |
| REF-HA | - | 440 | - | 220 | 656 | 344 | 562 | - | 2.20 | 120 | 5.0 |
| LA-FA | 286 | - | 154 | 220 | 636 | 334 | 545 | - | 4.40 | 180 | 5.2 |
| HA-FA | - | 286 | 154 | 220 | 636 | 334 | 545 | - | 4.40 | 170 | 5.3 |
| LA-CC1 | 286 | - | 154 | 220 | 649 | 341 | 556 | 4.40 | 2.20 | 40 | 3.9 |
| HA-CC1 | - | 352 | 88 | 220 | 649 | 341 | 556 | 2.64 | 2.20 | 60 | 4.3 |
| LA-BA1 | 286 | - | 154 | 220 | 646 | 339 | 553 | - | 2.20 | 40 | 3.7 |
| LA-BA2 | 286 | - | 154 | 220 | 646 | 339 | 553 | - | 2.2 | 80 | 4.5 |
| HA-BA1 | - | 286 | 154 | 220 | 646 | 339 | 553 | - | 2.20 | 40 | 2.0 |
| HA-BA2 | - | 286 | 154 | 220 | 646 | 339 | 553 | - | 2.20 | 50 | 5.5 |

## 2.4.2 Exposure

On May 8$^{th}$, 2021 the cubes were placed on a field exposure test area located at the Technical University of Denmark (Kgs. Lyngby, Denmark, GPS coordinates: 55.79103, 12.52619), shown in Figure 1. The surfaces with pins were the top face (measuring North-South and East-West length changes) and the South-West exposed face (measuring vertical and horizontal length changes) as suggested in reference [20]. The measurements were systematically done in the morning, preferably before sun exposure. Meteorological data including temperature, relative humidity and rainfall were continuously recorded by a climate station located on the roof of the building facing the exposure site.

*Figure 1: Field exposure site at the Technical University of Denmark (Kgs. Lyngby, Denmark).*

## 2.5 Overview of expansion tests

Table 6 presents an overview of the mixes produced, as well as the type of PC used (LA or HA). A dash means that no mix was produced for a given test due to material unavailability.

Field cubes were cast first to maximise the exposure duration. Whenever possible, both PC-LA and -HA were used to study the effect of the PC alkali content. Regarding accelerated tests, TI-B 51 was used as the starting point, where PC-LA was chosen to avoid expansion during curing. The same binders were chosen for ASTM C1567, to facilitate the comparison between mortar bar tests. Then, based on mortar bars expansions, it was chosen to use only one type of PC per SCM in AAR-10 to limit the size of the experimental matrix. Thus, BA1, BA2 and GB were tested in combination with PC-LA to assess their potential to trigger ASR expansion, and the other SCMs were tested with PC-HA to evaluate their efficacy in preventing ASR expansion.

*Table 6: Overview of the mixes produced. Blue: PC-LA, Red: PC-HA.*

| | ASTM C1567 | TI-B 51 | AAR-10 | Field |
|---|---|---|---|---|
| Ref | ● | ● | ●● | ●● |
| FA | ● | ● | ● | ●● |
| CC1 | - | ● | ● | ●● |
| CC2 | ● | ● | ● | - |
| BA1 | ● | ● | ● | ●● |
| BA2 | ● | ● | ● | ●● |
| SSA | ● | ● | ● | - |
| CB | ● | ● | ● | - |
| GB | ● | ● | ● | - |

## 2.6 Free alkali content and transport properties

Previous publications reported results about the free alkali content [13] and the transport properties [14] of paste samples made with the same binders as in the present paper. The specimens were cast with w/b = 0.5 and sealed cured at 20°C until testing. The free alkali content was determined by Cold Water Extraction at 28 and 140 days. Transport properties were documented via the non-steady-state chloride migration coefficient and the bulk electrical conductivity at 28 days. It was shown that both values correlated well for sealed cured samples, and that the results obtained on paste were reasonably equivalent to those on concrete.

# 3 Results

This section first presents the results from each expansion test. Subsequently, the outcomes are summarised and compared for each mix. Finally, the results are combined with free alkali contents and transport properties. Three mixes were chosen to illustrate the condition of the samples at the end of the tests (Ref, BA1 and FA). All raw data and calculations are available online, see reference [21].

## 3.1 ASR expansion tests

### 3.1.1 Mortar bar tests

The results from mortar bar tests are displayed in Figure 2. In ASTM C1567 (left), only one mix expanded more than the reference (BA2). Three mixes had no expansion (CC2, FA and SSA). For most curves the expansion rate decreased over time, but no sharp dropped is visible as in TI-B 51. Most curves had not levelled off after 14 days and would probably have continued to expand.

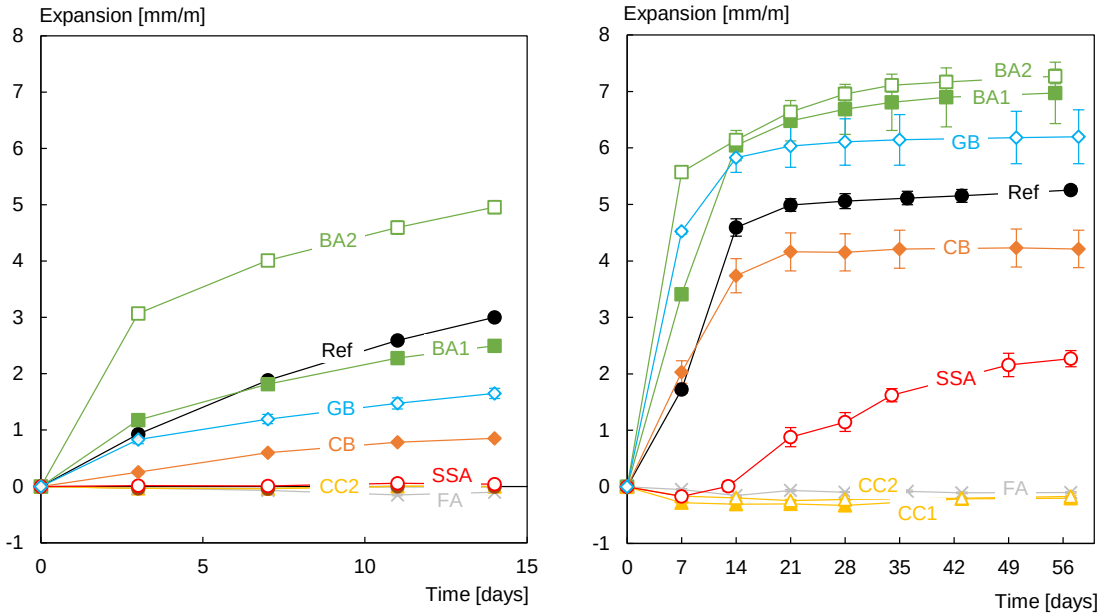


*Figure 2: Expansion measured in mortar bar tests. Left: ASTM C1567. Right: TI-B 51 (measurements were performed until 20 weeks, but all curves levelled off from 8 weeks). Note that only two specimens were measured for GB in ASTM C1567 (one broke during demoulding).*

Expansions in the TI-B 51 (right) were measured up to 20 weeks, however all curves levelled off from 8 weeks. For the sake of clarity, it was therefore chosen to plot only the first 8 weeks. Three mixes showed no expansion at all (CC1, CC2 and FA), three expanded more than the reference (BA1, BA2 and GB), and two

did expand but less and/or slower than the reference (SSA and CB). No significant expansion was measured during curing (maximum: 0.4 mm/m). For most mixes which expanded, the expansion rate dropped significantly after 1-2 weeks of exposure. Overall, larger expansions were reached compared to ASTM C1567.

Visual inspections carried out during TI-B 51 are in agreement with the expansion trends show in Figure 2. Typical signs of ASR damage were visible at the surface, including map cracking and pop outs. Some examples after 8 weeks of exposure are shown in Figure 3. No picture of ASTM C1567 is shown due to a white opaque layer covering the surface of the specimens.

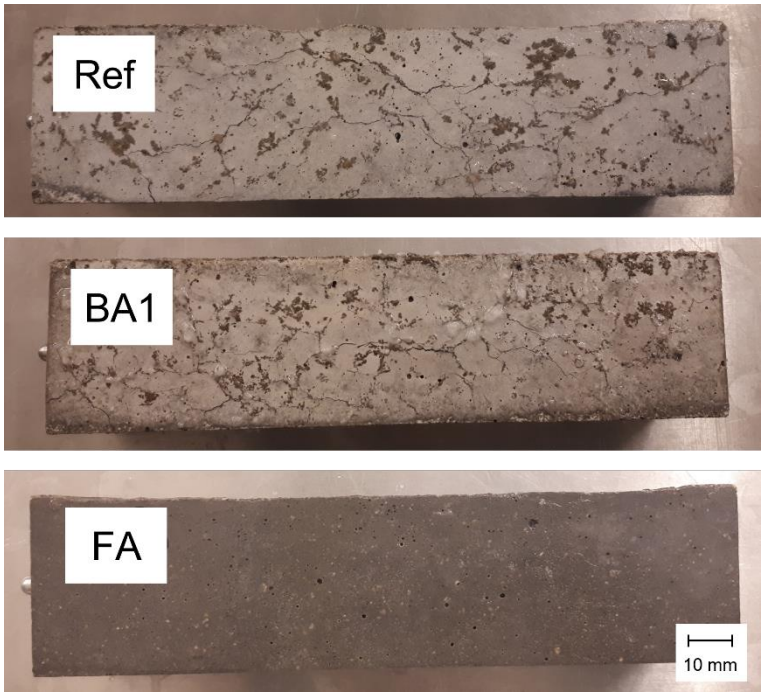


*Figure 3: Photographs of TI-B 51 samples after 8 weeks of exposure. Cracked are clear visible on Ref and BA1, while the surface of FA is intact.*

### 3.1.2 Concrete prism tests

The expansions measured in AAR-10 are presented in Figure 4. The specimens are still stored in the laboratory and will be monitored until 2 years. All mixtures cast with PC-LA expanded, except the reference with plain PC. For the two biomass ashes, the curves took off almost immediately after the beginning of the exposure. On the contrary, it took 3 to 6 months for the specimens with glass (LA-GB) to start expanding. The expansions flattened out after 1 year of exposure or less. On the opposite, none of the mixtures cast with PC-HA expanded, except the reference.

Figure 5 shows the condition of some of the specimens after 1.25 years of exposure. It can be seen that all specimens have dark stains surrounding the white

flint particles, including the specimens that did not expand (PC-LA and HA-FA). Pop-outs were observed when handling the specimens. A severe leaching is visible on the specimens which expanded the most (PC-HA and LA-BA1).

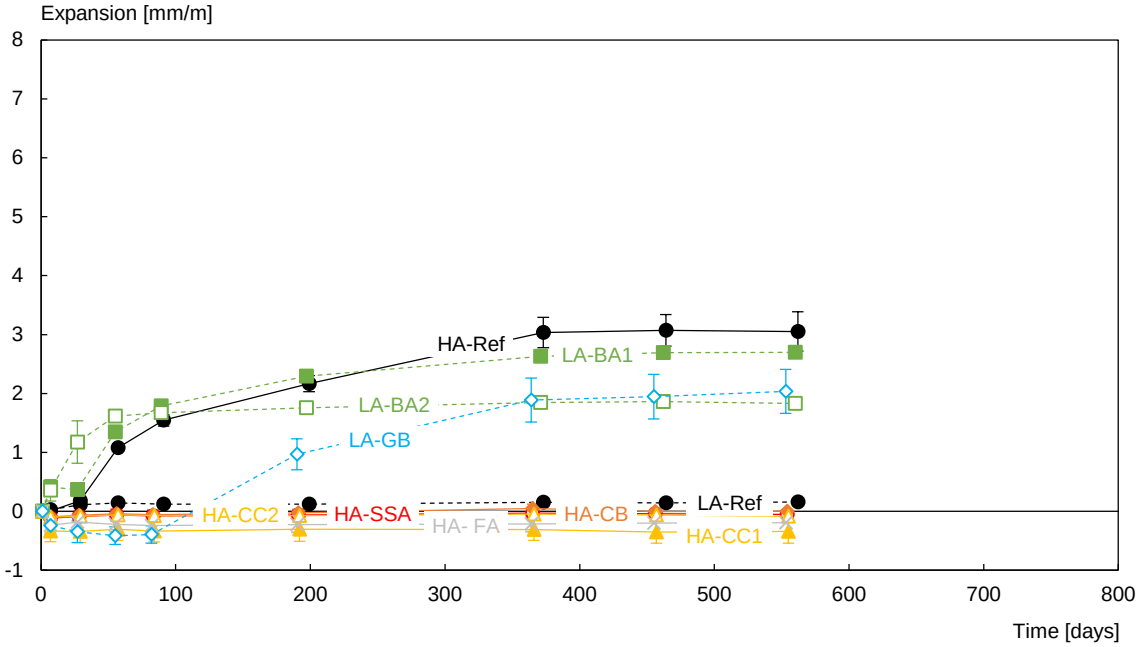


*Figure 4: Expansion measured in AAR-10. Note that after 1.25 years, only two prisms were measured for LA-Ref and HA-Ref. The third prisms were taken out for further inspections, not reported here.*

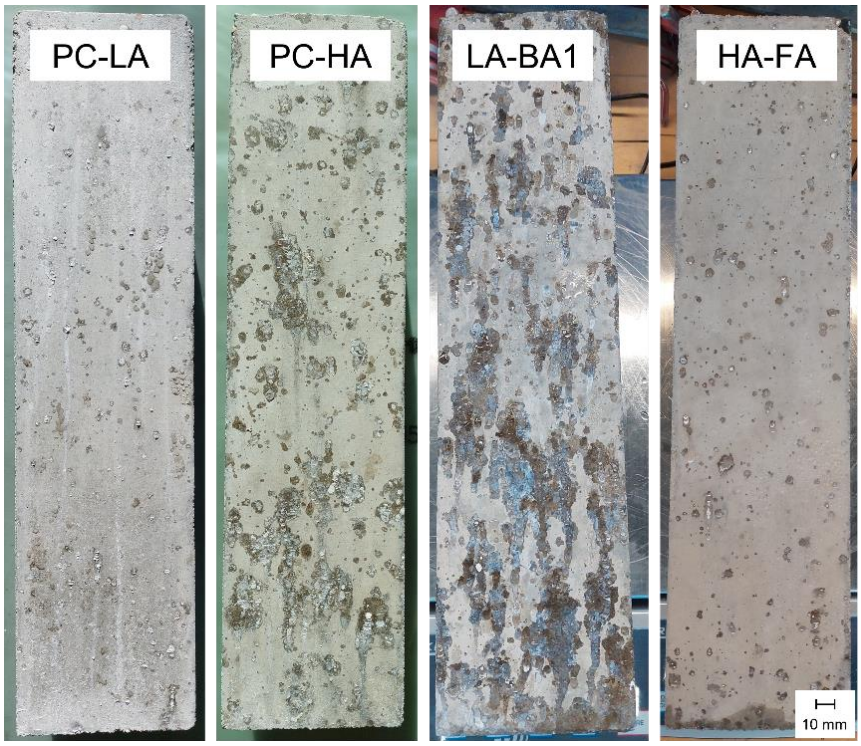


*Figure 5: AAR-10 specimens after 1.25 years of exposure.*

The alkali leaching measured by sampling the solution at the bottom of the test containers is shown in Figure 6, where $Na_2O_{eq}$ is expressed in % of total (left) and in kg/m$^3$ left in the specimens (right). Overall, the more expansion the larger leaching, except for GB. All SCMs used with PC-HA lowered leaching by at least 50% compared to HA-Ref, the largest reduction being obtained with FA, CC1 and CC2. The values are slightly lower than the ones reported by Lindgård et al. [7] for the same test, but still in the same order of size. It should be mentioned Figure 6 does not account for the alkalis that may be present in the felt cloth covering the containers' walls, so the actual alkali leaching is likely to be higher [7,18].

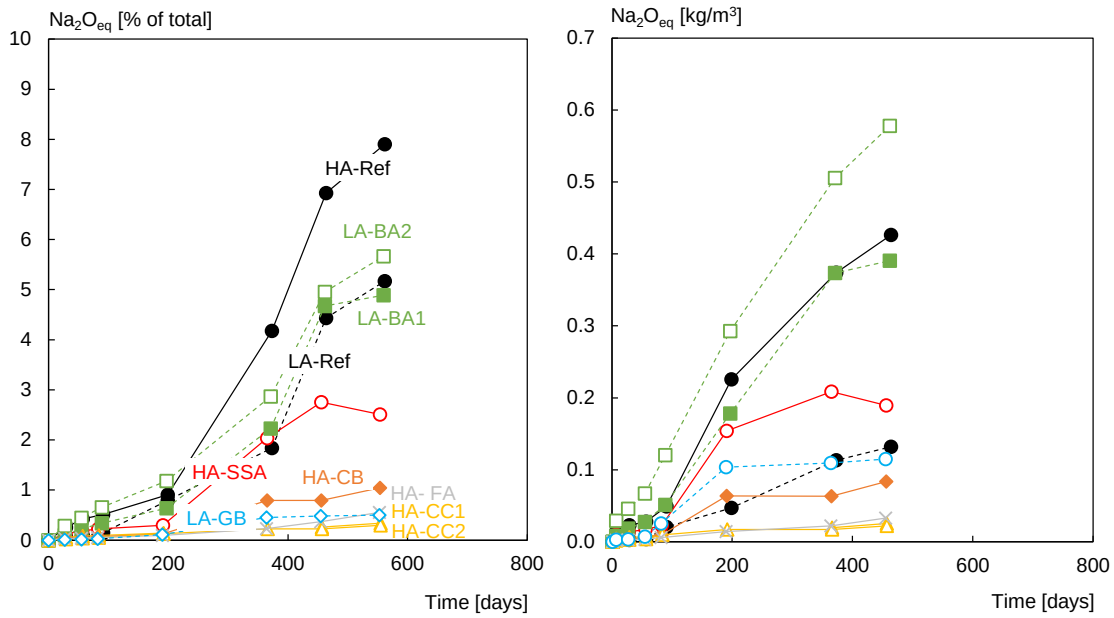


*Figure 6: Alkali leaching in AAR-10. Left: in % of total $Na_2O_{eq}$. Right: in kg/m$^3$ $Na_2O_{eq}$.*

### 3.1.3 Field exposure cubes

The expansion curves of the exposure cubes are plotted on Figure 7, together with the meteorological data for the corresponding period. No significant difference between the top and the side surfaces were observed, except for LA-BA2 and HA-BA2 where the side surface expanded more (order of size: 1 mm/m). The reference cube containing PC-LA did not show any expansion (nor any visible sign of damage) after 2 years. On the contrary, the reference cube with PC-HA started to expand after a few weeks of exposure and reached the highest level of expansion of all cubes after 2 years. All mixes containing biomass ashes expanded extremely fast, with a moderate influence of the PC alkali content. It should be noted that HA-BA2 expanded by 1.06% during sealed curing at 20°C, which must be added to the values shown in Figure 6 to get the total expansion. The fact that HA-BA1 and HA-BA2 expanded less than PC-HA is probably due to fast expansion,

cracking and therefore alkali leaching of the specimens. On the opposite, FA was able to prevent the expansion in all cases. Finally, it can be seen that 20 wt.% CC1 was not enough to prevent the expansion with PC-HA, which took off after about 1 year of exposure. The top surfaces of some of the cubes are shown in Figure 8.

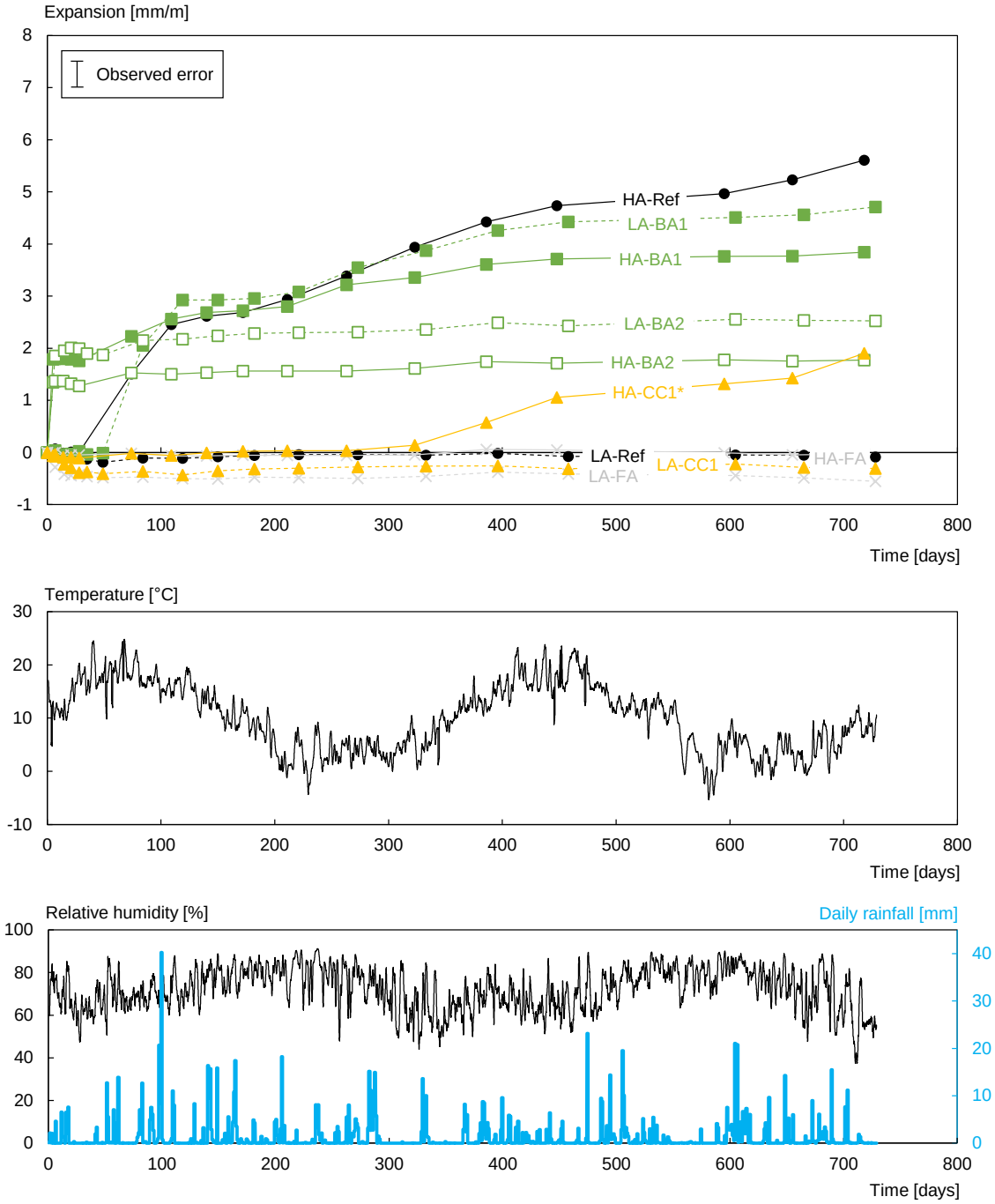


*Figure 7: Average expansion of field exposure cubes and meteorological conditions. *) 20 wt.% cement replacement only (35 wt.% for all other mixtures). Note that HA-BA2 expanded by 1.06% during the 4 weeks of sealed curing at 20°C. The error is based on observations made on twin cubes located on the same exposure site.*

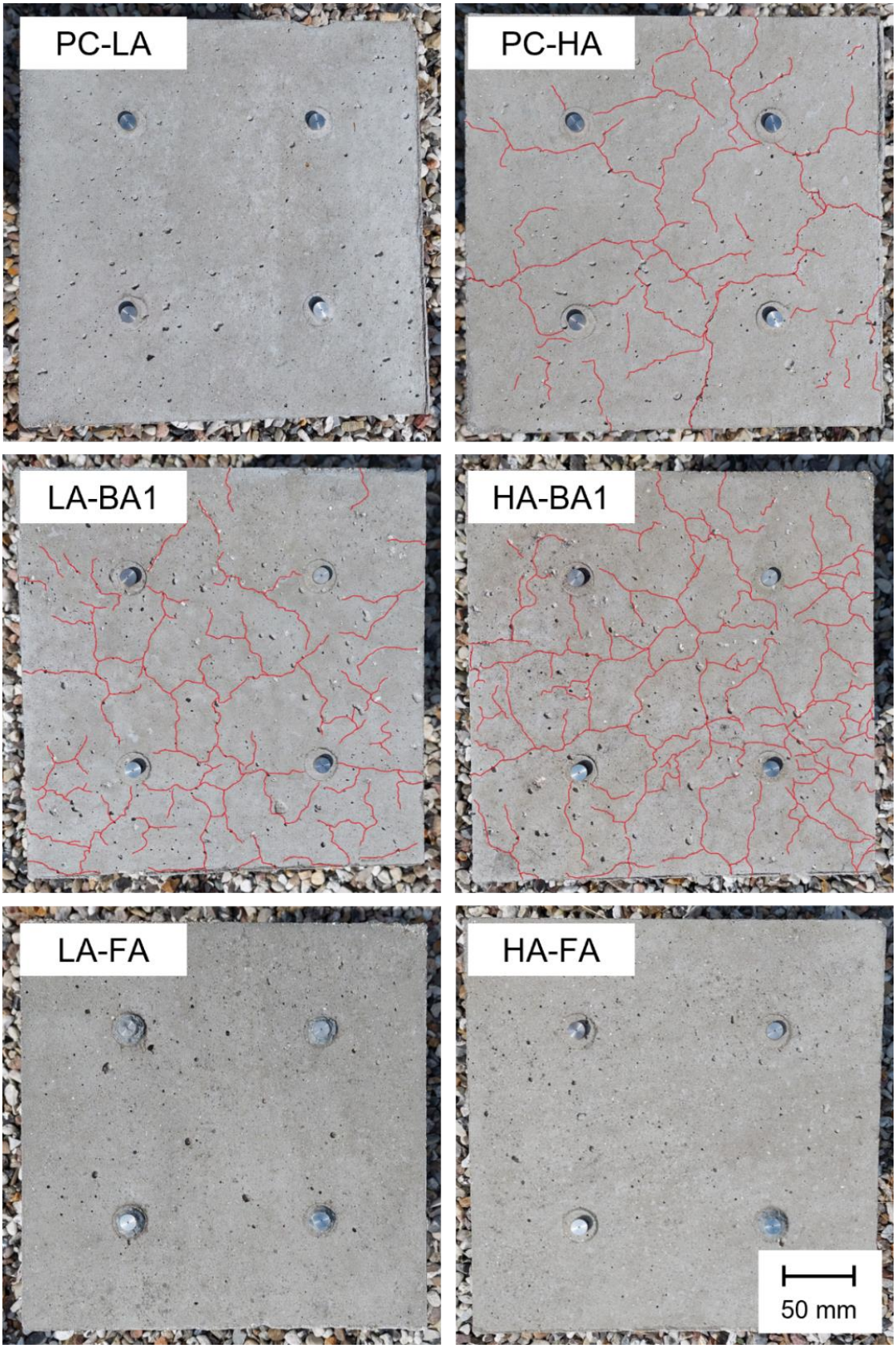


*Figure 8: Top surface of concrete cubes after 2 years of outdoor exposure. The cracks visible on the pictures with a magnification ×1.5 were marked in red.*

## 3.2 Correlation between the binder properties and ASR expansion

All the expansion data presented previously are now compared to the free alkali content and the chloride migration coefficient determined on corresponding paste samples. The comparison is presented in Figure 9, where each expansion test is presented in a different graph.

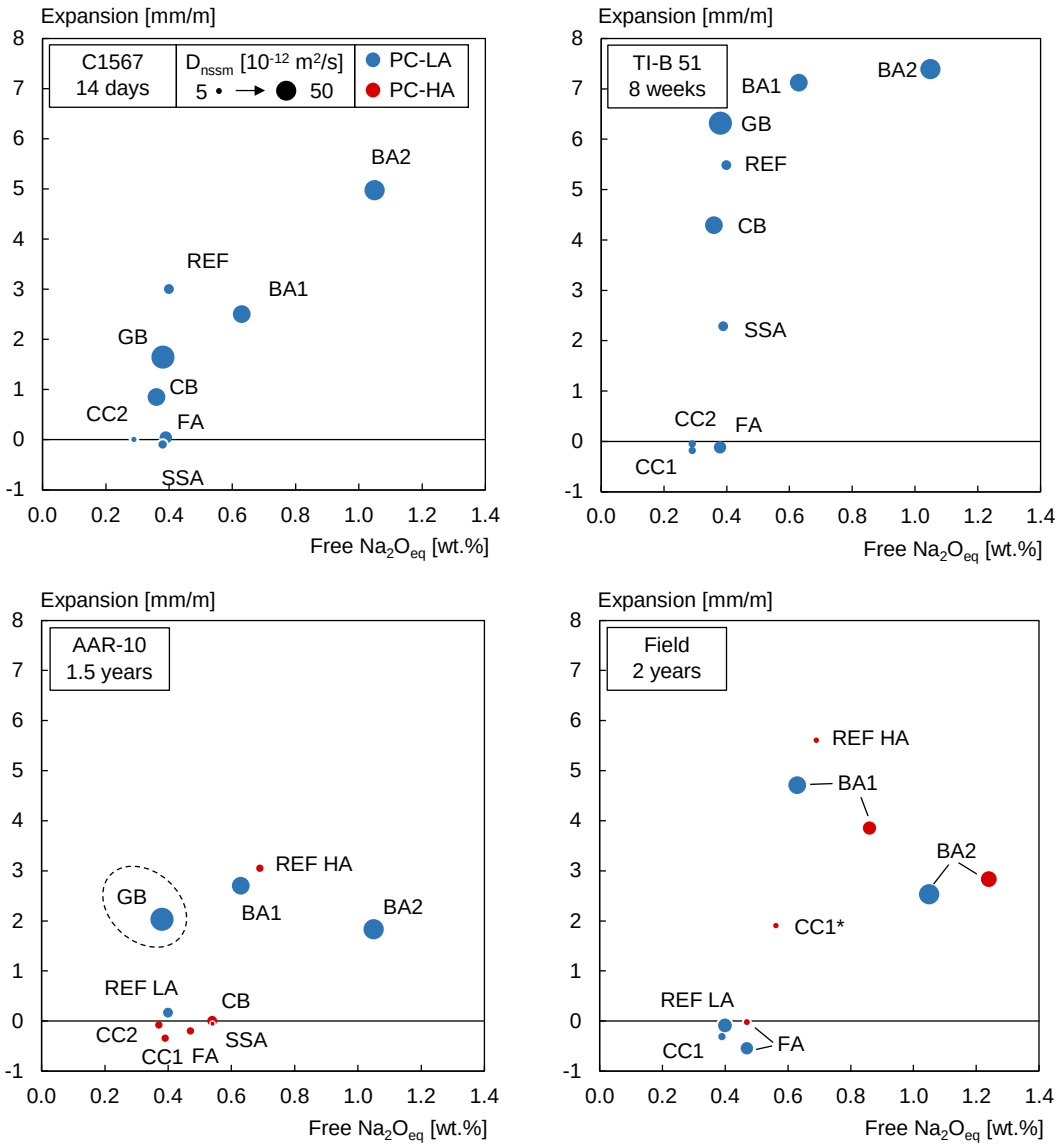


*Figure 9: Expansion in the different tests as a function of the free alkali content determined on paste samples [13]. The size of the marker indicates the non-steady-state chloride migration coefficient [14]. *) For HA-CC1, the free alkali content and the migration coefficient were linearly interpolated from the paste results (20 wt.% CC1 in field cube vs. 35 wt.% in paste specimens).*

Note that for HA-CC1 in the field, the free alkali content and the migration coefficient were measured on paste with 35 wt.% CC1, while the cube only contains 20 wt.%. Therefore, a linear interpolation of the paste results was made to account for the different replacement level of CC1.

The reason for choosing the free alkali content (wt.%) instead of the alkali concentration (mmol/L), as it was done previously [10–12], is because the free alkali content is easier to determine and less sensitive to the w/b [22]. As such, the free alkali content can be seen as a binder property, while concentrations are paste properties. Moreover, in the present case, the expansion tests had similar w/b (0.47 to 0.50), so the concentration variations for a given binder are limited.

For mortar bar tests, it is difficult to conclude on any relationship between the free alkali content and the expansion. A linear fit in Figure 9 would result in a $R^2$ of 0.72 for ASTM C1567 and 0.44 for TI-B 51. If plotting the expansion as a function of the migration coefficient, the $R^2$ is equal to 0.25 for ASTM C1260 and 0.53 for TI-B 51. In both tests, five mixes have similar free alkali contents but different levels of expansion (Ref FA, SSA, CB and SSA). The fact that CB expanded more than SSA and FA may be explained by a larger migration coefficient, which favoured NaCl ingress. However, this cannot explain why the reference mix performed worse than the other mixes having a similar free alkali content (SSA and FA).

For concrete tests, there seems to be a threshold for the free alkali content below which no expansion occurs, which is similar to what other authors observed [10,11]. The threshold appears to be around 0.5 - 0.6 wt.% $Na_2O_{eq}$ for the binder, corresponding to a free alkali loading of 2.2 - 2.6 kg/m$^3$. Above this value, there is no clear link between expansion, free alkali content and migration coefficient. The case of GB is peculiar in AAR-10 (circled in Figure 9), because the specimens expanded significantly while the free alkali content displayed was relatively low.

# 4 Discussion

## 4.1 Comparison of expansion data

A comparison of the expansions obtained in the different tests is shown in Table 6. The expansion of the reference specimens is well above the limit for reactive aggregates in mortar tests (1 mm/m), as expected. The same observation can be made in AAR-10 and in the field for PC-HA reference mixes considering the proposed limits of 0.40 and 0.50 mm/m, respectively [23]. When examining Figures 4 and 7, it is somehow surprising to have similar kinetics between the two concrete tests because the outdoor exposure conditions were not favourable (the

average air temperature over the two years was 9.9°C, and the RH was around 70%) [24]. This is likely to be a coincidence, potentially induced by other factors affecting ASR such as rainfalls and solar insolation [25].

Regarding PC-LA mixes, the AAR-10 specimens will probably never expand due to the significant amount of alkalis leached out. However, the outcome for the field cube is more uncertain. The cube is bigger and has a smaller surface-to-volume ratio than AAR-10 specimens (factor 2.5), which should contribute to less alkali leaching - everything else being equal [26]. However, leaching also occurs in the field, but it is more complex to measure [27]. Moreover, the exposure conditions vary from one site to another, which makes it difficult to compare with results from the literature.

*Table 7: Summary of expansion test results. For each mix, the top and bottom row correspond to LA-PC and HA-PC respectively. Red: Expansion larger than the reference. Orange: Expansion lower than the reference but still higher than the acceptance limit. Green: Expansion below the acceptance limit. †) 20 wt.% of replacement only. *) with an additional 1.06% of expansion during curing.*

| In mm/m | | ASTM C1567 (14 days) | TI-B 51 (8 weeks) | AAR-10 (1.5 years) | Field (2 years) |
|---|---|---|---|---|---|
| Acceptance limit | | 1.00 | 1.00 | 0.40 | 0.50 |
| Ref | PC-LA | 3.00 | 5.26 | 0.14 | -0.09 |
| | PC-HA | - | - | 3.07 | 5.61 |
| FA | PC-LA | -0.10 | -0.10 | - | -0.55 |
| | PC-HA | - | - | -0.20 | -0.03 |
| CC1 | PC-LA | - | -0.20 | - | -0.31 |
| | PC-HA | - | - | -0.35 | 1.90† |
| CC2 | PC-LA | 0.00 | -0.17 | - | - |
| | PC-HA | - | - | -0.07 | - |
| BA1 | PC-LA | 2.50 | 6.97 | 2.69 | 4.71 |
| | PC-HA | - | - | - | 3.85 |
| BA2 | PC-LA | 4.96 | 7.27 | 1.86 | 2.53 |
| | PC-HA | - | - | - | 1.78* |
| SSA | PC-LA | 0.04 | 2.27 | - | - |
| | PC-HA | - | - | -0.04 | - |
| CB | PC-LA | 0.85 | 4.21 | - | - |
| | PC-HA | - | - | 0.00 | - |
| GB | PC-LA | 1.65 | 6.20 | 1.95 | - |
| | PC-HA | - | - | - | - |

In most cases for blended mixes, the different tests also agree as to which SCMs prevent or amplify the expansion. However, several exceptions can be noted:

- BA1 and GB expanded less than the reference in ASTM C1567, while they expanded more in all other tests.
- SSA expanded above the acceptance limit in TI-B 51 but showed no expansion in ASTM C1567 nor in AAR-10, even though it was blended with PC-HA.
- A similar situation occurred for CB, but the mix did expand in ASTM C1567 (although it remained below the acceptance limit).

The discrepancies for mortar bar tests may stem from interactions between the materials and the surroundings, inducing phenomena that would not occur otherwise. As an example, it is known that the high temperature in ASTM C1567 destabilises sulphate-bearing phases like ettringite. Sulphate ions are then released into the pore solution, which lowers the hydroxide ion concentration. This in turns results in a pH drop, which impedes the ASR process [28]. It could be hypothesised that other reaction occurs between the external compounds present in the exposure solutions and some mineral phases. Since the tests have different solutions and different compounds, thermodynamic equilibria may be shifted differently, leading to different results.

From the available data, AAR-10 and field cubes always led to the same conclusion. The field cube cast with CC1 has a different replacement level as in AAR-10, therefore it is not considered as a mismatch. As mentioned before, several inconsistencies were observed with mortar bar tests, which questions their ability to reliably assess the efficacy of SCMs. This is particularly true for alternative SCMs (BA, SSA and CB). The most problematic case among the presented ones is certainly BA1 expanding less than the reference in ASTM C1567, but significantly more and/or faster in the others, especially in the field.

It must be mentioned that 2 years is a short exposure duration compared to most other field studies. Nevertheless, it was chosen to show the results due to the unusual fast expansion for most mixes. However, caution should be taken in drawing conclusions for the mixes which did not expand. As an example, several cubes similar to LA-Ref have been cast and exposed since 2017 on the same exposure site (same reactive aggregate, but from different batches). Some of these cubes have expanded, not necessarily the oldest, while others have not. Even though no reason can be given with certainty so far, it seems that this concrete composition is in a sensitive area for ASR onset.

## 4.2 Influence of the binder properties

The concept of alkali threshold for reactive aggregates has been used for many years [29], and led to the implementation of a maximum alkali loading in concrete typically around 3 kg/m$^3$ $Na_2O_{eq}$. It should be emphasised that the term "threshold" must be used with caution. In the present case, it refers to the expansion fashion only, i.e. whether the internal stresses are strong enough to make the solid matrix swell. It does not imply anything about the dissolution of amorphous silica from ASR-reactive particles, nor the formation of ASR products. It is therefore more likely to be an apparent threshold, resulting from a multi-stage process, than a chemical threshold for the ASR onset.

Even though the value of 3 kg/m$^3$ $Na_2O_{eq}$ may not be safe for all aggregates [30], it is still widely used. For plain PC, assuming that around 70% of the alkalis are free [13], a total alkali loading of 3 kg/m$^3$ corresponds to a free alkali loading of 2.1 kg/m$^3$, which is close to the threshold range mentioned earlier. The main difficulty is to evaluate the contribution of SCMs, which is done when using the free alkali content. A more comprehensive discussion on the topic can be found in [13].

Although the free alkali content seems to be a promising indicator of the ASR performance of a binder, it may be safer not to rely exclusively on it before more data have been collected. Indeed, in addition to the effect of alkalis, other compounds in the pore solution may affect the ASR. This is for instance the case of aluminium, which was found to slow down the dissolution of silica [31,32]. Another potential effect to consider is the alkali release from aggregates, which can increase the free alkali loading. This topic is currently under investigation to find a suitable method for anticipating the amount releasable, but there are already indications that the contribution may be significant with certain types of aggregates [33].

It should be mentioned that the binder properties showed in Figure 7 were determined on paste samples sealed cured at 20°C for 28 days, hence a maturity of 28 Mdays. However, the maturity reached at the end of the expansion tests is very different: assuming an apparent activation energy of 33.5 kJ/mol, it means approx. 160 Mdays in ASTM C1567, 230 Mdays in TI-B 51, 1200 Mdays in AAR-10 and 500 Mdays in the field [34]. Changes in maturity influence the ongoing pozzolanic reactions, which induces a refinement of the pore structure and the binding or release of alkali metals. In addition, the free alkali content is also affected by some alkali metals being bound to ASR products, as well as alkali leaching. On this last point, the results presented in Figure 6 suggest that AAR-10 is relatively effective to prevent significant alkali leaching, as all values measured were below 10% of the total content for all mixes.

This difference in maturity might explain the behaviour of GB in AAR-10. A limited amount of sodium was found at 28 days in the paste, but reactivity measurements indicated that GB eventually started to react and release sodium into the pore solution at a later stage [13]. Therefore, the free alkali content of GB plotted in Figure 9 may be not representative of the actual content in AAR-10 specimens. However, if this is the case, one would expect more alkali leaching since the specimens are cracked. As Figure 6 shows that the leaching is roughly the same in LA-GB and LA-Ref, this suggests that there is not a large difference in free alkalis between the two mixes. Another possible explanation is that GB may not act as an SCM, but rather like a reactive aggregate. Indeed, it is known that the behaviour of glass changes as a function of its fineness [35]. In the present case, the pozzolanic activity may be negligible due to the relatively coarse particle size ($d_{50}$ = 67 µm).

## 4.3 Practical use

In the Danish requirements, TI-B 51 is the required test to document the ASR performance of binders that are not included in the standards yet (EN 206 DK NA). However, the test was initially designed to evaluate aggregate reactivity [17], and the mechanism by which NaCl triggers ASR is still not clear. Several mechanisms were proposed as to how NaCl acts, such as pH increase via portlandite dissolution and consumption [36], formation of calcium chloroaluminates via an expansive process [37] and enhanced dissolution of amorphous silica [38]. A better understanding of the mechanism would help to assess whether the test is fundamentally acceptable for testing SCMs or not. However, the data presented earlier show that it is difficult to interpret the results, in particular for the mixes which do expand but less than the reference.

The results from the field cubes also demonstrate that comparing the performance of two mixes should be done by looking at the full expansion curve, and not only at the expansion values at a given point in time. For example, in Figure 7, the mixes BA1 and BA2 with PC-HA expanded faster than HA-Ref, even though they had a lower expansion after 2 years. In addition, expansion during curing was registered for HA-BA2 (approximately 1 mm/m). Another possible situation, although not observed here, is that of a specimen which starts to expand just before the end of the test but stays below the acceptance limit. In all these cases, a careful evaluation of the results must be conducted. Alternatively, more requirements can be set, e.g. an intermediate limit for the expansion or a limit for the expansion rate in the final period of the test.

The Danish field experience with this reactive sand (Øde Hastrup) is that if the initial alkali content of the concrete is low, ASR only occurs due to spreading and penetration of de-icing salts (NaCl) into the concrete. If no de-icing salts are present, using low alkali cement (typical in Denmark) is enough to prevent ASR damage [39]. To the author's knowledge, there is no case in Denmark of a structure intentionally cast with reactive aggregates and preventive measures. In a more general context, previous work showed that using low alkali PC might not be sufficient to prevent ASR with certain types of aggregates, in particular highly reactive ones [40]. Thus, the results showed in Figure 9 are probably strongly aggregate dependant. Since the number of datapoints is rather limited, it would be valuable to have more mixes in the sensitive range 0.45-0.65 wt.% free $Na_2O_{eq}$ to confirm the threshold behaviour. In parallel, field testing should be continued to evaluate the correlation with laboratory results over a longer exposure period.

# 5 Conclusion

This study investigated the effect of various SCMs on ASR expansion under field exposure and accelerated conditions as per ASTM C1567, TI-B 51 and RILEM AAR-10. The results were also put into perspective with regards to some binder characteristics, namely the free alkali content and transport properties. The following points can be concluded:

- AAR-10 and field exposure led to identical conclusions with respect to the reactivity of sand containing porous opaline flint and the effect of the PC alkali content.
- The effect of a given SCM on the ASR expansion varies depending on the accelerated test chosen. Among the three accelerated tests carried out, AAR-10 showed the best correlation with field results.
- For all tests, including field testing, the assessment of a mix should not be made only in comparison with the reference mix at a given point in time. The shape of the curve and the possible expansion during curing must be accounted for.
- For concrete tests (AAR-10 and field), there seems to be a threshold free alkali loading below which no expansion occurs for the reactive aggregate tested, around 2.2 - 2.6 kg/m$^3$ free $Na_2O_{eq}$. However, field testing must be continued and ideally completed by other mix designs in the sensitive area to confirm this trend in the long term.
- The effect of transport properties is less clear but may still be a reasonable explanation for some of the features, in particular in mortar bar tests.

# Acknowledgements

The work presented is part of an industrial PhD project financed by the Danish Road Directorate and a joint grant from Innovation Fund Denmark (Innovationsfonden) and Realdania under the program Circular Built Environment. The financial support is gratefully acknowledged. We thank the Research and Quality Centre of Aalborg Portland for the XRF analyses, as well as the following companies for supplying the materials: EasyMining (sewage sludge ash), Emineral (biomass ashes), Norcem (PC-HA) and Norrecco (crushed brick). In addition, a warm thank you to Miriam E. Krüger (TU Munich) for the characterisation of aggregates.

# References

[1] M. Thomas, B. Fournier, K. Folliard, J. Ideker, M. Shehata, Test methods for evaluating preventive measures for controlling expansion due to alkali-silica reaction in concrete, Cem Concr Res. 36 (2006) 1842–1856. https://doi.org/10.1016/j.cemconres.2006.01.014.

[2] M.-A. Bérubé, J. Duchesne, D. Chouinard, Why the accelerated mortar bar method ASTM C1260 is reliable for evaluating the effectiveness of supplementary cementing materials in suppressing expansion due to alkali-silica reactivity, Cement Concrete and Aggregates. 17 (1995) 26–34. https://doi.org/10.1520/CCA10333J.

[3] M. Thomas, F. Innis, Use of the Accelerated Mortar Bar Test for Evaluating the Efficacy of Mineral Admixtures for Controlling Expansion due to Alkali-Silica Reaction, Cement, Concrete, and Aggregates. 21 (1999) 157–164. https://doi.org/10.1520/CCA10429J.

[4] V. Sirivivatnanon, P. Thomas, M. Joshua Tapas, T. Nhu Nguyen, Reliability of AMBT and CPT in testing the effectiveness of SCM to mitigate alkali–silica reaction of field concrete, Constr Build Mater. 369 (2023) 130510. https://doi.org/10.1016/j.conbuildmat.2023.130510.

[5] B. Fournier, R. Chevrier, A. Bilodeau, P.-C. Nkinamubanzi, N. Bouzoubaa, Comparative field and laboratory investigations on the use of supplementary cementing materials (SCMs) to control alkali-silica reaction (ASR) in concrete, in: H. de M. Bernardes, N.P. Hasparyk (Eds.), Proceedings of the 15th International Conference on Alkali-Aggregate Reaction in Concrete, Sao Paulo (Brasil), 2016.

[6] J. Duchesne, M.-A. Bérubé, Long-term effectiveness of supplementary cementing materials against alkali–silica reaction, Cem Concr Res. 31 (2001) 1057–1063. https://doi.org/10.1016/S0008-8846(01)00538-5.

[7] J. Lindgård, M.D.A. Thomas, E.J. Sellevold, B. Pedersen, Ö. Andiç-Çakir, H. Justnes, T.F. Rønning, Alkali-silica reaction (ASR) - Performance testing: Influence of specimen pre-treatment, exposure conditions and prism size on alkali leaching and prism expansion, Cem Concr Res. 53 (2013) 68–90. https://doi.org/10.1016/j.cemconres.2013.05.017.

[8] B. Fournier, J. Lindgård, B.J. Wigum, I. Borchers, Outdoor exposure site testing for preventing Alkali-Aggregate Reactivity in concrete – a review, in: M.G. Alexander, H. Beushausen, F. Dehn, P. Moyo (Eds.), Proceedings of the 5th International Conference on Concrete Repair, Rehabilitation and Retrofitting, MATEC Web of Conferences, Cape Town (South Africa), 2018: p. 03002. https://doi.org/10.1051/matecconf/201819903002.

[9] D. Hooton, B. Fournier, Long-term alkali-silica mitigation of high-alkali concrete with cement replacements, Proceedings of Institution of Civil Engineers: Construction Materials. 175 (2022) 125–136. https://doi.org/10.1680/jcoma.21.00049.

[10] M.H. Shehata, M.D.A. Thomas, Use of ternary blends containing silica fume and fly ash to suppress expansion due to alkali-silica reaction in concrete, Cem Concr Res. 32 (2002) 341–349. https://doi.org/10.1016/S0008-8846(01)00680-9.

[11] M. Bagheri, B. Lothenbach, K. Scrivener, The effect of paste composition, aggregate mineralogy and temperature on the pore solution composition and the extent of ASR expansion, Mater Struct. 55 (2022) 192. https://doi.org/10.1617/s11527-022-02015-6.

[12] M. Kasaniya, M.D.A. Thomas, Role of the alkalis of supplementary cementing materials in controlling pore solution chemistry and alkali-silica reaction, Cem Concr Res. 162 (2022). https://doi.org/10.1016/j.cemconres.2022.107007.

[13] M. Ranger, M.T. Hasholt, Cold Water Extraction for determination of the free alkali metal content in blended cement pastes, CEMENT. (2023) 100079. https://doi.org/10.1016/j.cement.2023.100079.

[14] M. Ranger, M.T. Hasholt, Relationship Between Chloride Migration, Bulk Electrical Conductivity and Formation Factor of Blended Cements, *Submitted for Publication*.

[15] S. Chatterjee, Z. Fördös, N. Thaulow, Alkali-silica reaction - Danish experience, in: R.N. Swamy (Ed.), The Alkali-Silica Reaction in Concrete, 1991.

[16] Teknologisk Institut, TI-B 51 - Test method for alkali-silica reactivity of sand (in Danish: Prøvningsmetode Sands alkalikiselreaktivitet), 1985.

[17] S. Chatterji, An accelerated method for the detection of alkali-aggregate reactivities of aggregates, Cem Concr Res. 8 (1978) 647–650. https://doi.org/10.1016/0008-8846(78)90047-9.

[18] T.F. Rønning, B.J. Wigum, J. Lindgård, Recommendation of RILEM TC 258-AAA: RILEM AAR-10: determination of binder combinations for non-reactive mix design using concrete prisms - 38 °C test method, Mater Struct. 54 (2021). https://doi.org/10.1617/s11527-021-01679-w.

[19] T.F. Rønning, J. Lindgård, I. Borchers, ASR performance testing concepts - RILEM AAR-10, AAR-11 and AAR-12, in: A.L. Batista, A.S. Silva, I. Fernandes, L.O. Santos, J. Custódio, C. Serra (Eds.), Proceedings of the 16th International Conference on Alkali-Aggregate Reaction in Concrete, Volume 1, Lisbon (Portugal), 2022: pp. 653–661.

[20] B.J. Wigum, J. Lindgård, G.J. Einarsson, Alkali Aggregate Reactions in Concrete - Establishing an outdoor exposure site, Mannvit, Iceland, 2013.

[21] M. Ranger, Dataset for journal article “Laboratory and field investigations of alkali-silica reaction prevention by supplementary cementitious materials: influence of the free alkali loading,” DTU Data. (2023). https://doi.org/10.11583/DTU.23799918.

[22] G. Plusquellec, M.R. Geiker, J. Lindgård, J. Duchesne, B. Fournier, K. De Weerdt, Determination of the pH and the free alkali metal content in the pore solution of concrete: Review and experimental comparison, Cem Concr Res. 96 (2017) 13–26. https://doi.org/10.1016/j.cemconres.2017.03.002.

[23] J. Lindgård, B. Fournier, T.F. Rønning, M.D.A. Thomas, Alkali–aggregate reaction: performance testing, exposure sites and regulations, Proceedings of the Institution of Civil Engineers - Construction Materials. 169 (2016) 189–196. https://doi.org/10.1680/jcoma.15.00077.

[24] B. Fournier, J.H. Ideker, K.J. Folliard, M.D.A. Thomas, P.-C. Nkinamubanzi, R. Chevrier, Effect of Environmental Conditions on Expansion in Concrete due to Alkali-Silica Reaction (ASR), Mater Charact. 60 (2009) 669–679. https://doi.org/10.1016/j.matchar.2008.12.018.

[25] Y. Kawabata, K. Yamada, T. Kawakami, Y. Sagawa, Environmental impacts on expansion of concrete due to alkali–silica reaction, Magazine of Concrete Research. 75 (2023) 723–733. https://doi.org/10.1680/jmacr.22.00158.

[26] J. Lindgård, Ö. Andiç-Çakir, I. Fernandes, T.F. Rønning, M.D.A. Thomas, Alkali-silica reactions (ASR): Literature review on parameters influencing laboratory performance testing, Cem Concr Res. 42 (2012) 223–243. https://doi.org/10.1016/j.cemconres.2011.10.004.

[27] J. Lindgård, T. Østnor, B. Fournier, Ø. Lindgård, T. Danner, G. Plusquellec, K. De Weerdt, Determining alkali leaching during accelerated ASR performance testing and in field exposed cubes using cold water extraction (CWE) and μXRF, in: Proceedings of the 5th International Conference on Concrete Repair, Rehabilitation and Retrofitting, MATEC Web of Conferences, Cape Town (South Africa), 2018. https://doi.org/10.1051/matecconf/201819903004.

[28] F. Golmakani, R.D. Hooton, Impact of pore solution concentration on the accelerated mortar bar alkali-silica reactivity test, Cem Concr Res. 121 (2019) 72–80. https://doi.org/10.1016/j.cemconres.2019.02.008.

[29] R.G. Sibbick, C.L. Page, Threshold alkali contents for expansion of concretes containing British aggregates, Cem Concr Res. 22 (1992) 990–994. https://doi.org/10.1016/0008-8846(92)90123-D.

[30] M.D.A. Thomas, Field studies of fly ash concrete structures containing reactive aggregates, Magazine of Concrete Research. 48 (1996) 265–279. https://doi.org/10.1680/macr.1996.48.177.265.

[31] T. Chappex, K.L. Scrivener, The influence of aluminium on the dissolution of amorphous silica and its relation to alkali silica reaction, Cem Concr Res. 42 (2012) 1645–1649. https://doi.org/10.1016/j.cemconres.2012.09.009.

[32] M. Bagheri, B. Lothenbach, M. Shakoorioskooie, K. Scrivener, Effect of different ions on dissolution rates of silica and feldspars at high pH, Cem Concr Res. 152 (2022) 106644. https://doi.org/10.1016/j.cemconres.2021.106644.

[33] M.-A. Bérubé, J. Duchesne, J.F. Dorion, M. Rivest, Laboratory assessment of alkali contribution by aggregates to concrete and application to concrete structures affected by alkali–silica reactivity, Cem Concr Res. 32 (2002) 1215–1227. https://doi.org/10.1016/S0008-8846(02)00766-4.

[34] P.F. Hansen, E.J. Pedersen, Maturity computer for controlled curing and hardening of concrete (in Danish), Nord Betong. 1 (1977) 21–25.

[35] R. Idir, M. Cyr, A. Tagnit-Hamou, Pozzolanic properties of fine and coarse color-mixed glass cullet, Cem Concr Compos. 33 (2011) 19–29. https://doi.org/10.1016/j.cemconcomp.2010.09.013.

[36] S. Chatterji, A.D. Jensen, N. Thaulow, P. Christensen, Studies of alkali-silica reaction. Part 3. Mechanisms by which NaCl and $Ca(OH)_2$ affect the reaction, Cem Concr Res. 16 (1986) 246–254. https://doi.org/10.1016/0008-8846(86)90141-9.

[37] M.-A. Bérubé, J. Frenette, Testing Concrete for AAR in NaOH and NaCl solutions at 38°C and 80°C, Cem Concr Compos. 16 (1994) 189–198. https://doi.org/10.1016/0958-9465(94)90016-7.

[38] A. Heisig, L. Urbonas, R.E. Beddoe, D. Heinz, Ingress of NaCl in concrete with alkali reactive aggregate: effect on silicon solubility, Mater Struct. 49 (2016) 4291–4303. https://doi.org/10.1617/s11527-015-0788-y.

[39] J. Lindgård, B. Grelk, B.J. Wigum, J. Trägårdh, K. Appelqvist, E. Holt, M. Ferreira, M. Leivo, Nordic Europe, in: I. Sims, A. Poole (Eds.), Alkali-Aggregate Reaction in Concrete - A World Review, CRC Press, 2017: pp. 277–320.

[40] B. Fournier, A. Bilodeau, N. Bouzoubaa, P.-C. Nkinamubanzi, Field and Laboratory Investigations on the Use of Fly Ash and Li-Based Admixtures to Prevent ASR in Concrete, in: Sixth International Conference on Durability of Concrete Structures, Leeds (United Kingdom), 2018.

Paper V

# Predicting the effect of SCMs on ASR in the accelerated mortar bar test with artificial neural networks

Maxime Ranger [a,b], Marianne Tange Hasholt [b], Ricardo Antonio Barbosa [c], Lene Højris Jensen [a]

[a] Danish Road Directorate, Hedehusene, Denmark

[b] Technical University of Denmark, Kongens Lyngby, Denmark

[c] Danish Technological Institute, Taastrup, Denmark

*Published in Proceedings of the 16th International Conference on Alkali-Aggregate Reaction in Concrete – Volume II, pp. 389 – 400, May 2022, Lisbon (Portugal)*

# Abstract

Supplementary cementitious materials (SCMs) are an efficient way to both mitigate ASR and reduce the carbon footprint of concrete. Identifying possible new materials and assessing their suitability regarding ASR have become major issues, since the amount of traditional SCMs such as fly ash is declining. Accelerated mortar bar test has been widely used to test different materials with various replacement levels, and a substantial amount of data is available in the literature. This study explores the possibility of using artificial neural networks to analyse this large dataset. Attention is drawn on the relationship between the chemical composition of the binder and the reduction in expansion brought by the addition of SCMs, compared to the reference mixes with cement only. Using a baseline case with only the CaO and $SiO_2$ contents of the binder as inputs, one can see that the individual addition of other compounds ($Al_2O_3$, $Fe_2O_3$, MgO, $SO_3$ and $Na_2O_{eq}$) does improve the neural network performance. Combining them altogether improves the performance even further, although the assumption of independence of inputs may no longer be valid. After training, the artificial neural network is able to predict with a relatively good accuracy the SCM effect: the reduction in expansion is successfully predicted within ± 20 percentage points for more than 90% of the dataset. However, uncertainties remain on the quantitative effect of each oxide, which could be investigated further by performing other types of regression on the same dataset. Besides, increasing the dataset size to fully exploit the potential of artificial neural networks and investigating methods to shed light on the input-output relationship are also promising leads to strengthen the analysis.

# Keywords

Accelerated mortar bar test, alkali-silica reaction, artificial neural network, supplementary cementitious materials.

# 1 Introduction

Supplementary cementitious materials (SCMs) play an important role in reducing the influence of concrete on global warming. Amongst all concrete constituents, cement has by far the largest $CO_2$ contribution, typically around 70% [1]. Traditional SCMs such as fly ash, silica fume or GGBF slag provide good examples of circularity, by upcycling industrial by-products. As a twofold effect, they can both reduce the carbon footprint of concrete by

substituting part of the cement and improve concrete durability. However, these materials come from industries emitting large amounts of $CO_2$, which are also at the core of environmental challenges. In Denmark, coal-fired power plants are currently phased out, which will make fly ash no longer available locally in the coming years. It is therefore necessary to find alternatives and assess their suitability.

Alkali-silica reaction (ASR) is one of the major concrete deterioration mechanisms that has been studied for more than 70 years. ASR is a chemical reaction taking place in the pore solution of concrete between alkali hydroxides ($OH^-$, $Na^+$ and $K^+$) and amorphous silica from aggregates dissolved at high pH [2]. The alkalis mostly come from cementitious materials, but some aggregates can also bring a significant contribution [3]. Traditional SCMs have proven to be an efficient way to mitigate deleterious ASR, and some extensive research have been carried out to document their effect [4]. One of the biggest challenges with ASR is the slow speed of reaction, as it can take some decades before seeing any sign of damage in field structures. Accelerated tests are therefore necessary to evaluate the ASR risk within a reasonable amount of time prior to construction. Two main accelerated tests have been used so far: the accelerated mortar bar test, AMBT (ASTM C1260/C1567, CAN/CSA A23.2-25A/28A, RILEM AAR-2), and the concrete prism test, CPT (ASTM C1293, CAN/CSA A23.2–14A, RILEM AAR-3). Although these tests were initially developed for assessing aggregate reactivity, they have also been used to evaluate the effect of SCMs on the ASR expansion. While the literature provides numerous test results for both AMBT and CPT with traditional SCMs, new SCMs have mostly been tested only with AMBT so far.

New SCMs, such as calcined clays, biomass ashes, sewage sludge ashes or waste construction materials (glass, brick) may have a higher alkali content than traditional materials. Their diversity is also reflected by a wide range of chemical compositions. A few studies have focused on the relationship between the chemical composition of fly ashes and the expansion of mortar bars containing these materials in the AMBT [5,6]. Attempts were made to correlate a chemical index, derived from the chemical composition, to the normalized expansion at 14 days by means of a non-linear regression analysis. This approach was subsequently applied to other types of SCMs [7,8].

Regression analysis refers to problems where it is intended to make a qualitative prediction of a variable, which is dependent of independent inputs [9]. One traditional way of performing regression analysis is to find the

mathematical function that represents the relationship between the inputs and the output the best. This can take the form of curve fitting, where the general form of the function is known but some fitting parameters have to be adjusted. However, nowadays machine learning offers new possibilities to analyse large datasets, almost without any assumption on the input-output relationship. Artificial neural network (ANN) is one type of modelling in machine learning and can be used for both classification and regression problems [10]. ANNs perform usually quite well for making predictions, and they also have the advantage of being easy to use once the model has been set, by changing the number of inputs for instance.

The objective of the present work is to investigate how the chemical composition of SCMs influences the expansion of mortar bars in the AMBT, even if the AMBT is considered as a rapid screening test that does not itself reliably predict the performance of concrete. This is done by performing regression on a large dataset with ANNs, which aims to find out what the generic relationship is and move from experimental measurements towards empirical generalization.

# 2 Artificial neural networks

Machine learning has now become a well-known tool for analysing large datasets. Machine learning is typically divided into three categories: unsupervised learning, supervised learning and reinforced learning. Amongst these three, supervised learning is probably the most comparable to the usual learning process of the human brain [10]. This can be seen as an iterative process, based on the “learning from mistakes” principle. Given a problem, some inputs and the current knowledge, an attempt is made to solve the problem, and an answer is generated. Then, the answer is compared to the solution. If a difference is noticed, the way of processing the inputs is modified, and a new answer is proposed. This process continues until the difference between the answer and the solution is judged as acceptable.

In machine learning, the artificial neural network (ANN) approach is one of the tools that allow supervised learning. The following gives an overall description and introduction to how they operate, as well as the basis for the model developed later in this paper.

## 2.1 Structure of an ANN

The ANNs mimic the structure of the human brain. An ANN is made of three distinct parts: the input layer, the hidden layer(s) and the output layer. They can be identified as the dendrites, the synapses and the axon in a biological neuron [11]. In the ANN, each neuron is connected to all neurons of the subsequent layer, and a weight $w_{ij}$ is associated to each connection. This structure can be seen in Figure 1.

The role of an artificial neuron is to classify inputs. A single input value is calculated by summing up all the weighted inputs connected to the neuron. Then, this value passes through a so-called activation function. In its simplest form, i.e. the step function, the activation function returns 0 if the input value is below a threshold limit, 1 otherwise. However, the step function is not appropriate for ANNs, because of the non-continuous gradient. For this reason, the sigmoid is often preferred as the default activation function [12]. To facilitate the classification process, an offset value can be added to the input value of the activation function. Such offset is called a bias, denoted as $b_j$. Biases are essentially giving one more degree of freedom in order to make the classification more accurate [11].

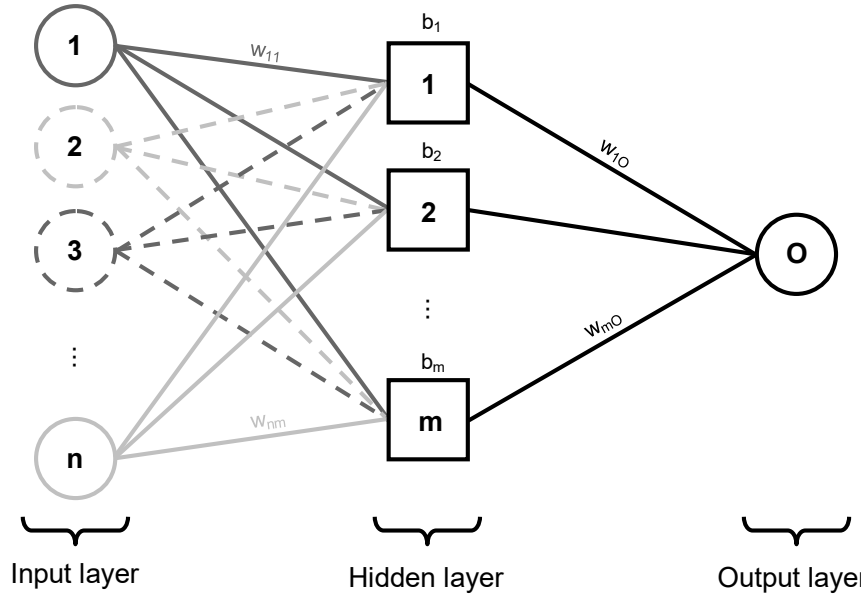


*Figure 1: Structure of an artificial neural network, with a single hidden layer.*

Once data have gone through all hidden neurons, they reach the output layer. This process is referred to as forward propagation [11]. The calculated output is then compared to the real output, by means of a loss function. The minimization of the loss function is done through a process called

backpropagation. Different methods exist, but the Levenberg-Marquardt algorithm has proven to be quite efficient for non-linear functions. In short, it consists of a combination between the steepest descent (stable but slow) and the Gauss-Newton (unstable but fast) algorithms, by means of an adaptive combination coefficient $\mu$. The term adaptive refers to the fact that $\mu$ is updated after each iteration, typically by multiplying or dividing it by a fixed factor. As an example, if the performance improves between two iterations, $\mu$ is reduced, and the calculation scheme gets closer to the Gauss-Newton algorithm. On the other hand, if the performance does not improve enough, $\mu$ is increased and make the steepest descent part dominant [13].

## 2.2 Architecture

The ANN is somehow similar to a system of equations to solve. Let $I$, $H$ and $O$ be respectively the number of input neurons, hidden neurons and output neurons. The total number of unknows $N_u$ is given by Equation (1). The number of equations $N_{eq}$ depends on the number of training data points $N_{tr}$, via Equation (2).

$$N_u = (I + 1)\, H + (H + 1)\, O \tag{1}$$

$$N_{eq} = N_{tr}\, O \tag{2}$$

As any system of equations, it can only be solved if $N_u \leq N_{eq}$, which can also be expressed as a condition on the number of hidden neurons by means of Equation (3).

$$H \leq \frac{(N_{tr} - 1)\, O}{I + O + 1} \tag{3}$$

For a classical system of equations, the equality case in Equation (3) would correspond to a system with a unique solution. On the other hand, the strict inequality would result in an over-constrained system. However, when using an ANN, the relationship that contains the loss function is not an equality, but only a minimization relationship. Therefore, the solution depends on how many training data are available: the higher $N_{tr}$, the better the generalization. Thus, for ANNs it is often required that $N_u \ll N_{eq}$, so that Equation (3) will rather take the form of an inequality, as shown in Equation (4).

$$H \ll \frac{(N_{tr} - 1)\, O}{I + O + 1} \tag{4}$$

## 2.3 Training

During the training stage, supervised learning is performed. It consists in a succession of forward and back propagations on the training subset, each cycle being called an epoch. Thus, after each epoch, the weights and biases are updated to improve the training performance. In the meantime, the updated ANN is applied to the validation subset, without backpropagation. The validation subset can therefore be used to test whether the ANN is trained enough or not [10]. If the validation performance does not improve from one epoch to the following ones, the training stops.

## 2.4 Overfitting

One major risk against generalization is overfitting. Taking a human-like image, overfitting corresponds to a situation where the training consists of solely learning by heart a set of problem-solution. When a new problem arises, it does not match with any of the combinations that have been learnt. Therefore, the answer is mainly a guess, and may significantly deviate from the actual solution. The following briefly presents a few methods to prevent overfitting.

### 2.4.1 Regularization

Overfitting in ANNs typically results in large values for the weights. One way to avoid it is to implement regularization, which aims to add a penalty to the loss function if some weights become too large [10]. A commonly used method, the Bayesian regularization, consists of adding the sum of the squares of the weights to the loss function. The optimization of the loss function will therefore result in a balance between minimizing the error and minimizing the weights [12].

### 2.4.2 Cross-validation

In cross-validation, the learning process of a given ANN architecture is repeated several times, by changing the validation dataset [10]. In k-fold cross-validation, the learning dataset (training + validation) is divided into k subsets, and k iterations are performed by using each subset once for validation. Note that for cross-validation, the test dataset remains unchanged. The principle of cross-validation is illustrated in Figure 2.

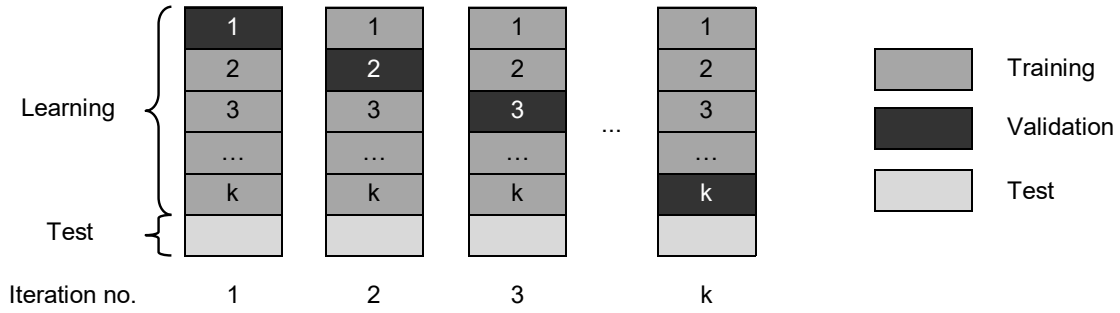


*Figure 2: Principle of k-fold cross-validation.*

### 2.4.3 Early stopping

Early stopping consists in stopping the training after a limited number of iterations, i.e. before the loss function converges. This may result in a slightly reduced training performance, but it prevents the neural network from becoming overtrained.

## 2.5 Limitations

ANNs usually perform quite well for making predictions. However, because their structure is highly non-linear, it is still quite difficult to understand the reasoning behind the answer, i.e. the mathematical equation governing the outputs as a function of the inputs. This is a typical example of the trade-off that exists between interpretability and accuracy of the model in data analysis [9]. Therefore, one possibility is to implement a regression analysis apart from the ANN, which is easier to interpret but may be less accurate. Then, both performances can be compared, and one can assess whether the use of an ANN can significantly improve the accuracy of the prediction or not.

# 3 Data collection

A literature review was made to collect data from accelerated mortar bar tests performed on a variety of SCMs. In order to compare the data on a fair basis, several criteria were applied for the data selection. First, the dataset was restricted to results obtained from a standard accelerated mortar bar test, i.e. ASTM C1260/1567 or CAN/CSA A23.2-25A/28A. However, a tolerance was applied for tests where the w/b ratio was slightly modified (in most cases, 0.50 instead of 0.47 required).

The second criterion dealt with the expansion of the reference bars. The present paper focuses on the expansion obtained in the AMBT when using SCMs, and not on the reactivity of aggregates. Therefore, it was chosen to select tests only

made with aggregates where the expansion of the reference test was larger than 0.2% after 14 days of exposure. Finally, the materials were filtered from their chemical composition, in order to only keep tests where the contents in $SiO_2$, $Al_2O_3$, $Fe_2O_3$, MgO, CaO, $SO_3$ and $Na_2O_{eq}$, for both cement and SCM, are available. It was chosen to consider $Na_2O_{eq}$ instead of $Na_2O$ and $K_2O$ separately to maximize the size of the dataset, as the distinct contents of $Na_2O$ and $K_2O$ were not always reported. In addition, SCMs for which the LOI was larger than 10% or for which the sum of all seven constituents mentioned before was lower than 90% were excluded.

This resulted in a selection of 92 different SCMs and a total of 467 data points. Note that the dataset included some tests performed with the same binder on different reactive aggregates. An overview of the dataset is presented in Table 1, and a ternary diagram of the materials is plotted in Figure 3.

*Table 1: Overview of the dataset (*: origin not known). The table continues on the next page.*

| Source | Type of SCM | Type and origin of aggregate | Number of datapoints |
|---|---|---|---|
| [8] | Fly ash class C & F, GGBF slag, Silica fume | River aggregate, Kızılırmak river (TUR) | 119 |
| [14] | Fly ash class C & F | Limestone, Spratt (CAN)<br>Rhyolite, New Mexico (USA)<br>Argillite, North Carolina (USA)<br>Quartzite, South Dakota (USA) | 40 |
| [6] | Fly ash class C & F | Sand – Volcanic rock, Oregon (USA)<br>2 types of reactive sand, Texas (USA) | 36 |
| [15] | Fly ash class C & F | Reactive sand, * | 34 |
| [16] | Fly ash class C & F, Calcined clay | Rhyolite, Wyoming (USA)<br>Reactive sand, Idaho (USA)<br>Rhyolite – Andesite, New Mexico (USA)<br>Glacial deposit - Shale, Iowa (USA) | 32 |
| [17] | Fly ash class C & F | Soda-lime glass sand, * | 20 |
| [7] | Fly ash class F, GGBF slag, Silica fume | 2 types of reactive sand, Colombia | 20 |
| [18] | Calcined clay | Reactive sand, * | 17 |
| [19] | Silica fume | Limestone, Spratt (CAN) | 16 |
| [20] | Fly ash class C & F | River sand, Arkansas river (USA) with reactive sand (Jobe), El Paso (TX-USA) | 16 |

| | | | |
|---|---|---|---|
| [21] | Fly ash class F, GGBF slag, Silica fume | River sand, Ahmetli (TUR)<br>Basaltic rock, Aliağa (TUR) | 12 |
| [22] | Fly ash class C, Natural pozzolan | Reactive sand, Texas (USA) | 12 |
| [23] | Metakaolin | Limestone, Spratt (CAN)<br>Greywacke – Argillite, Sudbury (CAN) | 8 |
| [24] | Ground glass, Natural pozzolan | Rhyolite, Thailand | 8 |
| [25] | Crushed brick | River aggregate, * | 7 |
| [26] | Fly ash class C & F | Reactive sand, Briggs (TX-USA) | 6 |
| [27] | Fly ash class F | River aggregate, Sakarya river (TUR) | 6 |
| [28] | Metakaolin, Fly ash class C | Reactive sand, Texas (USA) | 6 |
| [29] | Fly ash class F | River aggregate, Aras river (IRN) | 5 |
| [30] | Natural pozzolan | River aggregate, * | 5 |
| [31] | Metakaolin | Basaltic rock, Aliağa (TUR) | 5 |
| [32] | Rice hush ash | Reactive sand, River Plate/Chaco (ARG) | 5 |
| [33] | Co-fired biomass ash | Reactive sand, Texas (USA) | 5 |
| [34] | Fly ash class C, Crushed brick | Perlite, Turkey | 5 |
| [35] | Ground glass | Reactive sand, * | 4 |
| [36] | Fly ash class C & F, Silica fume | Limestone, Spratt (CAN) | 4 |
| [37] | Metakaolin | Greywacke, Western Cape (ZAF) | 4 |
| [38] | GGBF slag | Reactive aggregate, Wawa (CAN) | 4 |
| [39] | Ground glass, Fly ash class C | Limestone, Spratt (CAN) | 3 |
| [40] | Fly ash class C | Reactive sand, Texas (USA) | 3 |

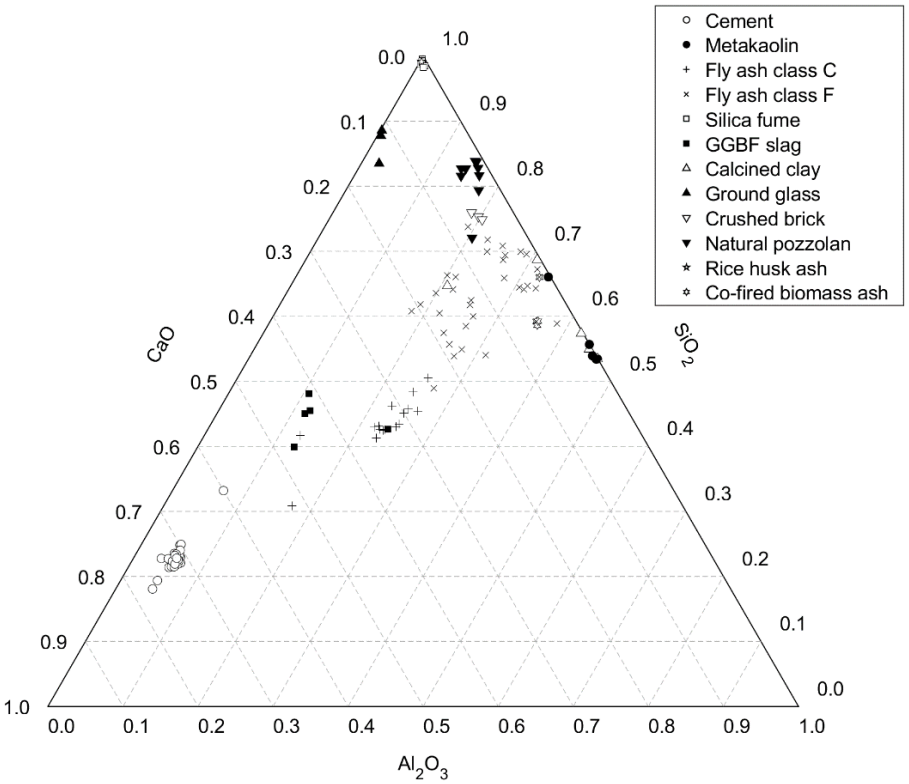


*Figure 3: Ternary diagram of the selected materials.*

# 4 Data analysis

The ANNs used for the present study were executed in MATLAB. Bayesian regularization combined with the Levenberg-Marquardt algorithm were implemented for the supervised training. The dataset was randomly divided into two subsets (85% for learning, 15% for test). The activation function was the sigmoid function, and the performance was assessed by calculating the mean square error.

## 4.1 Inputs

The inputs were derived from the partial chemical composition of the binder. The inclusion of one specific compound resulted in two values, namely the content by mass in the cement $X_{cem}$ and in the SCM $X_{SCM}$. These values were then weighted by the replacement level $RL$ according to Equation (5), so that $x_{cem}$ and $x_{SCM}$ were used as inputs for the model.

$$\begin{cases} x_{cem} = X_{cem} \cdot RL \\ x_{SCM} = X_{SCM} \cdot RL \end{cases} \quad (5)$$

It is desirable to have independent inputs for ANNs. However, when considering the chemical composition, the variables are strictly not independent, as their sum

should be lower than 100%. This is particularly true when considering the primary oxides, that account for the largest part of the composition usually.

Finally, input data were automatically normalized when using the *feedforwardnet* function in MATLAB.

## 4.2 Output

Since most data were from studies carried out with different aggregates, the expansion values obtained were not directly comparable. One way of overcoming this issue was to normalize the expansion $y$ with the expansion of the associated reference test $y_{ref}$, as shown in Equation (6).

$$\hat{y} = \frac{y}{y_{ref}} \tag{6}$$

## 4.3 Choice of the architecture

Equation (4) gives a condition on the maximum number of hidden neurons. Given that the number of training data (68% of 467, as the learning subset is divided into 5 for cross-validation, where each validation fold represents 17% of the entire dataset – see the explanation in the next paragraph) was not extremely large, a factor 2 was applied to satisfy Equation (4), as shown per Equation (7).

$$H_{max} = \frac{1}{2}\,\frac{(N_{tr} - 1)\,O}{I + O + 1} \tag{7}$$

The choice of the architecture was based on a triple loop on the learning data subset only (Figure 4). The outer loop was an iteration on the number of hidden neurons, from 1 to $H_{max}$. The medium loop consisted of 30 iterations where the learning data subset was randomly divided for 5-fold cross-validation, therefore each fold corresponds to 17% of the initial dataset. The same set of initial weights and biases was used for each iteration, the set being randomly selected prior to running the algorithm.

For each iteration, the termination was based on the validation performance: the training stopped when the mean square error (MSE) on the validation subset did not decrease for 8 epochs in a row.

The training and validation MSE were calculated for each iteration and averaged for the two inner loops. This resulted in a plot of both MSE as a function of the number of hidden neurons. These curves typically decrease and stabilize. However, if the number of hidden neurons is too larger, the MSE for

validation may start to increase, which is a common sign of overtraining. The number of hidden neurons was finally selected as the minimum number of neurons for which the two MSE are less than 1% higher than their minimum value. This is illustrated in Figure 4. Note that there were a few exceptions, where this criterion could not be fulfilled. In such a case, the tolerance was increased until finding an appropriate number of neurons.

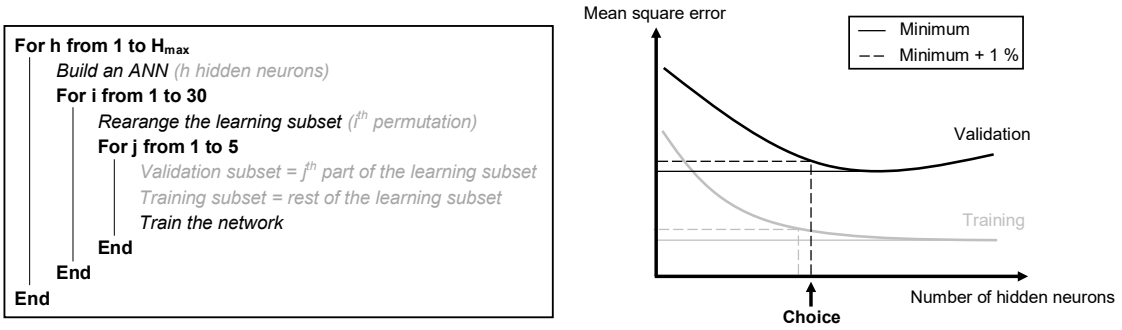


*Figure 4: Triple loop algorithm (left) and schematic graph for selecting the number of hidden neurons (right).*

## 4.4 Prediction

When the number of hidden neurons had been chosen, a new ANN was build based on the selected architecture. The new ANN was trained with the entire learning subset, i.e. the learning phase did not include any validation, in order to maximize the number of training data. In this case, early stopping was implemented to stop training, since the termination criterion used when choosing the architecture could no longer be applied. The maximum number of epochs corresponded to the average number of epochs performed during the choice of the architecture (i.e. after how many epochs the training stopped when performing cross-validation), for this specific number of neurons.

The results were split into the subset used for learning (85% of the dataset) and the test subset (15%). Note that before this stage, the test subset was not used at all, which made it ideal for making a final assessment of the neural network. For each subset, the coefficient of determination $R^2$ was calculated. The predictions were plotted against the experimental values in both cases. Besides, the residual errors were also displayed as a function of the replacement level. The residual error $r$ was calculated based on Equation (8), where the subscripts $p$ and $m$ respectively stand for predicted and measured.

$$r = \widehat{y_p} - \widehat{y_m} \tag{8}$$

## 4.5 Variables

Since the objective of the present study was to investigate the effect of the chemical composition of the binder on the AMBT expansion, 12 different combinations of inputs were used. The baseline combination only included $SiO_2$ and CaO, as they were considered to have the largest effect on the test result [5,6,8]. In order to stress the influence of other compounds, 5 combinations were formed by adding a third oxide ($Al_2O_3$, $Na_2O_{eq}$, $Fe_2O_3$, MgO or $SO_3$) in addition to $SiO_2$ and CaO. In a similar way, 5 other combinations were created by including all oxides except one. Finally, the last combination to be tested included all seven compounds.

# 5. Results

The chosen architecture and the performances obtained with the learning and the test subsets are given in Table 2, together with $H_{max}$ calculated from Equation (7) and the selected number of neurons H.

*Table 2: Architecture and performances of the ANN.*

| Compounds selected for defining the inputs | Combination | $H_{max}$ | H | Epochs | $R^2$ learning | $R^2$ test |
|---|---|---|---|---|---|---|
| $SiO_2$, CaO | 1 | 27 | 10 | 34 | 0.824 | 0.896 |
| $SiO_2$, CaO, $Al_2O_3$ | 2 | 20 | 8 | 31 | 0.852 | 0.879 |
| $SiO_2$, CaO, $Na_2O_{eq}$ | 3 | 20 | 8 | 25 | 0.849 | 0.879 |
| $SiO_2$, CaO, $Fe_2O_3$ | 4 | 20 | 8 | 34 | 0.853 | 0.901 |
| $SiO_2$, CaO, MgO | 5 | 20 | 6 | 27 | 0.837 | 0.906 |
| $SiO_2$, CaO, $SO_3$ | 6 | 20 | 10 | 35 | 0.878 | 0.893 |
| $SiO_2$, CaO, $Na_2O_{eq}$, $Fe_2O_3$, MgO, $SO_3$ | 7 | 11 | 7 | 30 | 0.909 | 0.873 |
| $SiO_2$, CaO, $Al_2O_3$, $Fe_2O_3$, MgO, $SO_3$ | 8 | 11 | 7 | 33 | 0.897 | 0.915 |
| $SiO_2$, CaO, $Al_2O_3$, $Na_2O_{eq}$, MgO, $SO_3$ | 9 | 11 | 7 | 30 | 0.912 | 0.902 |
| $SiO_2$, CaO, $Al_2O_3$, $Na_2O_{eq}$, $Fe_2O_3$, $SO_3$ | 10 | 11 | 10 | 31 | 0.919 | 0.922 |
| $SiO_2$, CaO, $Al_2O_3$, $Na_2O_{eq}$, $Fe_2O_3$, MgO | 11 | 11 | 9 | 33 | 0.918 | 0.844 |
| $SiO_2$, CaO, $Al_2O_3$, $Na_2O_{eq}$, $Fe_2O_3$, MgO, $SO_3$ | 12 | 10 | 7 | 31 | 0.915 | 0.914 |

Figure 5 shows the predicted normalized expansion plotted against the experimental normalized one for combination no. 12. The residual errors on the expansion as described per Equation (8), obtained with the same combination, are plotted against the cement replacement level in Figure 6.

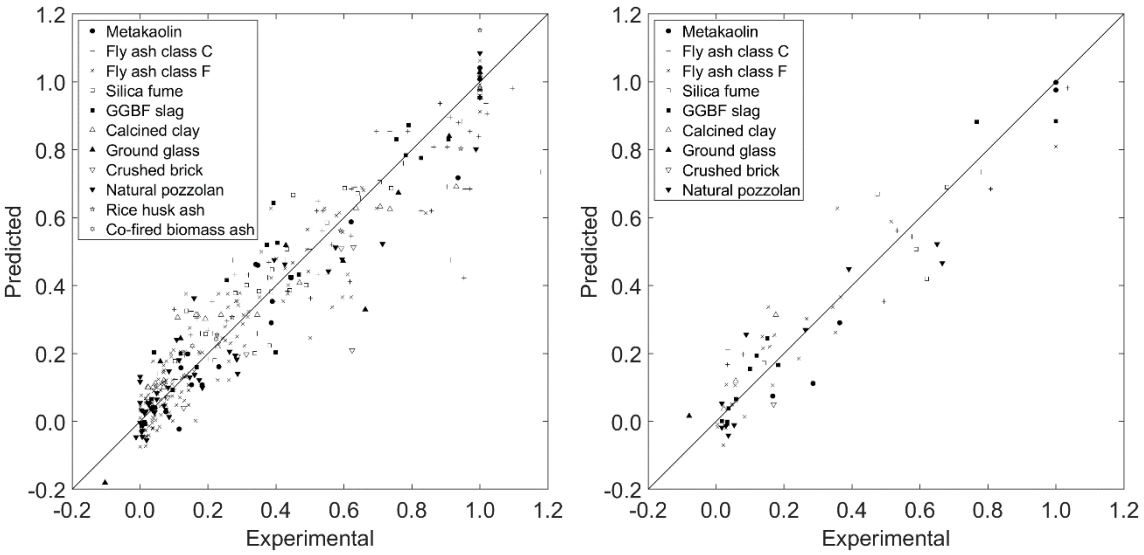


*Figure 5: Predicted vs. experimental normalized expansion for the learning data subset (left) and the test data subset (right), for combination no.12. The black solid line is a one-to-one line.*

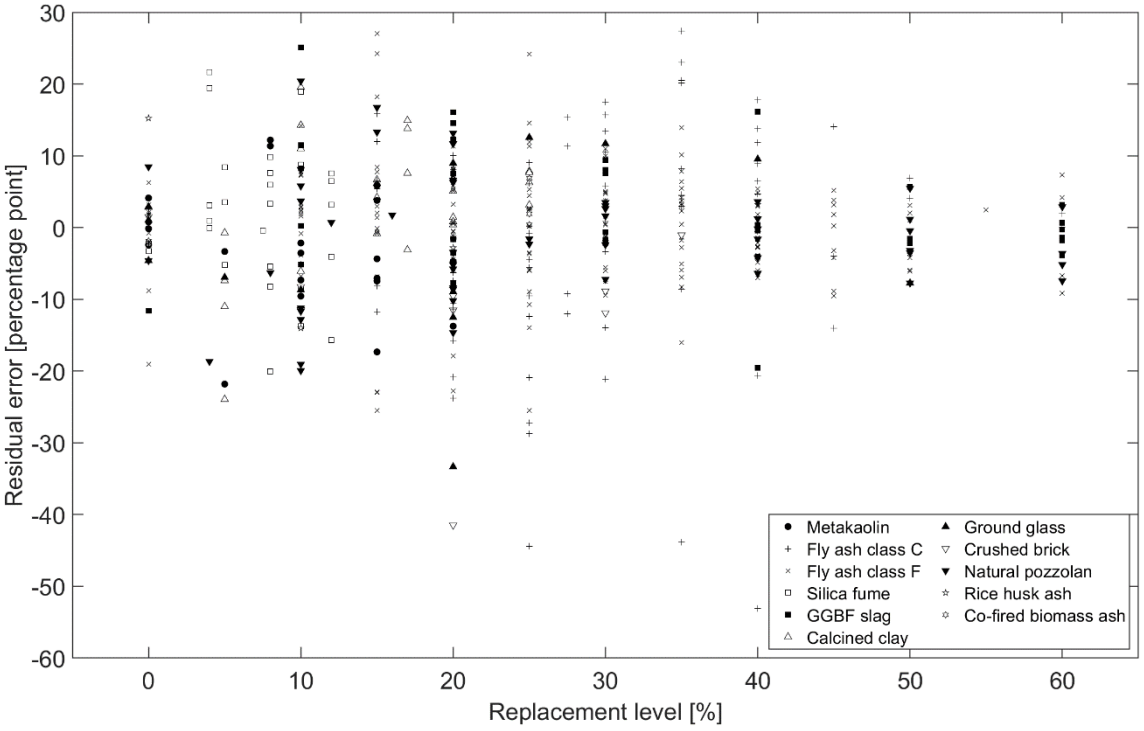


*Figure 6: Residual error as a function of the replacement level for combination no.12.*

# 6 Discussion

Considering combination no.1 as the baseline, the addition of each single oxide (combinations no.2 to no.6 in Table 2) improved the performance of the ANN for learning. The smallest improvement was obtained when considering MgO, while the largest gain occurred with $SO_3$. These two observations were consistent with a previous analysis, where the MgO content of the binder was found to have a quite poor correlation with the normalized expansion, while the $SO_3$ content had the fourth best $R^2$ value behind $SiO_2$, CaO and $Al_2O_3$ [5].

A reason for $SO_3$ to cause the best improvement in the present work could be due to a particularly large influence on a few datapoints, that where originally far away from the one-to-one line and strongly penalising the $R^2$ value. The ability of $Na_2O_{eq}$ to improve the fitting is also worth to mention. Besides the very low $R^2$ value reported elsewhere [5], it is also known that the alkali concentration of the pore solution during the AMBT is dramatically changed due to alkali exchanges with the NaOH test solution [41], therefore it is not expected to see an influence from the alkali content of the binder. When considering the test subset, the influences were more variable, which could be due to some sampling effects. As the test subset was much smaller that the learning one, the $R^2$ value could be significantly modified by even fewer datapoints.

When combining all seven oxides (combination no.12), the performances were logically improved, both compared to the baseline and to the effect of each individual oxide. This can graphically be seen in Figure 5, where there is a clear trend for the results to match with the one-to-one line.

Combinations no.7 to no.11 were tested to further investigate the influence of each oxide on the performance. For almost all of them, the removal of one oxide caused no significant change in performance for the learning subset. One explanation to this behaviour could be that when increasing the number of oxides, the assumption of independence between the inputs becomes less and less valid. The only exception was seen for combination no. 8, where $Na_2O_{eq}$ was removed. As mentioned before regarding combination no. 3, it was once again not expected that $Na_2O_{eq}$ would influence the quality of the fitting. However, the exact effect of the alkali content on the expansion is not clear. Indeed, understanding the way ANNs process the inputs to predict the outputs is known to be a challenge. Numerous methods have been proposed to explain

black box models [42], but it is still quite difficult to find the most appropriate technique for a given analysis.

The residual error plotted on Figure 6 shows the deviation of the prediction compared to the measured normalized expansion for combination no.12. Note that both subsets, learning and test, are combined on the figure. The average residual was 6.9 pp. (percentage point) for the learning subset, and 7.7 pp. for the test one. 53% of the values were within ±5 pp. for the learning subset, 77% within ±10 pp. and 94% within ±20 pp.. This was respectively 43%, 69% and 94% for the test subset. These results implied that in most cases, the ANN was able to predict the expansion reduction induced by the use of an SCMs, with an accuracy of 20 pp.. Although the accuracy was not high enough to predict the ability of an SCM to keep the expansion below 0.1% at 14 days, it could be used as a screening tool in order to evaluate the potential of an SCM to perform well in the AMBT.

The largest differences were difficult to explain. However, most of them seemed to be related to the shape of the curve when plotting the expansion obtained in the AMBT as a function of the replacement level. It was seen that for some materials, the efficacy of the SCM is not linear, but is closer to an S-shaped curve: there is little to none reduction in expansion at low replacement levels, whereas the expansion is almost completely prevented at high replacement levels. This is for instance the case for one type of glass [24], one brick [34], on rice husk ash [32] and some class C fly ashes [6,14,16]. As a result, the ANN sometimes predicted an S-shape while the behaviour was rather linear, leading to an overestimation of the normalized expansion, but also sometimes behaved the other way around.

Finally, it should be mentioned that by increasing the size of the dataset, e.g. to a couple of thousand data, the consistency between the performances obtained on the learning and the test subsets would likely be improved, in particular by removing sampling effects and covering a broader range of materials.

# Conclusion

Artificial neural networks bring new possibilities to analyse large datasets, especially when the input-output relationship is not well-established. The present work has shown that an ANN could be used as a screening tool with a relatively good accuracy to estimate the ability of an SCM to reduce the ASR expansion measured in the AMBT.

However, analysing the effect of each compound turned to be quite challenging. Although the addition of more inputs compared to CaO and $SiO_2$ alone had an evident benefit on the accuracy of the prediction, the quantitative evaluation of their impact remained unclear. Moreover, the assumption on the independence of the inputs may no longer be valid when increasing the number of inputs, as they are bound by an inequality (sum lower than 100%). The present approach would probably benefit from using an even larger dataset, to widen the scope of materials and eliminate sampling effects. In parallel, investigating methods to extract knowledge from the ANN would help lifting the veil on the weaknesses of the model, although finding the most appropriate method is still challenging.

Finally, as the reliability of the prediction is closely related to the reliability of the input data, the choice of AMBT data can be questioned, particularly because the AMBT is far to be the best and appropriate test to evaluate effectiveness of SCMs against ASR. However, it should be noted that the present ANN model was designed to investigate the effect of the chemical composition of SCMs on the ASR expansion and did not aim to focus on a specific test method. In this respect the AMBT was chosen because, to the authors' knowledge, it offers the largest and most diverse dataset in the literature concerning SCMs and ASR expansion. Nevertheless, the model can easily be transposed to datasets obtained with other test methods such as the CPT or outdoor exposure blocks, as soon as a sufficient amount of data is available.

# Acknowledgements

The authors gratefully acknowledge the financial support of Innovation Fund Denmark (Innovationsfonden) and Realdania for the present research project. We would also like to thank Line Clemmensen (DTU Compute) for the fruitful discussions and insights about artificial neural networks.

# References

[1] C.V. Nielsen, Carbon footprint of concrete buildings seen in the life cycle perspective, in: Proceedings NRMCA 2008 Concrete Technology Forum, 2008: pp. 1–14.

[2] F. Rajabipour, E. Giannini, C. Dunant, J.H. Ideker, M.D.A. Thomas, Alkali-silica reaction: Current understanding of the reaction mechanisms and the knowledge gaps, Cem Concr Res. 76 (2015) 130–146. https://doi.org/10.1016/j.cemconres.2015.05.024.

[3] H.C.B. Thomsen, B. Grelk, R.A. Barbosa, K.K. Hansen, Alkali Release from Typical Danish Aggregates to Potential ASR Reactive Concrete, XXIIIth Symposium on Nordic Concrete Research & Development. (2017).

[4] M. Thomas, The effect of supplementary cementing materials on alkali-silica reaction: A review, Cem Concr Res. 41 (2011) 1224–1231. https://doi.org/10.1016/j.cemconres.2010.11.003.

[5] L.J. Malvar, L.R. Lenke, Efficiency of fly ash in mitigating alkali-silica reaction based on chemical composition, ACI Mater J. 103 (2006) 319–326.

[6] K.A. Schumacher, J.H. Ideker, New Considerations in Predicting Mitigation of Alkali-Silica Reaction Based on Fly Ash Chemistry, Journal of Materials in Civil Engineering. 27 (2015) 04014144.

[7] J. Cassiani, M. Dugarte, G. Martinez-Arguelles, Evaluation of the chemical index model for predicting supplementary cementitious material dosage to prevent the alkali-silica reaction in concrete, Constr Build Mater. 275 (2021). https://doi.org/10.1016/j.conbuildmat.2020.122158.

[8] M. Mahyar, S.T. Erdoğan, M. Tokyay, Extension of the chemical index model for estimating Alkali-Silica reaction mitigation efficiency to slags and natural pozzolans, Constr Build Mater. 179 (2018) 587–597. https://doi.org/10.1016/j.conbuildmat.2018.05.217.

[9] G. James, D. Witten, T. Hastie, R. Tibshirani, An Introduction to Statistical Learning - With application in R, Springer, 2013. https://doi.org/10.1007/978-1-4614-7138-7.

[10] P. Kim, MATLAB Deep Learning, Apress, 2017. https://doi.org/10.1007/978-1-4842-2845-6.

[11] U. Kamath, J. Liu, J. Whitaker, Deep Learning for NLP and Speech Recognition, Springer International Publishing, 2019. https://doi.org/10.1007/978-3-030-14596-5.

[12] D.J. Livingstone, Artificial Neural Networks: Methods and Applications, Humana Press, 2008.

[13] H. Yu, B.M. Wilamowski, Levenberg-Marquardt Training, in: Intelligent Systems, CRC Press, 2018: pp. 12–1.

[14] P.R. Rangaraju, J. Desai, Effectiveness of Fly Ash and Slag in Mitigating Alkali-Silica Reaction Induced by Deicing Chemicals, Journal of Materials in Civil Engineering. 21 (2009) 19–31.

[15] A. Kruse, A. Jasso, K. Folliard, R. Ferron, M. Juenger, T. Drimalas, Characterizing Fly Ash, Report FHWA/TX-13/0-6648-1, 2012, Center for Transportation Research, University of Texas at Austin.

[16] W. Touma, D. Fowler, R. Carrasquillo, Alkali-silica reaction in Portland cement concrete: testing methods and mitigation alternatives, Report ICAR -301-1f, Austin, 2001.

[17] S.M.H. Shafaatian, A. Akhavan, H. Maraghechi, F. Rajabipour, How does fly ash mitigate alkali-silica reaction (ASR) in accelerated mortar bar test (ASTM C1567)?, Cem Concr Compos. 37 (2013) 143–153. https://doi.org/10.1016/j.cemconcomp.2012.11.004.

[18] C. Li, J.H. Ideker, T. Drimalas, The efficacy of calcined clays on mitigating alakli-silica reaction (ASR) in mortar and its influence on microstructure, RILEM Bookseries. 10 (2015) 211–217. https://doi.org/10.1007/978-94-017-9939-3_26.

[19] A.M. Boddy, R.D. Hooton, M.D.A. Thomas, Effect of product form of silica fume on its ability to control alkali-silica reaction, Cem Concr Res. 30 (2000) 1139–1150. https://doi.org/10.1016/S0008-8846(00)00297-0.

[20] W.J. Phillips, Alkali Silica Reaction Mitigation Using High Volume Class C Fly Ash, Thesis and dissertations, University of Arkansas, Fayetteville 2015.

[21] H. Yazici, A. Beglarigale, K. Tosun Felekoğlu, S. Türkel, Comparing the alkali-silica reaction mitigation potential of admixtures by using different accelerated test methods, Constr Build Mater. 197 (2019) 597–614. https://doi.org/10.1016/j.conbuildmat.2018.11.227.

[22] R.I. Cano, Evaluation of Natural Pozzolans as Replacements for Class F Fly Ash in Portland Cement Concrete, MSc Thesis, The University of Texas at Austin, 2013.

[23] T. Ramlochan, M. Thomas, K.A. Gruber, Effect of metakaolin on alkali-silica reaction in concrete, Cem Concr Res. 30 (2000) 339–344. https://doi.org/10.1016/S0008-8846(99)00261-6.

[24] T. Meesak, S. Sujjavanich, Effectiveness of 3 different supplementary cementitious materials in mitigating alkali silica reaction, Mater Today Proc. 17 (2019) 1652–1657. https://doi.org/10.1016/j.matpr.2019.06.195.

[25] L. Turanli, F. Bektas, P.J.M. Monteiro, Use of ground clay brick as a pozzolanic material to reduce the alkali-silica reaction, Cem Concr Res. 33 (2003) 1539–1542. https://doi.org/10.1016/S0008-8846(03)00101-7.

[26] C.S. Shon, S.L. Sarkar, D.G. Zollinger, Application of modified ASTM C1260 test for fly ash-cement mixtures, Transp Res Rec. 1834 (2003) 93–106. https://doi.org/10.3141/1834-12.

[27] K. Yildirim, M. Sümer, Comparative analysis of fly ash effect with three different methods in mortars that are exposed to alkali silica reaction, Compos B Eng. 61 (2014) 110–115. https://doi.org/10.1016/j.compositesb.2014.01.004.

[28] R.D. Moser, A.R. Jayapalan, V.Y. Garas, K.E. Kurtis, Assessment of binary and ternary blends of metakaolin and Class C fly ash for alkali-silica reaction mitigation in concrete, Cem Concr Res. 40 (2010) 1664–1672. https://doi.org/10.1016/j.cemconres.2010.08.006.

[29] B. Ahmadi, M. Shekarchi, Use of natural zeolite as a supplementary cementitious material, Cem Concr Compos. 32 (2010) 134–141. https://doi.org/10.1016/j.cemconcomp.2009.10.006.

[30] F. Bektas, L. Turanli, P.J.M. Monteiro, Use of perlite powder to suppress the alkali-silica reaction, Cem Concr Res. 35 (2005) 2014–2017. https://doi.org/10.1016/j.cemconres.2004.10.029.

[31] Ş. Yazici, H.Ş. Arel, D. Anuk, Influences of Metakaolin on the Durability and Mechanical Properties of Mortars, Arab J Sci Eng. 39 (2014) 8585–8592. https://doi.org/10.1007/s13369-014-1413-z.

[32] G. Rodríguez De Sensale, Effect of rice-husk ash on durability of cementitious materials, Cem Concr Compos. 32 (2010) 718–725. https://doi.org/10.1016/j.cemconcomp.2010.07.008.

[33] C.R. Shearer, N. Yeboah, K.E. Kurtis, S.E. Burns, Evaluation of biomass fired and co-fired fly ash for alkali-silica reaction mitigation in concrete, in: T. Drimalas, J.H. Ideker, B. Fournier (Eds.), Proceedings of the 14th International Conference on Alkali-Aggregate Reactivity in Concrete, Austin, TX, 2012.

[34] F. Bektas, Use of ground clay brick as a supplementary cementitious material in concrete-hydration characteristics, mechanical properties, and ASR durability, PhD Thesis, Iowa State University, 2007.

[35] N. Schwarz, H. Cam, N. Neithalath, Influence of a fine glass powder on the durability characteristics of concrete and its comparison to fly ash, Cem Concr Compos. 30 (2008) 486–496. https://doi.org/10.1016/j.cemconcomp.2008.02.001.

[36] M.-A. Bérubé, J. Duchesne, D. Chouinard, Why the accelerated mortar bar method ASTM C1260 is reliable for evaluating the effectiveness of supplementary cementing materials in suppressing expansion due to alkali-silica reactivity, Cement Concrete and Aggregates. 17 (1995) 26–34. https://doi.org/10.1520/CCA10333J.

[37] A.T. Bakera, M.G. Alexander, Properties of Western Cape Concretes with Metakaolin, in: MATEC Web of Conferences, EDP Sciences, 2018. https://doi.org/10.1051/matecconf/201819911011.

[38] D. Hooton, C.R. Donnelly, B. Clarida, C.A. Rogers, An assessment of the effectiveness of blast-furnace slag in counteracting the effects of alkali-silica reaction, in: M.-A. Bérubé, B. Durand, B. Fournier (Eds.), 11th International Conference on Alkali Aggregate Reaction, Québec City, 2000: pp. 1313–1322.

[39] C. Shi, Y. Wu, C. Riefler, H. Wang, Characteristics and pozzolanic reactivity of glass powders, Cem Concr Res. 35 (2005) 987–993. https://doi.org/10.1016/j.cemconres.2004.05.015.

[40] C.R. Shearer, The productive reuse of coal, biomass and co-fired fly ash, PhD Thesis, Georgia Institute of Technology, 2014.

[41] F. Golmakani, R.D. Hooton, Impact of pore solution concentration on the accelerated mortar bar alkali-silica reactivity test, Cem Concr Res. 121 (2019) 72–80.

[42] R. Guidotti, A. Monreale, S. Ruggieri, F. Turini, F. Giannotti, D. Pedreschi, A survey of methods for explaining black box models, ACM Comput Surv. 51 (2018).

Paper VI

# Reactivity of alternative supplementary cementitious materials assessed by the $R^3$ method

M. Ranger [a,b], J. Duchesne [c]

[a] Department of Environmental and Resource Engineering, Technical University of Denmark, Kgs. Lyngby, Denmark

[b] Danish Road Directorate, Copenhagen, Denmark

[c] Department of Geology and Geological Engineering, Laval University, Quebec City, Canada

*Accepted for the 16th International Congress on the Chemistry of Cement, September 2023, Bangkok (Thailand)*

# Abstract

The necessity to reduce carbon emissions in concrete production has accelerated the partial replacement of Portland cement by Supplementary Cementitious Materials (SCMs). As the range of SCMs studied is constantly expanding, screening tests to evaluate their reactivity have gained considerable attention. One example is the $R^3$ method, which consists in quantifying the chemical reactivity of an SCM in a simplified mixture simulating the environment of a cement paste. Different parameters measured by various techniques have been proposed in previous work: heat release, bound water, portlandite consumption and chemical shrinkage.

In the present study, the $R^3$ method was applied to both traditional and alternative SCMs, to further investigate the validation range of the method. The experimental matrix included limestone, fly ash, calcined clays, biomass ashes, crushed brick, glass beads and sewage sludge ash. Three parameters were measured: heat release by isothermal calorimetry, bound water by oven-drying and portlandite consumption by thermogravimetry. The results indicated that both heat release and bound water correlated well with the relative compressive strength at 28 days, even for alternative SCMs. Thus, the $R^3$ method appears as an efficient screening test to identify promising SCMs. In addition, the study confirmed the potential of bound water, which can be measured with basic equipment available in many laboratories.

As most SCMs were first tested as received, the particle size varied significantly between the materials. Crushing the SCMs did not always improve the reactivity, presumably only when the amorphous part was affected. Finally, the effect of sulphates and carbonates on the reactivity was tested. Both compounds influenced the measured parameters, but no conclusion could be drawn regarding the correlation with the compressive strength. Thus, it is suggested to keep both sulphates and carbonates in the $R^3$ mix design, following the initial idea of mimicking a cement paste environment.

# Keywords

Reactivity tests, Supplementary cementitious materials, Heat release, Bound water, Compressive strength.

# 1 Introduction

Supplementary Cementitious Materials (SCMs) are major assets for limiting the $CO_2$ emissions associated with the production of concrete. However, the availability of traditional SCMs, such as fly ash or blast furnace slag, is expected to be reduced, because of the global trend towards reducing the use of fossil resources and increasing the recycling of waste materials. To ensure a sufficient supply for the concrete industry, it is necessary to find alternative materials and assess their suitability as SCMs. Many binder properties should be tested, but the compressive strength is among the first characteristics to document. In the process of developing new binders, a screening test able to determine the potential of a material to be used as an SCM is of major interest. This is the purpose of the $R^3$ method, which was one of the key topics of RILEM TC 267-TRM, see Li et al. (2018). The method consists of reactivity measurements of a paste made of portlandite, SCM, alkalis, sulphates, carbonates, and water, aiming at isolating the SCM reaction while simulating the environment of a cement paste. After 7 days of curing at 40°C, the SCM reactivity can be quantified by different parameters: heat release, bound water, portlandite consumption and chemical shrinkage. Previous work has already shown a fairly good correlation of heat release and bound water with the relative compressive strength at 28 days for traditional SCMs, see Londono-Zuluaga et al. (2022).

# 2 Research significance

The present study focused on assessing whether the $R^3$ method is effective with alternative SCMs. Two materials were ground finer in an attempt to increase their reactivity and study the effect on $R^3$ results. Finally, the influence of sulphates and carbonates on two SCMs was also investigated.

# 3 Materials and methods

The chemical composition of the SCMs measured by X-Ray Fluorescence (XRF) is shown in Table 1.

$R^3$ pastes were prepared by mixing the constituents in the following proportions: 11.11 g of SCM, 33.33 g of portlandite, 60.00 g of deionised water, 0.24 g of KOH, 1.20 g of $K_2SO_4$ and 5.56 g of calcite.

*Table 4: Chemical composition of the SCMs (measured by XRF). *: spherical particles.*

| Oxide | Limestone | Fly ash | Calcined clay | | Biomass ash | | Sewage sludge ash | Crushed brick | Glass beads* |
|---|---|---|---|---|---|---|---|---|---|
| | LL | FA | CC1 | CC2 | BA1 | BA2 | SSA | CB | GB |
| $SiO_2$ | 2.0 | 56.2 | 46.6 | 49.0 | 25.5 | 23.2 | 56.8 | 63.4 | 72.0 |
| $Al_2O_3$ | 0.4 | 23.8 | 17.4 | 17.3 | 4.8 | 4.3 | 8.4 | 11.2 | 0.7 |
| $Fe_2O_3$ | 0.12 | 6.90 | 9.58 | 9.74 | 1.80 | 1.93 | 19.57 | 4.32 | 0.17 |
| MgO | 0.3 | 1.8 | 2.5 | 2.5 | 3.5 | 4.0 | 0.9 | 1.2 | 3.8 |
| CaO | 54.2 | 3.9 | 9.7 | 10.1 | 34.1 | 30.9 | 1.4 | 9.0 | 9.1 |
| $Na_2O$ | 0.03 | 0.49 | 0.92 | 0.81 | 0.87 | 0.71 | 1.03 | 2.81 | 13.63 |
| $K_2O$ | 0.06 | 1.64 | 2.47 | 2.66 | 4.93 | 7.35 | 2.43 | 0.43 | 0.21 |
| $TiO_2$ | 0.03 | 0.93 | 0.97 | 0.97 | 0.28 | 0.29 | 1.54 | 0.63 | 0.07 |
| $P_2O_5$ | 0.11 | 1.02 | 0.21 | 0.24 | 2.91 | 3.03 | 2.97 | 0.15 | 0.01 |
| $SO_3$ | 0.08 | 0.79 | 0.97 | 0.98 | 4.58 | 12.66 | 0.38 | 0.63 | 0.24 |
| $Na_2O_{eq}$ | 0.07 | 1.57 | 2.54 | 2.55 | 4.12 | 5.55 | 2.63 | 2.91 | 13.77 |
| LOI | 42.52 | 1.57 | 7.97 | 4.94 | 15.83 | 10.26 | 3.77 | 5.37 | 0.09 |
| Sum | 100.0 | 99.6 | 99.8 | 99.7 | 99.8 | 99.6 | 99.4 | 99.8 | 100.0 |
| Density [kg/m$^3$] | 500 | 2300 | 2700 | 2700 | 2620 | 2650 | 2650 | 2640 | 2500 |
| $d_{50}$ [µm] | 4 | 18 | 10 | 39 | 16 | 70 | 11 | 43 | 67 |

## 3.1 Compressive strength

The compressive strength at 28 days was tested on mortar bars containing 65% of CEM I 52.5 N and 35% of SCMs. The relative compressive strength was calculated with respect to a mix containing 100% CEM I. A correction was made for the air content, on the basis of 5% strength loss for 1 % of air.

## 3.2 Techniques to quantify reactivity

Isothermal calorimetry was performed at 40°C on a paste sample of approximately 30 g (Calmetrix I2000). Heat release was measured for up to 7 days. For bound water, paste samples of approximately 8 g were cast into plastic vials and cured at 40°C. After 7 days, the samples were crushed and dried for 24h at 40°C followed by 2h at 350°C. Bound water was defined as the mass loss between 40 and 350°C.

On the same samples as for bound water, hydration was stopped after 7 days using the double solvent exchange method. The amount of portlandite was quantified by thermogravimetric analysis (NETZSCH STA 449 F3 Jupiter®,

from 30 to 950°C at 10°C/min) using the tangential method. The results were corrected for the portlandite purity (86%).

# 4 Results and discussion

Figure 1 shows the relative compressive strength at 28 days plotted against the different $R^3$ parameters. The best correlation is obtained with heat release ($R^2$ = 0.79), followed by bound water (0.73) and portlandite consumption (0.59). This is consistent with the trends reported by Li et al. (2018), confirming that both heat release and bound water are well correlated with the compressive strength. Portlandite consumption presents some inconsistencies for biomass ashes, which might be latent hydraulic materials. This is similar to previous results obtained for blast furnace slag, see Li et al. (2018). It should be noted that SCMs may behave differently in mortars and $R^3$ pastes, e.g. because of the filler effect or the particle shape.

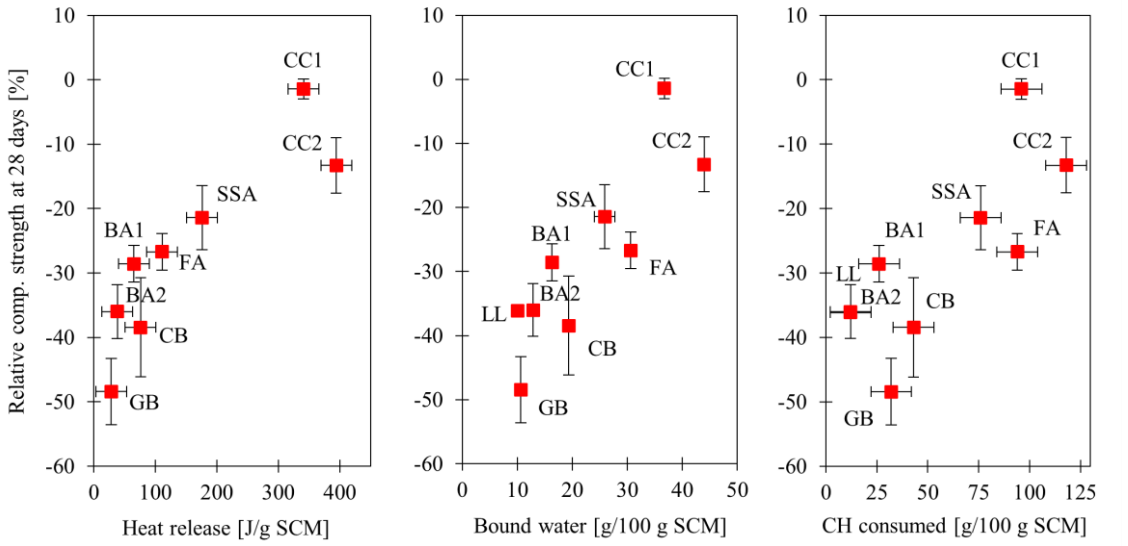


*Figure 1: Relative compressive strength at 28 days plotted against $R^3$ results at 7 days: heat release (left), bound water (centre), portlandite consumption (right). Note: the heat release was not measured for LL.*

As heat release and bound water lead to similar conclusions, the latter appears to be a promising parameter for screening potential SCMs on an industrial scale. As the method requires basic and affordable laboratory equipment, it could be useful to identify new potential SCMs and estimate their reactivity. In this respect, an important parameter is the particle size of the SCM, which affects the specific surface area and thus the dissolution rates. As shown in Table 2, the bound water content more than doubles when the glass particles are crushed to cement-like particle sizes. Conversely, no changes are observed

when reducing the particle size of brick powder. This is probably because crushing only affects the crystalline non-reactive phases, while the amorphous phases are already fine enough. Thus, $R^3$ tests can also be used in a pre-optimisation process to assess whether the gain in reactivity with a finer material is worth the energy used for grinding.

*Table 5: Bound water at 7 days as a function for different particle sizes. *For glass, coarse particles are spherical, while fine particles are more angular due to grinding.*

| Material | Glass beads* | | Crushed brick | |
|---|---|---|---|---|
| Particle size ($d_{50}$) | Coarse (67 µm) | Fine (9 µm) | Coarse (43 µm) | Fine (13 µm) |
| Bound water at 7 days [g/100 g SCM] | 11 | 25 | 19 | 17 |

Table 3 shows the results obtained with regular $R^3$ pastes, and modified $R^3$ systems without sulphates and no carbonates. For both calcined clay and fly ash, the presence of sulphates and carbonates increases bound water and portlandite consumption, but reduces heat release. These changes are likely due to changes in the phase assemblage. In the absence of sulphate, ettringite is not formed as shown in Avet et al. (2016), which could explain the lower amount of bound water. In the presence of calcite, Avet et al. (2022) reported a slightly lower heat release, which is in agreement with the present results. However, it is not possible to conclude on the influence of sulphates and carbonates on the correlation with the compressive strength. In the absence of further evidence, and because the current mixture already gives satisfactory results, it is proposed to follow the regular $R^3$ design and include both sulphates and carbonates in the mixture.

*Table 6: $R^3$ results for mixes with and without sulphate and carbonates. BW = bound water, HR = heat release, CHC = portlandite consumption.*

| Sulphates and carbonates | Fly ash | | | Calcined clay 2 | | |
|---|---|---|---|---|---|---|
| | BW [g/100 g SCM] | HR [J/g SCM] | CHC [g/100 g SCM] | BW [g/100 g SCM] | HR [J/g SCM] | CHC [g/100 g SCM] |
| With | 31 | 111 | 94 | 44 | 394 | 118 |
| Without | 24 | 135 | 59 | 39 | 407 | 83 |

# 5 Conclusions

As alternative SCMs attract increasing attention due to the expected shortage of traditional SCMs, screening test methods can help identify the most promising materials. In the present work, the $R^3$ method was successfully applied to a range of alternative SCMs and showed a satisfactory correlation with the relative compressive strength at 28 days. The influence of the particle size of the SCMs on the reactivity was also studied, illustrating the possibility to use the $R^3$ method to assess whether pre-processing the materials is worthwhile. Finally, no clear conclusion can be drawn regarding the effect of sulphates and carbonates on the correlation with the compressive strength. However, the phase assemblage is probably more realistic in their presence. Unless proven otherwise, it is suggested that they should be kept in the mix.

# Acknowledgements

The work presented is part of an industrial PhD project financed by the Danish Road Directorate and a joint grant from Innovation Fund Denmark (Innovationsfonden) and Realdania under the program Circular Built Environment. This financial support is gratefully acknowledged. The Research and Quality Centre of Aalborg Portland is warmly thanked for XRF analyses.

# References

Avet et al. (2016), "Development of a new rapid, relevant and reliable ($R^3$) test method to evaluate the pozzolanic reactivity of calcined kaolinitic clays", *Cement and Concrete Research*, 85: 1-11

Avet et al. (2022) "Report of RILEM TC 267-TRM phase 2: optimization and testing of the robustness of the $R^3$ reactivity tests for supplementary cementitious materials", *Materials and Structures*, 55(3): pp. 92

Li et al. (2018) "Reactivity tests for supplementary cementitious materials: RILEM TC 267-TRM phase 1", *Materials and Structures*, 51(6): pp. 151

Londono-Zuluaga et al. (2022) "Report of RILEM TC 267-TRM phase 3: validation of the $R^3$ reactivity test across a wide range of materials", *Materials and Structures*, 55(5): pp. 142

Paper VII

# Cold Water Extraction as a method to determine the free alkali content of cementitious binders

M. Ranger [a,b], M.T. Hasholt [b], and R.A. Barbosa [c]

[a] Department of Environmental and Resource Engineering, Technical University of Denmark, Kgs. Lyngby, Denmark

[b] Danish Road Directorate, Copenhagen, Denmark

[c] Danish Technological Institute, Taastrup, Denmark

*Accepted for the 16th International Congress on the Chemistry of Cement, September 2023, Bangkok (Thailand)*

# Abstract

The alkali content ($Na_2O$ and $K_2O$) of cement is of major importance when evaluating the risk of developing Alkali-Silica Reaction (ASR) in concrete. During hydration, alkali metals (Na and K) can either be bound to unreacted particles, bound to hydrates, or free in the pore solution. The latter category is the most critical one with respect to ASR, but its quantification remains more complex than the total content.

Blended cements containing e.g. fly ash or calcined clay are known to have less free alkalis than ordinary Portland cement, despite a larger total amount. Thus, using the total content to classify cements or calculate the alkali loading of a concrete mix may result in irrelevant figures regarding ASR. A procedure enabling to quantify free alkalis, which can be performed in most cement laboratories, would therefore be a useful tool.

This paper introduces the possibility to use Cold Water Extraction (CWE) as a method to determine the free alkali content of a cementitious binder. CWE is a technique aiming at extracting the pore solution of hardened samples, which can be performed with standard laboratory equipment. Three different cement types were investigated: a CEM I, a CEM II/B-M (35% clinker replacement) and a prototype CEM II/C-M (50% clinker replacement), all manufactured with the same clinker. The more traditional Pore Water Extraction method was also performed to benchmark CWE results. The free alkali content was determined after performing extraction on paste samples cured for 28 days at 20°C. Both methods indicated the same trends, namely lower relative and absolute free contents for blended cements compared to CEM I. The results were also in agreement with expansions obtained with the Danish accelerated mortar bar test (TI-B 51), which is currently prescribed in the Danish standards when total alkalis requirements cannot be met.

# Keywords

Alkalis, Alkali-Silica Reaction, Blended Cement, Cold Water Extraction.

# 1 Introduction

Alkali-Silica Reaction (ASR) is a well-known concrete deterioration mechanism which can severely affect structures. ASR requires the presence of a reactive aggregate, a high alkali content ($Na_2O$ and $K_2O$) and a high relative

humidity. If the use of reactive aggregates cannot be avoided, a typical prevention measure consists in keeping the pH low by limiting the alkali content of the binder, see Fournier and Bérubé (2000). Even though the pH (or $[OH^-]$) is often mentioned as the key driving factor of ASR, it is known that the chemistry of the pore solution can often be described by $[Na^+] + [K^+] \approx [OH^-]$, see for instance Kasaniya and Thomas (2022). Thus, it seems reasonable to use the sum of alkali metals ions (referred to as "free") as an estimate of the hydroxide ion concentration. However, one must be careful with such assumption, in particular when other ions are present in significant amounts (e.g. $Cl^-$ or $SO_4^{2-}$). While the total alkali content is routinely determined when manufacturing cementitious materials (e.g. by X-Ray Fluorescence, XRF), the free alkali content requires to extract the pore solution and determine its alkali metal content. Plusquellec et al. (2017) published a review on the different methods related to this topic. The so-called "Pore Water Extraction" method (PWE) is the most common procedure in the literature, but it requires a specific and expensive equipment able to squeeze out the pore solution from a hardened sample. The complexity of the setup therefore limits its use outside research laboratories. An alternative to PWE is the "Cold Water Extraction" method (CWE), which consists in leaching a crushed sample into an extraction liquid with basic laboratory equipment. Both methods allow to calculate either the concentration in the pore solution or the free content of alkali metals, however the amount of pore solution may greatly affect the results, see Tuinukuafe et al. (2022) and Ranger et al. (2023).

As long as Portland cement is used, the ratio between free and total alkalis is rather constant, previous studies reporting values between 60 to 80%, see Ranger et al. (2023). However, the ratio changes significantly when blended cement is used, as supplementary cementitious materials (SCMs) are known to have a larger total alkali content than Portland cement but a lower free content due to alkali metal binding on hydration products. Using the total alkali content across all types of cements may therefore result in serious inconsistencies between the declared value and the ASR performance of the binder.

In Denmark, the standard DS/INF 135 is used to classify cements into four categories depending on the total alkali content of the clinker: extra low ($\leq 0.4$ wt.% $Na_2O_{eq}$), low ($\leq 0.6$), moderate ($\leq 0.8$) and high ($> 0.8$). This rule applies to CEM I, CEM II/A-V and B-V, and CEM II/A-M and B-M. For other binders, ASR documentation is required via the Danish accelerated mortar bar test (TI-B 51, immersion in a saturated NaCl solution for 8 or 20 weeks).

# 2 Research significance

Because of the complexity to determine the free alkali content, the total content is generally the default parameter in ASR regulations. However, the total alkali content does not correlate with ASR expansion when blended cements are used. Thus, this work investigates the possibility of using CWE to determine the free alkali content of a cementitious binder, to allow a more fair comparison between Portland cements and blended cements. The study also focuses on using a method that can be applied at an industrial scale.

# 3 Materials and methods

Three binders were investigated: a CEM I, a CEM II/B-M and a prototype CEM II/C-M (respectively 35 and 50% clinker replacement with calcined clay and limestone), all produced with the same clinker. The chemical composition of the cements measured by XRF is given in Table 1.

*Table 7: Chemical composition of the cements (determined by XRF).*

| Oxide | CEM I | CEM II/B-M | CEM II/C-M |
|---|---|---|---|
| $SiO_2$ | 19.2 | 22.1 | 26.6 |
| $Al_2O_3$ | 5.2 | 6.4 | 8.5 |
| $Fe_2O_3$ | 3.67 | 3.95 | 4.94 |
| MgO | 1.0 | 1.1 | 1.4 |
| CaO | 63.4 | 54.2 | 45.7 |
| $Na_2O$ | 0.33 | 0.38 | 0.45 |
| $K_2O$ | 0.38 | 0.69 | 1.09 |
| $SO_3$ | 3.14 | 2.73 | 2.47 |
| Loss on ignition | 3.21 | 7.86 | 7.88 |
| $Na_2O_{eq}$ (total) | 0.58 | 0.83 | 1.17 |
| Fineness [$m^2/kg$] | 430 | 700 | - |
| Density [$kg/m^3$] | 3140 | 3020 | - |

Paste samples were cast with w/b = 0.50 and sealed-cured before performing CWE (28 and 140 days) and PWE (28 days). CWE was caried out following the procedure described in Ranger et al. (2023): crushing paste to obtain 20.0 g between 0.5 and 1 mm, leaching for 5 min in 20 g of deionised water and filtering. PWE was done by squeezing a sample at a pressure of 1000 MPa for 15 min. The content of Na and K in the solutions were determined by ICP-

OES. The amount of pore solution was determined by drying a piece of paste in a desiccator containing silica gel and stored at 40°C until reaching constant mass. The detailed formulas to derive the free alkali content are shown in Ranger et al. (2023).

In parallel, the TI-B 51 method was conducted using a typical Danish reactive sand containing porous opaline flint (Øde Hastrup). Mortars bars (40 x 40 x 160 mm) were cast with w/b = 0.50 and a sand-to-cement ratio of 3. The bars were cured in deionised water for 28 days at 20°C before being immersed in a saturated NaCl solution kept at 50°C. The expansion of the bars was measured up to 20 weeks.

# 4 Results and discussion

Figure 1 presents the free alkali content determined for the three cements with two parameters varying: the extraction method (left) and the curing time (right).

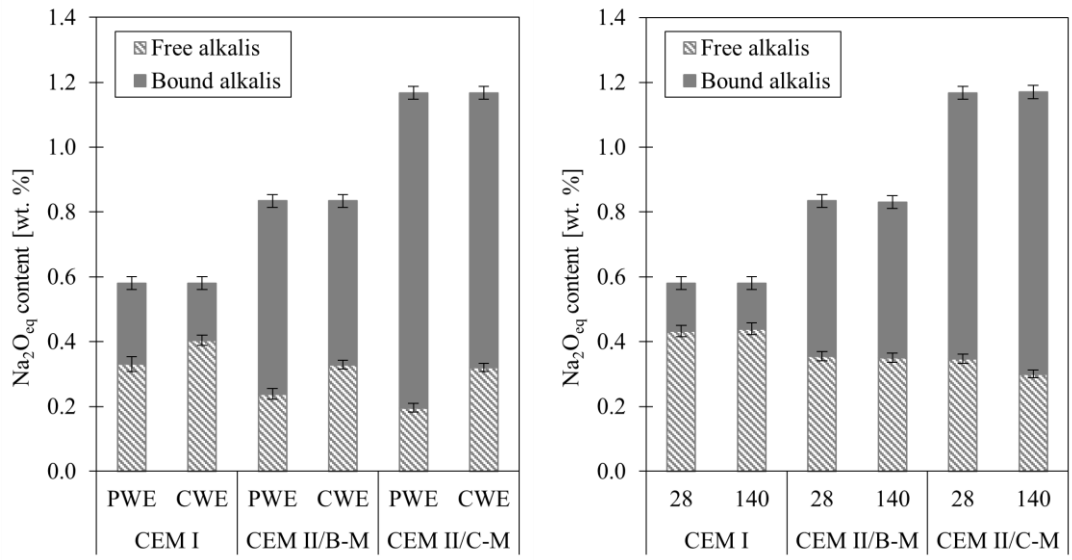


*Figure 1: Free and bound alkali content: comparison between CWE and PWE at 28 days (left), comparison between CWE at 28 and 140 days (right).*

Independently of the method used (CWE or PWE), the free alkali content in pastes produced with blended cements is lower than in pastes with CEM I, despite the rise in total alkalis induced by SCMs (Figure 1, left). These results were expected, as other authors reported a decrease of the concentrations of alkali metal ions in the pore solution for limestone calcined clay cements, see Nguyen et al. (2018). Although CWE and PWE show the same trend, CWE systematically results in higher values than PWE. In CWE, leaching in water

induces the dissolution of portlandite, so that the leaching solution has more Ca than the initial pore solution. Consequently, the thermodynamic equilibrium between the C-S-H and the leaching solution is shifted toward a higher Ca/Si of the C-S-H, thereby reducing its alkali metal binding capacity. More data and a detailed discussion can be found in Ranger et al. (2023). The practical implication is that CWE probably tends to overestimate free alkalis, which is however on the safe side. Moreover, it can also be seen that the curing time has a limited influence on the results (Figure 1, right). Only CEM II/C-M presents a slight drop from 28 to 140 days, probably due to the pozzolanic reaction binding more alkali metals over time.

Blended cements also perform better than CEM I in the TI-B 51 test (Figure 2). However, a clear difference can be seen between CEM II/B-M and CEM II/C-M, the latter showing no expansion after 20 weeks of exposure. This behaviour can hardly be explained by the free alkali content, which is almost equal for the two cements. Since the TI-B 51 is an immersion test, a possible explanation is that the two cements influence transport properties in different ways, so that the resistance to ion and/or water ingress is a major factor influencing the test outcome. This point is currently under investigation. According to the Danish standards (national annex of EN 206), the TI-B 51 test must be used to document the ASR performance of a cement that is not already included in the Danish standards. In practise, the test outcome is also used to decide on the alkali classification of the cement. For instance, it may be chosen to exclude the alkalis from the SCM in the calculations if a blended cement causes less than a Portland cement.

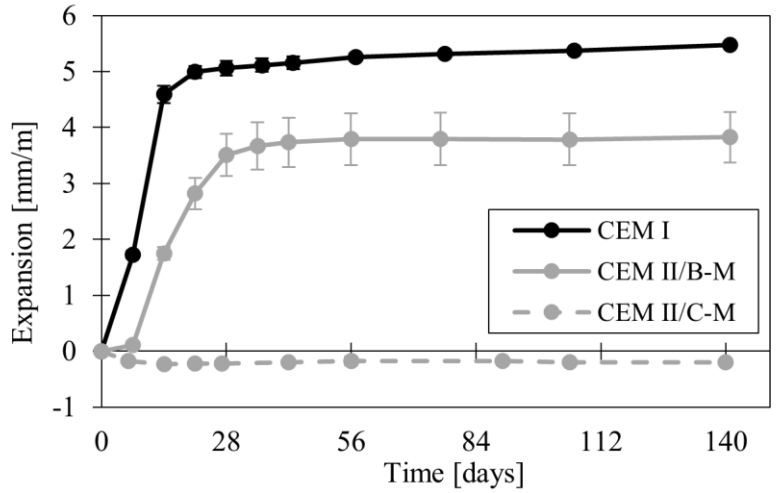


*Figure 2: Expansions measured in the TI-B 51 test.*

When making an alkali classification of cements, the free alkali content seems to be a parameter that is more chemically meaningful than the TI-B 51 expansion. In this respect, CWE is a relatively simple method to measure the free alkali content directly. It should be emphasised that the free alkali content is only one parameter affecting ASR. Thus, for mitigation purposes, more testing is required.

# 5 Conclusions

With the increasing use of blended cements, it is important to compare all types of cements on a relevant basis, i.e. with suitable parameters for a given purpose. While blended cements often perform better than Portland cements against ASR, they usually have a larger total alkali content because of the presence of SCMs. The present work investigated a method, namely Cold Water Extraction, to determine the free alkali content of cementitious binders, which seems more appropriate than the total content in an ASR context. CWE can be performed on paste samples with standard laboratory equipment, and the results suggest that 28 days of curing at 20°C are sufficient to obtain a value of appropriate accuracy. Additional binders are currently under investigation to further explore the potential of the method.

# Acknowledgements

This work is part of an industrial PhD project financed by the Danish Road Directorate and a joint grant from Innovation Fund Denmark (Innovationsfonden) and Realdania under the program Circular Built Environment. This financial support is gratefully acknowledged. The Research and Quality Centre of Aalborg Portland is warmly thanked for supplying CEM I and CEM II/B-M, hosting Pore Water Extraction tests, and performing XRF analyses. Finally, we would like to acknowledge the support of the CALLISTE project for developing and supplying the prototype CEM II/C-M.

# References

Fournier and Bérubé (2000) “Alkali-aggregate reaction in concrete: a review of basic concepts and engineering applications”, *Canadian Journal of Civil Engineering*, *27*(2): 167–191

Kasaniya and Thomas (2022) “Role of the alkalis of supplementary cementing materials in controlling pore solution chemistry and alkali-silica reaction”, *Cement and Concrete Research*, 162: pp. 107007

Nguyen et al. (2018) “Engineering properties of limestone calcined clay concrete”, *Journal of Advanced Concrete Technology*, *16*(8): 343–357

Plusquellec et al. (2017) “Determination of the pH and the free alkali metal content in the pore solution of concrete: Review and experimental comparison”, *Cement and Concrete Research*, 96: 13–26.

Ranger et al. (2023) “Pore solution alkalinity of cement paste as determined by Cold Water Extraction”, *Cement*, 11: pp. 100055.

Tuinukuafe et al. (2022) Estimating $Na^+$ and $K^+$ concentrations of the pore solution based on ex-situ leaching tests and thermodynamic modeling, *RILEM Technical Letters*, 7: 88–97.